Oncolytic adenoviruses expressing transgenes targeting the tumor stroma to enhance the antitumor efficacy

Jana de Sostoa Pomés

UNIVERSITAT DE BARCELONA
FACULTAT DE FARMÀCIA I CIÈNCIES DE L'ALIMENTACIÓ
PROGRAMA DE DOCTORAT EN BIOMEDICINA

ONCOLYTIC ADENOVIRUSES EXPRESSING TRANSGENES TARGETING THE TUMOR STROMA TO ENHANCE DE ANTITUMOR EFFICACY

JANA DE SOSTOA POMÉS

2019

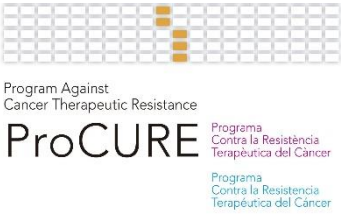

UNIVERSITAT DE BARCELONA

FACULTAT DE FARMÀCIA I CIÈNCIES DE L'ALIMENTACIÓ

PROGRAMA DE DOCTORAT EN BIOMEDICINA

ONCOLYTIC ADENOVIRUSES EXPRESSING TRANSGENES TARGETING THE TUMOR STROMA TO ENHANCE THE ANTITUMOR EFFICACY

JANA DE SOSTOA POMÉS

2019

Memòria presentada per Jana de Sostoa Pomés per optar al grau de Doctor/a per la Universitat de Barcelona

Dr. Ramon Alemany Bonastre	Dr. Francesc Viñals Canals	Jana de Sostoa Pomés
Director	Tutor	Autora

TABLE OF CONTENTS

ABBREVIATIONS **7**

SUMMARY **13**

RESUM… **17**

INTRODUCTION **21**

1. Virotherapy of cancer **23**

2. Oncolytic adenoviruses **24**

2.1 Adenovirus classification *25*

2.2 Virion structure *25*

2.3 Genome structure *26*

2.4 Biology of the Infectious cycle *27*

2.4.1 Adsorption and entry 27

2.4.2 Early gene expression and DNA replication 28

2.4.3 Late gene expression and virion assembly 29

2.5 Design of tumor-selective oncolytic adenoviruses *31*

2.5.1 Transductional and transcriptional targeting 31

2.6 ICO15K *33*

2.7 Arming oncolytic adenoviruses with therapeutic transgenes *34*

2.8 Clinical experience with oncolytic adenoviruses *36*

2.9 Limitations of oncolytic adenoviruses *38*

2.9.1 Oncolytic adenovirus tumor delivery and targeting 39

2.9.2 Stromal barriers 39

2.9.3 Immune responses 41

3. Antitumor immune responses **41**

3.1 Tumor-induced immune evasion *43*

3.2 Oncolytic adenovirus-mediated antitumor immune responses *44*

3.3 Strategies to improve antitumor immune responses with oncolytic adenoviruses *46*

3.3.1 Stimulatory molecules encoded in oncolytic adenoviruses 46

3.3.2 Combination of oncolytic viruses with other immunotherapies 47

4. Antiviral immune responses **49**

4.1 Bispecific T-cell engagers (BiTEs) *50*

4.1.1 Structure 50

4.1.2 Mode of action 51

4.1.3 Clinical applications 52

5. Toxin-based therapeutic approaches **54**

5.1 Immunotoxins: a new tool for cancer therapy *54*

5.1.1 Structure 54
5.1.2 Ribosome-inactivating proteins 55
5.2 GDEPT therapy *57*
OBJECTIVES **59**
MATERIALS AND METHODS **63**
1. Handling of bacteria **65**
1.1 Preparation of electrocompetent bacteria *65*
1.2 Transformation of competent bacteria by electroporation *65*
1.3 Plasmidic DNA extraction from bacterial cultures *66*
1.3.1 Small and large scale of DNA preparations 66
1.4 Homologous recombination in bacteria *67*
2. Cell culture **69**
2.1 Cell lines *69*
2.2 Maintenance of cell cultures *70*
2.3 Cell counting *70*
2.4 Cell freezing and cryopreservation *70*
2.5 Mycoplasma test *71*
2.6 Isolation, cryopreservation and thawing of human PBMCs and T cells *71*
2.7 Fluorescent labeling of cells with CFSE *72*
3. Recombinant adenoviruses **72**
3.1 Transgenes design *72*
3.1.1 BiTE design 72
3.1.2 Immunotoxin design 74
3.1.3 NfrA design 75
3.2 Construction of transgene-expressing oncolytic adenovirus *76*
3.2.1 Construction of BiTE-expressing oncolytic adenovirus 76
3.2.2 Construction of immunotoxin-expressing oncolytic adenovirus 76
3.2.3 Construction of vector-encoded immunotoxin 76
3.2.4 Construction of NfrA-expressing oncolytic adenovirus 77
3.3 Adenovirus generation by calcium phosphate transfection *77*
3.4 Clone isolation by plaque purification assay *78*
3.5 Amplification and purification of adenoviruses *78*
3.5.1 Amplification of oncolytic adenoviruses 79
3.5.2 Purification of oncolytic adenoviruses 79
3.6 Titration of adenoviruses *80*
3.6.1 Determination of physical viral particles by spectrophotometry 80
3.6.2 Determination of functional viral particles by anti-hexon staining 81
3.7 Characterization of oncolytic adenoviruses *81*
3.7.1 Isolation of viral DNA from infected cells (Hirt's) 81

3.7.2 Isolation of viral DNA from purified viral particles 82
3.7.3 Characterization of viral genomes by restriction enzymes 82
3.7.4 Characterization of viral DNA by sequencing 83
4. Production and titration of lentiviral vectors 84
5. Recombinant adenovirus-based *in vitro* assays 85
5.1 Adenovirus-mediated cytotoxicity assay 85
5.2 Adenovirus production assay 85
5.3 Production of supernatants 86
5.4 Immunology techniques 86
5.4.1 Antibodies and flow cytometry 86
5.4.2 Preactivation and expansion of human T cells 87
5.4.3 Generation of genetically-modified T cells 88
5.4.4 Binding assays 88
5.5 Co-culture-based in vitro assays 88
5.5.1 T-cell activation assays 88
5.5.2 T-cell proliferation assay 89
5.5.3 Cell-mediated cytotoxicity assays 89
5. *In vivo* assays with recombinant adenoviruses 90
5.6 Mouse models and procedures 90
5.7 Detection of transcripts in tumors by real-time PCR 91
5.8 Immunohistochemistry of OCT-embedded tumor sections 92
6. Statistical analysis 92
RESULTS.. 93
1. Optimization of replication-dependent transgene expression from an oncolytic adenovirus 95
1.1 Generation and characterization of luciferase-expressing oncolytic adenoviruses 95
1.2 Characterization of transgene expression in vivo 99
1.3 Impact of transgene expression from an oncolytic adenovirus in therapeutic efficacy in vivo 101
2. Fap-targeting bispecific T cell engager-armed oncolytic adenovirus 102
2.1 Generation and characterization of an oncolytic adenovirus secreting a FAP-targeting BiTE 102
2.2 Cells infected with ICO15K-FBiTE secrete FBiTE molecules which specifically bind to target and effector cells 107
2.3 Supernatants from ICO15K-FBiTE-infected cells induce activation and proliferation of T cells 111
2.4 Combining viral oncolysis with FBiTE-mediated killing improves therapeutic activity in vitro 114
2.5 ICO15K-FBiTE increases tumor T-cell retention and accumulation in vivo 117
2.6 ICO15K-FBiTE-mediated oncolysis enhances antitumor efficacy in vivo 119
2.7 ICO15K-FBiTE improves the antitumor activity by depletion of FAP 122
3. Targeting the tumor stroma with an immunotoxin or prodrug 126
3.1 Oncolytic adenovirus expressing FAP-targeted immunotoxin 126

3.1.1 Construction of different anti-FAP-toxin-secreting oncolytic adenoviruses 126
3.1.2 FAP-specific binding of immunotoxins secreted by infected cells 128
3.1.3 *In vitro* cytotoxicity of oncolytic adenovirus expressing immunotoxin 130
3.2 Expression vector-encoded immunotoxin 133
3.2.1 Generation of expression vector-encoded immunotoxin 133
3.2.2 Binding of secreted immunotoxin to FAP-expressing cells 134
3.2.3 Specific cytotoxicity of FAP-positive cells by supernatants-containing immunotoxin 136
3.3 Nfra-armed oncolytic adenovirus 137
3.3.1 Generation of NfrA-secreting oncolytic adenovirus 137
3.3.2 *In vitro* characterization of oncolytic adenovirus expressing NfrA 138

DISCUSSION 143

1. Optimization of replication-dependent transgene expression from an oncolytic adenovirus 145

2. FBiTE-armed oncolytic adenovirus 151

3. Targeting the tumor stroma with an immunotoxin or a prodrug 165

CONCLUSIONS 171

REFERENCES 175

ANNEX 203

LIST OF FIGURES

Figure 1. Principle of cancer virotherapy. 23
Figure 2 Adenovirus virion structure. 26
Figure 3. The genome structure and major transcript units of human Ad5. 27
Figure 4. Infectious cycle of human adenoviruses 30
Figure 5. Δ24 selectivity mechanism. 33
Figure 6. Schematic representation of the ICO15K genome modifications. 34
Figure 7. Challenges to effective OVs therapy *in vivo*. 38
Figure 8. Generation and regulation of antitumor immunity. 43
Figure 9. Antitumor immunity by OV therapy. 45
Figure 10. Generation and structure of a BiTE. 51
Figure 11. Mode of action of BiTE. 52
Figure 12. Structural representation of the tree generations of immunotoxins. 55
Figure 13. The mechanism of GDEPT systems.. 58
Figure 14. Schematic representation of the oncolytic adenoviruses used in this project. 96
Figure 15. Cytotoxicity profile of the different cLUC-expressing viruses 98
Figure 16. Kinetics and efficiency of transgene expression by recombinant viruses. 99
Figure 17. Efficacy and kinetics of luciferase activity *in vivo* 100
Figure 18. Antitumor efficacy of different cBiTE-expressing viruses. 102
Figure 19. Schematic structure representation of the ICO15K-FBiTE and the different ICO15K-mFBiTE viruses used in this study. 105
Figure 20. Viral production from cell extracts (CE) and supernatants (SN) of ICO15K-IIIa-FBiTE and ICO15K-40SA-FBiTE. 106
Figure 21. Comparative cytotoxicity profile of ICO15K-IIIa-FBiTE and ICO15K-40SA-FBiTE. 107
Figure 22. FAP and CD3 expression of the cell lines used in this project. 108
Figure 23. Binding assay of FBiTE and mFBiTE expressed by BiTE-expressing viruses. 110
Figure 24. Evaluation of cytokine production. 112
Figure 25. FBiTE molecules expressed from ICO15K-FBiTE-infected cells induce T-cell proliferation. 114
Figure 26. Enhanced FBiTE-expressing viruses-mediated cytotoxicity of FAP-positive cells 115
Figure 27. FBiTE-mediated killing of FAP-positive non-infected cells 116
Figure 28. Cytotoxicity of CFSE-stained-murine or human CAFs.. 117
Figure 29. Characterization of GFP- and CBG Luciferase-expressing T cells 118
Figure 30. Increased T cell accumulation in ICO15K-FBiTE tumors. 119
Figure 31. Enhanced antitumor efficacy of ICO15K-FBiTE in the presence of T cells. 121
Figure 32. Antitumor activity in absence of T cells.. 122
Figure 33. Depletion of tumor stroma by ICO15K-FBiTE. 124
Figure 34. A549 tumor tissue characterization.. 125
Figure 35. Schematic representation of the immunotoxin-expressing viruses used in this section. 127
Figure 36. Binding assay of the immunotoxins secreted by infected cells. 130

Figure 37. Cytotoxicity of M5-Sarcin-expressing viruses 131
Figure 25. Immunotoxin-mediated cytotoxicity. 132
Figure 39. Construction and *in vitro* characterization of ICO15K-ONCO-FAP. 133
Figure 40. Diagram of the immunotoxin expressed by GT4082. 134
Figure 41. Binding assays of immunotoxins expressed from HEK293-transfected cells 136
Figure 42. Cytotoxicity of immunotoxin-containing supernatants of HEK293 transfected cells. 136
Figure 43. Construction of NfrA-expressing ICO15K.. 137
Figure 44. Cytotoxic curves of viruses in permissive and semi-permissive cell lines. 139
Figure 45. Activity of NfrA expressed by ICO15K-NfrA. 140
Figure 46. NTR-dependent bystander effect of SN34668. 141
Figure 47. Dual targeting of cancer and tumor stroma using OVs encoding stromal cell-targeted BiTEs. 152

LIST OF TABLES

Table 1. Ongoing clinical trials on OAds in cancer therapy. 37
Table 2. Clinical trials of BiTEs. 53
Table 3. Cell lines used in this thesis. 69
Table 4. Primers used for the detection of mycoplasma 71
Table 5. Primers used to obtain the M5-Sarcin, ESC11-Sarcin and ONCO-FAP for being inserted in an expression vector. 75
Table 6. Conditions used to obtain the M5-Sarcin, ESC11-Sarcin and ONCO-FAP. 75
Table 7. Primers used for adenovirus and transgenes sequencing. 83
Table 8. PCR conditions for adenovirus and transgenes sequencing. 83
Table 9. Plasmids for the generation of lentiviral vectors 84
Table 10. List of antibodies used for flow cytometry. 87
Table 11. Primers used for the detection of viral genomes and FBiTE molecules. 91
Table 12. PCR conditions for the detection of viral genomes and FBiTE molecules 92
Table 13. PCR conditions for the detection of FAP cDNA. 92
Table 14. Characterization of purified viruses used in *in vivo* assays 97
Table 15. Characterization of purified viruses used for the antitumor efficacy assay. 102
Table 16. Characterization of purified virus 104
Table 17. Description of the NTR prodrug or pre-prodrug used *in vitro* and *in vivo* assays 138
Table 18. Characterization of purified virus 138

ABBREVIATIONS

%	Percentage
Å	Årmströng
°C	Centigrade degrees
Δ24	*delta*24 mutation, deletion of 24 bp in E1A protein
µF	microfarad
µg	microgram
µL	microliter
µm	micrometer
Ω	Ohm
AAALAC	Association for Assessment and Accreditation of Laboratory Animal Care
ABD	Albumin-Binding Domain
ABP	Albumin-Binding Peptide
Ad	Adenovirus
ADP	Adenovirus Death Protein
ALT	Alanine Transaminase
AST	Aspartate Transaminase
ATCC	American Type Cell Culture
BAC	Bacterial Artificial Chromosome
Bak	Bcl-2 homologous antagonist/killer
Bax	Bcl-2-associated X protein
BCA	Bicinchoninic Acid Assay
bp	base pairs
BSA	Bovine Serum Albumin
C4BP	Complement Binding Protein-4
$CaCl_2$	Calcium chloride
CAR	Coxsackievirus B and Adenovirus Receptor
CCE	Clarified Cell Extract
CD4 and 8	Cluster of differentiation 4 and 8
cDNA	complementary DNA
CE	Cell Extract
CFSE	Carboxyfluorescein succinimidyl ester
Cm	Chloramphenicol
cm	centimeter
CMV	Cytomegalovirus

CO_2	Carbon dioxide
CPE	Cytopathic effect
CR	Complement Receptors
CRAd	Conditionally Replicative Adenovirus
CsCl	Cesium chloride
CTL	Cytotoxic T Lymphocyte
CTLA-4	Cytotoxic T-Lymphocyte-Associated Protein 4
DAB	3,3'-Diaminobenzidine
DAPI	4',6-Diamidino-2-phenylindole dihydrochloride
DNA	Deoxyribonucleic acid
DC	Dendritic cell
ddH_2O	bi-distilled water
ddDNTP	2',3' dideoxynucleotides
DMEM	Dulbecco's Modified Eagle's Medium
DMSO	Dimethyl sulfoxide
DNA	Deoxyribonucleic Acid
dNTP	Nucleoside triphosphate
EDTA	Ethylenediaminetetraacetic acid
ELISA	Enzyme-Linked ImmunoSorbent Assay
ELISPOT	Enzyme-Linked Immunospot Assay
FACS	Fluorescence Activated Cell Sorting
FBS	Fetal Bovine Serum
FDA	Food and Drug Administration
FIX	Coagulation factor IX
FX	Coagulation factor X
g	acceleration of gravity
g	gram
GALV	Gibbon Ape Leukemia Virus
GM-CSF	Granulocyte Macrophage-Colony Stimulating Factor
h	hour
H_2O_2	Hydrogen peroxide
HA	Hyaluronic acid
HCl	Chloridric acid
HDAC	Histone deacetylases
HEK293	Human Embryonic Kidney 293
HEPES	4-(2-hydroxyethyl)-1-piperazineethanesulfonic acid

IC_{50}	Inhibitory Concentration 50
IFN	Interferon
Ig	Immunoglobulin
IL	Interleukin
IP	Intraperitoneal
IT	Intratumoral
ITR	Inverted Terminal Repeats
IU	International Units
IV	Intravenous
IVIS	*In Vivo* Imaging System
K	Kozak sequence
KH_2PO_4	Monopotassium phosphate
Kan	Kanamycin
kb	kilobase
KC	Kupffer Cell
KCl	Potassium chloride
L	Liter
LITR	Left Inverted Terminal Repeat
LRP	Lipoprotein Receptor-related Protein
LSEC	Liver Sinusoid Endothelial Cell
LU	Light Units
mA	Milliampere
mAb	monoclonal antibody
mg	milligram
MHC	Major Histocompatibility Complex
min	minute
mL	milliliter
MLP	Major Late Promoter
MLU	Major Late transcription Unit
mm	millimeter
mm^3	cubic millimeter
mM	millimolar
MOI	Multiplicity of Infection
mRNA	Messenger Ribonucleic Acid
MSA	Mouse Serum Albumin
MSC	Mesenchymal Stem Cell

MTT	3-(4,5-Dimethylthiazol-2-yl)-2,5-Diphenyltetrazolium Bromide
MVA	Modified Vaccinia Ankara
NAbs	Neutralizing antibodies
NaCl	Sodium chloride
NaH_2PO_4	Monosodium phosphate
Na_2HPO_4	Disodium phosphate
NaOH	Sodium hydroxide
NDV	Newcastle Disease Virus
NF-κβ	Nuclear factor Kappa-light-chain-enhancer of activated B cells
ng	nanogram
NK	Natural Killer
nm	nanometer
OCT	Optimum Cutting Temperature compound
OD	Optical Density
p	photons
pA	polyadenylation sequence
PAMP	Pathogen-Associated Molecular Pattern
PBS	Phosphate Buffered Saline
PCR	Polymerase Chain Reaction
PEG	Polyethylene Glycol
p.i.	Post-infection or post-injection
pg	picogram
PMA	Phorbol Myristate Acetate
pmol	picomol
PRR	Pattern Recognition Receptor
PS	Penicillin-Streptomycin
PSA	Prostate-Specific Antigen
Rb	Retinoblastoma
RGD	Arginine-glycine-aspartic acid
RITR	Right Inverted Terminal Repeat
RNA	Ribonucleic Acid
rpm	revolutions per minute
RPMI	Roswell Park Memorial Institute
RT	Room Temperature
RT-PCR	Real-Time PCR
SA	Splicing Acceptor

SD	Standard Deviation
SDS	Sodium dodecyl sulfate
SEM	Standard Error of the Mean
SFC	Spot forming colony
SPARC	Secreted Protein Acidic and Rich in Cysteine
Sr	Steradian
SR	Scavenger Receptor
Strep	Streptomycin
TAE	Tris-Acetate-EDTA
TAP	Transporter Associated to Antigen Processing
TE	Tris-EDTA
TGF-β	Transforming Growth Factor-β
TL	Track-Luc cassette (eGFP-Luciferase)
TLP	Tripartite Leader
TNF	Tumor Necrosis Factor
TLR	Toll-Like Receptor
TP	Terminal Protein
TRAIL	TNF-related apoptosis-inducing ligand
Tris	Tris(hydroxymethyl)aminomethane
TU	Transducing Unit
V	Volt or Volume
VA	Virus-Associated
vp	viral particle
VSV	Vesicular Stomatitis Virus
VV	Vaccinia Virus
WHO	World Health Organization
wt	wild type

Amino acids

F Phe, phenylalanine	**S** Ser, serine	**Y** Tyr, tyrosine	**K** Lys, lysine	**W** Trp tryptophan
L Leu, leucine	**P** Pro, proline	**H** his, histidine	**D** Asp, aspartic acid	**R** Arg, arginine
I Ile, isoleucine	**T** Thr, threonine	**Q** Gln, glutamine	**E** Glu, glutamic acid	**G** Gly, glycine
M Met, methionine	**A** Ala, alanine	**N** Asn, asparagine	**C** Cys, cysteine	**V** Val, valine

Nucleotides

A adenine **T** thymine **G** guanine **C** cytosine **U** uracil

SUMMARY

Oncolytic virus (OV)-based therapies have an emerging role in the treatment of solid tumors, involving both direct cell lysis and immunogenic cell death. Nonetheless, tumor-associated stroma limits the efficacy of oncolytic viruses by forming a barrier that block efficient viral penetration and spread. Another important hurdle for the efficacy of OVs is the antiviral immune responses, where virus-specific infiltrating T cells clear adenovirus-infected cells without compromising tumor burden.

In this thesis, these hurdles have been addressed in separate chapters. We first hypothesized that arming an oncolytic adenovirus with a FAP-targeting bispecific T cell engager (FBiTE) could retarget infiltrated lymphocytes towards cancer-associated fibroblasts (CAFs), enhancing viral spread and favoring antitumor rather than anti-viral immune responses. The engineered ICO15K-expressing FBiTE virus showed similar infectivity and replication potency than the non-armed virus. FBiTE-mediated binding of $CD3^+$ effector T cells and FAP^+ target cells led to T-cell activation, proliferation, and cytotoxicity against FAP-positive cells *in vitro*. *In vivo,* FBiTE expression increased intratumoral accumulation of T cells and decreased the level of FAP, a marker of CAFs, in tumors. Finally, the antitumor activity of the FBiTE-armed adenovirus was superior to the parental virus. The data presented in this thesis strongly supports that the combination of viral oncolysis of cancer cells and FBiTE-mediated cytotoxicity of FAP-expressing CAFs might be an effective strategy to overcome a key limitation of oncolytic virotherapy, encouraging its further clinical development.

Aiming to induce stroma disruption, we secondly generated a panel of oncolytic adenoviruses expressing FAP-targeting immunotoxins and a nitroreductase (NfrA)-activatable prodrug. During the development of these projects, we successfully rescued and characterized all the viruses. However, although immunotoxins molecules were properly expressed and secreted from modified-virus infected cells, no promising results were obtained. In contrast, NfrA-armed virus showed replication-dependent enzymatic activity on target cells, leading to increased oncolytic potency *in vitro*. These preliminary results indicate that this last strategy could be considered to foster viral spread in stroma-abundant tumors, encouraging its validation in an *in vivo* setting.

RESUM

Les teràpies basades en virus oncolítics pel tractament de tumors sòlids es consideren molt prometedores degut a la seva capacitat de combinar la lisi directa de cèl·lules canceroses i la mort cel·lular per l'activació del sistema immune. No obstant, l'estroma associat al càncer forma una barrera que bloqueja la penetració i distribució del virus en el tumor, limitant l'eficàcia dels virus oncolítics. Una altra limitació important és la resposta immune contra el virus. Les cèl·lules T citotòxiques específiques contra el virus que infiltren el tumor eliminen, normalment, les cèl·lules infectades per l'adenovirus sense comprometre la massa tumoral.

En aquesta tesi, aquestes limitacions han estat abordades en capítols separats. Primer va m hipotetitzar que un adenovirus oncolític armat amb un *bispecific T cell engager* (BiTE) contra FAP (FBiTE) podria redirigir els limfòcits infiltrats contra els fibroblasts associats al càncer (CAFs), millorant la distribució viral i afavorint la resposta antitumoral vers l'antiviral. El virus ICO15K que expressa el FBiTE va mostrar un patró d'infectivitat i de replicació similars al virus no armat. La unió de les cèl·lules T efectores $CD3^+$ i les cèl·lules diana FAP^+ mitjançada pel FBiTE va provocar l'activació, la proliferació i la citotoxicitat de les cèl·lules T contra la cèl·lules FAP positives *in vitro*. *In vivo*, l'expressió de FBiTE va induir l'acumulació intratumoral de les cèl·lules T i la disminució dels nivells de FAP, un marcador de CAFs, en els tumors. Finalment, l'activitat antitumoral dels adenovirus armats amb el FBiTE va ser superior que la del virus parental. Els resultats presentats en aquesta tesi aporten fortes evidències que la combinació de l'oncolisi viral de les cèl·lules canceroses i la citotoxicitat dels CAFs FAP^+ mitjançada pel FBiTE pot ser una estratègia efectiva per superar les limitacions claus de la viroteràpia. Aquests resultats incentiven el desenvolupament d'aquesta estratègia pel seu ús en la clínica.

Amb l'objectiu de destruir l'estroma, vam generar un panell d'adenovirus oncolítics que expressaven diferents immunotoxines específiques contra FAP i una nitroreducatasa (NfrA) activadora de prodroga. Durant el desenvolupament d'aquests projectes, vam obtenir i caracteritzar tots els virus. No obstant, encara que les diferents immunotoxines van ser adequadament expressades i secretades per les cèl·lules infectades pels virus, no vam obtenir cap resultat prometedor. El virus armat amb la NfrA, en canvi, va mostrar una activació enzimàtica depenent de la replicació del virus en les cèl·lules diana, incrementant la potència oncolítica del virus *in vitro*. Aquests resultats preliminars indiquen que aquesta última estratègia podria fomentar la distribució viral en tumors rics en estroma i incentiven la seva validació en models animals.

INTRODUCTION

1. VIROTHERAPY OF CANCER

Oncolytic viruses (OVs) are emerging as important agents in cancer treatment. OVs are therapeutically useful viruses that selectively infect and damage cancerous tissues without causing harm to normal tissues (S. J. Russell, Peng, and Bell 2012) (**Figure 1**). OVs can replicate and produce more cancer-specific progeny virions, conferring them an uncommon feature in the field of pharmacology: a selective drug that amplifies itself within the targeted cells of the patient. Furthermore, as replicating biotherapeutics, OVs can be delivered systemically or locoregionally and therefore have the potential to act at both primary and metastatic tumor sites.

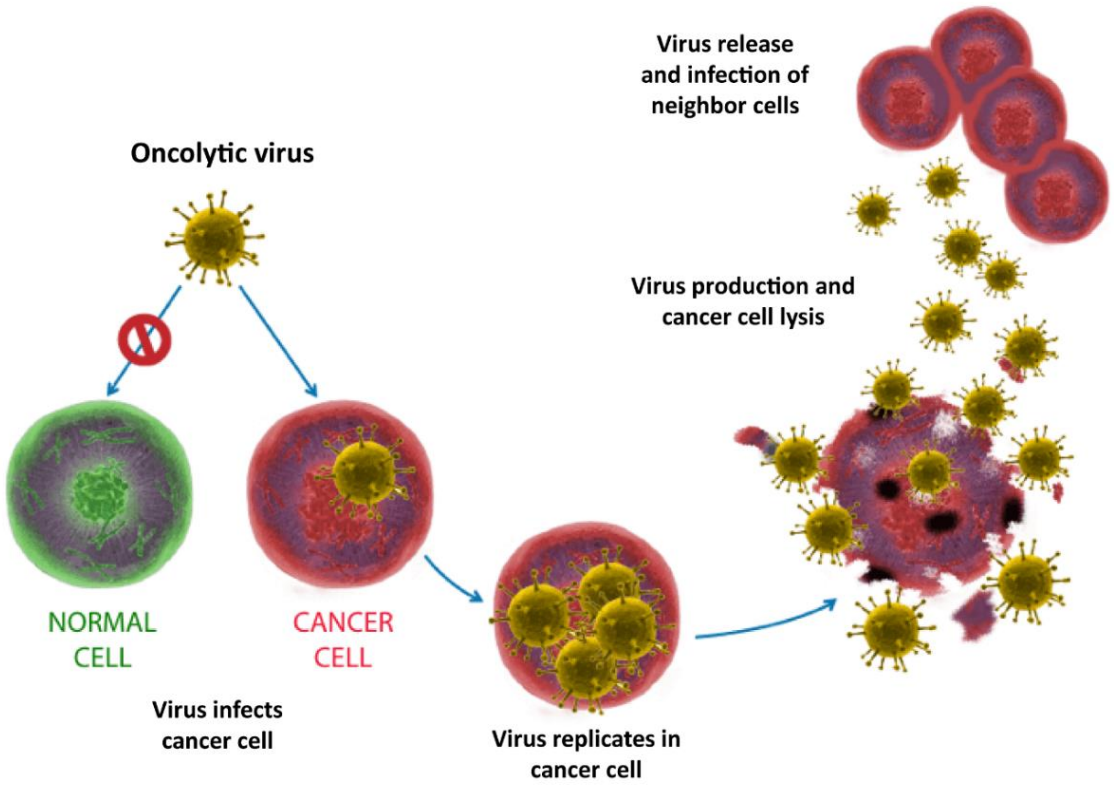

Figure 1. Principle of cancer virotherapy. The oncolytic virus infects preferably cancer cells and selectively replicates in them. If a normal cell is infected the replication cycle is aborted. Virus replication leads to cancer cell lysis and release of the viral progeny. The new generated viruses infect neighbor cells and initiate new replicative cycles, disseminating throughout the tumor mass until, ideally, its eradication.

The viral infection leads to tumor regression through two distinct mechanisms: direct killing of tumor cells by replication-dependent induced cell death and promotion of an

antitumor response towards tumor cells, including non-infected cells, by inducing immunogenic cell death. All types of immunogenic cell death, such as immunogenic apoptosis, necrosis, and autophagic cell death, are characterized by the release of tumor-associated antigens (TAAs) in combination with damage-associated immune responses (DAMPs), viral pathogen-associated molecular patterns (PAMPs) and pro-inflammatory cytokines (Bartlett et al. 2013).

The history of viral therapy of cancer dates back to the turn of the 20th century when Dr. George Dock observed spontaneous regressions of acute lymphoblastic leukemia after a presumed influenza infection (Dock 1904). From that moment on, viruses from nine virus families have reached phase I-III clinical trials, and for some of these viruses derivates with different genetic modifications are being studied (Cattaneo et al. 2008). Globally, there are three approved OVs for marketing as cancer therapeutics: ONYX-015 (also known as Oncorine), an oncolytic adenovirus (OAd) that was approved in China in 2005 for the treatment of head and neck cancer (Polyak 2011); Rigvir, an oncolytic reovirus approved for the treatment of advanced melanoma in Estonia, Latvia, Poland, and Belarus (Doniną et al. 2015); and the Granulocyte-macrophage colony-stimulating factor (GM-CSF)-expressing HSV T-Vec (also termed IMLYGIC or talimogene laherparepvec) was approved in the USA, Europe, and Australia for the treatment of advanced or non-resectable melanoma (Coffin 2016).

2. ONCOLYTIC ADENOVIRUSES

Among the OVs studied to date, adenoviruses (Ads) hold features that make them good virotherapy candidates. These include low pathogenicity, a lytic replication cycle, the ability to infect proliferating and quiescent cells, and an efficient gene transfer mechanism. Furthermore, Ads have been key models in molecular biology by contributing to the progress of understanding processes such as DNA replication, RNA splicing, cell cycle control, and oncogenic transformation, among others (Berk 2005; Howley and Livingston 2009). This wide knowledge about the molecular biology of Ad infection makes it fairly easy to modify its genome.

2.1 ADENOVIRUS CLASSIFICATION

Ads are members of the *Adenoviridae* family. In human, 57 serotypes have been identified and classified into seven subgroups or species (A-G, subgroup B is further divided into B1 and B2), based on the cross-reactivity patterns of neutralizing antibodies (Hall, Blair Zajdel, and Blair 2010). Ads are common human pathogens that cause a range of infections from mild, self-limited respiratory viral infections, conjunctivitis and diarrhea to severe disseminated disease (Ison 2006). Within the same subgroup, the pathogenicity and tissue tropism are similar. The human adenovirus serotype 5 (Ad5) (subgroup C) has been the most widely used in the fields of gene therapy, cancer virotherapy, and vaccination. Ad5 mainly infects epithelial cells from the respiratory tract, causing mild respiratory symptoms similar to a common cold. Ad5 is the serotype used in this thesis.

2.2 VIRION STRUCTURE

Ads are icosahedral non-enveloped, double-stranded DNA virus. Viral DNA and associated core proteins such as pV, pVII, Mu (pX), and terminal protein (TP), are encased in an icosahedral capsid with 20 triangular faces and has a diameter of 60-90 nm. Each of the triangular faces is constituted by 12 copies of hexon trimer (polypeptide II). Complexes formed by the pentameric penton base (polypeptide III) and trimeric fiber (polypeptide IV) form the vertices. Fiber protein, which radiates from the 12 vertices of the virion, is structured in 3 domains: the N-terminal tail, that attaches to the penton base, a central *shaft*, and a C-terminal globular *knob* domain that functions as the cellular attachment site. Moreover, other minoritary proteins such as protein IIIa, VI, VIII, and IX make up the capsid, acting as cement between hexons (**Figure 2)**.

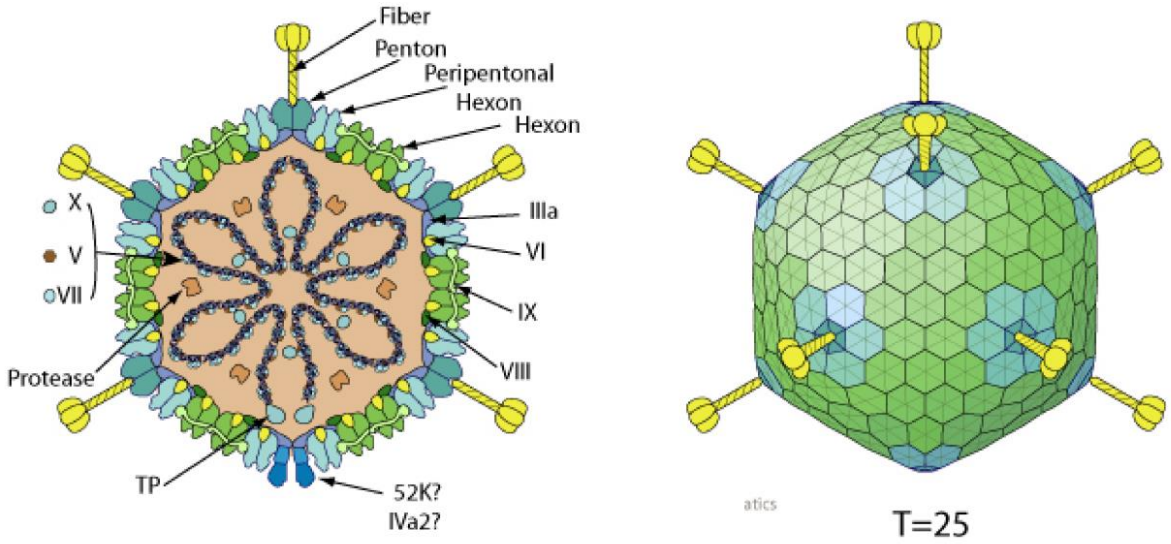

Figure 2 Adenovirus virion structure. Schematic representation of the capsid and core proteins of an adenovirus. Imaged taken from https://viralzone.expasy.org/4?outline=all_by_species.

2.3 GENOME STRUCTURE

The human Ad5 genome is a ~36 kb linear molecule of double-stranded DNA flanked by two inverted terminal repeats (ITR) at both ends of the molecule, which contain the viral DNA replication origins. Genetic information is organized in overlapping transcription units on both strands. Extensive splicing leads to the translation of over 50 proteins, from which 11 are structural virion proteins. Adenovirus genes are classified in three major groups, depending on the time course of their expression during viral replicative cycle: six early (E) transcription units (E1A, E1B, E2, E3, and E4), three delayed-early units (IX, IVa2 and E2 late), and one late (L) transcription unit that is processed to generate five families of late mRNAs (L1 to L5) (Verma and Weitzman 2005) (**Figure 3**), whose expression is under the control of the major late promoter (MLP) and produce the structural proteins of the capsid. In addition, Ad genome also contains the viral-associated (VA) genes that codify for one or two non-coding RNAs, which are involved in translational control during infection.

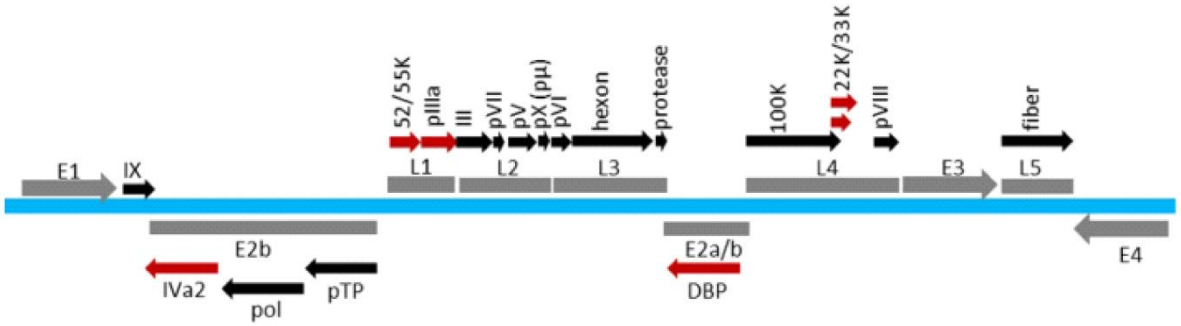

Figure 3. The genome structure and major transcript units of human Ad5. The Ad5 genome is composed of 36 kb linear double-stranded DNA (viral genome shown in blue). The Ad5 genes are temporally transcribed as early units (E1 to E4) or late unit (L1 to L5) in both directions (shown in grey). Proteins expressed from various regions are indicated above or below the region (black). Factors involved in Ad packaging are shown in red. Image adapted from (Ahi and Mittal 2016).

2.4 BIOLOGY OF THE INFECTIOUS CYCLE

Ads are lytic viruses. The virus cycle can be divided in two phases: the early phase which comprises virus entry and internalization into host cell, endosome escape, transport to nucleus, transcription of early genes and genome replication; and the late phase which comprises transcription and translation of late genes, assembly of structural proteins to form the capsids, and genome encapsidation. The virus cycle finalizes with the lysis of the host cell and the release of the virus progeny to the extracellular media.

2.4.1 Adsorption and entry

The first step in the infection-cycle is gaining access to the host cell. It occurs through primary interaction between the fiber knob and the coxsackie adenovirus receptor (CAR), a 46 kDa transmembrane receptor and a member of the immunoglobulin (Ig) superfamily (Bewley 1999). This initially adhesion is temporary and insufficient, but a secondary interaction between an exposed RGD (Arg-Gly-Asp) motif located on the penton base protein and the αVβ3, αVβ5, α5β1, and αvβ1 integrins results in viral cell internalization (**Figure 4, step 1**) (Nemerow 2000). This viral internalization is mediated via clathrin-mediated endocytosis, followed by partial capsid disassembly upon acidification of the endosome. Endosomal escape is modulated by the lytic action of protein VI, after which the nucleocapsid is translocated to the perinuclear envelope along the microtubule network (Wiethoff et al. 2005). Transport to the nuclear pore complex involves the

microtubule-dependent motor, cytoplasmic dynein, which facilitates Ad attachment to microtubules (**Figure 4, steps 2-4**) (Kelkar et al. 2004). After reaching the nucleus, the capsid is completely disassembled, and the viral DNA is translocated through the nuclear pore complex for subsequent transcription and replication (**Figure 4, step 5**).

2.4.2 Early gene expression and DNA replication

Once the viral genome enters the nucleus, the E1A is the first transcription unit expressed, which produce multiple mRNAs and several proteins due to alternative RNA splicing. From these mRNAs, two are predominantly produced in the early infection phase: the 12s, encoding the 243R protein and the 13s, which encodes the 289R protein. The main function of these proteins is the *trans*-activation of the other early transcription units (E1B, E2A, E2B, E3, and E4) and the induction of the cells to enter the S phase. This latter function, which is a prerequisite for Ad replication, is achieved by the sequestration of members of the retinoblastoma (Rb) protein family, which are tumor suppressor proteins that inhibit the cell cycle via binding to E2F transcription factors (Berk 2005; Howley and Livingston 2009). These E2F transcription factors are crucial in cell-cycle regulation as they promote the expression of S phase-related genes. As a result of this E1A-mediated S-phase induction and of its *trans*-activator activities, the other early transcription units are expressed and produce proteins which cover key functions in the replication cycle of Ads. The main function of the E1B gene products (19K and 55K) is the inhibition of apoptosis. The 55K protein inactivates the pro-apoptotic tumor suppressor p53, whose accumulation is triggered by the E1A-mediated cell cycle deregulation, while the 19K protein inactivates down-stream mediators of p53-independent apoptotic pathways. The deregulation of the cell cycle caused by E1A results in the accumulation of the tumor suppressor p53, which induces apoptosis as a cell defense mechanism. The genes in E2 region encode for the proteins required for the replication of the genome including the DNA polymerase (Ad pol), the preterminal protein (pTP) and the single-stranded DNA binding protein (ssDBP). E3 gene products are involved in the evasion of the host antiviral immune response in order to avoid the destruction of the infected cell before completing the cycle. For instance, E3-19K sequesters the major histocompatibility complex (MHC) class I molecules in the endoplasmic reticulum, preventing its transport to the cell surface. Furthermore, it can also interfere in the loading of peptides onto MHC class I molecules by binding to the transporter associated to antigen processing (TAP). Finally, the E4 transcriptional unit is

involved in viral replication, stability and transport of viral mRNA, and it also mediates the expression of the late genes (**Figure 4, steps 6-15**).

2.4.3 Late gene expression and virion assembly

Once the gene products of the early phase have accumulated and the viral genome has begun to replicate, the major late promote (MLP) is regulated by a transcriptional complex made up of a dimer of IVa2 and the non-structural protein, L4 33K (W. C. Russell 2009). The MLP regulates the expression of genes from the major late transcription unit (MLTU), which encodes for 15 to 20 different mRNAs derived from a single pre-mRNA by differential splicing and polyadenylation (**Figure 4, steps 16-19**). Most late proteins are expressed from regions L1-L5 and correspond to structural proteins and proteins involved in virion assembly and genome packaging. Once the late phase genes are expressed and accumulated in the cytoplasm, structural proteins are transported to the nucleus, where DNA encapsidation and virion assembly takes place (**Figure 4, steps 20-21**). At this point, the Ad protease cleaves a subset of the structural proteins into their mature form in order to generate infectious Ad particles. Finally, cell lysis and progeny release occurs, mediated by the adenovirus death protein (ADP) which is expressed from the E3 transcription unit (**Figure 4, step 22**), the only early gene that is expressed during the late phase.

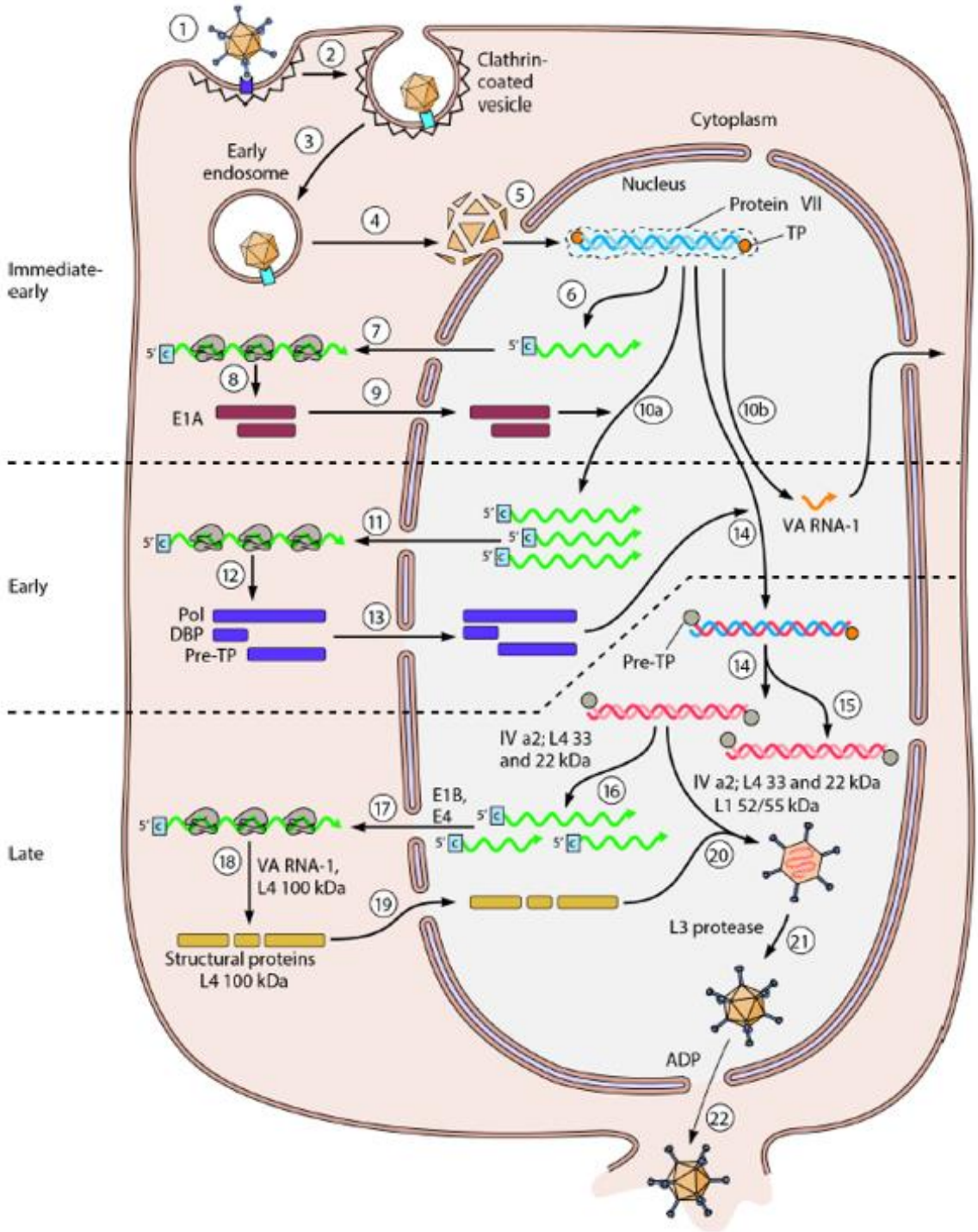

Figure 4. Infectious cycle of human adenoviruses. The infection cycle of adenoviruses can be divided into time-specific events: adenovirus cell entry (steps 1-3), capsid disassembly and genome import into the nucleus (steps 4-5), immediate-early E1A gene expression (steps 6-9), E1A-mediated transcription of viral early genes (step 10a), translation of viral early proteins (steps 11-13), viral DNA replication (steps 14-15), transcription and translation of viral late genes (steps 16-19), capsid assembly and virion maturation (steps 20-21) and progeny virus release (step 22). Image from (Flint et al. 2015).

2.5 DESIGN OF TUMOR-SELECTIVE ONCOLYTIC ADENOVIRUSES

A fundamental requirement in the development of OAds is to restrict their replication to tumor cells by means of genetic engineering. There are two main strategies for improving this selectivity. The first is the transductional targeting of Ads, which aims at restricting Ad entry to tumor cells at the level of virus receptor binding. The second strategy is based on the restriction of Ad replication to tumor cells by manipulating the different Ad transcription units and is termed post-entry targeting.

2.5.1 Transductional and transcriptional targeting

Transductional targeting of Ad aims at enhanced or specific transduction of the target cell. The goal is to abrogate the broad tropism of Ad5 for normal epithelial cells and/or enhance the virus infectivity toward CAR-deficient tumor cells. Transductional targeting strategies involve one or two modifications of the viral capsid: a first (optional) detargeting step to ablate the native tropism of the virus, and a second retargeting step to direct it towards cancer-specific receptors. Three main strategies have been developed to detarget Ads which involve: (i) genetic ablation of the native tropism determinants (CAR, integrins, and heparan sulfate proteoglycans (HSPGs), (ii) chemical modifications of viral coat using polymer-based strategies (polyethylene glycol (PEG), N-[2-hydroxypropyl]methacrylamide (HPMA)), and (iii) 'genetic pseudotyping' between different Ads serotypes (Coughlan et al. 2010; Glasgow, Everts, and Curiel 2006). Regarding retargeting, systems to modify Ad tropism are based in (i) the addition of an adapter molecule to crosslink the virus to a target cellular receptor, or (ii) the genetic modifications of the viral capsid (Glasgow, Everts, and Curiel 2006).

With regard to tumor retargeting, genetic insertion of retargeting ligands in different capsid locations such as the C-terminus of the fiber, the HI loop of the fiber, the penton base, certain hypervariable regions (HVRs) of the hexon and the minor capsid protein pIX has been described (Coughlan et al. 2010). From these, the most successful to date is the incorporation of the RGD-4C peptide (CDCRGDCFC) that targets with high affinity αvβ3 and αvβ5 integrins, which are commonly overexpressed in different types of cancer (Cripe et al. 2001; Dmitriev et al. 1998). This peptide has been the best model of transductional retargeting of Ads, as it has been genetically incorporated into different locations of the fiber of Ad species B, C, and F (Bayo-Puxan et al. 2009; Hesse et al. 2007; Matsui et al.

2011; Murakami et al. 2010; Toyoda et al. 2008). Furthermore, the efficacy of the insertion of the RGD-4C peptide into the HI loop of the fiber from an oncolytic adenovirus is currently being tested in clinical trials for glioma and ovarian cancer (S. J. Russell, Peng, and Bell 2012).

Transcriptional selectivity limits transgene expression to target tissues and can be achieved by two means, genetic complementation (Fueyo et al. 2000; O'Shea et al. 2004) or through the use of tumor- or tissue-specific promoters (TSP) to drive viral replication (Bauerschmitz et al. 2006; Hernandez-Alcoceba et al. 2000; Tsukuda et al. 2002). The first is based on mutations or deletions in key Ad replication genes, which can be compensated only in cancer cells (Nettelbeck 2003). One of the best examples is the AdΔ24 which carries a 24-base pair deletion in the E1A region responsible for the interaction with the pRb (Fueyo et al. 2000). As mentioned before, E1A-mediated sequestration of pRb releases the E2F transcription factor, leading to S-phase induction and viral replication in normal cells. Importantly, the pRb pathway is deregulated in almost 90% of cancers, resulting in constitutively E2F-mediated transcription of cell cycle control genes. Thus, in normal cells in which no pRb deregulation is observed, the Δ24-E1a protein will fail to interact with the pRb protein, resulting in halted viral gene transcription and replication (**Figure 5**). Conversely, the constitutive E2F-mediated transcription of S phase genes in cancer cells allows viral gene transcription and replication. The second approach, which is based on the insertion of tumor-specific promoters or other regulatory sequences in the Ad genome to drive viral gene expression only in cancer cells, has been successfully in OAds using promoters such as the prostate-specific antigen (PSA), the human telomerase reverse transcriptase (hTERT), MUC1, AFP and tyrosinase, among others (Nettelbeck 2003).

More recently, other tropism-modifying strategies have been used. A notable new strategy is the application of microRNA targeting to oncolytic viruses, which takes advantage of differential expression of certain microRNA species in tumor and normal tissues. Insertion of liver-specific microRNA binding sites in the 3' untranslated region (UTR) of the gene encoding E1A of an OAds eliminated its hepatotoxicity without destroying tumor cell-killing activity (Cawood et al. 2009, 2011; Ros, Villanueva, and Fillat 2015).

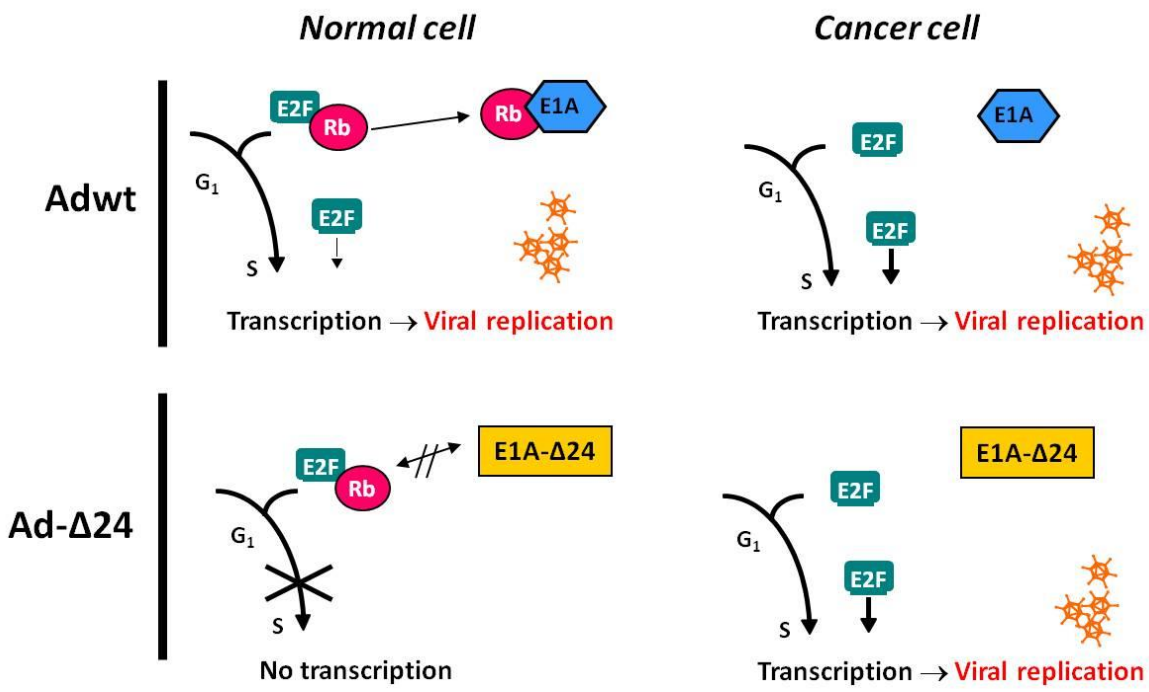

Figure 5. Δ24 selectivity mechanism. E1A protein binds and inactivates Rb to induce S phase of cell cycle and viral replication. In tumor cells this function is redundant, since Rb pathway is truncated and E2F is already free. In normal cells, Δ24 deletion avoids the dissociation of Rb and E2F and no viral replication occurs. Image taken from (Rodríguez García 2015).

2.6 ICO15K

ICOVIR15K (abbreviated ICO15K) is an OAd that combines several of the transcriptional and transductional targeting strategies described above to generate a highly tumor-specific OAd. Regarding transcriptional targeting, the endogenous promoter of E1A has been modified by incorporating eight extra E2F-responsive sites organized in four palindromes and one extra Sp-1-binding site in the *E1a* endogenous promoter (Juan J. Rojas et al. 2010) (**Figure 6A**). This modified promoter confers the virus with high selectivity for actively dividing cells and only increases 151 bp the adenovirus genome, allowing the insertion of foreign transgenes due to its small size compared to the other tumor-specific promoters (**Figure 6B**). In addition, this virus also contains the Δ24 deletion in E1A described above, which abrogates the interaction of this protein with pRb. As for transductional targeting, ICO15K incorporates an RGDK motif replacing the KKTK heparan sulfate glycosaminoglycan-binding domain in the fiber shaft (**Figure 6C)**. This modification, which targets integrins, reduces hepatic tropism and increases tumor transduction, therefore reducing Ad-mediated hepatotoxicity and improving antitumor efficacy *in vivo* (Bayo-Puxan

et al. 2009; J. J. Rojas et al. 2012). This virus has shown potent antitumor efficacy and favorable toxicity profiles in several xenograft models, and we currently use it as a platform to incorporate novel modifications or transgenes to improve its antitumor potency (Fajardo et al. 2017; Sonia Guedan et al. 2010; Alba Rodríguez-García et al. 2015).

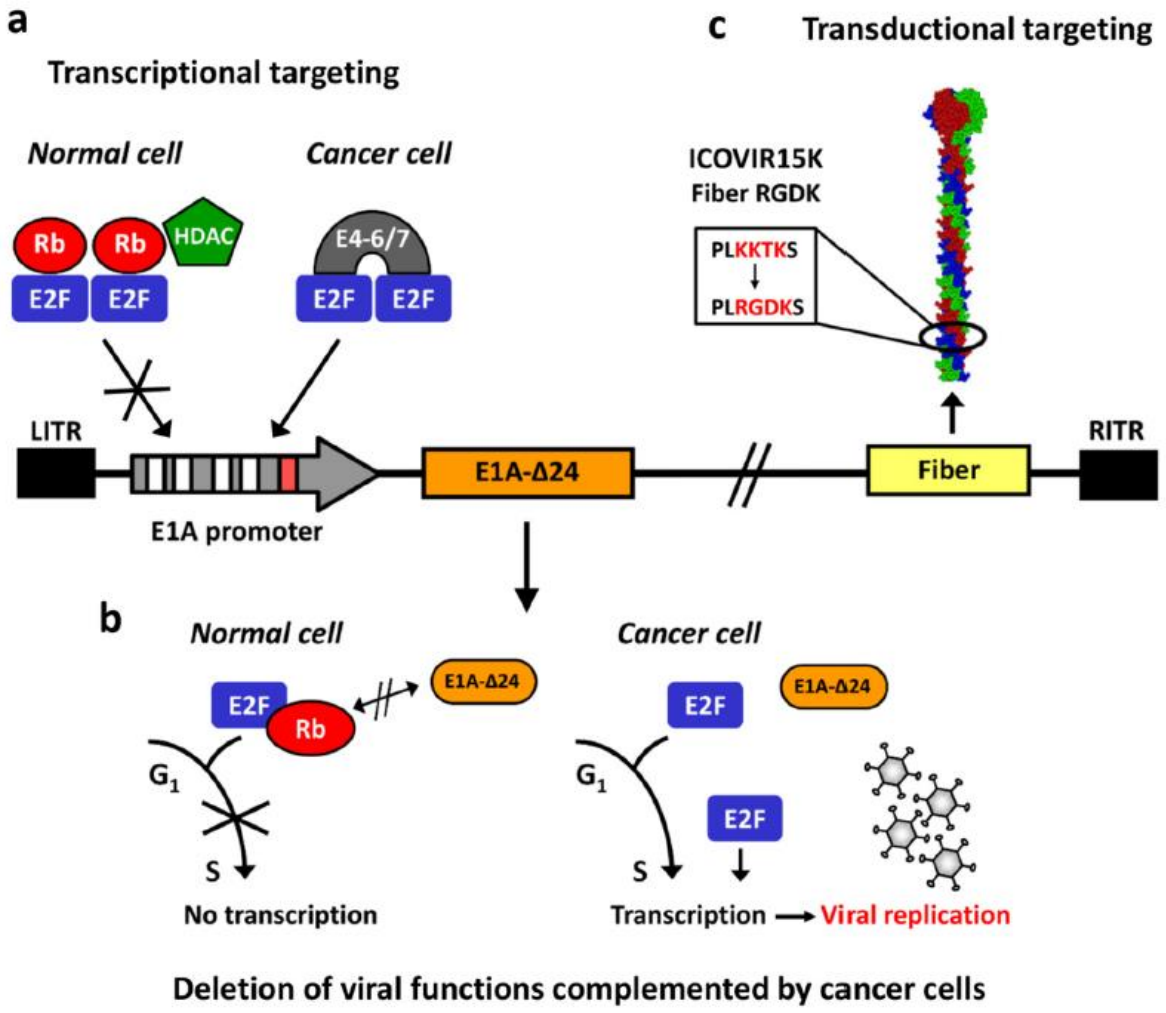

Figure 6. Schematic representation of the ICO15K genome modifications. **A.** ICO15K contain the modified E1A promoter with four E2F boxes (white squares) and one Sp1 box (red square), and (**B**) the truncated E1A-Δ24 protein to confer selectivity for tumor cells. **C.** The RGD motif is inserted in the in the fiber *shaft* replacing the KKTK domain. Image adapted from (Rojas Expósito 2017).

2.7 ARMING ONCOLYTIC ADENOVIRUSES WITH THERAPEUTIC TRANSGENES

The discovery of the genetic basis of malignancy has in part promoted the development of cancer gene therapy. Arming oncolytic viruses with genes that encode prodrug convertases

or therapeutic proteins can enhance their potency. OAds can be engineered to encode therapeutic transgenes with varying modes of action including “suicide genes” or prodrug convertase genes whose encoded protein converts a harmless prodrug to a diffusible anticancer drug (FitzGerald et al. 2011; Ladd et al. 2011), a “radioconcentrator gene” so that infected tumor cells are able to concentrate a β-emitting radioisotope that damages adjacent uninfected tumor cells (Barton et al. 2008), and it can be also engineered to express one or more genes capable of amplifying the immune-mediated killing of uninfected tumor cells. These transgenes can be either inserted as a cassette with its own promoter and polyadenylation (polyA) signal, or as an extra adenoviral transcription unit controlled by the viral gene expression machinery (Nettelbeck 2008). For the former, transgene expression can be controlled by constitutive promoters (*e.g.* CMV) or by tissue-specific promoters to add another level of specificity (Carette et al. 2005). For the second strategy, transgenes can be linked to viral proteins such as *E1a* via sequences that will not affect protein function (*e.g.* internal ribosome entry sites, IRES) or by adding a splice acceptor and a polyA signal that will promote transgene expression from the MLP. Controlling transgene expression from viral promoters is particularly appealing for the generation of armed OAds, since restricting its expression to virus replication adds another level of selectivity. Additionally, MLP-driven transgene expression will be restricted to the late phase of the replication cycle, which is important in cases where the therapeutic protein can reduce the viability of infected cells, thereby impairing the completion of the infection cycle. Transgene cassettes have been successfully inserted in different regions of the adenovirus genomes including E1, E3, or E4. Also, some of these regions (*e.g.* E3) can be fully replaced by the transgene without altering virus replication (Nettelbeck 2008). Transgenes coupled to splice acceptors and polyA signals can be inserted in various regions downstream of the MLP (Jin, Kretschmer, and Hermiston 2005). One drawback of OAds compared to other bigger viruses is the restriction in transgene size that can be incorporated in its genome. The maximum packaging size for the Ad genome is 38kb, which is approximately 2kb over the wild-type (wt) size (Bett, Prevec, and Graham 1983; Ghosh-Choudhury, Haj-Ahmad, and Graham 1987). Since some OAds are modified with tumor-specific promoters, this further restricts the space available for transgene insertion. In the case of ICO15K, which has a genome size of 36.1kb, the maximum tolerated transgene size to be inserted is approximately 1.9kb. As mentioned above, a strategy to

increase the available space in the Ad genome involves the replacement of some viral regions such as E3.

2.8 CLINICAL EXPERIENCE WITH ONCOLYTIC ADENOVIRUSES

To date, several OAds have been tested in the clinic involving different types of tumors and routes of administration. In the early 2000s, multiple phase I and II clinical trials were completed using the first modified OAd, ONYX-015, developed by Onyx Pharmaceuticals (Bischoff et al. 1996; Ganly et al. 2000). This virus has a deletion of the E1B-55K gene, which is responsible for binding and inactivation of the master cell cycle regulator p53 (Blackford and Grand 2009). Further studies revealed that the E1B-55K deletion negatively affected the oncolytic properties of these OAds (O'Shea et al. 2004). Intratumoral application of this virus was initiated in patients with squamous carcinomas of the head and neck (HNSCC) or with pancreatic cancer, obtaining as a result a safety profile and moderate but promising antitumor activity (Ganly et al. 2000). Later, a phase II was initiated to evaluate the combination of ONYX-015 and standard cisplatin-based chemotherapy in recurrent HNSCC patients. Of 30 patients, 19 (63%) experienced an objective tumor response, including eight (27%) complete responses (Khuri et al. 2000). However, long-term survival was not improved. Other bad prognosis tumor types such as pancreatic carcinoma or glioblastoma were treated with intratumoral injections of ONYX-015, without observing toxicity or objective responses. Therefore, further development of ONYX-015 was abandoned in the United States, and the rights were taken over by the Chinese company Shanghai Sunway Biotech. Then, H101, an oncolytic adenovirus that has genetic modifications very similar to those of ONYX-015 (deletion of E1B-55kDa and a part of E3), became the world's first oncolytic virus to be approved for human use in 2005 when China's State Food and Drug Administration approved it as a commercial drug for head and neck squamous cell carcinoma, based on the efficacy observed in a clinical trial conducted in China.

The Delta-D24-RGD (also named DNX-2401) is a derivative of Ad5-D24, a 24-base pair (bp) deletion-based OAd whose fiber region is modified by incorporating an integrin binging RGD-4C motif, allowing CAR-independent infection cancer cells (see section 3.5.1). This virus is currently under clinical investigation (**Table 1**). A phase I clinical trial evaluating the intraperitoneal administration of DNX-2401 in ovarian cancer patients revealed similar toxicity

profiles to those observed in the clinical trials described above (Kimball et al. 2010). Interestingly, signs of virus replication were observed in ascites from these patients, as virus DNA copy numbers raised in 30% of the patients 3 days after inoculation. A more recent trial has evaluated the potential of DNX-2401 for the treatment of recurrent malignant glioma. Complete regressions and partial responses were observed in patients receiving intratumoral virus administrations, and the data suggest that antitumor immune responses complement the oncolytic action of the virus. As mentioned above, DNX-2401 received fast-track status and orphan drug designation by the FDA for the treatment of malignant glioma in 2016 (New drugs/Drug news 2014).

Overall, several OAd have shown antitumor potential and good tolerance in varying scenarios and approaches, reinforcing the potential of this treatment if further research is performed. Notwithstanding, events of striking tumor shrinkage are relatively rare, especially in single-agent approaches. To conclude indisputable success, therefore, there is still a long way to go.

Trial number	Phase	Cancer type	Oad type	Description
NCT03029871	I	NSCLC	Ad5-yCD/mutTKSR39rep-ADP	5-FC and vGCV
NCT03178032	I	DIPG	DNX-2401 (Ad-Δ24-RGD)	-
NCT03003676	I	Melanoma	ONCOS-102 (Ad5/3-D24-GM-CSF)	Pembrolizumab and CP
NCT03072134	I	Glioma	NSC-CRAd-Survivin-pk7	Radiotherapy and chemotherapy
NCT02879669	Ib/II	Mesothelioma	ONCOS-102 (Ad5/3-D24-GM-CSF	Pemetrexed/cisplatin and CP
NCT02705196	I/II	Pancreatic	LOAd703	Gemcitabine and nabpaclitaxel
NCT02555397	I	Prostate	Ad5-yCD/mutTKSR39rep-hIL12	-
NCT03190824	II	Melanoma	OBP-301 (Telomelysin)	-
NCT03281382	I	Pancreatic	Ad5-yCD/mutTKSR39rep-hIL12	5-FC
NCT02045602	I	Advanced solid tumors	VCN-01	Gemcitabine and Abraxane®
NCT02798406	II	GBM and GS	DNX-2401	Pembrolizumab

Table 1. Ongoing clinical trials on OAds in cancer therapy. Table adapted from (Goradel et al. 2018).

2.9 LIMITATIONS OF ONCOLYTIC ADENOVIRUSES

Despite de potential of OVs as anticancer agents, clinical studies point out the need to tackle their limitations to further improve their therapeutic efficacy. Beyond the difficulties of reaching enough tumor cells by the intravenous route of administration, other hurdles for the success of virotherapy imposed by the tumor microenvironment (TME) need to be addressed (**Figure 7**) (Marchini, Scott, and Rommelaere 2016).

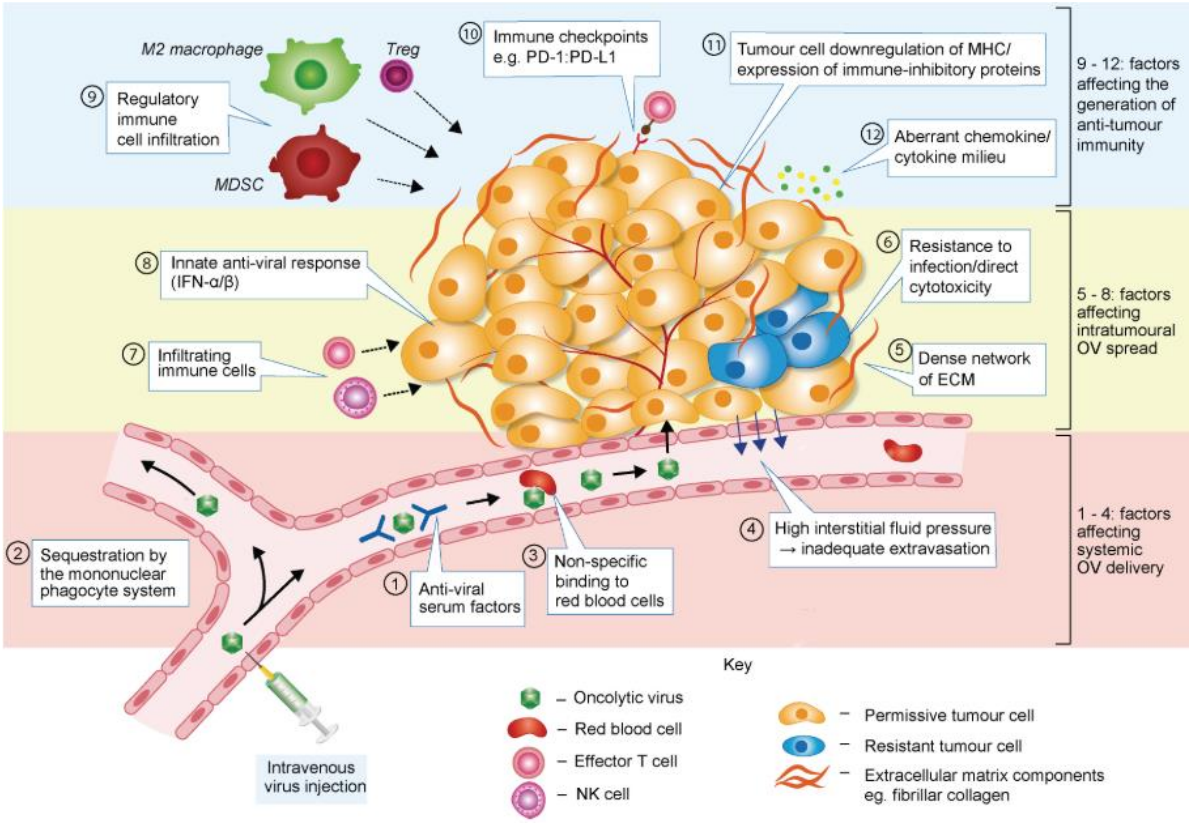

Figure 7. Challenges to effective OVs therapy *in vivo*. When delivered to tumors via bloodstream, most of the initial dose is retained by the liver. Moreover, Ovs can be neutralized by the interaction with blood cells, the complement or neutralizing antibodies (box 1-3). Once the target site is reached an additional hurdle is posed by high interstitial fluid pressure within the tumor (box 4). Following extravasation, or after intratumoural OV injection, several factors may limit intratumoural viral spread and therapeutic effectiveness: tumor stroma (*e.g* extracellular matrix (ECM)) (box 5), anti-viral activity and/or cancer resistance to OAd-mediated cell killing (box 6-12). Image adapted from (Marchini, Scott, and Rommelaere 2016).

2.9.1 Oncolytic adenovirus tumor delivery and targeting

One of the main limitations of oncolytic virotherapy is the accurate and efficient delivery of the virus. In order for an OV to establish a niche within the tumor after systemic administration, the OV has to bypass the liver that may actively sequester a percentage of the administered dose (Alemany, Suzuki, and Curiel 2000) (phagocyted by Kupffer cells). This hepatic tropism reduces the distribution of the infused Ads into the tumor. Importantly, specific binding to serum factors such as pre-immune immunoglobulin M, complement, anti-viral cytokines and macrophages may result in the rapid neutralization and clearance of a virus by the reticuloendothelial system (Duffy et al. 2012). Pre-existing immunity to human Ad5 generally exists, and when is the case, neutralizing antibodies (NAbs) may severely hinder systemic delivery (Bradley et al. 2012; Fausther-Bovendo and Kobinger 2014). Elements other than immune factors may also impede intravenous OV delivery. Non-specific binding of OVs to blood cells has been noted in the case of Ad (Lyons et al. 2006), and the characteristically high interstitial fluid pressure within a tumor disfavors extravasation of virions from the tumor vasculature.

To date, several strategies have been developed to overcome those obstacles. As for NAbs of the virus, chemical shielding of the Ad capsid with synthetic polymers or the replacement of HVR from one Ad serotype to another have shown useful to evade NAbs (see section 3.5.1). In addition, our group has recently shown the advantages of inserting an albumin-binding domain in the hexon to shield the virus from NAbs, which improves its blood persistence after systemic administration (L. A. Rojas et al. 2016). The use of patient-derived autologous cells, such as mesenchymal stem cells (MSCs) or monocytes, as cell carriers to deliver the virus to tumors has also been explored (Bunuales et al. 2012; Nakashima, Kaur, and Chiocca 2010). Other strategies involving genetic modification of capsid proteins to improve tumor targeting and reduce liver transduction have already been discussed in section 3.5.1.

2.9.2 Stromal barriers

After reaching the tumors, one of the major obstacles to successful oncolytic therapy is the presence of stroma in tumors, formed by different types of cells (*e.g.* immune cells, MSCs, Cancer-associated fibroblasts (CAFs), extracellular matrix (ECM) compounds, built by structural and adhesive proteins (*e.g.* fibronectin, laminin, collagen and elastin),

proteoglycans and glycoproteins (Hynes and Naba 2012; Kalluri 2016). Stroma not only creates physical barriers that limit OAd spread across the tumor, but also induces tumor progression by enhancing the survival, proliferation, stemness, metastasis, and an immunosuppressive microenvironment that limits tumor immunity, ultimately promoting cancer progression, but also enhancing resistance to therapy (Kalluri 2016). Moreover, in contrast to cancer cells, CAFs are partly resistant to OAd infection and thus represent a physical barrier for virus spread *in vivo* (M. Verónica Lopez et al. 2009).

Targeting ECM components or CAFs are the main strategies to improve OAd spread within the tumor. Alteration of the microenvironment by administering exogenous enzymes directly to the tumor or by arming viruses to encode recombinant enzymes can facilitate viral spread. For example, arming OVs with ECM-degrading enzymes is commonly exploited to enhance viral penetration in solid tumors (Smith, Breznik, and Lichty 2011). In our group, delivery of a hyaluronidase-expressing OAd (VCN-01) showed improved dissemination and therapeutic activity in a human melanoma xenograft model by enzymatically targeting hyaluronan, a sulfated glycosaminoglycan component of the tumor extracellular matrix (Sonia Guedan et al. 2010; Alba Rodríguez-García et al. 2015) and this virus is currently under clinical investigation for the treatment of advanced pancreatic cancer (NCT02045602). Other proteins that modulate the configuration of ECM have been used to increase viral spread and antitumor efficacy in several tumor models. For instance, small molecules such as relaxin and decorin have been expressed from OAds, aiming to inhibit collagen production and upregulate the expression of matrix metalloproteases (MMP) that participate in the degradation of this connective tissue protein (Ganesh et al. 2007; Kim et al. 2006; Yoon, Hong, and Yun 2017). Regarding the strategies to target CAFs, a bioselection of adenoviruses in CAFs developed in our group indicated that a truncation of the i-leader protein could enhance the virus release and propagation in these cells (Puig-Saus et al. 2012), enhancing the activity of OVs. Another strategy that specifically targets these stromal cells has been the use of the SPARC promoter to control the virus replication (M. Verónica Lopez et al. 2009). These viruses induce oncolysis in fibroblasts and have shown potent *in vitro* cytotoxicity in stroma-rich ovarian xenograft models (M. Veronica Lopez et al. 2012).

2.9.2.1 Cancer-associated fibroblasts (CAFs)

2.9.3 Immune responses

Besides delivery and stromal barriers, the immune system has been long identified as a major challenge for the success of OAds in cancer patients. The mammalian adaptive immune system has evolved to restrict the replication and spread of invading pathogens. For oncolytic virus-based therapeutics, this is a double-edged sword. On the one hand, these defense mechanisms pose an impediment to the delivery and spread of oncolytic viruses, reducing viral replication, early clearance and decreasing antitumor efficacy. On the other hand, tumors have an immuno-suppressive environment in which the immune system is silenced in order to avoid the immune response against cancer cells. The delivery of OVs into the tumor wakes up the immune system so that it can facilitate a strong and durable response against the tumor itself. Both innate and adaptive immune responses contribute to this process, producing an immune response against tumor antigens and facilitating immunological memory. These opposing views opened the debate whether the immune system is a friend or foe for OAds. Therefore, finding a balance between antitumor and antiviral immunity is, under this new light, a priority for researchers. Optimization of viral replication and propagation as well as the generation of anticancer immunity remains a significant challenge facing OV. With a better understanding of the complex immunological interactions between OVs, tumor cells, and the host immune system, the next generation of OVs will be poised to realize the full immunotherapeutic potential of OV.

Based on both the physical barriers and pro-tumorigenic functions of tumor stroma and the strong antiviral immune responses that limit OV therapy, this thesis mainly focuses on overcoming these limitations. Thus, in the coming sections, the different immunological hurdles for OAds and strategies developed to overcome these will be discussed in detail.

3. ANTITUMOR IMMUNE RESPONSES

Cancer is characterized by the accumulation of a variable number of genetic alterations and the loss of normal cellular regulatory processes (Tian et al. 2011). These events have long been known to result in the expression of neoantigens, differentiation antigens, or cancer testis antigens, which can lead to presentation of peptides bound to MHC I

molecules on the surface of cancer cells, distinguishing them from their normal counterparts. Since the work of Boon *et al.*, we have known that these cancer-specific peptide-MHC I complexes can be recognized by $CD8^+$ T cells produced spontaneously in cancer patients. For an antitumor immune response to lead to effective killing of cancer cells, a series of stepwise events must be initiated (Boon et al. 1994).

The initiation of antitumor immunity begins with the capture of antigens derived from tumors by DCs, which process them for presentation or cross-presentation on MHC class I and II molecules. Tumor-antigen-loaded DCs migrate to draining lymph nodes where, under stimulating signaling conditions, will elicit antitumor effector T-cell responses. T cells interact with the complex formed by the presented peptide and the MHC molecules in DCs by specific T cell receptors (TCR), initiating a signaling cascade that leads to its activation. In addition, costimulatory signals are needed, and its nature determines the kind of response that will be triggered. In the absence of immunogenic stimulus, DCs will instead induce tolerance, anergy, or the production of regulatory T cells (T_{regs}). DCs also trigger B cell and NK cell responses, which may contribute to antitumor immunity. Finally, cancer-specific T cells might enter the tumors, where they will recognize specifically tumor cells that present the tumor antigen associated to MHC class I molecules on its surface (Mellman, Coukos, and Dranoff 2011) (**Figure 8**). Production of cytokines and activation of $CD4^+$ T cells are also required to generate a potent and sustained response.

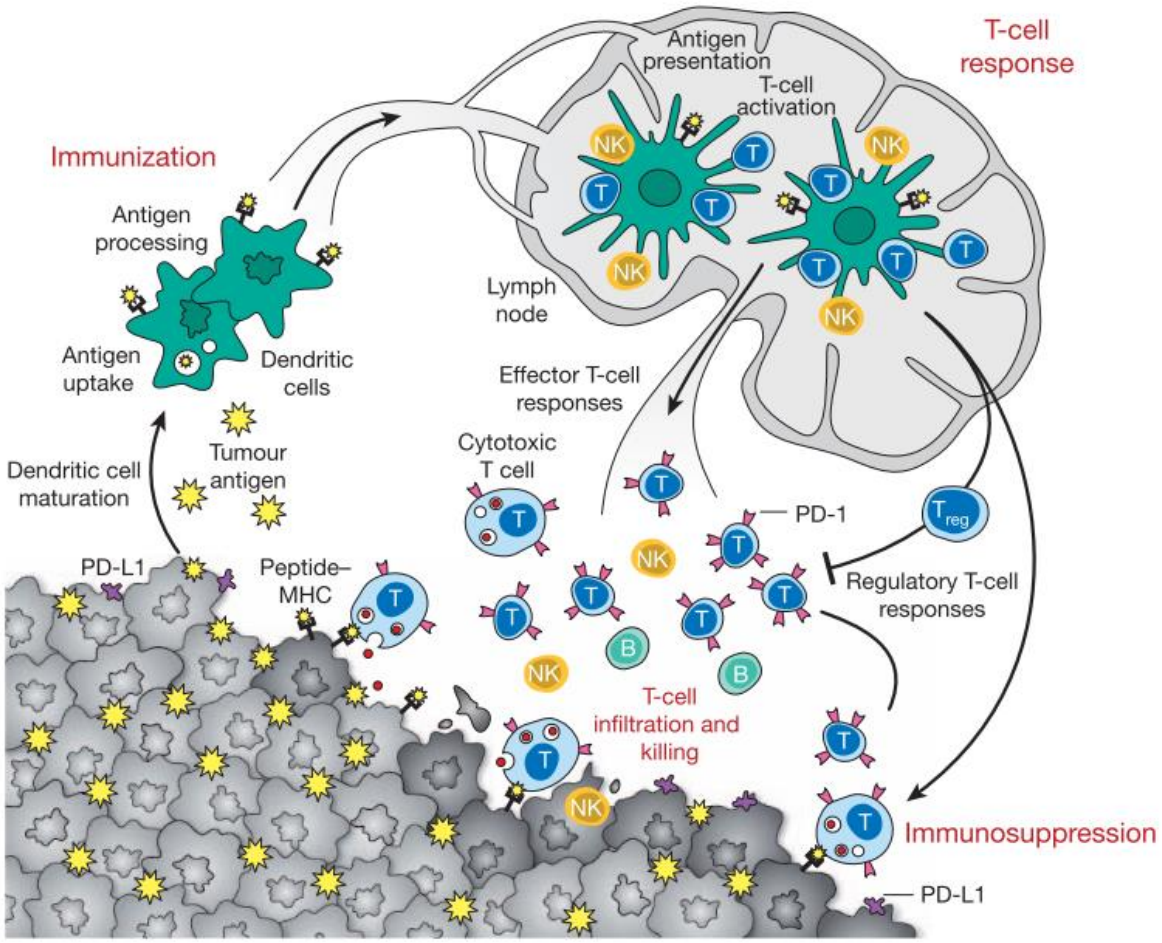

Figure 8. Generation and regulation of antitumor immunity. Antitumor immune responses start with the capture and processing of tumor-associated antigens by DCs for presentation on MHC class II or cross-presentation on class I molecules. Then, DCs migrate to draining lymph nodes where, in the presence of an immunogenic stimulus, will elicit anticancer effector T-cell responses in the lymph node. On the contrary, without such stimulus, DCs will induce tolerance. In the lymph node, antigen presentation to T cells will elicit a response depending on the type of DC maturation stimulus received and on the interaction of T-cell co-stimulatory molecules with their surface receptors on DCs. Antigen-educated T cells will exit the lymph node and enter the tumor bed, where immunosuppressive defense mechanisms produced by tumors oppose effector T-cell function. Image obtained from (Mellman, Coukos, and Dranoff 2011).

3.1 TUMOR-INDUCED IMMUNE EVASION

The escape phase represents the failure of the immune system either to eliminate or to control transformed cells, allowing surviving tumor cell variants to grow in an immunologically unrestricted manner. Cancer cells develop several strategies to circumvent both innate and adaptive immunological defenses. For instance, cancer cells secrete factors such as adenosine, prostaglandin E2, transforming growth factor- β (TGF-β)

and vascular endothelial growth factor-A (VEGF-A) that exert multiple direct and indirect immunosuppressive activities (Gabrilovich et al. 1999; Wrzesinski, Wan, and Flavell 2007). These mediators may function in the suppression of DCs, indirectly inhibiting T-cell penetration into the tumor bed or directly suppressing effector T-cell activation while enhancing the function of T_{reg} cells. Tumor cells can also directly escape T-cell recognition by downregulating MHC class I or by disabling other components of the antigen processing machinery. Shedding of soluble NKG2D ligands such as MIC-A or MIC-B can severely compromise the ability of NK cells to function in the TME. In addition, tumor cells may upregulate surface ligands, which mediate T-cell anergy (or exhaustion), including PD-L1 and other ligands to inhibitory T-cell receptors. In addition to T_{reg} cells, other suppressive lymphocyte subsets have been reported including IL-10 producing B cells and B regulatory cells, type II NKT cells, NK cells and γδ T cells. Myeloid lineage cells also promote immune suppression in tumors, such as the myeloid-derived suppressor cells (MDSC) (Gabrilovich and Nagaraj 2009). Finally, tumor stroma cells have also an important immunomodulatory role. CAFs can promote the recruitment and function of immunosuppressive cells through different mechanisms (Takahashi et al. 2017; Ziani, Chouaib, and Thiery 2018).

3.2 ONCOLYTIC ADENOVIRUS-MEDIATED ANTITUMOR IMMUNE RESPONSES

To date, oncolysis mediated by OAds has been shown to induce antitumor immune responses directed to neoepitopes in preclinical and clinical studies (Kanerva et al. 2013; Woller et al. 2015). In fact, Ad is considered one of the most immunogenic of viruses, inducing robust adaptive immune responses (Afkhami, Yao, and Xing 2016). In our group, we have also demonstrated virus-induced antitumoral immune response with an iRGD-modified hyaluronidase-armed OAd, observing partial antitumoral effects (Al-Zaher et al. 2018). As briefly described in section 2, all types of immunogenic cell death, such as immunogenic apoptosis, necrosis and autophagic cell death, are characterized by the release of TAAs in combination with DAMPs and PAMPs (Bartlett et al. 2013; Inoue and Tani 2014). Following the secretion of DAMPs and cytokines, more innate immune cells, such as macrophages, DCs, NK cells and neutrophils infiltrate the tumor environment. The immune stimulating cytokine secretion leads to maturation of APCs and hence presentation of TAAs and viral antigens to activate the adaptive immune system in the lymph nodes. Cytotoxic T cells will start infiltrating the tumor again and specifically

eliminate cancer cells. Overall, it is now evident that OV therapy can revert the immune-suppressive tumor environment from "cold" to "hot" (**Figure 9**) (Marelli et al. 2018).

Despite these encouraging evidences, further studies have also suggested that oncolysis alone will likely not be sufficient to induce long lasting antitumor immune responses. OAds alone have been reported to fail at promoting tumor-specific antitumor immune responses in immunocompetent mice, and only their combination with tumor peptide-loaded DCs could trigger such responses (Woller et al. 2011). Furthermore, *in vitro* studies have demonstrated that oncolysates from OAd-infected melanoma cells fail to induce DC maturation unless cytokines and co-stimulatory signals are added to the cultures (Schierer et al. 2012). These data, in combination with the strong evidence of the importance of antitumor immune responses for virotherapy, has promoted the development of OAds with improved immunomodulatory properties.

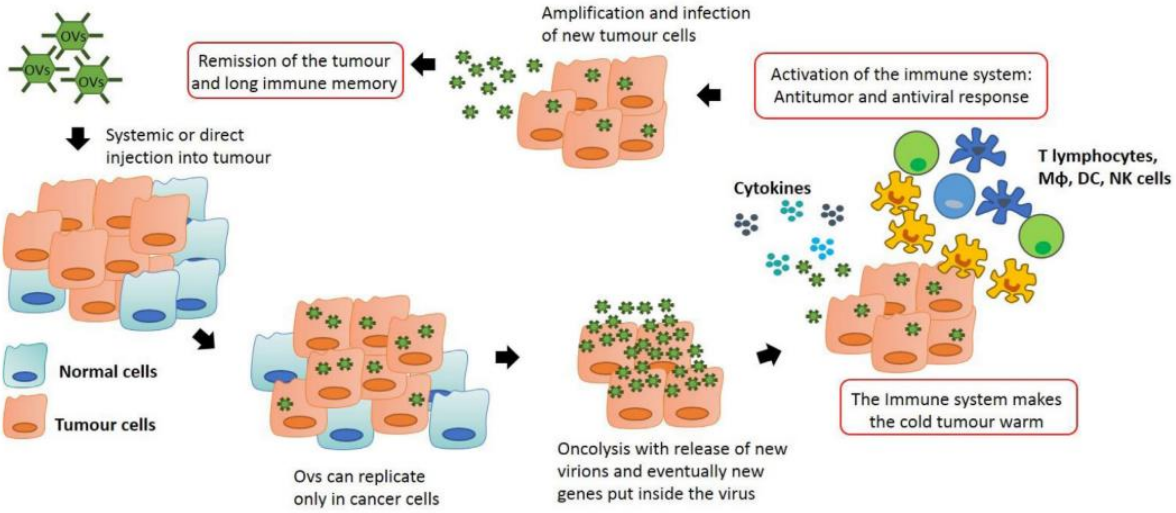

Figure 9. Antitumor immunity by OV therapy. The injection of OV stimulates the immune system which is recruited into the tumor, skewing the neoplastic mass from an immuno-suppressive environment to an inflammatory site. Macrophages and T lymphocytes are key players in this process, producing cytokines that can recruit other immune cells and actively destroy cancer cells. This action generates an immunological memory that mat avoid cancer recurrence and synergizes with the oncolytic action of the viruses, potentially leading to tumor remission. Image adapted from (Marelli et al. 2018).

3.3 STRATEGIES TO IMPROVE ANTITUMOR IMMUNE RESPONSES WITH ONCOLYTIC ADENOVIRUSES

Based on the OAd-mediated beneficial effects on the immune system described above, several approaches have been further developed to enhance antitumor immune responses and efficacy. The main strategies will be discussed in detail in the next sections.

3.3.1 Stimulatory molecules encoded in oncolytic adenoviruses

To improve immune responses against the tumor, immunostimulatory factors such as granulocyte-macrophage colony-stimulating factor (GM-CSF), TNF-α, Interleukin (IL)-2, IL-12, IL-15, IL-18, and IL-24 can be embedded into the genome of OAds (Cerullo et al. 2010). One of the most effective immunostimulatory factors is the GM-CSF. Its antitumor properties could be related to stimulation of DCs and direct recruitment of NK cells (Dranoff 2003). GM-CSF-armed OAds have shown promise as potent inducers of antitumor immunity in preclinical and clinical studies (Bristol et al. 2003; Cerullo et al. 2010; Du et al. 2014; Nishio et al. 2014; Ramesh et al. 2006; Ranki et al. 2016). As an example, a Phase I clinical trial with the GM-CSF-armed OAd CG0070 showed complete response rate of 48.6% in bladder cancer patients (Ramesh et al. 2006). IL-12 is another antitumor cytokine which is produced by stimulated macrophages, DCs, monocytes, and activated B cells. It has been shown that antitumor activity of IL-12 is related to enhancing the proliferation of both CTL and NK cells, increasing susceptibility of tumor cells to T cell-mediated cytotoxicity (Trinchieri, Pflanz, and Kastelein 2003). Lee *et al.* engineered E1B-55K-deleted OAds to express IL-12 and B7-1, a costimulatory molecule on APCs (YKL-IL12/B7) (Y. S. Lee et al. 2006). They demonstrated that intratumoral injections in melanoma tumor-bearing mice resulted in tumor regression, the longevity of survival, increasing of IL-12, and IFN-γ production, and augmentation of $CD4^+$ and $CD8^+$ T-cells infiltration into tumor tissues. Li *et al.* ((Li et al. 2016) used CCL21- and IL21-armed OAds in which E1A expression was under the control of the human telomerase reverse transcriptase (hTERT) promoter. This OAd was able to induce migration, suppress tumor cell growth, and increase CTL cytotoxicity *in vitro*. In another study by this group, Ad-CD40L-CCL20 showed similar results (G. Y. Liu et al. 2015). In addition to oncolysis effects, antitumoral functions of Ad-CD40L-CCL20 could be related to the induction of DC maturation and T-cell activation by CD40L and CCL20. Another example is the Ad5/3-hTERT-E1A-hCD40L, a chimeric OAd with the CD40 ligand in

the E3 region and with E1A controlled by the tumor-restricted hTERT promoter. This virus showed enhanced efficacy and immunomodulatory properties *in vitro* and *in vivo* compared to the parental virus (Diaconu et al. 2012). IL-2, an attractive molecule in gene therapy of cancers, has shown antitumor efficacy through stimulation of T-cell proliferation and differentiation (Havunen et al. 2017). TNF-α, like IL-2, is not only able to activate immune cells (Hirvinen et al. 2015) but also produces other chemokines and cytokines, induces antitumor inflammation (Balkwill 2009), and causes apoptosis and necrosis of cancer cells (Mocellin et al. 2005). Havunen *et al.* engineered an OAd for expressing human IL-2 and TNF-α (Ad5/3-E2Fd24-hTNFa-IRES-hIL12 or TILT-123). The combination of TILT-123 with tumor infiltrated lymphocytes (TILs) was able to completely cure the animals and at three months follow-up cured animals remained tumor free.

3.3.2 Combination of oncolytic viruses with other immunotherapies

3.3.2.1 Immune checkpoint inhibitors

One of the new approaches that have been emerged in treating various types of cancers is the use of inhibitors against immune checkpoint proteins such as programmed cell death protein 1 (PD-1) and cytotoxic T lymphocyte-associated 4 (CTLA-4). Interactions of PD-1 or CTLA-4 on the surface of cytotoxic T cells with their ligand programmed death ligand-1 (PD-L1) and cluster differential 80 (CD80)/cluster differential 86 (CD86) on APCs, respectively, help evasion of cancer cells from T lymphocytes (Dine et al. 2017). After the discovery of CTLA-4 and PD-1, other inhibitory receptors expressed on T cells such as lymphocyte activation gene 3 (LAG-3), T cell immunoglobulin mucin 3 (TIM-3) and CD200 have been also described (Pardoll 2012).

Therefore, combining OAds with antibodies against these checkpoint inhibitors is an attractive approach to cancer therapy. One strategy that has been evaluated in preclinical studies is the generation of OAds expressing full-length anti-CTLA-4 antibodies. An example of this is the chimeric virus Ad5/3-D24aCTLA4, an OAd expressing anti-CTLA4 mAbs. Supernatants from Ad5/3-D24aCTLA4-infected cells increased the activation of PBMCs from cancer patients when compared to the parental virus (Dias et al. 2012). Another strategy that is currently under investigation is the direct combination of OAds with FDA-approved checkpoint inhibitors. For instance, the Ad5-Δ24-RGDOX, which expresses OX40L with anti-PD-L1 antibody in glioma-bearing mice, increased long-term survival rate up to

58% (Jiang et al. 2017). Combination of Pembrolizumab (anti-PD-1 antibody) and DNX-2401 (Ad5-Δ24-RGD) is under evaluation in a multi-center Phase II clinical trial (NCT02798406). Other combinations of different OAds with anti-PD1 and anti-PD-L1 blocking antibodies for the treatment of different malignancies have been recently registered (NCT02636036, NCT03003676).

3.3.2.2 Adoptive T-cell therapy

Clinical use of adoptive cell therapies to treat cancer has gained great interest in recent years. Immunotherapy using *ex vivo*-expanded tumor infiltrated lymphocytes (TILs) was pioneered by Steven Rosenberg in the 1980s, and adoptive T-cell therapy (ACT) is currently gaining ground in the form of receptor-engineered immune cell therapy (chimeric antigen receptor (CAR)T-cell therapy). Nevertheless, these advances alone may not be sufficient to reverse the effects of the immune-suppressive nature of the TME.

Therefore, the intrinsic immunomodulatory properties of OAds have encouraged their combination with TILs or CARs as a strategy to improve tumor efficacy. Regarding TIL therapy, Tähtinen *et al.* used the B16.OVA tumor model to demonstrate that intratumoral administrations of a chimeric Δ24-based OAd improved the efficacy of adoptively transferred OVA-specific $CD8^+$ T cells (Tahtinen et al. 2015). More recently, the combination of OAd with TILs from pancreatic and melanoma tumors from Syrian hamsters has shown improved antitumor efficacy compared to the virus or TIL transfer alone (Siurala et al. 2016). This study is particularly interesting, since OAds show permissive replication in the Syrian hamster cancer model and thus represent a scenario that more closely resembles the oncolytic process in humans. These studies suggest that OAds might be promising tools for improving ACT of TILs.

CART-cell therapy involves genetic modification of patient's autologous T cells to express a CAR specific for a TAA, following by *ex vivo* cell expansion and re-infusion back to the patient. Despite the exciting results obtained in clinical trials of hematological malignancies, CART cells have shown limited success in solid tumors. Therefore, OAds have been proposed as attractive tools to enhance its antitumor activity in solid tumors. An Δ24-based OAd encoding RANTES and IL-15 has been used as a strategy to increase the persistence and infiltration of CART cells in the tumors (Nishio et al. 2014). In line with this, the combination of an OAd encoding TNF-α and IL-2 with CART cells targeting mesothelin

showed enhanced T-cell proliferation, persistence, function and infiltration in solid tumors, leading to improved antitumor efficacy. Finally, we have recently demonstrated that combining a EGFR-BiTE-armed OAd with CART cells improve CART-cell activation and proliferation *in vitro* and *in vivo*, thereby enhancing T-cell-mediated cytotoxicity (Wing et al. 2018). These studies highlight the potential of using OAds to improve CART-cell therapy.

4. ANTIVIRAL IMMUNE RESPONSES

As described above, there is now ample evidence that the potent antiviral immune responses contribute to oncolytic virus antitumor efficacy. However, the virus-specific $CD8^+$ T cell immune responses may become immunodominant over immune responses against exogenous antigens (Harrington et al. 2002; Restifo 2001; Sharpe et al. 2001). Importantly, even when tumor antigen is expressed by an OAd or displayed in its capsid, the virus proteins are likely to be immunodominant, masking the immune responses to delivered transgenes, capsid-displayed TAA and other tumor-restricted epitopes (Frahm et al. 2012; Schirmbeck et al. 2008). Additionally, tumor-bearing immunocompetent mice treated with armed OAds showed increased antiviral immune responses with concomitant loss of transgene expression in the tumors (Gibson et al. 2015). Thus, OAd-infected cells are often cleared from the tumor microenvironment by infiltrating virus-specific CTLs before clinical responses are observed. These facts support the need of balancing antiviral and antitumor immune responses for the success of virotherapy with OAds.

Different strategies have already been proposed in order to modulate the antiviral immune response. Coating the adenoviral capsid with MHC-I-restricted tumor-specific peptides has shown to overcome the immunodominance of an OAd by favoring antitumor immune responses *in vivo* (Capasso et al. 2016). We have also demonstrated that OAds encoding tumor-associated epitopes fused to the viral protein E3-19K promote MHC-I epitope presentation independently from TAP protein, leading to antitumor immune responses which compensate adenoviral epitope immunodominance (A. Rodríguez-García et al. 2015). Another interesting approach to favor antitumor rather than antiviral immune responses is the so-called oncolysis-assisted DC vaccination in which DCs loaded with tumor-specific epitopes are administered during the treatment with oncolytic viruses. Woller *et al.* have shown that the intratumor or intravenous delivery of OAds into immunocompetent mice fails to promote tumor-specific antitumor immune responses as a

result of increased antiviral immune responses (Woller et al. 2011). However, when combined with DCs loaded with tumor-specific epitopes, OAds promote a shift from virus- to tumor-specific antitumor immune responses. Finally, a virus-selective transient tolerization using IL-10 induced DCs prior to the virotherapy treatment to foster responses against tumor antigens or epitopes is currently being addressed in our group (unpublished data).

In summary, antiviral immune responses can intrinsically limit OV infection, spread, and overall therapeutic efficacy. However, there is increasing evidence that virus-mediated destruction or damage of tumors can lead to an antitumor immune response (Sobol et al. 2011). Thus, novel strategies to minimize the antiviral immune response for successful virus growth and retreatment, but to stimulate antitumor responses, would provide an opportunity to tilt this balance in favor of the therapeutic benefit. In this thesis, we propose the use of anti-FAP bispecific T-cell engager (BiTE) antibody as a strategy to redirect antiviral T cells to attack tumor stroma and to improve therefore the virus spread within the tumor.

4.1 BISPECIFIC T-CELL ENGAGERS (BITES)

4.1.1 Structure

BiTE antibody constructs comprise tandemly-arranged single-chain variable fragments (scFvs). One scFv binds the TCR CD3ε subunit and the other binds a tumor-associated surface antigen (TAA). Both scFv are connected with a serine-glycine linker, which is generally constructed of three or more SGGGG repeats, making the peptide sufficiently long and flexible to allow both scFv to associate in a functional conformation (**Figure 10**). The length of this linker determines therefore the flexibility of movement between the two scFvs and can be adjusted by including more or fewer repeats to optimize binding to both target cells. The dual specificity of the BiTE is achieved in approximately 55 kDa in size and 11 nm in length, a structure that is much smaller than a traditional antibody molecule. To date, BiTEs have been developed to target several TAA antigens for a variety of both hematological and solid tumors.

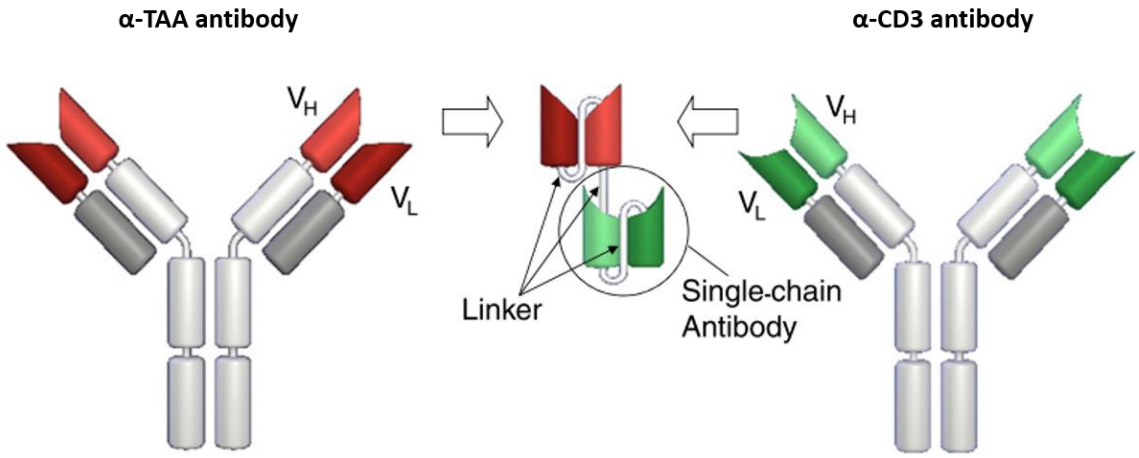

Figure 10. Generation and structure of a BiTE. Variable domains (V_H and V_L) of a monoclonal antibody are joined together by non-immunogenic linkers, generating single-chain antibodies (scFv, circle). One of the scFv recognizes a TAA (red) and the other recognizes the epsilon chain of the CD3 corepector in the TCR complex (green). Both scFvs are further linked by a short flexible peptide. Image adapted from (Nagorsen et al. 2012).

4.1.2 Mode of action

The simultaneous binding of the BiTE to the CD3 on T cells and to the TAA on target cells leads to the formation of the immunological synapse due to the close proximity of both membranes, leading to polyclonal T-cell activation, expansion and lysis of the protein-expressing target cells. Activation of the T cells, as evidenced by the expression of activation markers (*e.g* CD25 and CD69) and by the secretion of pro-inflammatory cytokines (*e.g.* IFN-ɣ and TNF-α), is achieved only in the presence of target cells independent of TCR specificity, co-stimulation, or peptide antigen presentation (Offner et al. 2006). Once activated, T cells release perforin and granzyme B directly into the target cell, provoking a pro-apoptotic cascade in target cells. Finally, T cells disengage from dying cells, proliferate and produce new cytotoxic granules before being engaged by BiTEs to neighboring tumor cells (**Figure 11)**. BiTEs can exert potent cytotoxic activities, with half maximal cell lysis (EC_{50}) typically falling in the femto- and picomolar range (i.e. $10^{-1} \times 10^4$ pg/mL) (Wolf et al. 2005). In addition, a recent study demonstrated that BiTEs can also mediate a bystander tumor cell killing of nearby cells lacking the targeted antigen. T cells activated by BiTEs in the presence of target-positive cells release cytokines that diffuse locally and bind to proximal target-negative cells (Ross et al. 2017). These cytokines do not lead to direct cytotoxicity effects but upregulate cell surface molecules, such as ICAM-1 and FAS, on bystander cells, leading to T cell-mediated killing of target-negative cells even

in the absence of a regular cytolytic synapse. The authors also show that diffusion of T cell-derived cytokines is restricted to nearby bystander cells in solid tumors, limiting therefore extratumoral toxicities.

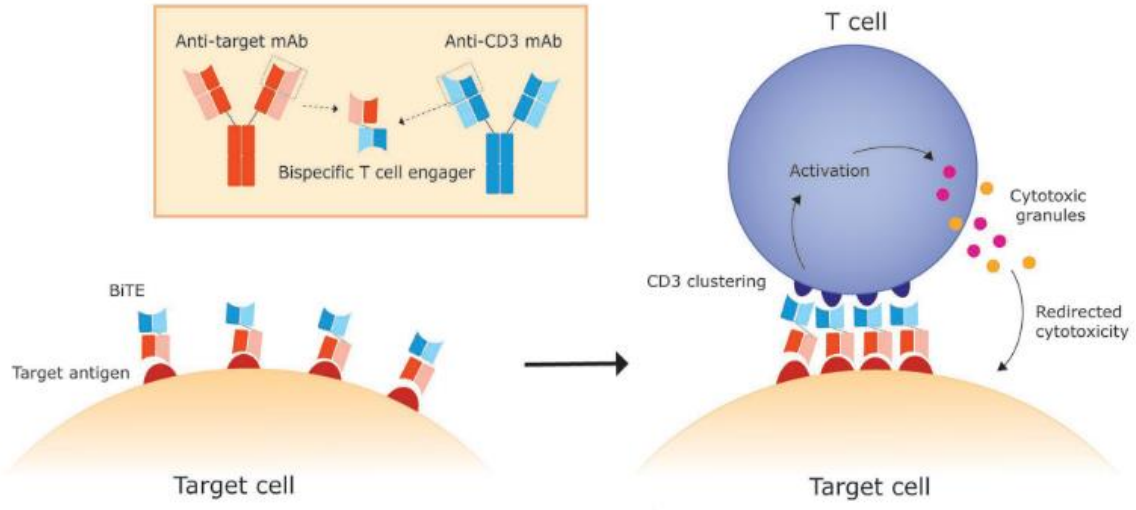

Figure 11. Mode of action of BiTE. Engagement by BiTE antibody constructs leads to activation and polyclonal expansion of T cells. The activation of T cells requires the presence of target cells. Upon binding of the BiTE antibody construct to both CD3 on T cells and the TAA on target cells, the formation of an immunological synapse is forced, thereby bypassing MHC/antigen-dependent activation of T cells. Subsequent to formation of the immunological synapse, apoptosis of the target cell is induced. Image taken from (Scott et al. 2018).

4.1.3 Clinical applications

To date, BiTEs targeting one of more than ten different TAAs have been evaluated in clinical studies (**Table 2**). From these, those targeting CD33, Ephrin receptor tyrosine kinase A2 (EphA2), carcinoembryonic antigen (CEA), B-cell maturation antigen (BCMA), epithelial cell adhesion molecule (EpCAM) and Prostate-specific membrane antigen (PSMA) are under investigation in Phase I clinical trials for the treatment of different malignancies. Most certainly, the best example of the potential of BiTEs for cancer treatment is Blinatumomab (also named Blincyto), which targets CD19. This BiTE has shown an overall response rate of 40% in patients with Philadelphia chromosome-negative relapsed or refractory B-cell precursor acute lymphoblastic leukemia (R/R ALL) and has been therefore granted approval by the FDA for the treatment of this condition. Blinatumomab has been further evaluated for other hematological malignancies. A recent study of a Phase I clinical

trial of Blinatumomab for the treatment of patients with Relapsed/Refractory Non-Hodgkin Lymphoma (R/R NHL) has reported overall response rates of 69% and a Phase II clinical trial is currently ongoing with expanded cohorts (Goebeler et al. 2016).

For the treatment of solid tumors, only the results of the Phase I dose-escalation clinical trial with the anti-CEA BiTE MEDI-565/AMG 211 for the treatment of gastrointestinal adenocarcinomas have been reported (Pishvaian et al. 2016). The BiTE was given weekly by intravenous infusion over 3 hours on days 1 through 5 for 4 weeks. Different doses were evaluated with or without dexamethasone pre-treatment. MEDI-565 showed similar half-life in serum as Blinatumomab (*i.e.* 2.2 hours) and cytokine release syndrome (CRS) was observed in patients in the highest dose cohort, although these were mitigated by dexamethasone pre-treatment. No objective responses were observed and 28% showed stable disease as the best response. The results of this study highlight some of limitations of BiTEs for the treatment of solid tumors. As opposed to hematological malignancies, BiTEs will have to penetrate the tumor through the vasculature and reach a concentration high enough to exert their potency. It is likely that the treatment and concentration scheme used in that trial was not sufficient to observe clinical responses, and a regime similar to that used for patients treated with Blinatumomab will potentially improve the performance of this BiTE in the future.

BiTE molecule	Targets	Phase	Indications
Blinatumomab	CD19 x CD3	Approved	ALL
AMG 211/MT 211	CEA x CD3	I	Gastrointestinal cancer
AMG 110/MT 110	EPCAM x CD3	I (completed)	Solid tumors
MEDI-565/MT 111	CEA x CD3	I (completed)	Gastrointestinal adenocarcinoma
AMG 330	CD33 x CD3	I	AML
AMG 420	BCMA x CD3	I	Multiple myeloma
AMG 212/ MT 112	PSMA (FOLH1)/CD3	I	Prostate cancer

Table 2. Clinical trials of BiTEs. Adapted from (Yuraszeck, Kasichayanula, and Benjamin 2017) and (Sedykh et al. 2018).

5. TOXIN-BASED THERAPEUTIC APPROACHES

As described in section 2.9.2, tumor heterogeneity and anatomical barriers to virus spread remain major obstacles that prevent complete tumor eradication by OVs. Thus, we aim to overcoming limited virus infection and spread by engineering OAd to recombinant antibody fusion proteins (immunotoxins) or gene-directed enzyme prodrug for bystander killing of cells not reached or noninfectable (*e.g.* CAFs) by the virus. Thus, in this thesis we have tested the therapeutic potential of both approaches, an anti-FAP immunotoxin and a gene-directed enzyme prodrug encoded by an OAd.

5.1 IMMUNOTOXINS: A NEW TOOL FOR CANCER THERAPY

5.1.1 Structure

Immunotoxins are chimeric molecules embodied with a protein toxin and a ligand which is either a growth factor or an antibody. The ligand part of the immunotoxin recognizes and binds to an antigen of the target cell, allowing the internalization of the toxin-moiety and permitting its drift to the cytoplasm where it can destroy the cell. Target specificity of the chimeric protein is determined via the binding attributes of the chosen antibody. Various toxic agents from different sources are used in immunotoxin development, including tosins from bacteria (*e.g. Pseudomonas* exotoxin A, Diphteria toxin, Anthrax toxin), fungi (α-sarcin, restrictocin), plants (*e.g.* Ricin, abrin, saporin, gelonin) and human (*e.g.* Granzyme B, RNases).

Immunotoxins can be classified into generations, based on design and potency. The first-generation immunotoxins were made of a full-length toxin protein attached to whole monoclonal antibodies. Nevertheless, these immunotoxins could bind to normal cells. Loss of specificity, low stability, and heterogeneous composition were the flaws of the first-generation immunotoxins (Bosch and Rosich 2008). Cumulative knowledge on the structure and function of the toxins enabled the removal of their native non-specific cell binding domain, generating much more target-specific immunotoxins when conjugated to monoclonal antibodies (second-generation immunotoxins) (Kreitman 2009; Pastan et al. 2007). Although more specific, and thus better tolerated by animals, immunotoxins from the second generation were still chemically heterogeneous and their large size hindered them from penetrating solid tumors. In order to avoid heterogeneity, improve tumor

penetration and reduce production complexity and costs, in third generation immunotoxins the cell binding domain of the toxin is genetically replaced with a ligand or with a scFv or dsFv fragment (**Figure 12**). Another challenge in the field is the elimination of the immunogenicity of the toxin to human immune system (Mathew and Verma 2009).

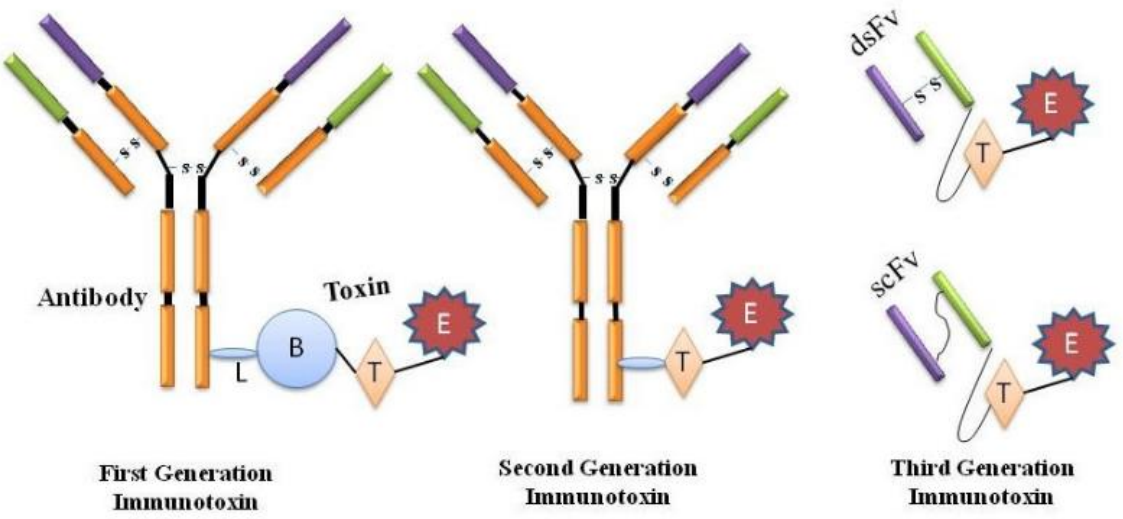

Figure 12. Structural representation of the tree generations of immunotoxins. First generation immunotoxins were prepared by chemically conjugating antibodies/ligands to intact toxin units or to toxins with attenuated cell binding capability. In second generation immunotoxins, truncated toxins that lack a cell binding domain were chemically conjugated to a targeting moiety. In third generation immunotoxins, the cell binding domain of the toxin is genetically replaced with a ligand or single-chain variable fragments (scFv) that are either genetically linked or held together by a disulfide bond (dsFv). L: chemical linker; B: binding domain of toxin; T: translocational domain of toxin; E: enzymatic domain of toxin; dsFv: double strans of variable of antibody; scFv: single-chain of fragment antibody.

5.1.2 Ribosome-inactivating proteins

Ribosome-inactivating proteins have been extensively studied because of their extraordinary efficiency against their target cells, making them excellent candidates as a toxin for immunotoxins. In this thesis, α-Sarcin and onconase toxins have been used for the construction of immunotoxins. They will be described in detail in next sections.

5.1.2.1 α-Sarcin

α-Sarcin is a potent polypeptide toxin (150 residues) secreted by the mold *Aspergillus giganteus* MDH 18894 (Olson et al. 1965) that belongs to the type I group (single polypeptide chain) of ribosome-inactivating proteins. It is the most significant member of a

family of fungal ribotoxins (Martínez-Ruiz et al. 1999). Ribotoxins behave as potent inhibitors of protein biosynthesis due to its highly specific ribonucleolytic activity, which cleaves a single phosphodiester bond of the larger molecule of rRNA located at a universally conserved site, known as the sarcin/ricin loop (SRL), leading to cell death by apoptosis (García-Ortega et al. 2010; Olombrada et al. 2014; Schindler and Davies 1977). Ribotoxins have several advantages for their use as immunotoxins toxic moiety, such as their small size, high thermostability, poor immunogenicity, resistance to proteases and, most importantly, their high efficiency in inactivating ribosomes (Lacadena et al. 2007). Accordingly, colon cancer-specific immunotoxins containing α-sarcin have already been designed and characterized (Gavilanes et al. 2012). In addition, a step further in the therapeutic use of the α-sarcin-based immunotoxin has been done showing the efficiency of the IMTXA33αs, which inhibits tumor growth as well as angiogenesis in nude mice harboring colon cancer xenografts (Tomé-Amat et al. 2015). This result can be considered the proof of concept that immunotoxins based on ribotoxins may be a unique therapeutic tool against different tumor pathologies. Moreover, an immunotoxin containing a deimmunized variant of α-sarcin showing a complete lack of T cell activation in *in vitro* assays have been recently described (Lacadena et al. 2016). These results support therefore the rationale of using the α-sarcin to design new immunotoxins.

5.1.2.2 Onconase

Onconase (ONC) is the smallest (12 kDa) known ribonuclease among enzymes belonging to the superfamily of RNase A. It was discovered by the Alfacell Corporation based on the observed antitumor activity in its source, *Rana pipiens* oocytes (Ardelt, Mikuslki, and Shogen 1991). The enzyme is cytostatic and cytotoxic to a variety of cancer cells in culture and exhibits potent antitumor activity *in vivo* (Darzynkiewicz et al. 1988; Mikulski et al. 1990). It also demonstrates strong immunomodulatory activity. All the observed biological activities of ONC depend on its enzymatic activity (i.e., on its ability to cleave phosphodiester bonds of RNA, especially tRNA). Thus, several properties of ONC seem to predispose this enzyme for potential clinical use, such as its resistance to the mammalian ribonuclease inhibitor and the unusually resistant to proteolysis due to its remarkable conformational stability. In addition, although ONC is an amphibian protein, it is well tolerated in humans. It may be administered repeatedly with no problems associated with immunogenicity, and its activity is not compromised by polyclonal antibodies. ONC has

been tested in phase I-III clinical trials, showing promising anticancer activities (Mikulski et al. 1993; Mikuslki et al. 2002). Importantly, ONC seems to be an ideal "effector" or "payload" molecule in potential targeted therapies. It compares favorably with plant or bacterial proteins used for the construction of immunotoxins as it is well tolerated in humans and distinctly more active (Saxena et al. 1991). For instance, its conjugate with an anti-CD22 antibody was found to be very effective in mice bearing human lymphoma and was exceptionally well tolerated by the animal models (Newton et al. 2001). More recently, Dirk Nettlebeck´s groupshowed antitumor efficacy both *in vitro* and *in vivo* with an immunotoxin ONC-anti-EGFR-encoding OAd (Fernández-Ulibarri et al. 2015), demonstrating that expressing immunotoxins from OAds may be a promising strategy for cancer therapy.

5.2 GDEPT THERAPY

Gene-directed enzyme prodrug therapy (GDEPT) is one of the successful prodrug delivery approaches and has shown great promise in cancer therapy. GDEPT utilizes transgenes which encode enzymes that can convert prodrugs into active therapeutic metabolites. GDEPT usually comprises a three-component system: an inactive drug (prodrug), a gene coding for an enzyme that converts inactive prodrug to an active drug, and a carrier. **Figure 13** illustrates the basic mechanisms of the GDEPT system for the treatment of cancer. In the first step, the coding gene is cloned into a vector or OV and delivered to a tumor cell. The gene is then transcribed into an mRNA which later is translated into the enzyme inside the tumor cell. Finally, a prodrug is administered systemically and absorbed by the same cell; the prodrug can then be converted to a cytotoxic drug by the enzyme inside the cell. What makes the GDEPT an attractive therapy also includes a bystander effect. The effect is achieved via different mechanisms (*e.g.,* passive diffusion) to achieve meaningful tumor regression and durable clinical response.

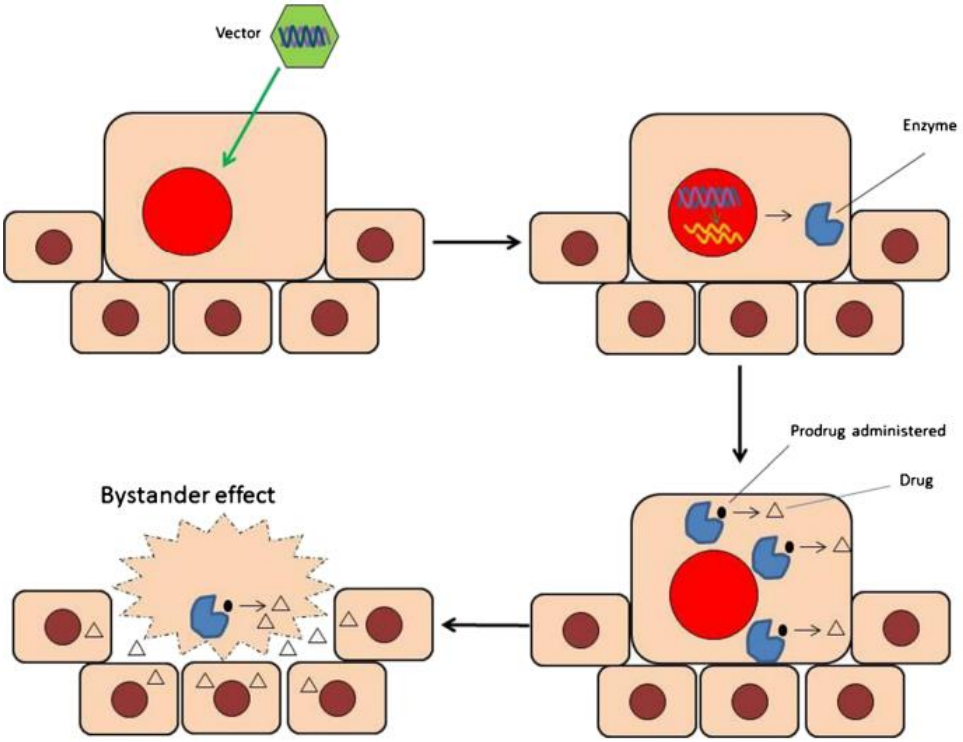

Figure 13. The mechanism of GDEPT systems. Image take from (Zhang, Kale, and Chen 2015).

One of the challenges of GDEPT is the development of efficient gene delivery systems to optimize enzyme gene expression and improve the efficacy of GDEPT. A variety of delivery systems have been explored for targeting GDEPT systems into tumors, and viruses have demonstrated to be excellent vectors for delivery of the therapeutic genes required for GDEPT (also named virus-directed enzyme-prodrug therapy (VDEPT)). An *E. coli* nitroreductase (NTR) gene (nfsB)-armed ONYX-411 in combination with SN 28343 prodrug resulted in 62,5% mice being tumor-free on day 120.

OBJECTIVES

Based on the pro-tumorigenic functions and physical barriers of tumor stroma and the strong antiviral immune responses that limit oncolytic virus (OV) therapy, the destruction of cancer-associated fibroblast (CAFs) by arming OVs with Fibroblast Activation Protein (FAP)-targeting Bispecific T-cell Engagers (BiTEs) or with other cytotoxic proteins may increase the antitumor efficacy of OVs.

The general objective of this thesis was to generate and characterize different oncolytic adenoviruses armed with genes that target stromal cells, and in particular cancer-associated fibroblasts, as a strategy to improve antitumor efficacy. To achieve this goal, specific objectives were set for three independent projects:

Improve replication-dependent transgene expression from an oncolytic adenovirus

- Generate a panel of oncolytic adenoviruses expressing luciferase in different locations of the genome and under different splicing acceptors.
- Characterize the efficacy profile and the luciferase expression of the luciferase-armed oncolytic adenoviruses *in vitro* and *in vivo*.
- Assess whether stronger levels of a therapeutic transgene expression can enhance antitumor efficacy *in vivo.*

Characterize a FAP-targeting bispecific t cell engager-armed oncolytic adenovirus

- Generate ICO15K-based oncolytic adenoviruses expressing BiTEs targeting FAP.
- Characterize the oncolytic properties and the efficacy profile of the BiTE-expressing adenoviruses *in vitro*.
- Characterize the functionality of BiTEs expressed from virus-infected cells.
- Evaluate the antitumor activity and the effect on the tumor stroma of the FBiTE-expressing oncolytic adenovirus in immunodeficient mice models.

Targeting the tumor stroma with an immunotoxin or a prodrug-activation strategy

- Generate and characterize oncolytic adenoviruses expressing different FAP-targeted immunotoxins.
- Generate and characterize oncolytic adenoviruses expressing a nitroreductase (NfrA)-activatable prodrug.

MATERIALS AND METHODS

1. HANDLING OF BACTERIA

In order to obtain enough amounts of plasmid DNA to be easily manipulated, its amplification in bacteria was required. For this reason, the plasmid should have a replication origin that allows its replication on the desired strain and a gene that confers resistance to an antibiotic in order to select the bacteria and avoid contaminations. In this work, the *Escherichia coli* strains DH5α and DH10B have been used with this purpose. Moreover, SW102 strain has been used to perform homologous recombination.

1.1 PREPARATION OF ELECTROCOMPETENT BACTERIA

The bacteria stock was conserved at -80°C with 15% glycerol. In order to induce competence, the glycerinate was scratched with a sterile pipette tip into 10 mL of LB (1% Tryptone, 0.5% Yeast Extract, 0.5% NaCl) and it was grown overnight at 37°C in agitation in a 50 mL Falcon tube. Next day, the 10 mL preculture was grown in 1 L of LB at 37ºC in agitation until the culture reached an OD_{600} of 0.6-0.7. The bacterial solution was distributed in 250 mL bottles (suitable for centrifugation in SORVALL centrifuge) and kept 40 minutes on ice in order to stop bacterial growth. Further manipulation of bacteria was carried on at 4ºC. Next, bacteria were centrifuged 15 minutes at 4000 *g* and 4ºC in a SORVALL centrifuge, supernatant was discarded, and the pellet was washed with cold bi-distilled (dd)H_2O water (4ºC). This centrifugation/washing process was repeated 3 times and in the last wash the pellet was resuspended in 45 mL of water with 10% glycerol. Bacteria were centrifuged one more time and, finally, resuspended in 3 mL of water containing 10% glycerol. The OD_{600} of a 1:100 dilution of the suspension was determined. OD value should be close to 1 (which is equivalent to $2.5x10^8$ bacteria/mL). Finally, the bacterial suspension was distributed in 50 µL aliquots that were immediately frozen on dry ice. Aliquots were stored at -80°C.

1.2 TRANSFORMATION OF COMPETENT BACTERIA BY ELECTROPORATION

Frozen DH5α electrocompetent *E. coli* aliquots (50 µL) were thawed on ice and mixed with a maximum of 10 µL pre-cooled DNA (10-1000 pg for retransformations or >200 ng of recombinations). The mixture was gently mixed, incubated 5 minutes on ice and transferred into ice-cold 0.2 cm electroporation cuvettes. Bacteria were electroporated at 50 µF, 1500 V and 125 Ω with the Electro Cell Manipulator™ ECM 630. Immediately, bacteria were resuspended in 1 mL of tempered LB and incubated for 30-60 minutes in

agitation at 37ºC. The suspension was plated on LB plates supplemented with the corresponding selection antibiotic and incubated 37ºC overnight. The next day, one clone was inoculated in 5 mL (for small scale isolation of DNA: mini-preps) or 50-200 mL (for large scale isolation of DNA: midi-preps) LB supplemented with the corresponding antibiotic. These cultures were used to isolate plasmid DNA as described below.

1.3 PLASMIDIC DNA EXTRACTION FROM BACTERIAL CULTURES

Plasmid DNA was obtained from saturated *E. coli* cultures grown in LB with antibiotic according to protocols based on an alkaline lysis with SDS. DNA was prepared at small and large scale.

1.3.1 Small and large scale of DNA preparations

Small scale DNA preparations (mini-preps) were performed following an adapted protocol described by Birnboim and Doly (Birnboim and Doly 2009). A colony grown in a LB-antibiotic dish was inoculated in 3 mL of LB-antibiotic and incubated overnight at 32ºC (for *E. coli* strain SW102) or 37ºC (for *E. coli* DH5α). 2 mL of the overnight cultures were centrifuged, and pellets were resuspended in 200 µL of pre-cooled solution 1 (25 mM Tris-HCl pH 8, 10 mM EDTA, 50 mM glucose). 200 µL of freshly prepared solution 2 (SDS 1%, NaOH 0.2 M) were added and the mixture was blended by inversion. Finally, 200 µL of pre-cooled solution 3 (3 M potassium acetate, 11.5% acetic acid) were added and the mixture was blended again by inversion until a white precipitate appears. The mixture was incubated 5 minutes on ice and centrifuged 15 minutes at 15000 g. Next, the clear supernatant was collected without taking the white pellet that corresponds to cellular DNA, proteins and SDS, and 2 volumes of ethanol were added. The mixture was incubated 15 minutes at room temperature (RT) and plasmid DNA was precipitated by centrifugation during 10 minutes at 15000 *g*, supernatant was discarded and the pellet was washed with 70% ethanol. It was centrifuged again 5 minutes at 15000 *g*, supernatant was discarded and the pellet was dried. Finally, plasmid DNA was resuspended in 50 µL of TE.

Large scale DNA preparations (midi-preps) were prepared from 200 mL of saturated bacteria culture using the PureLink™ HiPure Plasmid Midiprep Kit (Invitrogen), following manufacturer's instructions.

1.4 HOMOLOGOUS RECOMBINATION IN BACTERIA

Homologous recombination performed in this work have been conducted in bacteria using the high efficiency system developed by Richard Stanton (Stanton et al. 2008), who kindly gave us the plasmid pAdZ5-CV5-E3^{+} in SW102 strain of *E. coli*. This plasmid contains the adenovirus genome type 5 (E1^{-}) as a bacterial artificial chromosome (BAC) with chloramphenicol (Cm) resistance gene. This system works using phage *λ* genes Redγβα, which are controlled by a temperature inducible promoter, whose activation can be triggered by a temperature of 42ºC. Electroporation of the heat-shocked bacteria with a DNA fragment flanked by homology arms (>30bp) to the targeted site in the BAC will result in the insertion of the DNA by homologous recombination. *SacB* and *Ampicillin* (Amp) resistance genes from Stanton *et al.* protocol were replaced by *rpsL-neo* cassette, as it is a faster and more cost-effective method (S. Wang et al. 2009).

Modification was performed in two steps. In the first step (positive selection), the *rpsL-neo* cassette is inserted in the region of interest of the adenovirus genome. This first fragment had homology regions (about 40 bp) with the site we wanted to modify on each end. The neo gene in the *rpsL-neo* cassette confers resistance to kanamycin. Thus, positive selection can be achieved by plating of the bacteria after electroporation in LB agar plates supplemented with kanamycin (kana) and chloramphenicol (Cm). In the second step (negative selection), the heat-shocked bacteria containing the pAdZ-rpsL-neo are electroporated with the DNA of interest flanked by homology arms targeting the region where the *rpsL-neo* cassette is inserted. The *E. coli* strain SW102 is intrinsically resistant to streptomycin (Strep) due to mutations in the *rpsL* gene but introducing the wild-type *rpsL* gene into the bacteria exerts dominant phenotypic effects over mutated *rpsL* (Stavropoulos and Strathdee 2001). After the second transformation, recombinant clones were those that had incorporated the inserted DNA and had lost *rpsL-neo* cassette, being consequently sensitive to Kana and resistant to Strep.

The plasmid pAdZ5-CV5-E3^{+} provided by Richard Stanton was modified in order to obtain pAdZ-ICOVIR-15K plasmid, backbone that has been used for all the modifications described in this thesis.

The procedure that has been followed to perform recombinations is as follows. For positive selection, glycerinates of the bacteria containing the pAdZ-ICOVIR-15K plasmid

were scratched with a sterile pipette tip, inoculated in 5 mL of LB media including Cm + Strep antibiotics (12.5 µg/mL, and 1 mg/mL, respectively) and incubated overnight at 32ºC and constant agitation. Then 25 mL of LB Cm + Strep were inoculated with 0.5 mL of the previous culture and incubated 32ºC with agitation until it reached an OD_{600} between 0.5-0.6. At this moment, culture was divided in two Falcon tubes with equal volumes. One of the tubes was kept on ice until further processing (non-induced). The other tube was induced by heat-shock at 42ºC for 15 minutes in a water bath, followed by chilling on ice for 15 minutes (induced). From that moment, manipulation was performed on ice in order to ensure transformation efficiency. Both cultures (induced and non-induced) were centrifuged 5 minutes at 4000 *g* at 4°C and supernatant was discarded. Bacteria pellet was resuspended in 12 mL of cold ddH_2O water and centrifugation was repeated. This washing step was repeated thrice and, after the final step, the pellet was resuspended in approximately 300 µL ddH_20. 50 µL-aliquots of the induced and uninduced cultures were transformed with ≥200 ng of the *rpsL-neo* DNA flanked by the desired homology arms. Bacteria were recovered in 1 mL of LB and incubated 2 hours at 32ºC with constant agitation. From this recovery, 100 µL were plated into LB plates containing Cm and Kan (12.5 µg/mL, and 15 µg/mL, respectively) and incubated overnight at 32ºC. About 20-24 hours later, the number of colonies on the plates of induced and non-induced cultures was counted to determine the recombination efficiency. Then, colonies from induced plates were picked and inoculated in 4 mL LB supplemented with Cm and Kana and incubated at 32ºC and 250 rpm. Next day, mini-preps of DNA were performed (see section 1.3.1). For screening of recombinant clones, 17,5 µL of the mini-preps were digested with the corresponding restriction enzymes (New England Biolabs and Takara/Clonetech) at 37°C for 1 hour and separated by electrophoresis on 1% agarose gels. Positive clones were stored at -80°C in LB with 15% (v/v) glycerol. The pAdZ-ICOVIR-15K-rpsLNeo plasmid, containing the *rpsL-neo* cassette after the fiber region of the adenovirus genome was previously generated in our group using this positive selection method.

A similar procedure was followed for the second step, in which the clones obtained in the previous step were inoculated in 5 mL of LB Cm + Kan and cultured overnight at 32ºC. Next day, the bacteria were made competent for its transformation by electroporation as described previously. Again, 200 ng of DNA (insert) containing the desired modification were transformed. After the recovery incubation, 100 µL from a 1:10 and 1:25 dilution were plated in LB agar supplemented with Cm and Strep and plates were incubated

overnight at 32ºC. Next day, colonies were picked and inoculated in 4 mL of LB-Cm + Strep and incubated overnight at 32ºC in agitation. Recombinant clones were screened and stored as above, and the correct insertion of the genes was confirmed by sequencing (see section 3.7.4). Midi-preps from the sequenced positive clones were prepared (see section 1.3.1) and used for transfection (see section 3.3).

2. CELL CULTURE

2.1 CELL LINES

The cell lines used in this thesis for the *in vitro* and *in vivo* experiments are summarized in the following table:

Cell line	Tumor type	Origin	Medium	FBS
A549	Lung adenocarcinoma	Human	DMEM	10%
A431	Epidermoid carcinoma	Human	DMEM	10%
HEK-293	Embryonic kidney	Human	DMEM	10%
293FT	Embryonic kidney	Human	DMEM+NEEA	10%
HT1080	Fibrosarcoma	Human	DMEM	10%
Jurkat	Acute T-cell leukemia	Human	RPMI	10%
hCAF	Prostate adenocarcinoma	Human	DMEM+NEEA	10%
HPAC	Pancreatic adenocarcinoma	Human	DMEM	10%
CMT-64.6	Lung adenocarcinoma	Mouse	DMEM	10%
Tramp-C2	Prostate adenocarcinoma	Mouse	DMEM	10%

Table 3. Cell lines used in this thesis.

The cancer cell lines A549, A431, HEK-293, 293FT, HT1080, Jurkat and HPAC were obtained from the American Type Culture Collection (ATCC, Manassas, VA, USA). hCAFs (Human CAFs pf179) were kindly provided by Varda Rotter (Weizmann Insitute of Science, Israel). The murine Tramp-C2 cell line was obtained from Dr. NM Greenberg (Baylor College of Medicine, Houston, TX). 293, 293mFAP and 293hFAP cell lines were obtained from Dr. Eric Tran (National Institutes of Health, Bethesda, MD). CMT.64 cell line was provided by Dr. Stephan Kubicka (Hannover Medical School, Hannover, Germany) and the most permissive clone to adenovirus infection was isolated and expanded, generating the CMT-64.6. Murine CAFs (mCAFs) were isolated from HPAC tumors as described (Berdiel-Acer et al.

2014). All cells were maintained in either DMEM or RPMI (Gibco, Thermo Fisher Scientific) supplemented with 10% FBS (Gibco, Thermo Fisher Scientific) previously inactivated by heating at 56°C for 30 minutes and penicillin-streptomycin (PS, Gibco-BRL, Barcelona, Spain) (100 U/mL and 100 µg/mL, respectively) at 37ºC and 5% CO_2. To generate FAP-expressing cell lines, HT1080 and A431 cells were transduced with a lentivirus encoding either the mouse or the human FAP cDNA (Dharmacon). FAP-expressing cells were sorted and expanded. HT1080 and A431 cells stably expressing mouse FAP or human FAP are designated as HT-mFAP and HT-hFAP or A431-mFAP and A431-hFAP, respectively. Tramp-C2-GFPLuc cell line was generated by sorting of Tramp-C2 cells that had previously been transduced with a lentiviral vector encoding GFP and luciferase. All cell lines were routinely tested for mycoplasma (see section 2.5).

2.2 MAINTENANCE OF CELL CULTURES

Cells were incubated at 37°C in a humidified atmosphere with 5% CO_2 in the presence of the corresponding medium. When cultures reached 80-90% confluence, cells were washed once with PBS and detached with trypsin-EDTA. To stop the reaction, cells were resuspended to a final volume of 10 mL in the corresponding medium supplemented with 5-10% (v/v) FBS. These cell suspensions were used to split the cells 1:6 to 1:20 depending on the cell line.

2.3 CELL COUNTING

To determine cell numbers, the automatic counting was performed with a cell counter TC20™ (Bio-Rad) according to the manufacturer's instructions.

2.4 CELL FREEZING AND CRYOPRESERVATION

For long term storage, cells were collected by trypsinization and pelleted by centrifugation. Cell pellets were resuspended in cold freezing medium (90% FBS, 10% DMSO). Cell suspension was distributed in cryotubes at 1 mL/tube and placed in a Mr. Frosty freezing container for its freezing at -80°C for 24 hours. Next day, cryotubes were stored in a liquid nitrogen tank. For cell thawing, cells were rapidly thawed in a water bath at 37ºC. Cells were diluted in pre-warmed medium and trespassed to a 15 mL Falcon tube. Centrifugation at 1000 *g* was carried out for 5 minutes and the pellet of cells was resuspended in fresh medium and seeded at an appropriate density.

2.5 MYCOPLASMA TEST

All cell lines were routinely tested for mycoplasma contamination by PCR using the following primers:

Primer	Sequence (5'→ 3')
MICO-1	GGCGAATGGGTGAGTAACACG
MICO-2	CGGATAACGCTTGCGACTATG

Table 4. Primers used for the detection of mycoplasma.

As a template for the PCR, medium from cells that had been in overconfluence and absence of antibiotics for at least 7 days were used. If the result was positive, cells were treated with Plasmocin™ (Invivogen) at 25 µg/mL for 2 weeks, and then the cells were tested again.

2.6 ISOLATION, CRYOPRESERVATION AND THAWING OF HUMAN PBMCS AND T CELLS

All experiments were approved by the ethics committees of the University Hospital of Bellvitge and the Blood and Tissue Bank (BST) from Catalonia. Blood samples were obtained from the BST from Catalonia and the Human Immunology Core of the University of Pennsylvania. Peripheral blood mononuclear cells (PBMCs) of healthy donors were isolated from the blood by ficoll (Rafer) density gradient centrifugation in Leucosep tubes (Greiner Bio-one) following manufacturer's recommendations. Erythrocytes were removed by incubation with ACK lysing buffer (Lonza) and thrombocytes were removed by centrifugation of the PBMCs at 1000 *g* for 10 minutes and aspiration of the supernatant. T cells were isolated from blood samples with the RosetteSep Human T-Cell Enrichment Cocktail (STEMCELL Technologies) according to the manufacturer's instructions. PBMCs and T cells were cryopreserved in FBS supplemented with 10% DMSO in aliquots of 1-5 × 10^7 cells/vial. For thawing, PBMCs or T cells cryovials were quickly thawed in a water bath at 37ºC and washed once with 10 mL RPMI supplemented with 10% FBS and 10 mM HEPES (Gibco) by centrifugation. Cells were resuspended at a concentration of 3 × 10^6 cells/mL and incubated overnight for the recovery of the cells prior to the experiments.

2.7 FLUORESCENT LABELING OF CELLS WITH CFSE

Trypsinized cancer cells or T cells were centrifuged at 500 *g* for 5 minutes and pellets were resuspended in 1 × 10^6 cells/1 mL of 1µM Carboxyfluorescein succinimidyl ester (CFSE) (Sigma) diluted in PBS. Cancer cells were incubated at 37ºC for 20 minutes protected from light and T cells for 1 minute at RT. After the incubation, the reaction was blocked with equal volumes of 5% FBS in PBS. Cells were centrifuged at 500 *g* for 5 minutes and pellets were resuspended either in the corresponding medium supplemented with 10% FBS. After resuspension, cells were counted, and cell concentration was adjusted as needed.

3. RECOMBINANT ADENOVIRUSES

All adenoviruses used in this thesis are derived from the human adenovirus serotype 5 (Ad5). The virus ICOVIR-15K has been previously described (J. J. Rojas et al. 2012).

3.1 TRANSGENES DESIGN

3.1.1 BiTE design

FBiTE

FBiTE was generated by joining the scFvs anti-FAP and anti-CD3ε with a GGGGS flexible linker. The anti-CD3 scFv sequence of the Blinatumomab BiTE was obtained from patent application WO2004106381. The anti-FAP sequence (M5) was derived from patent application US 2009/0304718 A1. The FAP5 and anti-CD3 variable regions were connected by a $(G_4S_1)_3$ and a $(G_2S_1)_4GG$ linker, respectively. The FBiTE was arranged V_L(M5)-V_H(M5)-V_H(CD3)-V_L(CD3) and contained an N-terminal signal peptide derived from the mouse immunoglobulin light chain for mammalian secretion, and a FLAG tag at the C-terminal for detection. The FBiTE construct included a left (upstream of the BiTE starting codon) and a right (downstream of the last BiTE codon) homology arms. The left homology region included the kozac, the IIIa splicing acceptor and extra DNA base pairs from the adenovirus genome. The right homology arm included the stop codon, the polyA signal and extra base pairs from the adenovirus genome. Both arms were homologous to the sequences flanking the *rpsL-neo* cassette in the pAdZ-ICOVIR-15K-rpsL-neo plasmid. The FBiTE-coding region was optimized for human codon usage avoiding Ssp1 and AfeI restriction sites, and the

whole construct, including the regulatory and homology sequences, was synthesized by Baseclear.

mFBiTE

The anti-mouse CD3 scFv was derived from the hamster monoclonal antibody 145.2C11 (Stone et al. 2012a). The anti-FAP was the same than the FBiTE. The 2C11 and M5 variable regions were connected by a $(G_4S_1)_3$ and a $(G_2S_1)_4GG$ linker, respectively, and both scFV were connected to each other by a GGGS flexible linker. The mFBiTE construct was arranged V_H(2C11)-V_L(2C11)-V_H(M5)-V_L(M5) and it included the peptide signal from the mouse Ig heavy chain and a FLAG tag at the N- and C-terminus of the protein, respectively. The mFBiTE construct included the same homology arm described for the FBiTE. The mFBiTE-coding region was optimized for human codon usage avoiding Ssp1 and AfeI restriction sites, and the whole construct, including the regulatory and homology sequences, was synthesized by Baseclear.

2C11-M5

Both the anti-mouse CD3 and the anti-mouse/human FAP scFvs were the same than the mFBiTE. In this case, the 2C11 and M5 variable regions were connected by a $(G_4S_1)_3$ and a $(G_2S_1)_3GG$ linker, respectively, and both scFv were connected to each other by a GGGS flexible linker. The 2C11-M5 construct was also arranged V_H(2C11)-V_L(2C11)-V_H(M5)-V_L(M5). The rest was the same than mFBiTE .

M5-2C11

The only difference compared to 2C11-M5 was the arrangement. In this case, M5-2C11 construct was arranged V_L(M5)-V_H(M5)-V_H(2C11)-V_L(2C11) .

M5-2C11.2

The only difference compared to M5-2C11 was the linker between 2C11 variable regions. In this design, we changed the linker $(G_2S_1)_3GG$ for the $(G_4S_1)_3$.

M5-2C11.3

Finally, we design the M5-2C11.2 changing the arrangement of the M5 variable regions, from V_L(M5)-V_H(M5)-V_H(2C11)-V_L(2C11) to V_H(M5)-V_L(M5)-V_H(2C11)-V_L(2C11) .

3.1.2 Immunotoxin design

M5-Sarcin

M5-Sarcin was generated by joining the scFv anti-FAP described above and the ribonuclease α-Sarcin with the GGCGGCCGC flexible linker. α-Sarcin sequence was obtained from the collaborator with this project, Javier Lacadena (Univerdad Complutense de Madrid). The M5-Sarcin was arranged V_L(M5)-V_H(M5)-Sarcin and contained an N-terminal signal peptide derived from the mouse immunoglobulin light chain for mammalian secretion, and a His tag at the C-terminal for detection. As described in FBiTE, this construct included a left and a right homology arms. The left homology region included the kozac, the IIIa splicing acceptor and extra DNA base pairs from the adenovirus genome. The right homology arm included the stop codon, the polyA signal and extra base pairs from the adenovirus genome. Both arms were homologous to the sequences flanking the *rpsL-neo* cassette in the pAdZ-ICOVIR-15K-E4-rpsL-neo plasmid. The M5-Sarcin-coding region was optimized for human codon usage avoiding HpaI and Pml I restriction sites, and the whole construct, including the regulatory and homology sequences, was synthesized by Baseclear

To generate an expression vector encoding the protein, the M5-Sarcin-conding region was amplified by PCR using the primers described in Table 5 and the conditions described in Table **6**. The sequence of the restriction enzyme Age I was added at the N-terminal and Not I at the C-terminal.

MO36-Sarcin

This construct was designed as the M5-Sarcin construct but replacing the scFv anti-FAP5 for the anti-FAP MO36. The sequence of scFv MO36 was obtained from Brocks *et al* (Brocks et al. 2001). MO36-Sarcin was only inserted in the adenovirus genome (see M5-Sarcin).

ESC11-Sarcin

To generate the ESC11-Sarcin, the scFv FAP5 was replaced for the scFv ESC11. This anti-FAP sequence (ESC11) was derived from patent application US 20120258119 A1. ESC11-Sarcin was designed as described in M5-Sarcin.

This construct was generated to be inserted to both the adenovirus genome (see M5-Sarcin) and to the expression vector (see Table 5 and Table 6).

ONCO-FAP

To generate the ONCO-FAP, the ribonuclease Onconase was fused to the scFv anti-FAP (FAP5) with a $(G_4S_3)_3$ flexible linker. The sequence of the Onconase was obtained from Fernández-Ulibarri *et al* (Fernández-Ulibarri et al. 2015). This protein was arranged Onconase- V_L(M5)-V_H(M5). This construct included the kozac, the 40SA splicing acceptor and the homology arms to be inserted in the adenovirus genome.

ONCO-FAP was designed to be inserted to both the adenovirus genome (see M5-Sarcin) and to the expression vector (see **Table 5** and **Table 6**).

Gene	Sequence 5'→3'	Description
F-KLA.AgeI	CGTACCGGTCCACCATGGGATGGTC	To obtain M5-Sarcin
R-M5S.NotI	CCTGGCGGCCGCTTTATTAGTGGTGGTGATGG	To obtain M5-Sarcin
F-ES.AgeI	CGTACCGGTCCACCATGGGCTGGAGCT	To obtain ESC11-Sarcin
R-NotI	CCTGGCGGCCGCTTTATTAGTGGTGGTGGTGGTGGTG	To obtain ESC11-Sarcin and ONCO-FAP
F-AgeI	CGTACCGGTCCACCATGGGATGGTCCTGTATTAT	To obtain ONCO-FAP

Table 5. Primers used to obtain the M5-Sarcin, ESC11-Sarcin and ONCO-FAP for being inserted in an expression vector.

Stage	Description	Temperature	Time	Cycles
1	Initial denaturation	95ºC	2 minutes	1
2	Denaturation	94ºC	1 minute	24
	Annealing	55ºC	1 minutes	
	Extension	72ºC	2 minutes	
3	Final extension	72ºC	7 minutes	1
4	Pause	4ºC	∞	1

Table 6. Conditions used to obtain the M5-Sarcin, ESC11-Sarcin and ONCO-FAP.

3.1.3 NfrA design

NfrA

NfrA was designed in collaboration with Adam Patterson (University of Auckland). NfrA was generated to be inserted only in the adenovirus genome. NfrA sequence (obtained from Adam Patterson) included a left and a right homology arms. The left homology region included the kozac, the IIIa splicing acceptor and extra DNA base pairs from the adenovirus genome. The right homology arm included the stop codon, the polyA signal and extra base pairs from the adenovirus genome. Both arms were homologous to the sequences flanking the *rpsL-neo* cassette in the pAdZ-ICOVIR-15K-rpsL-neo plasmid.

3.2 CONSTRUCTION OF TRANSGENE-EXPRESSING ONCOLYTIC ADENOVIRUS

3.2.1 Construction of BiTE-expressing oncolytic adenovirus

The BiTE constructs were excised from pUC57 plasmids by exploiting the SspI and AfeI restriction sites included in their sequence. These sites were designed so that the overhangs generated after restriction retained the homology to the target sequences in the pAdZ-ICOVIR-15K-rpsL-neo plasmid. The pUC57 plasmids containing the BiTE constructs were digested with SspI and AfeI enzymes (New England Biolabs) according to the manufacturer's instructions. Digestions were separated by gel electrophoresis and the band corresponding to the BiTE constructs were sliced from the gel. DNA gel extraction was performed with the QIAquick gel extraction kit (QIAGEN) according the manufacturer's instructions. This DNA was used for homologous recombination in bacteria in order to generate the plasmids pAdZ-ICO15K-FBiTE, pAdZ-ICO15K-mFBiTE and pAdZ-ICO15K-2C11-M5, pAdZ-ICO15K-2C11-M5.2 and pAdZ-ICO15K-2C11-M5.3 (see section 1.4).

3.2.2 Construction of immunotoxin-expressing oncolytic adenovirus

Immunotoxins were obtained excising the pUC57 with the restriction sites Hpa I and Pml I. Oncolytic adenovirus expressing the different immunotoxins were generated as described in section 3.2.1. They were named pAdZ-ICO15K-M5-Sarcin, pAdZ-ICO15K-ESC11-Sarcin, pAdZ-ICO15K-MO36-Sarcin and pAdZ-ICO15K-ONCO-FAP.

3.2.3 Construction of vector-encoded immunotoxin

For the generation of an expression vector encoding the immunotoxins described above, the plasmid GT4082 was used. GT4082 is a mammalian expression vector that constitutively expresses the Green Fluorescent Protein (GFP) under the CMV promoter and

contains an ampicillin selectable marker. The GFP cassette is flanked by the restriction sites Age I and Not I. Immunotoxins sequences, that included the restriction sites Age I in N-terminal and Not I in C-terminal (see section 3.1.2), and the GT4082 plasmid were digested by these same restriction enzymes (New England BioLabs). Digestions were separated by gel electrophoresis and the band corresponding to our immunotoxins (inserts) and to the linearized GT4082 (vector) without the GFP were sliced from the gel. DNA gel extraction was performed with the Monarch® DNA gel extraction kit (New England BioLabs) according to manufacturer's instructions. Linearized vector and digested inserts were ligated with the T4 DNA Ligase (New England BioLabs) following manufacturer's instructions (molar ratio of 1:5 vector to insert). Competent cells were transformed (see section 1.2) with 1-5 µL of the ligation and incubated overnight at 37ºC. Next day, mini-preps of DNA were performed (see section 1.3.1) for screening of ligated clones. Resulting good clones were named GT4082-M5-Sarcin, GT4082-ESC11-Sarcin and GT4082-ONCO-FAP.

3.2.4 Construction of NfrA-expressing oncolytic adenovirus

NfrA encoded by oncolytic adenovirus was generated as described in section 3.2.1. It was named pAdZ-ICO15K-NfrA.

3.3 ADENOVIRUS GENERATION BY CALCIUM PHOSPHATE TRANSFECTION

Once the desired modifications have been incorporated into the viral genome, this recombinant viral DNA needs to be introduced into packaging cells to generate the adenovirus. For this purpose, HEK-293 cells were transfected with the plasmid containing the viral genome by the calcium phosphate-based method. For the transfection with pAdZ plasmids, previous linearization of the viral genome is not required since these plasmids incorporate a self-excising system. Once the plasmid enters the cell, the endonuclease I-SceI is expressed and releases the viral genome. This system increases the efficiency of the transfection, as circular DNA is transfected more efficiently than linear DNA. After the transfection, the viral cycle begins, and after several rounds of replication (about 7 days post-transfection), foci of cytopathic effect are clearly seen.

For transfection, monolayers of HEK-293 cells seeded in 6-well plates at a confluence of 60-80% were used. For each plasmid to be transfected the following mixture was prepared in a 1.5 mL tube:

- 19.5 µL of CaCl2 2 M
- 3 µg of DNA
- ddH_2O up to a final volume of 162 µL

This solution was mixed up softly for 10 seconds, and another 1.5 mL tube containing 162 µL of HBS 2X (NaCl 274 mM, HEPES 50 mM, and NaH_2PO_4 1.5 mM in H_2O, pH adjusted to 6.95-7.05 with NaOH) was prepared. The solution containing the DNA was added drop by drop to the tube containing the HBS while air was being bubbled with a pipette. The mixture was incubated for 20 minutes at RT and added drop-wise to the plate. 2 hours later calcium phosphate precipitates became visible and at 16 hours post-transfection the medium was removed and exchanged by fresh medium.

When the cytopathic effect (CPE) foci were visible (approximately 5-7 days post-transfection), cells were collected together with the supernatant (cell extract, CE) and underwent 3 rounds of freeze/thaw cycles to completely release the viral particles from the cells. This cell extract (CE) was used for further amplification steps.

3.4 CLONE ISOLATION BY PLAQUE PURIFICATION ASSAY

Serial dilutions from the transfection CE, ranging from 10^{-1} to 10^{-7}, were prepared in DMEM 5% FBS. 100 µL of each dilution was used to infect one 6-well of 80% confluent A549 cells for 4 hours at 37ºC. After removing the media and washing of the cells with PBS, 3 mL of a 1:1 solution of DMEM 5% FBS and 1% agarose pre-warmed was added to the cells. Once solidified, 2 mL of fresh medium were added over the agarose matrix. The plates were incubated at 37ºC until the appearance of plaques was evident (5-8 days post infection). To select clones, the medium was removed, and the plaques were picked through the agarose matrix using a pipette tip. The aspirated agarose/medium was resuspended in 500 µL of DMEM 5% FBS and used for further amplifications steps.

3.5 AMPLIFICATION AND PURIFICATION OF ADENOVIRUSES

Amplification and purification allow the obtainment of sufficient amounts of adenovirus and in the appropriated formulation to be used for *in vitro* and *in vivo* assays. The amplification of the adenovirus is based on the propagation of the virus through culture plates of larger sizes at each passage and in bigger amounts. The purification of the

adenovirus is based on its separation from the cell debris by ultracentrifugation steps in cesium chloride. Both processes are described in the following sections.

3.5.1 Amplification of oncolytic adenoviruses

After clone selection, 250 µL from the clone suspension were used to infect a 6-well of confluent A549 cells. When cytopathic effect (CPE) was observed cells were harvested and subjected to 3× freeze/thaw cycles. From this point on, viruses were sequentially amplified by scaling up as follows: 6-well → 1 × 100mm dish → 1 × 15cm dishes → 18 × 15cm dishes. In general, 1:20 dilutions of the viral suspension from each step were used as inoculum for the next expansion step, while the rest was stored at -80°C as backup stocks. The general process for virus propagation consisted of an infection and harvesting steps. Infections were performed in DMEM 5% FBS and dishes were incubated for 3-4 days until cells were detached or showed evident signs of CPE. For harvesting, infected cells were collected by pipetting and subjected to 3x freeze/thaw cycles. In the final harvesting step, cell pelleted by centrifugation and cells were resuspended in a maximum volume of 10 mL before performing freeze/thaw cycles for purification. 50 mL of supernatants were also collected for the first round of ultracentrifugation.

3.5.2 Purification of oncolytic adenoviruses

Oncolytic adenoviruses were purified by cesium chloride (CsCl) density gradient centrifugation. Prior to the preparation of the CsCl gradients, cell pellets were subjected to three freeze/thaw cycles to release the viruses from the cells. Debris was cleared by centrifugation at 1000 *g* for 10 minutes, and the supernatant was collected. Cell pellets were resuspended in 10mL of the supernatant stored in the last step of the amplification process, and tubes were centrifuged again to wash the pellet. This process was repeated until a final volume of 42mL of virus supernatant was reached. Discontinuous CsCl gradients were prepared in ultracentrifugation tubes (Beckman Coulter) using 2 solutions at different concentrations. For the first layer of the gradient, 2.5 mL of a solution with a concentration of 1.35 g/mL were added to the bottom of the tubes. The second layer consisted of 2.5 mL of a CsCl solution at 1.25 g/mL, and it was carefully added on top of the first layer. Gradients were completed by carefully adding 7.5 mL of the virus on top of the second layer of the gradient. Tubes were ultracentrifuged for 2 hours at 150000 *g* (35000 rpm, SW40 Ti rotor, Beckman) and 10°C. With these conditions, viral particles are

separated from cell debris according to size and appear as 2 bands at the interface between 1.25 and 1.35 g/mL layers. The upper band corresponds to empty viral capsids and was removed by suction. The lower band of interest was collected and placed on ice in a 50 mL Falcon tube. For further purification and concentration, a second centrifugation step using a continuous CsCl gradient was performed. The solution containing the virus was brought up to 24 mL with the CsCl solution at 1.35 g/mL and distributed into 2 ultracentrifuge tubes. The second centrifugation was carried out overnight at the same conditions of the first one. After centrifugation, the upper band was discarded by suction and the band corresponding to the full viral particles was collected in a maximum volume of 2 mL. Buffer exchange was performed with PD-10 desalting columns (GE healthcare Life Sciences) according to the manufacturer's instructions. Viruses were eluted from columns with 2 mL Tris-NaCl, supplemented with glycerol to a final concentration of 5% (v/v) and stored in 20 µL to 500 µL aliquots at -80°C for long term storage.

3.6 TITRATION OF ADENOVIRUSES

3.6.1 Determination of physical viral particles by spectrophotometry

This method is used to quantify the viral particles (vp) from a purified adenovirus stock without discrimination between infective or defective particles. It is based on the determination of the absorbance of viral DNA at a wavelength of 260 nm.

Three different dilutions (1:5, 1:10, and 1:20) of the purified viral stock were prepared in lysis buffer (Tris 10 mM, EDTA 1 mM, 0.1% SDS, pH 8.0) and incubated for 10 minutes at 56°C. Then, the OD_{260} and OD_{280} was measured using a NanoDrop ND-1000 UV/VIS spectrophotometer. The final concentration of the virus was calculated with the following formula, considering that the extinction coefficient of adenoviruses is 1.1×10^{12} per OD unit:

$$Titer\ (vp/mL) = OD_{260\,nm} \times sample\ dilution \times 1.1 \times 10^{12}$$

The ratio between the absorbance at 260 nm and 280 nm gives an idea of the integrity of the purified sample. It should be around 1.3.

3.6.2 Determination of functional viral particles by anti-hexon staining

This method is based on the detection of positive cells for the immunostaining of the viral protein hexon in monolayers of HEK-293 cells infected with serial dilutions of the virus. This technique allows the determination of functional infective viral particles (Transducing Units, TU) in purified stocks and cell extract samples.

Serial 1:10 dilutions of the viral stock were prepared in DMEM 5% FBS in triplicates in a final volume of 100 µL in 96-well plates. HEK-293 cells (1×10^5 cells) were added to the wells in a volume of 50 µL and plates were incubated for 36 hours at 37ºC. Medium was removed by suction and the cells were dried for 5 minutes at RT. To fix and permeabilize the cells, 100 µL/well of cold methanol were added and incubated 10 minutes at -20ºC. Methanol was removed, and wells were washed twice with PBS^{++} containing 1% BSA. Cells were incubated for 1-2 hour at 37ºC with 1:5 diluted anti-hexon antibody obtained from the hybridoma 2Hx-2 (ATCC, Manasas, VA, USA). Cells were then washed thrice and incubated with an anti-mouse secondary antibody conjugated with the fluorochrome Alexa-488 (Thermo Fisher Scientific) diluted 1:500 for 1-2 hour. Finally, cells were washed three times and the viral titer was determined by counting stained cells using an inverted fluorescence microscope. To calculate the concentration of transducing units (TU) in the stock, the following formula was used:

$$Functional\ titer\ (TU/mL) = \frac{Mean\ of\ positive\ cells}{100\ \mu L} \times Dilution\ factor \times 1000\ \mu L$$

3.7 CHARACTERIZATION OF ONCOLYTIC ADENOVIRUSES

3.7.1 Isolation of viral DNA from infected cells (Hirt's)

This method has been used for the analysis and validation of the clones obtained in the plaque formation assay.

For this, A549 cells seeded in a 100 mm plate were infected with the corresponding adenovirus until complete CPE was observed. Cells were harvested and centrifuged 5 minutes at 1000 *g*. Supernatant was discarded and the cell pellet was resuspended in 1 mL of PBS. Cell suspension was pelleted again by centrifugation and resuspended in 350 µL of ddH_20. 350 µL of Hirt's solution 2X (10 mM Tris pH 8.0, 20 mM EDTA, 1.2% SDS, and 200

µg/mL of proteinase K) were added to the cell suspension and the sample was mixed and incubated for 1 hour at 56ºC. 200 µL of NaCl 5 M were added dropwise while vortexing, and the mixture was incubated at 4ºC for 8-16 hours until a white precipitate (corresponding to the cellular DNA) appeared. In order to eliminate this cellular DNA, the suspension was centrifuged for 30 minutes at 15000 *g* and 4ºC and the upper clear phase containing the viral DNA was collected. Incubation with RNAse at a final concentration of 100 µg/µL was carried out for 1 hour at 37ºC. Samples were mixed with one volume phenol-chloroform and centrifuged for 5 minutes at 13000 *g*. The upper phase containing the DNA was collected, mixed with two volumes of ethanol supplemented with 2% sodium oxaloacetate and incubated for 1 hour at -20ºC. Samples were centrifuged for 20 minutes at 13000 *g*, the supernatant was discarded and pellets were washed once with 70% ethanol. Finally, the supernatant was discarded and air-dried DNA pellets were resuspended in 25 µL TE pH 8.0.

3.7.2 Isolation of viral DNA from purified viral particles

This method has been used to verify the identity of each generated virus purified stock. 50 µL-aliquot of purified virus were used. Usually, an input of $2x10^{10}$ vp results in yields of 1 µg of viral DNA.

To this aliquot, we added:

- EDTA pH 8.0 (16 µL 0.5 M)
- SDS (20 µL 10%)
- Proteinase K (8 µL, 10 mg/mL)
- TE pH 8.0 up to 400 µL

Samples were incubated for 2 hours at 56ºC in order to dissociate viral particles. DNA was isolated by phenol-chloroform extraction and ethanol precipitation as described above. DNA pellets were resuspended in 25 µL TE pH 8.0.

3.7.3 Characterization of viral genomes by restriction enzymes

Genomes of recombinant adenoviruses were characterized by restriction analysis to confirm genome stability during amplification. For this, 500 ng of adenovirus DNA was digested with the corresponding restriction enzyme according to the manufacturer's

instructions. DNA from the parental adenovirus (*i.e.* ICO15K) was included as a control for comparison. Digestion patterns were evaluated by gel electrophoresis on 1% agarose gels.

3.7.4 Characterization of viral DNA by sequencing

Adenovirus genomes were sequenced to discard potential recombinations with the wild-type *E1a* present in HEK-293 cells during the transfection–mediated adenovirus rescue, and to discard mutations in the transgenes after the amplification process in A549 cells. The primers for the sequencing of the different regions of the adenovirus genomes are described in **Table 7.** Primers used for adenovirus and transgenes sequencing.

Span	Primer	Sequence (5'→ 3')	To sequence
Fiber	Fiber up	CAAACGCTGTTGGATTTATG	Transgenes inserted after fiber
	Fiber down2	GGCTATACTACTGAATGAA	
E4	Ad35566F	CACCACTCGACACGGCACCA	Transgenes inserted after E4
	Ad35825R	GGGCGGAGTAACTTGTATG	
Ad	Oligo7	GGAACACATGTAAGCGACGGATGTGG	Modified *E1a* promoter
	Ad670F	ATCTTCCACCTCCTAGCCAT	Δ24 mutation

Table 7. Primers used for adenovirus and transgenes sequencing.

Sequencing was performed with the BigDye™ Terminator v3.1 Cycle Sequencing Kit (Applied Biosystems, Thermo Fisher Scientific). For the sequencing setup, 10 µL-reaction mixes were prepared containing 100-200 ng DNA, 3.2 pmol of the primer, 2 µL 5X Sequencing Buffer, 2 µL Reaction Mix and ddH_2O to complete the final volume. The PCR conditions are listed in **Table 8.** PCR conditions for adenovirus and transgenes sequencing.

Stage	Description	Temperature	Time	Cycles
1	Initial denaturation	96ºC	1 minute	1
2	Denaturation	96ºC	30 seconds	24
	Annealing	50ºC	15 seconds	
	Extension	60ºC	2 minutes	
3	Pause	4ºC	∞	1

Table 8. PCR conditions for adenovirus and transgenes sequencing.

Reactions were sequenced by the core facility from the translational research laboratory at the Catalan Institute of Oncology or by Stabvida (Portugal).

4. PRODUCTION AND TITRATION OF LENTIVIRAL VECTORS

The lentiviruses used in this thesis were produced with 2nd or 3rd generation plasmids, described in **Table 9**. The plasmid pWPT-GFP was bought in Addgene and genetically modified to replace the GFP to encode human or murine FAP, generating the pWPT-hFAP and pWPT-mFAP, respectively. The plasmid pTRPE-CBG-T2A-GFP was kindly provided by Sònia Guedan (University of Pennsylvania).

Generation	Plasmid name	Plasmid type	Description
2nd	pMD2.g	Envelope	Encodes the VSV-G envelope
	pSPAx2	Packaging	Encodes the Gag, Pol, Rev and Tat proteins
	pWPT-hFAP or mFAP	Transfer	Encodes the human (hFAP) or murine FAP (mFAP)
3rd	pRSV-Rev	Packaging	Encodes the Rev protein
	pMDLg/pRRE	Packaging	Encodes the Gag and Pol proteins
	pMD2.g	Envelope	Encodes the VSV-G envelope
	pTRPE-CBG-T2A-GFP	Transfer	Encodes the click beetle green luciferase and GFP

Table 9. Plasmids for the generation of lentiviral vectors.

For lentivirus production, 293FT cells (8×10^6) were seeded in 15 cm plates in a total volume of 30 mL. The next day, the plasmids pMD2g (7 µg), pSPAx2 (14 µg) and the pWPT-hFAP/ mFAP (22 µg) for 2nd generation lentivirus and the plamids pRSV-Rev (18 µg), pMDLg/pRRE (18 µg), pMD2.g (7 µg) and the pTRPE-CBG-T2A-GFP plasmid (15µg) for 3rd generation lentivirus, were diluted in Opti-MEM (Gibco, Thermo Fisher Scientific) to a final volume of 1.4 mL and mixed with 60 µL plus reagent. The DNA mixture was added drop-wise into a tube containing 1.4 mL Opti-MEM and 60 µL Lipofectamine LTX (Thermo Fisher Scientific), and the tubes was mixed by finger vortexing. Transfection mixtures were incubated at RT for 20 minutes. After incubation, the medium from the 293FT cultures was removed and transfection mixtures were added drop-wise to the cells in order to cover the

whole monolayer. After one-minute incubation, 30 mL fresh medium was added to the plate. 24 hours post-transfection, the medium was harvested and stored at 4°C and fresh medium was added to the plates. The next day, the medium was harvested and both 24h and 48h supernatants were filtered through 0.45 µM filter units. Lentivirus preparations were concentrated by ultracentrifugation for 2 hours at 20000 rpm (82705 *g*) and 4°C with a SW28 Ti rotor (Beckman Coulter), supernatants were discarded and each virus pellet was resuspended in 200-400 µL RPMI 10% FBS. Aliquots (20-50 µL) were stored at -80°C.

TRPE-CBG-T2A-GFP-expressing lentiviral stocks were titrated on Jurkat cells. For this, 1:3 dilutions of the lentivirus in a final volume of 100 µL were prepared in 96-well plates. Jurkat cells (2×10^4) were seeded into each well and plates were incubated at 37°C for 72 hours. CBG-expressing Jurkat cells were evaluated by flow cytometry and the percentage of GFP^+ cells was determined for each dilution. To calculate the titer for each lentiviral preparation, the following formula was used:

$$Titer\ (TU/mL) = OD_{260\,nm}\left(\frac{\%\ positive\ cells}{100}\right) \times (2 \times 10^4\ cells) \times 20 \times Dilution$$

5. RECOMBINANT ADENOVIRUS-BASED *IN VITRO* ASSAYS

5.1 ADENOVIRUS-MEDIATED CYTOTOXICITY ASSAY

Different human or mouse cell lines (between 1.5×10^4 to 3×10^4 depending on the cell type) were seeded in 96-well plates in DMEM supplemented with 5% FBS. Cells were infected with serial dilutions of the parental virus (ICO15K) or the modified viruses starting from 200-1000 TU/cell. At day 4-6 post-infection plates were washed with PBS and stained for total protein content with the bicinchoninic acid (BCA) kit (Pierce Biotechnology). Absorbance was determined and the percentage of cell survival was calculated by normalization to the absorbance values of uninfected wells. The inhibitory concentration 50 (IC_{50}) was calculated with GraphPad Prism v6.02 (GraphPad Software Inc.) by using a dose-response non-linear regression with variable slope.

5.2 ADENOVIRUS PRODUCTION ASSAY

A549 (1×10^5) were seeded in 24-wells plates and incubated overnight. The next day, one of the wells was trypsinized and the total number of cells was determined. Cells were

infected with ICO15K, ICO15K-IIIa-FBiTE or ICO15K-40SA-FBiTE at an MOI of 20 in a final volume of 500 µL for 72 hours. After incubation, the cells were collected together with the supernatant and cell extracts were prepared by 3x freeze/thaw cycles. The functional titer was determined with the anti-hexon staining method (see section 3.6.2). Results are expressed as the number of TU produced by a single cell, taking into account the functional titer and the number of cells at the day of the infection.

5.3 PRODUCTION OF SUPERNATANTS

A549 cells ($1x10^7$) were seeded in 100 mm culture plates. When plates had 90% of confluence, medium was removed and cells were infected at MOI of 20 with ICO15K, or ICO15K-modified viruses in a final volume of 10 mL of DMEM supplemented with 5% FBS. 72h post-infection, supernatants were collected and centrifuged 5 min at 500 *g* to eliminate detached cells. Supernatants from uninfected cells were used as a mock control. For binding assays, supernatants were concentrated (approximately 20x) with Amicon Ultra-15 filter units with a molecular weight cutoff of 30 kDa (Merck Millipore) according to manufacturer's instructions. Aliquots of the supernatant were stored at -20°C for future analysis.

5.4 IMMUNOLOGY TECHNIQUES

5.4.1 Antibodies and flow cytometry

Flow cytometry analysis was performed with a Gallios cytometer (Beckman Coulter). The antibodies used in this thesis are listed and described in **Table 10**. Surface staining and washes were performed in PBS supplemented with 5% FBS and 0.01% NaN_3. Cells were stained cell viability with LIVE/DEAD fixable stain (Thermo Fisher Scientific) according to the manufacturer's instructions. For indirect surface staining, primary antibodies or isotype controls were incubated for 30 minutes on ice, followed by three washing steps and incubation with fluorochrome-coupled secondary antibodies for 30 minutes on ice. Direct surface staining was performed for 30 min on ice. All flow cytometry data were analyzed with the FlowJo software v7.6.5 and v10 (Tree Star).

Antibody	Specie	Clonality	Company	Concentration	Application
Anti-FLAG	Mouse	Monoclonal (M2)	Sigma-Aldrich	5µg/mL	Binding assays
Normal mouse IgG1a	Mouse	-	Santa Cruz Biotechnology	5µg/mL	Binding assays
Anti-FLAG	Rabbit	Polyclonal	Sigma-Aldrich	5µg/mL	Binding assays
Normal rabbit IgG	Rabbit	-	Santa Cruz Biotechnology	5µg/mL	Binding assays
Anti-HIS TAG	Mouse	Monoclonal (13/45/31-2)	Dianova	2µg/mL	Toxins detection by Western Blot
FITC anti-HIS TAG	Mouse	Monoclonal (13/45/31-2)	Dianova	5µg/mL	Toxins detection by flow cytometry
73.3	Mouse	-	-	5µg/mL	mFAP detection
Hybridoma F19	Mouse	-	-	100 µL	hFAP detection
Alexa Fluor 488 anti-mouse IgG	Goat	Polyclonal	Thermo Fisher Scientific	5µg/mL	Binding assays
Alexa Fluor 647 anti-mouse IgG	Goat	Polyclonal	Thermo Fisher Scientific	5µg/mL	Binding assays
Alexa Fluor 647 anti-Rabbit IgG	Goat	Polyclonal	Thermo Fisher Scientific	5µg/mL	Binding assays
APC streptavidin	-	-	Biolegend	2µg/mL	hFAP detection
Conj-anti-human CD3	Mouse	Monoclonal (OKT3)	Biolegend	Titration-dependent	T-cell proliferation
Conj-anti-human CD4	Mouse	Monoclonal (OKT4)	Biolegend	Titration-dependent	T-cell proliferation
Conj-anti-human CD8	Mouse	Monoclonal (SK1)	Biolegend	Titration-dependent	T-cell proliferation
Conj-anti-human CD45	Mouse	Monoclonal (H130)	Biolegend	Titration-dependent	T-cell proliferation

Table 10. List of antibodies used for flow cytometry.

5.4.2 Preactivation and expansion of human T cells

T cells were isolated as described in section 2.6. For stimulation, human T cells (1×10^6 cells/mL) were cultured with CD3/CD28 activating Dynabeads (Thermo Fisher Scientific) at a 1:3 bead-to-cell ratio. On day 3 after bead stimulation, T-cell cultures were fed with ¾ culture volumes of fresh medium. On day 5 after bead stimulation, beads were removed by placing the cultures on DynaMag-15 magnet (Thermo Fisher Scientific) and recovering the supernatants. Cells were counted with the TC20 automated counter by setting the gates from 8 µM to 14 µM (resting T cells have a mean diameter of 6 µM, whereas proliferating T cells have a mean diameter of 10 µM), and cultures were set to 1×10^6 cells/mL. From this day on, cells were fed daily to a concentration of 8×10^5 cells/mL. Cells were maintained in culture until day 10-11 after bead stimulation, when they were still in

the expansion phase and just before they returned to a resting state. Aliquots (1-10 × 10^7 cells) were cryopreserved in FBS supplemented with 10% DMSO.

5.4.3 Generation of genetically-modified T cells

For the generation of luciferase- T cells, transduction with the corresponding lentiviral vectors was carried out 24 h after bead-mediated T-cell activation (see section 5.4.2). For the generation of luciferase-expressing T cells, cultures were infected with the CBG-T2A-GFP vector at an MOI of 7.5. Transduced T-cell cultures were expanded and handled as described in section 5.4.2. T-cell preparations were characterized for the expression of the transgene and phenotyped for CD4 and CD8 T-cell subpopulations by flow cytometry (see section 5.4.1).

5.4.4 Binding assays

Target cells (2 × 10^5) or effector cells (1 × 10^5) were incubated with the different supernatants for 1 h on ice. Cells were washed 3x followed by incubation with the monoclonal M2 anti-FLAG antibody (Sigma Aldrich) for BiTE detection or with the monoclonal FITC anti-His tag (Dianova) for toxin detection for 30 minutes on ice. IgG1 isotype (Santa Cruz Biotechnology) was used as a control. Cells were washed 3x and anti-FLAG bound antibodies were detected by incubating cells with an Alexa Fluor 488- or 687-coupled goat anti-mouse IgG secondary antibody (Thermo Fisher Scientific) for 30 min on ice. Cells were evaluated by flow cytometry and 10000 events were acquired.

5.5 CO-CULTURE-BASED *IN VITRO* ASSAYS

5.5.1 T-cell activation assays

To evaluate human T-cell activation induced by the supernatants from virus-infected cells, cancer cells (3 × 10^4) and T cells (1.5 × 10^5) were seeded in 96-well plates in 100 µL medium. Co-cultures were mixed with 100 µL of the supernatants and incubated for 24h. Coculture supernatants were harvested, centrifuged at 500 *g* for 5 min to discard cells, and stored at -80°C. Supernatants were assessed for human cytokines IFN-ɣ, TNF-α, and IL-2 using the ELISA MAX Deluxe set (Biolegend), following the manufacturer's protocol.

5.5.2 T-cell proliferation assay

To asses T-cell proliferation induced by the supernatants from virus infected cells, cancer cells (3×10^4) and CFSE-labeled PBMCs or T cells (1.5×10^5) were seeded in 96-well plates in 100 µL medium. Co-cultures were mixed with 100 µL of the supernatants and incubated for 6 days (PBMCs) or 3 days (T cells). Cells were then stained for cell viability with LIVE/DEAD fixable stain (Thermo Fisher Scientific) followed by incubation with an anti-CD4 and anti-CD8 antibodies. Flow cytometry analysis was performed by acquiring 20000 events per sample.

5.5.3 Cell-mediated cytotoxicity assays

5.5.3.1 CFSE-cytotoxicity assay

CFSE-labeled target cells (3×10^4) were co-cultured with T cells (1.5×10^5) in 100 µL medium in 96-well plates. Co-cultures were mixed with 100 µL of the supernatants and incubated for 24 h. Co-cultures were trypsinized and stained with LIVE/DEAD fixable stain (Thermo Fisher Scientific) for 30 min at RT. After washing, cells were analyzed by flow cytometry and the percentage of $CFSE^+$/LIVE/$DEAD^+$ cells was determined. 10000 $CFSE^+$ events were acquired for each sample.

5.5.3.2 Bystander killing assay

For bystander killing assays, CFSE-labeled FAP-negative cells were cultured in the presence of T cells and its derivative mFAP or hFAP cells (E:T=5) and 100 µL of supernatants were added. After 24h, cells were trypsinized and stained with LIVE/DEAD fixable stain (Thermo Fisher Scientific) for 30 min at RT followed by incubation with an anti-CD45 antibody. mFAP- and hFAP-expressing cells were identified as a CFSE- hCD45- double negative cells. The percentage of $CFSE^+$/LIVE/$DEAD^+$ cells and $CFSE^{-/}hCD45^-$/LIVE/$DEAD^+$ cells was determined.

FBiTE-mediated cytotoxicity of FAP-positive non-infected cells was assessed infecting A549 cells in suspension with ICO15K or ICO15K-FBiTE (MOI=20). After 4 hours, infected cells were washed thrice with PBS. $3x10^4$ A549-infected cells were mixed with $3x10^4$ CFSE-labeled target cells (1:1), T cells (E:T=5) and supernatants (100 µL). After three days of incubation, co-cultures were stained and analyzed as described above.

5. *IN VIVO* ASSAYS WITH RECOMBINANT ADENOVIRUSES

5.6 MOUSE MODELS AND PROCEDURES

All the animal studies were performed at the IDIBELL facility (AAALAC unit 1155) and approved by the Ethics Committee for Animal Experimentation from Biomedical Research Institute of Bellvitge (IDIBELL).

For the realization of this work, male or female NOD/*scid*/*IL2rg*$^{-/-}$ (NSG) mice (bred in house) were used for the antitumor efficacy and biodistribution studies and female SCID/beige mice (Envigo) were used for transgene expression experiments. In all cases, 6-8 week-old mice with a body weight between 15 and 30 g were used. A549 ($4x10^6$), HPAC ($2x10^6$) or CMT-64.6 ($2x10^6$) cells were subcutaneously injected to both flanks. Once tumors reached a median volume of 120 mm^3, mice were randomized and treated as corresponded.

To evaluate T-cell trafficking to the tumor, mice bearing A549 tumors were treated intratumorally with PBS, ICO15K, or ICO15K-IIIa-FBiTE ($1x10^9$ vp/tumor). Four days later, $1x10^7$ preactivated GFP- and CBG-luciferase-expressing T cells (LUC-T-cells) were intravenously injected to treated mice. Mice were given an intraperitoneal injection of 15mg/mL D-luciferin potassium salt solution (Byosinth AG) and imaged daily for 7 days using IVIS Lumina XRMS Imaging System (PerkinElmer). Tumor radiance was measured by drawing a region of interest around the tumor contour.

For antitumor efficacy studies, mice were treated intratumorally with PBS, ICO15K, ICO15K-IIIa-FBiTE or ICO15K-40SA-FBiTE ($1x10^9$ vp/tumor). Four days later, $1x10^7$ preactivated T cells were intravenously injected once (A549) or twice (HPAC) to all mice. Tumors were measured twice or thrice a week with a digital caliper and tumor volume was determined with the equation V (mm^3) = $\pi/6 \times W^2 \times L$, where W and L are the width and the length of the tumor, respectively.

To evaluate transgene expression in the tumor, mice were treated intratumorally with PBS, ICO15K-IIIa-cLUC or ICO15K-40SA-cLUC ($1x10^9$ vp/tumor). Mice were given an intraperitoneal injection of 15mg/mL D-luciferin potassium salt solution (Byosinth AG) and imaged at day 3, 7, 12 and 15 after treatment using IVIS Lumina XRMS Imaging System

(PerkinElmer). Tumor radiance was measured by drawing a region of interest around the tumor contour.

5.7 DETECTION OF TRANSCRIPTS IN TUMORS BY REAL-TIME PCR

Frozen tumor samples were disrupted using a mortar and pestle under liquid nitrogen. RNA and DNA were isolated from approximately 25 mg of homogenized tissue with the DNA/RNA/protein kit (IBI Scientific). RNA samples were treated with the TURBO DNA-*free* kit (Thermo Fisher Scientific) to remove traces of genomic DNA. RNA (1µg) was retrotranscribed with the High-Capacity cDNA Reverse Transcription kit (Thermo Fisher Scientific). Real-time analysis was performed in a LightCycler 480 Instrument II (Roche). To quantify the viral genomes and FBiTE transcripts in the tumor, 100ng of DNA and 40ng of cDNA in the presence of SYBR Green I Master (Roche) were used, respectively. Standard curves for viral genomes and FBiTE were prepared by serial dilutions of known copy numbers of adenovirus plasmid and pUC57-FBiTE, respectively. The primers used for the detection of virus and FBiTE cDNA are listed in **Table 11** and PCR conditions are listed in **Table 12**. To assess murine FAP expression, 25 ng of cDNA were analyzed with the TaqMan Gene Expression Assay ref. Mm01329177_m1 (Thermo Fisher Scientific). A standard curve was prepared by serial dilutions of known copy numbers of a murine FAP-expressing plasmid. Human FAP-expressing plasmid was also included as negative control. The primers used for the detection of FAP cDNA are listed in **Table 11** and PCR conditions are listed in **Table 13**. In all cases, non-retrotranscribed RNA samples, in a quantity equivalent to the amount cDNA loaded in the PCR, were used for PCR to discard genomic DNA contamination.

Gene	Sequence 5'→3'	Description
Ad18852	CTTCGATGATGCCGCAGTG	For the detection of viral genome
Ad19047R	ATGAACCGCAGCGTCAAACG	For the detection of viral genome
qBiTEF	CGGCGAGAAAGTGACAATGAC	For the detection of FBiTE
qBiTER	TTGGTGAGGTGCCACTTTTC	For the detection of FBiTE

Table 11. Primers used for the detection of viral genomes and FBiTE molecules.

Stage	Description	Temperature	Time	Cycles
1	Activation	95ºC	10 minutes	1
2	Amplification cycles	95ºC	15 seconds	40

		60ºC	1 minute	
		72ºC	7 seconds	

Table 12. PCR conditions for the detection of viral genomes and FBiTE molecules.

Stage	Description	Temperature	Time	Cycles
1	Activation	50ºC	2 minutes	1
		95 ºC	10 minutes	
2	Amplification cycles	95ºC	15 seconds	40
		60ºC	1 minute	

Table 13. PCR conditions for the detection of FAP cDNA.

5.8 IMMUNOHISTOCHEMISTRY OF OCT-EMBEDDED TUMOR SECTIONS

To detect FAP and E1A-Adenovirus expression in tumors, immunohistochemistry (IHC) was performed using OCT-embedded sections (5 µm thick) of freshly frozen tumor tissues. Sections were fixed 5 minutes with 2% of PFA at room temperature and endogenous peroxidases were blocked by incubation in 3% H_2O_2. Next, sections were blocked for 1 hour with 10% of normal goat serum diluted in 1% BSA, PBS-Tween. All the incubations were performed in a humidity chamber. For FAP detection, primary antibody incubation was performed overnight at 4ºC using a biotinylated polyclonal sheep anti-human/mouse FAP antibody (5µg/mL) or its isotype sheep IgG (R&D systems) in PBS with 5% of goat serum. For adenovirus detection, the primary antibody used was an anti-Ad2/5 E1A antibody (Santa Cruz Biotechnology) diluted 1/200 in PBS. The next day, sections were incubated with ABC-HRP kit (Vectastain) for 30 min, followed by 5 min incubation with DAKO-DAB substrate (EnVision). Slides were dehydrated using standard protocols and counterstained with hematoxylin. Section were mounted in DPX (VWR International).

6. STATISTICAL ANALYSIS

Statistical analyses were performed using GraphPad Prism software v6.02. All results were expressed as means ±SD or SEM, as indicated. One-way ANOVA with Tukey *post hoc* test was used for differences between three or more groups in a single condition or time point. $P < 0.05$ was taken as the level of significance.

RESULTS

1. OPTIMIZATION OF REPLICATION-DEPENDENT TRANSGENE EXPRESSION FROM AN ONCOLYTIC ADENOVIRUS

1.1 GENERATION AND CHARACTERIZATION OF LUCIFERASE-EXPRESSING ONCOLYTIC ADENOVIRUSES

Oncolytic viruses are promising anticancer agents because they selectively kill cancer cells and multiply within a tumor, but their clinical benefit has so far been modest urging for development of new strategies with enhanced oncolytic efficacy. Their oncolytic potency might be improved by expressing a therapeutic gene from the virus genome, and both the mode of transgene expression and the locale of transgene insertion into the virus genome critically determine the efficacy of this approach. Although different oncolytic adenovirus armed with transgenes have already been tested in our laboratory, the needed of stronger levels of transgene expression without impairing the replication of the virus has been evident (Fajardo et al. 2017; Sonia Guedan et al. 2010).

The main goal of this project was to optimize the transgene expression inserted in the ICO15K oncolytic adenovirus without affecting its cytotoxic capacities. The ICO15K was previously developed in our laboratory and it incorporates palindromic E2F-1-binding sites in the E1A promoter and bears an RGDK motif replacing the KKTK heparan sulfate glycosaminoglycan-binding domain in the fiber shaft (J. J. Rojas et al. 2012). As this virus has shown favorable toxicity profiles and good tumor targeting *in vivo,* we chose it as a platform to incorporate into its genome all the transgenes tested in the present thesis.

In order to establish a strategy to exploit the adenoviral major late promoter (MLP) for transgene expression, we proposed the generation of the following panel of viruses (**Figure 14A**). To be able to visually an easily quantify the expression of the transgenes, we first decided to use the Cleek Beetle Green (CBG) luciferase as a transgene. We then inserted the luciferase gene under two different splicing acceptors, the IIIa and the 40SA. The IIIa splicing acceptor, which has been used in previous works in our laboratory, is the 3VDE endogenous splicing acceptor for the IIIa protein of the Adenovirus 5 (Ad5). In contrast, 40SA is the splicing acceptor of the long fiber gene of the Ad40 and has been reported to be an strong splicing acceptor (Carette et al. 2005). Both sequences are shown in **Figure 14B.** Moreover, we also tested the effect of these two splicing acceptors in two different

locations, after the fiber gene or between the E4 cassette and the RITR. The after-fiber location is closer or more proximal to the MLP than the after-E4 location. Thus, the ICO15K-IIIa-cLUC, the ICO15K-40SA-cLUC (which the transgenes are inserted after the fiber), the ICO15K-E4-IIIa-cLUC and the ICO15K-E4-40SA-cLUC (which the transgenes are located after the E4) oncolytic adenoviruses were generated (**Figure 14A**).

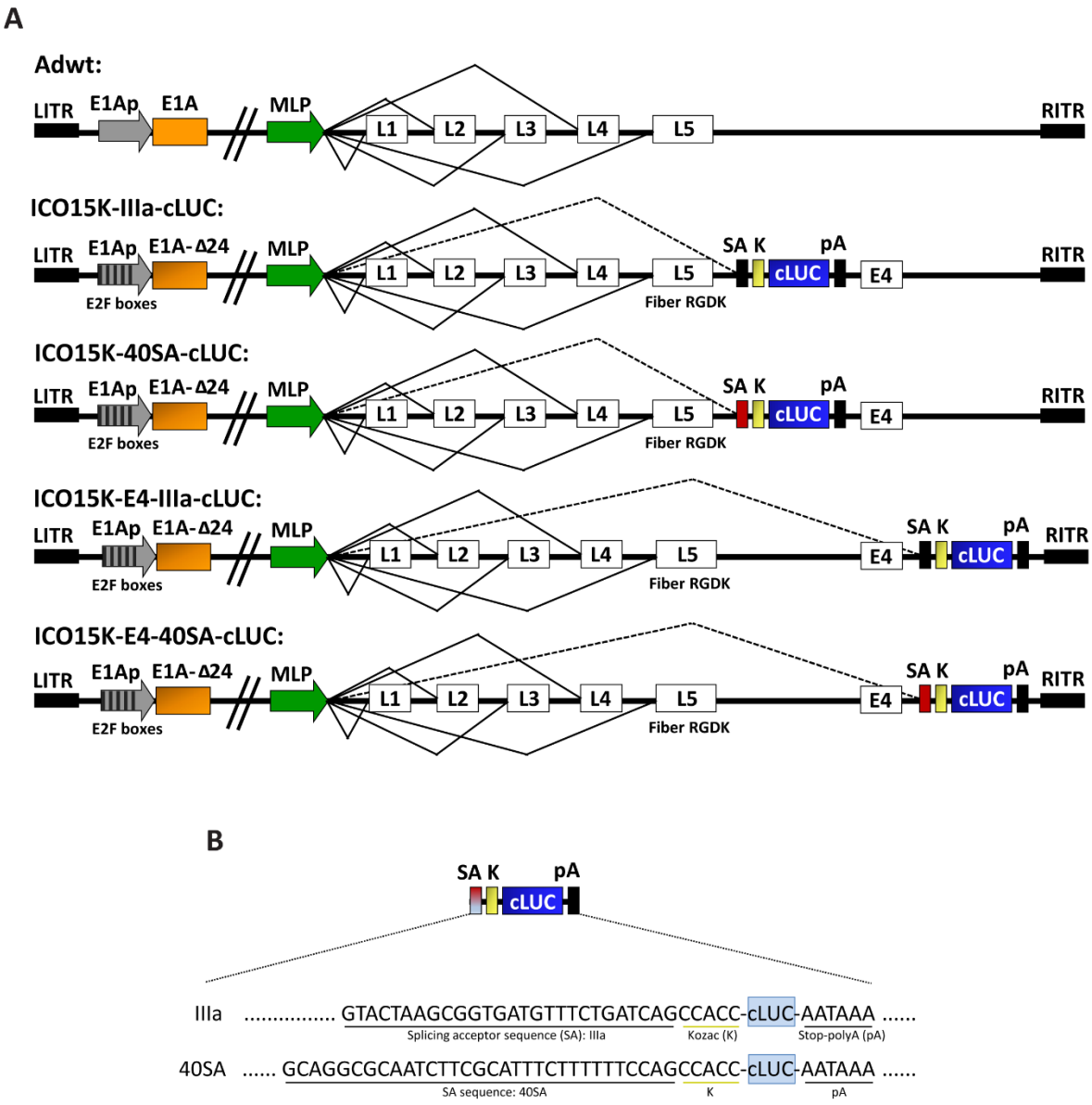

Figure 14. Schematic representation of the oncolytic adenoviruses used in this project. A. Main genetic modifications of each virus are highlighted. Adwt is the human Ad5 wild type virus; ICO15K-IIIa-cLUC, ICO15K-40SA-cLUC, ICO15K-E4-IIIa-cLUC and ICO15K-E4-40SA-cLUC are oncolytic adenoviruses which contain the modified E1a promoter (including four E2F boxes and one Sp1 box), the truncated E1A protein and the RGDK fiber to confer selectivity for tumor cells. All modified viruses contain the cLUC expression cass ette, but in the ICO15K-IIIa-cLUC the gene is inserted after the fiber and under the IIIa splicing acceptor (black SA box). The ICO15K-40SA-cLUC the gene is also after fiber, but under the 40SA splicing acceptor (red SA box). In contrast,

cLUC gene in ICO15K-E4-IIIa-cLUC and the ICO15K-E4-40SA-cLUC viruses is inserted after the E4 cassette with the splicing acceptor IIIa or 40SA, respectively. **B.** Sequences of the both IIIa (black boxes) and 40SA (red boxes) splicing acceptors.

Once the modified viruses were generated, amplified and purified, a comparative study was performed to characterize the effects and expression levels of the cLUC insertion in the two different locations and with two different splicing acceptors. The viral cytotoxic properties and the level of the transgene expression in two different *in vitro* and *in vivo* models were compared. The reference physical and functional titers obtained of the purified viruses (only after fiber viruses) are presented in **Table 14**. Similar physical and functional titers were obtained between viruses, which would facilitate its comparation for the *in vivo* applications. Further *in vitro* experiments were carried out with clarified cell extracts (CCE).

Virus	Physical titer (vp/mL)	Functional titer (TU/mL)	Physical:Functional ratio
ICO15K	2.1×10^{12}	2.06×10^{11}	10.19
ICO15K-IIIa-cLUC	1.06×10^{12}	1.20×10^{11}	8.84
ICO15K-40SA-cLUC	2.36×10^{12}	1.27×10^{11}	18.62

Table 14. Characterization of purified viruses used in *in vivo* assays.

The first feature to analyze was the cytotoxic profile between the parental and the four recombinant ICO15K viruses. To this end, the human A549 and the murine CMT-64.6 cell lines were infected in serial dilutions with all described-above viruses. These two cell lines were chosen to compare the level and persistence of the transgene expression between a highly sensitive cell line (A549) and a highly resistant murine cell line (CMT-64.6). Surprisingly, in the most permissive A549 model, both ICO15K-IIIa-cLUC and ICO15K-40SA-cLUC, which cLUC was inserted after fiber, were significantly less cytotoxic than the other 3 oncolytic viruses (**Figure 15**, left panel, the lower cytotoxicity or higher impairment is observed as shift of the curve to the right). Moreover, carrying the 40SA splicing acceptor after the fiber seems to induce the highest impairment. However, in the murine CMT-64.6, which is a semi-permissive cell line, although we observed a similar cytotoxic profile, differences were much less relevant (**Figure 15**, right panel). Overall, the *in vitro* potency

was more affected when cLUC gene was inserted after fiber compared to the viruses where the same gene was inserted after E4 into the genome.

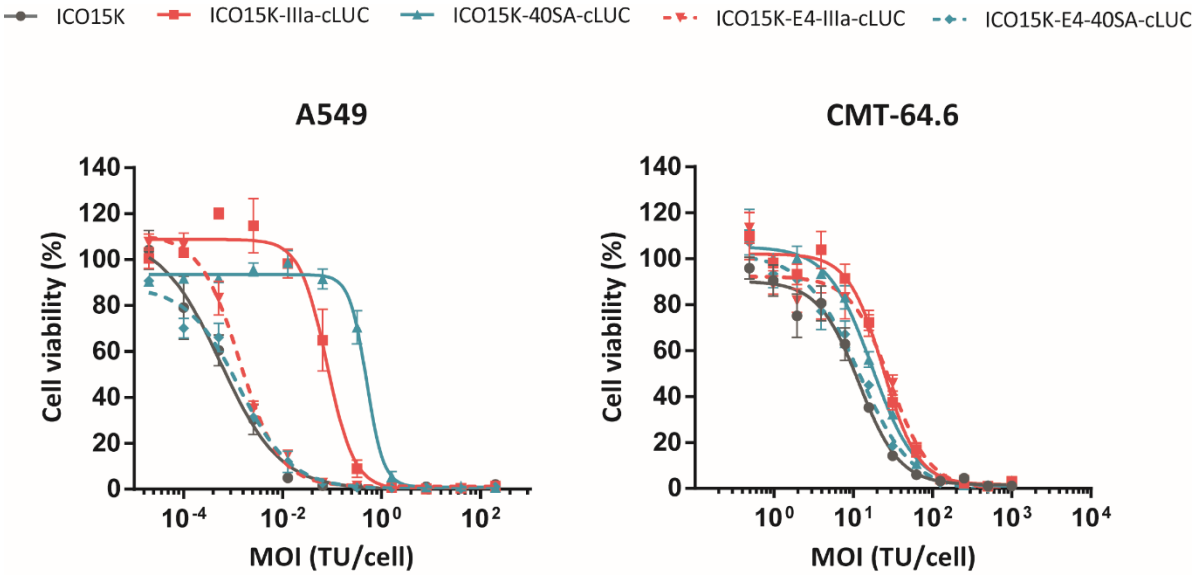

Figure 15. Cytotoxicity profile of the different cLUC-expressing viruses. A549 and CMT-64.6 cell lines were infected with serial dilutions, ranging from 200 (A549) or 1000 (CMT-64.6) to 0 MOIs, with the ICO15K, ICO15K-IIIa-cLUC, ICO15K-40SA-cLUC, ICO15K-E4-IIIa-cLUC or ICO15K-E4-40SA-cLUC viruses. After 6 (A549) or 7 days (CMT-64.6) post-infection, cell viability was determined by BCA staining. Mean ± SD of triplicates is plotted.

Next, we sought to test the magnitude and timing of the transgene expression by the different modified-viruses. For this purpose, we infected A549 cells with ICO15K-IIIa-cLUC, ICO15K-40SA-cLUC, ICO15K-E4-IIIa-cLUC or ICO15K-E4-40SA-cLUC viruses and luciferase activity was determined at 12, 24, 48 and 72 hours post-virus infection. At 12 hours post-infection, ICO15K-40SA-cLUC luciferase activity was already 3.5-fold superior compared to the other three viruses. Importantly, these differences were increasing during the time, reaching as much as 100-fold compared to the ICO15K-IIIa-cLUC, 5400-fold compared to the ICO15K-E4-40SA-cLUC and 24000-fold compared to the ICO15K-E4-IIIa-cLUC (**Figure 16**). Remarkably, both viruses with the cLUC gene inserted between E4 and RITR (distal to the MLP) showed significant less luciferase activity compared to the ones with after-fiber cLUC insertion (proximal to the MLP). These results indicate therefore that after-fiber location favors higher levels of transgene expression compared to E4 location. Regarding the splicing acceptor, we observed that the 40SA was significant stronger than the IIIa splicing acceptor. This data is consistent with those of Carette *et al*, who also reported

strong luciferase activities when using the 40SA splicing acceptor (Carette et al. 2005). Therefore, the cytotoxicity and expression results suggest that the more gene expression is achieved the lower is the cytotoxicity. If so, the inverse correlation between replication and transgene expression will pose the dilemma of which of these two parameters favor when arming an OAd to improve efficacy.

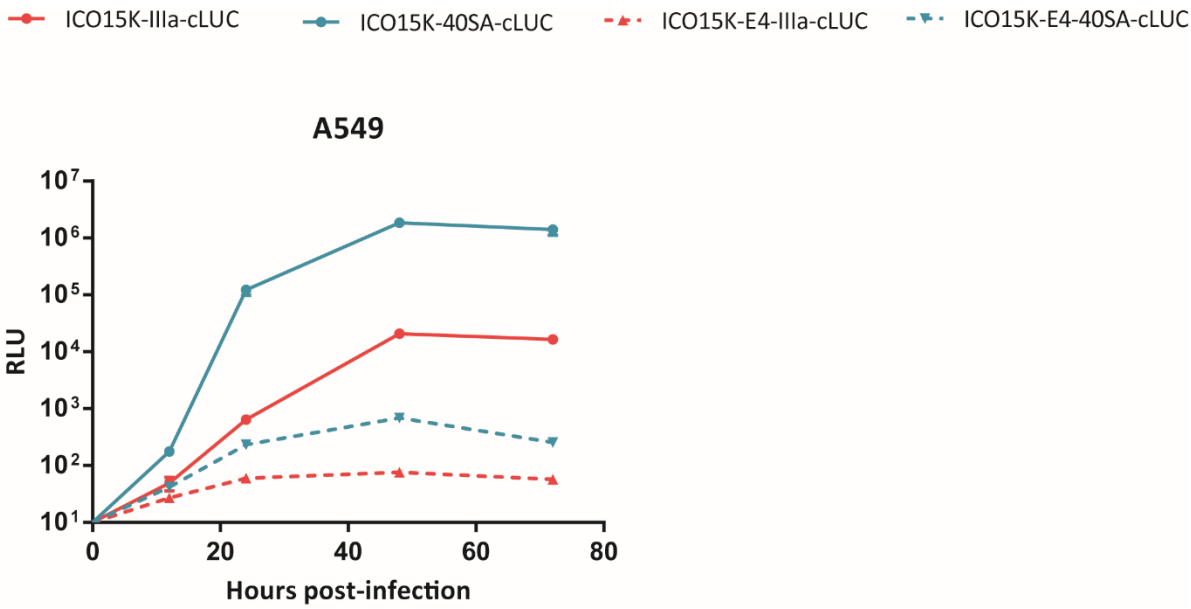

Figure 16. Kinetics and efficiency of transgene expression by recombinant viruses. A549 cells were infected with ICO15K, ICO15K-IIIa-cLUC, ICO15K-40SA-cLUC, ICO15K-E4-IIIa-cLUC or ICO15K-E4-40SA-cLUC at MOI 5 and luciferase activities were determined at indicated time points. Mean RLU logarithmic values ± SD of triplicates is shown.

1.2 CHARACTERIZATION OF TRANSGENE EXPRESSION *IN VIVO*

Once the *in vitro* comparative study between the different viruses was performed, we chose the ICO15K-IIIa-cLUC and ICO15K-40SA-cLUC as a candidate to test the transgene expression kinetics and the antitumor efficacy in a semi-permissive CMT-64.6 and a permissive A549 *in vivo* models. Hence, both CMT-64.6 and A549 tumors were implanted in scid-beige mice and when they reached a volume of 120mm^3, mice were intratumorally injected with the candidate viruses. After virus treatment, luciferase activity for *in vivo* bioluminescence imaging (IVIS) and tumor size were monitored. As shown in **Figure 17A**, both ICO15K-IIIa-cLUC and ICO15K-40SA-cLUC showed luciferase activity *in vivo*. However, and according with our earlier observation *in vitro*, the engineered ICO15K-40SA-cLUC virus showed remarkably more luciferase expression compared to its counterpart ICO15K-IIIa-

cLUC. None of the modified viruses significantly improved tumor growth when using CMT-64.6 semi-permissive cell line (**Figure 17B**). This lack of improved efficacy was expected as replication in the mouse model is too low to obtain efficacy and arming the virus with cLUC was not expected to add efficacy.

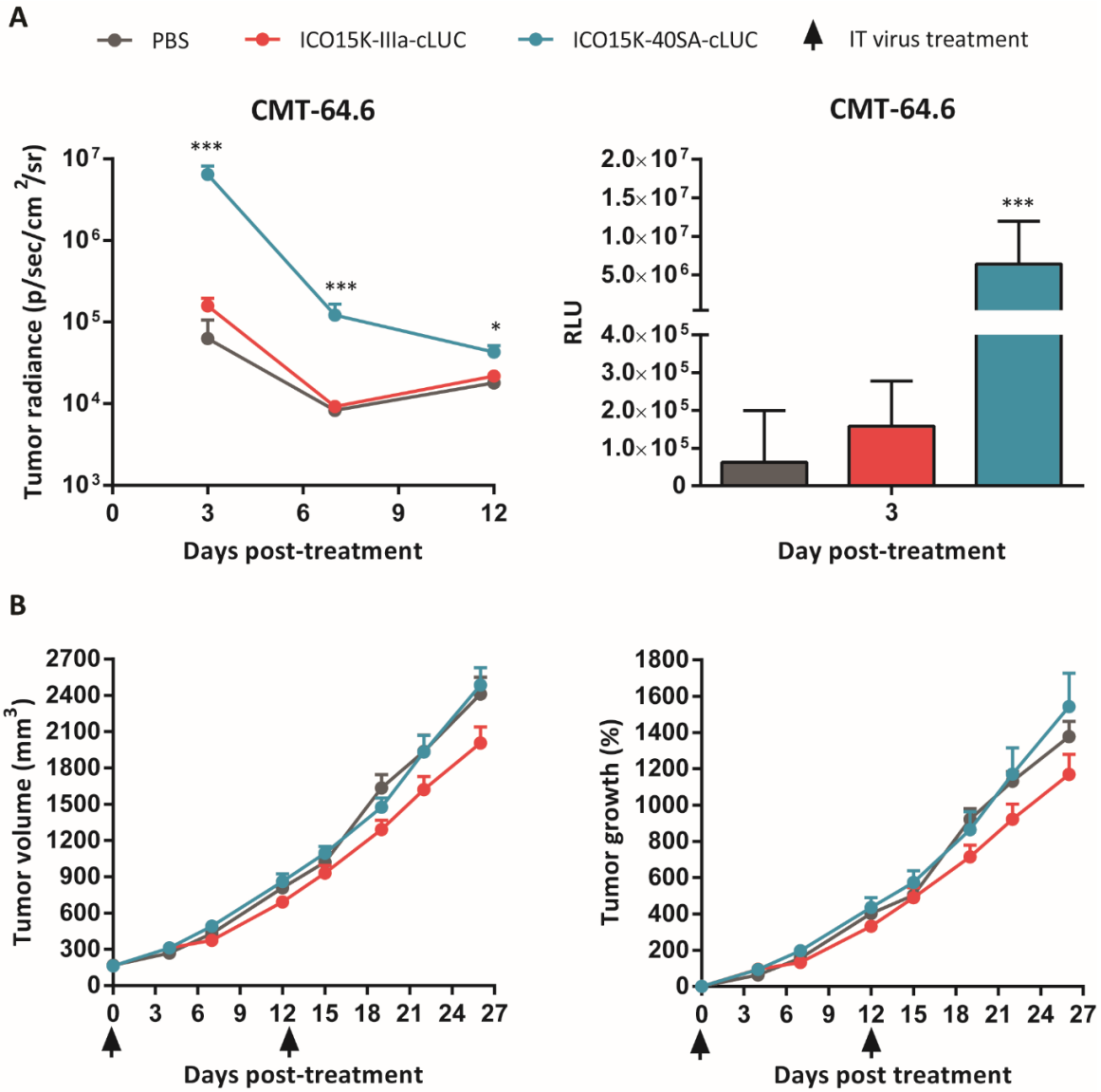

Figure 17. Efficacy and kinetics of luciferase activity *in vivo*. Subcutaneous CMT-64.6 xenografts were treated intratumorally with 2 x 10^9 vp/tumor of PBS, ICO15K, ICO15K-IIIa-cLUC or ICO15K-40SA-cLUC viruses. **A.** Comparative luciferase expression in different viruses was measured by *in vivo* imaging system (IVIS) at days 3, 6 and 12 after virus injection. **B.** Tumor size was measured every 3-4 days after tumor treatment. The mean tumor volume or tumor growth ± SEM of ≥ 10 tumors per group is shown. *, significant ($P < 0.05$) and ***, significant ($P < 0.0001$) by one-way ANOVA test with *post hoc* analysis of ICO15K-40SA-cLUC compared to PBS and ICO15K-IIIa-cLUC groups.

1.3 IMPACT OF TRANSGENE EXPRESSION FROM AN ONCOLYTIC ADENOVIRUS IN THERAPEUTIC EFFICACY *IN VIVO*

In order to determine whether improved significant transgene expression *in vitro* and *in vivo* using 40SA instead of the IIIa-splicing acceptor could favor the antitumor efficacy, we replaced the cLUC transgene for a therapeutic transgene. To assess the differences in antitumor efficacy, we first decided to use the cBiTE transgene, which has already been validated by Fajardo *et al*, for a therapeutic *in vivo* assay (Fajardo et al. 2017). cBiTE is a recombinant protein composed of two scFv connected through a flexible linker. One of the scFv recognizes the tumor-associated antigen EGFR, whereas the second scFv bind to the CD3 subunit in the T-cell receptor (TCR). As cBiTE has the ability to redirect T cells to kill $EGFR^+$-cancer cells, we hypothesize that higher amounts of cBiTE molecules within the tumor would increase T-cell activation and proliferation, improving therefore the overall antitumor efficacy. For this purpose, we then used the ICO15K-cBiTE (inserted after-fiber, under the splicing acceptor IIIa) from Fajardo *et al,* and the ICO15K-40SA-cBiTE and ICO15K-E4-40SA-cBiTE were generated, amplified and purified. Purified cBiTE-expressing viruses showed similar physical and functional titers (**Table 15.** Characterization of purified viruses used for the antitumor efficacy assay. Then, NSG mice bearing A549 tumor were treated with PBS or 2 x 10^9 vp/tumor of ICO15K-IIIa-cBiTE, ICO15K-40SA-cBiTE or ICO15K-E4-40SA-cBiTE, and after four days, all mice received an infusion of PBMCs. Tumor volume was regularly monitored. Unexpectedly, although significant higher expression of cBiTE molecules of ICO15K-40SA-cBiTE compared to the other viruses, it could not reduce tumor growth (**Figure 18**). This lack of efficacy could be given by the decreased cytotoxic capacities of the ICO15K-40SA-cBiTE shown *in vitro* (**Figure 15**), when using the 40SA-cLUC-expressing virus), which the infusion of T cells helped to compensate its loss, but not to improve the overall antitumor efficacy, or it could also be for an insufficient disponible functional T cells, which even haven high amounts of functional cBiTE molecules in the tumor, the lack of T cells would limit its complete therapeutic potential.

Virus	Physical titer (vp/mL)	Functional titer (TU/mL)	Physical:Functional ratio
ICO15K	2.1 x 10^{12}	2.06 x 10^{11}	10.19
ICO15K-IIIa-cBiTE	3.32 x 10^{12}	1.68 x 10^{11}	19.8
ICO15K-40SA-cBiTE	1.40 x 10^{12}	7.66 x 10^{10}	18.27

ICO15K-E4-40SA-cBiTE	2.76 x 10^{12}	2.06 x 10^{11}	13.38

Table 15. Characterization of purified viruses used for the antitumor efficacy assay.

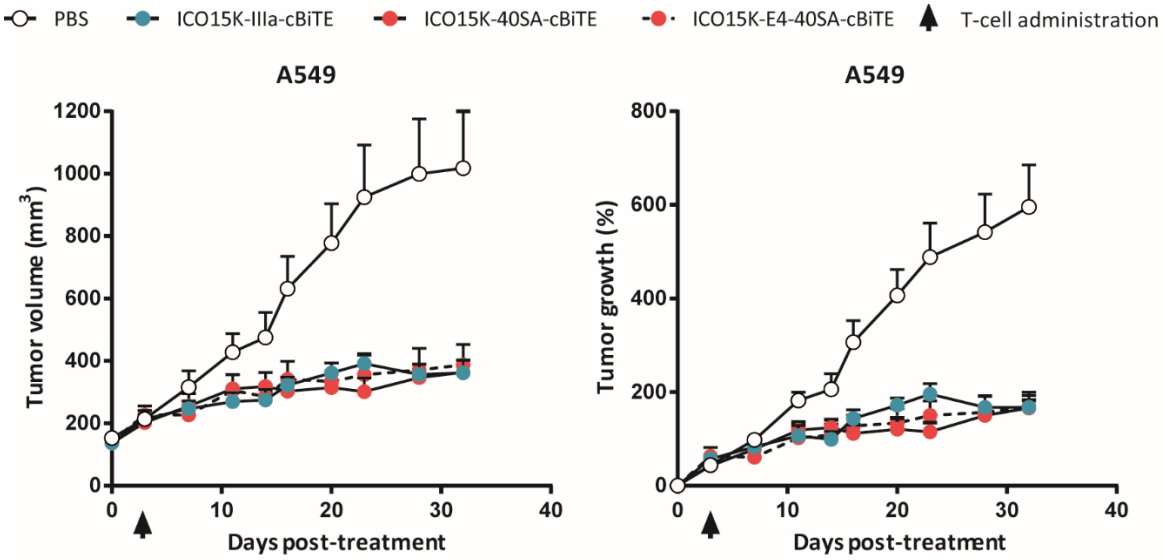

Figure 18. Antitumor efficacy of different cBiTE-expressing viruses. NSG mice with subcutaneous A549 lung tumors were treated with a single intratumoral injection of PBS, ICO15K-IIIa-cBiTE, ICO15K-40SA-cBiTE or ICO15K-E4-40SA-cBiTE at a dose of 2 x 10^9 vp per tumor. Fours days post-virus treatment, 1 x 10^7 of PBMCs were intravenously injected to all mice. The mean tumor volume or tumor growth ± SEM of ≥ 12 tumors per group is shown. *, significant ($P < 0.0001$) by one-way ANOVA test with *post hoc* analysis compared to PBS group.

2. FAP-TARGETING BISPECIFIC T CELL ENGAGER-ARMED ONCOLYTIC ADENOVIRUS

The results of this chapter generated the manuscript "Targeting the tumor stroma with an oncolytic adenovirus secreting a Fibroblast Activation Protein-targeted bispecific T-cell Engager", enclosed in the annex section.

2.1 GENERATION AND CHARACTERIZATION OF AN ONCOLYTIC ADENOVIRUS SECRETING A FAP-TARGETING BITE

One of the major obstacles to successful oncolytic therapy is the presence of stroma in tumors, formed by different types of cells and extracellular matrix (ECM) compounds. Stroma not only creates physical barriers that limit oncolytic adenovirus (OAd) spread across the tumor, but also induces tumor progression by enhancing the survival,

proliferation, stemness, metastasis, and an immunosuppressive microenvironment that limits tumor immunity, ultimately promoting cancer progression, but also enhancing resistance to therapy (Kalluri 2016). One attractive stromal target is the fibroblast activation protein-α (FAP), a transmembrane serine protease that is highly expressed on the cell surface of cancer-associated fibroblasts (CAFs), which represent the key component in the tumor microenvironment of many cancers.

We had previously reported the generation of an oncolytic adenovirus armed with a BiTE targeting the EGFR on tumor cells (ICO15K-cBiTE) (Fajardo et al. 2017). This approach, however, does not address the presence of a tumor stroma which can impair virus spread in the tumor. In order to simultaneously target cancer cells through virus-mediated oncolysis and to re-direct immune responses towards tumor stroma fibroblasts, in the present study we engineered the genome of the oncolytic adenovirus ICO15K to express a FAP-targeting BiTE (FBiTE) (**Figure 19**).

The FBiTE or the mFBiTE molecules were engineered by joining with flexible linkers (GS linkers) two scFvs, one specific for human or mouse CD3ε (FBiTE or mFBiTE, respectively) and the other for murine and human FAP. The FAP scFv sequence was specifically chosen to bind both murine and human to be able to target the murine CAFs infiltrated in human xenografted tumors in the *in vivo* experiments. The FBiTE and mFBiTE genes also contained an N-terminus signal peptide derived from the mouse immunoglobulin light chain for mammalian secretion, and a FLAG tag at the C-terminus for detection. For enhanced and correct translation of the proteins, the constructs included a kozak sequence upstream of the starting codon, and a polyA site downstream of the stop codon. The adenovirus IIIa splicing acceptor or the 40SA splicing acceptor were placed upstream of the kozak sequence in order to control de FBiTE expression from de Major Late Promoter (MLP). As we wanted to evaluate whether a higher BiTE production in the tumor would improve antitumor efficacy, we generated the ICO15K-IIIa-FBiTE, which expressed the FAP-targeting BiTE under the IIIa splicing acceptor and the ICO15K-40SA-FBiTE, where the IIIa splicing acceptor was replaced by the stronger splicing acceptor 40SA (Carette et al. 2005). In the case of the mFBiTE, five different OAds IIIa-expressing mFBiTE were designed (mFiBTE, 2C11-M5, M5-2C11, M5-2C11.2 and M5-2C11.3). We have previously demonstrated that the insertion of a transgene after the fiber gene using an adenoviral splicing acceptor favors its expression in a replication-dependent manner without interfering with viral

oncolysis (Fajardo et al. 2017; Sonia Guedan et al. 2010). Thus, the genome of ICO15K was genetically engineered by homologous recombination in bacteria to place the FBiTE or mFBiTE constructs downstream of the fiber gene as an L6 unit. The viruses ICO15K-FBiTE or the different versions of the ICO15K-mFBiTE were successfully rescued and clarified cell extracts (CCE) had similar functional titers as those of ICO15K. Only the parental ICO15K and the engineered ICO15K-IIIa-FBiTE and ICO15K-40SA-FBiTE were amplified and purified (**Table 16**).

Virus	Physical titer (vp/mL)	Functional titer (TU/mL)	Physical:Functional ratio
ICO15K	4.03×10^{12}	1.06×10^{11}	38.02
ICO15K-IIIa-FBiTE	3.07×10^{12}	7.43×10^{10}	41.25
ICO15K-40SA-FBiTE	3.60×10^{12}	6.60×10^{10}	54.55

Table 16. Characterization of purified virus.

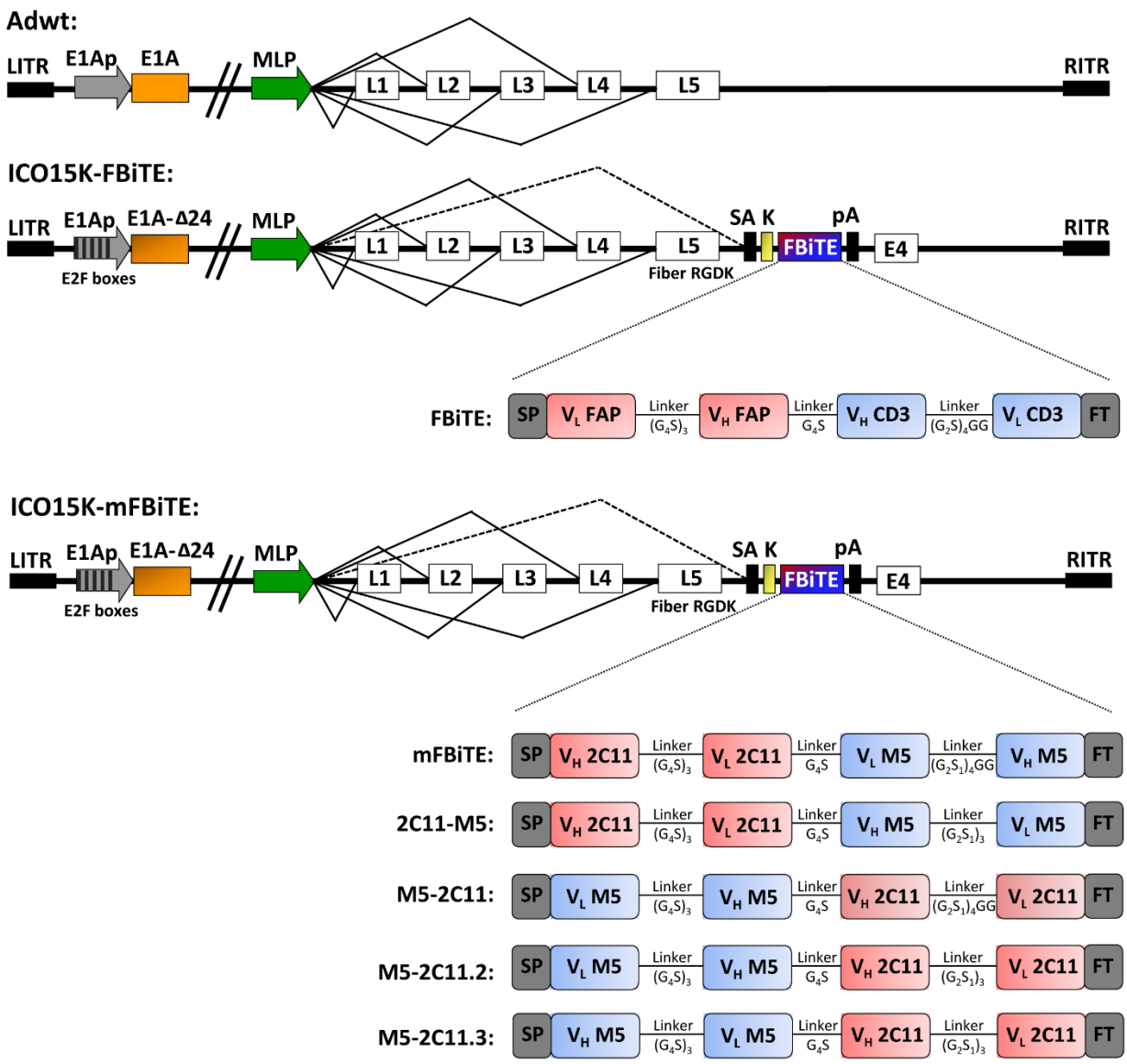

Figure 19. Schematic structure representation of the ICO15K-FBiTE and the different ICO15K-mFBiTE viruses used in this study. The virus ICO15K carries the Δ24 mutation in the E1a gene and its expression is controlled by palindromic E2F binding sites located in the promoter of the gene. This virus also contains an RGDK motif replacing the KKTK heparan sulfate glycosaminoglycan-binding domain in the shaft of the fiber (L5). FBITE molecule is formed by VL and VH domains of anti-mhFAP and human or mouse CD3Ɛ are connected by glycine and serine flexible linkers, flanked by the light chain immunoglobulin signal peptide (SP) and the FLAG tag (FT). FBiTE is inserted after the adenovirus fiber gene under the control of the major late promoter (MLP).

To evaluate whether the FBiTE insertion affected the viability and the oncolytic properties of the virus, we first compared the replication kinetics of ICO15K and ICO15K-IIIa-FBiTE, and ICO15K-40SA-FBiTE in A549 cells. We observed a minor loss in the production yields in cell extracts and supernatants of ICO15K-FBiTE compared to the parental virus but a high

loss of production yields in supernatants of ICO15K-40SA-FBiTE, indicating that using the splicing acceptor 40SA instead of the IIIa decreases the proper replication of the virus (**Figure 20**). These results are consistent with data described in section 1.1.

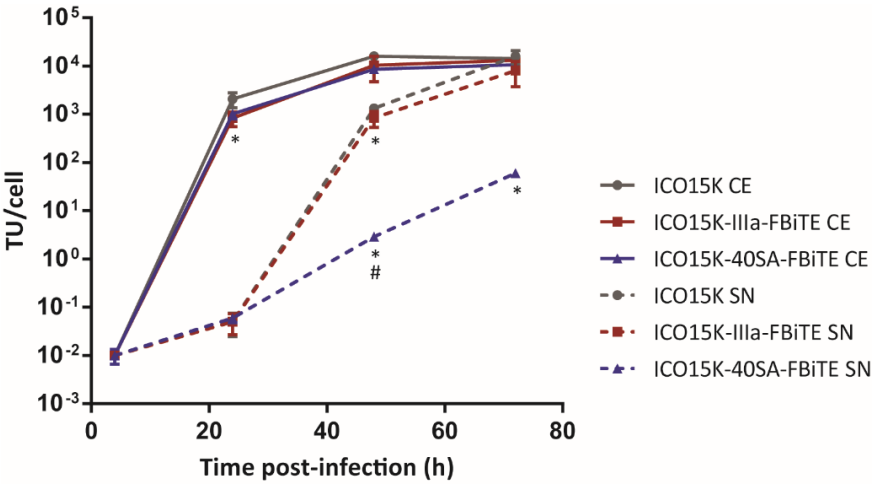

Figure 20. Viral production from cell extracts (CE) and supernatants (SN) of ICO15K-IIIa-FBiTE and ICO15K-40SA-FBiTE. A549 cell line was infected with ICO15K, ICO15K-IIIa-FBiTE or ICO15K-40SA-FBiTE. At indicated time points, cell extracts and supernatants were harvested and titrated by an anti-hexon staining-based method. Mean values ± SD are plotted (n=3). TU, transducing units. CE, cell extract. SN, supernatant.

We next assessed the killing kinetics of the virus in dose-response cytotoxicity assays in three cancer cell lines (A549, HT1080, and hCAF). As shown, the IIIa-FBiTE-expressing adenovirus conserved oncolytic properties despite slight increases in IC_{50} values compared to the parental virus. However, the 40SA-FBiTE-expressing adenovirus showed between 2-186-fold loss of cytotoxic capacities compared to both the IIIa-FBiTE and the parental virus, mainly for the A549 cell line (**Figure 21**).

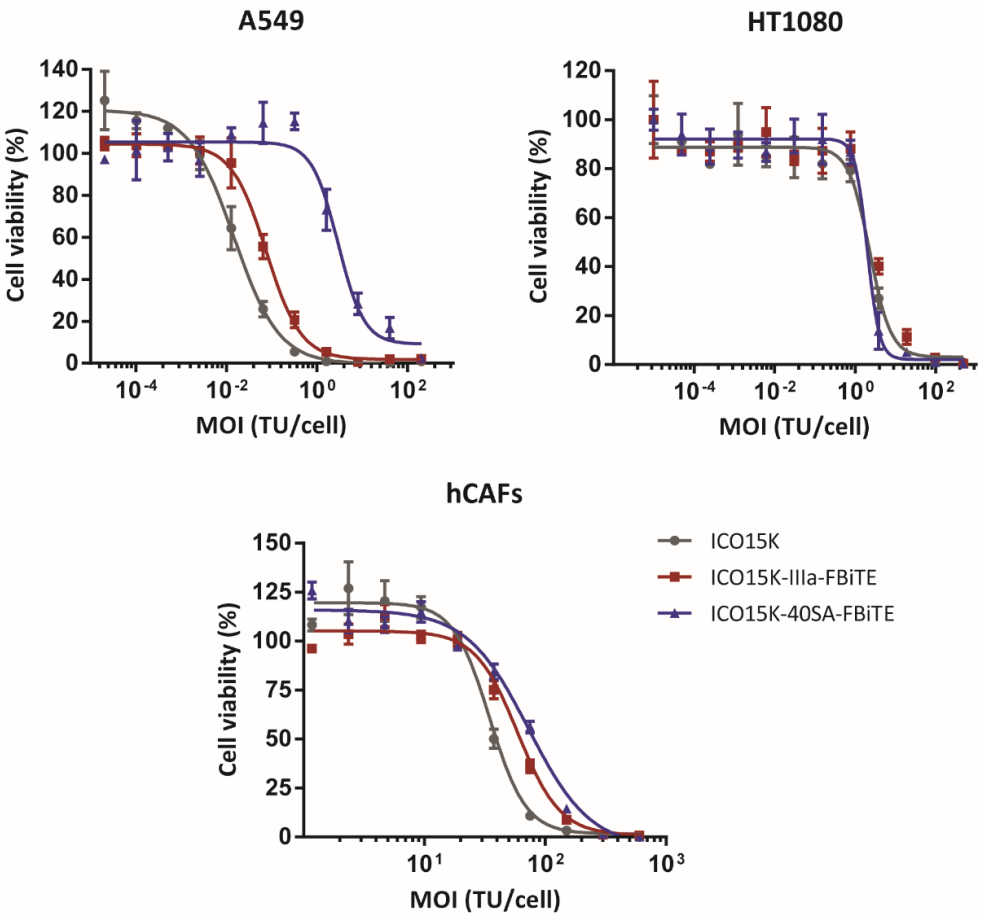

Cell line	IC_{50} ICO15K	IC_{50} ICO15K-IIIa-FBiTE	Fold change vs. ICO15K	IC_{50} ICO15K-40SA-FBiTE	Fold change vs. ICO15K
A549	0.01455±0.006	0.07578±0.02	5.2x	2.894±2.25	189x
HT1080	2.883±1.3	4.197±1.987	1.5x	2.491±1.351	0.86x
hCAFs	33.25±4.9	56.87±7.2	1.7x	69.74±14.8	2x

Figure 21. Comparative cytotoxicity profile of ICO15K-IIIa-FBiTE and ICO15K-40SA-FBiTE. A549, HT1080 and hCAFs cell lines were incubated with serial dilutions of ICO15K, ICO15K-IIIa-FBiTE or ICO15K-40SA-FBiTE, with multiplicity of infections (MOIs) ranging from 200 (A549) or 600 (HT1080 and hCAFs) to 0 TU/cell. Viability was measured at day 6 post-infection for A549 and HT1080 and at day 7 for hCAFs. Mean values ± SD are plotted (n=3).

2.2 CELLS INFECTED WITH ICO15K-FBITE SECRETE FBITE MOLECULES WHICH SPECIFICALLY BIND TO TARGET AND EFFECTOR CELLS

To characterize the FBiTE, a panel of FAP-expressing cancer cell lines, FAP^+ human and murine CAFs and also $CD3^+$ Jurkat were used. In all cases, FAP-negative cell lines were used as a negative control (**Figure 22**).

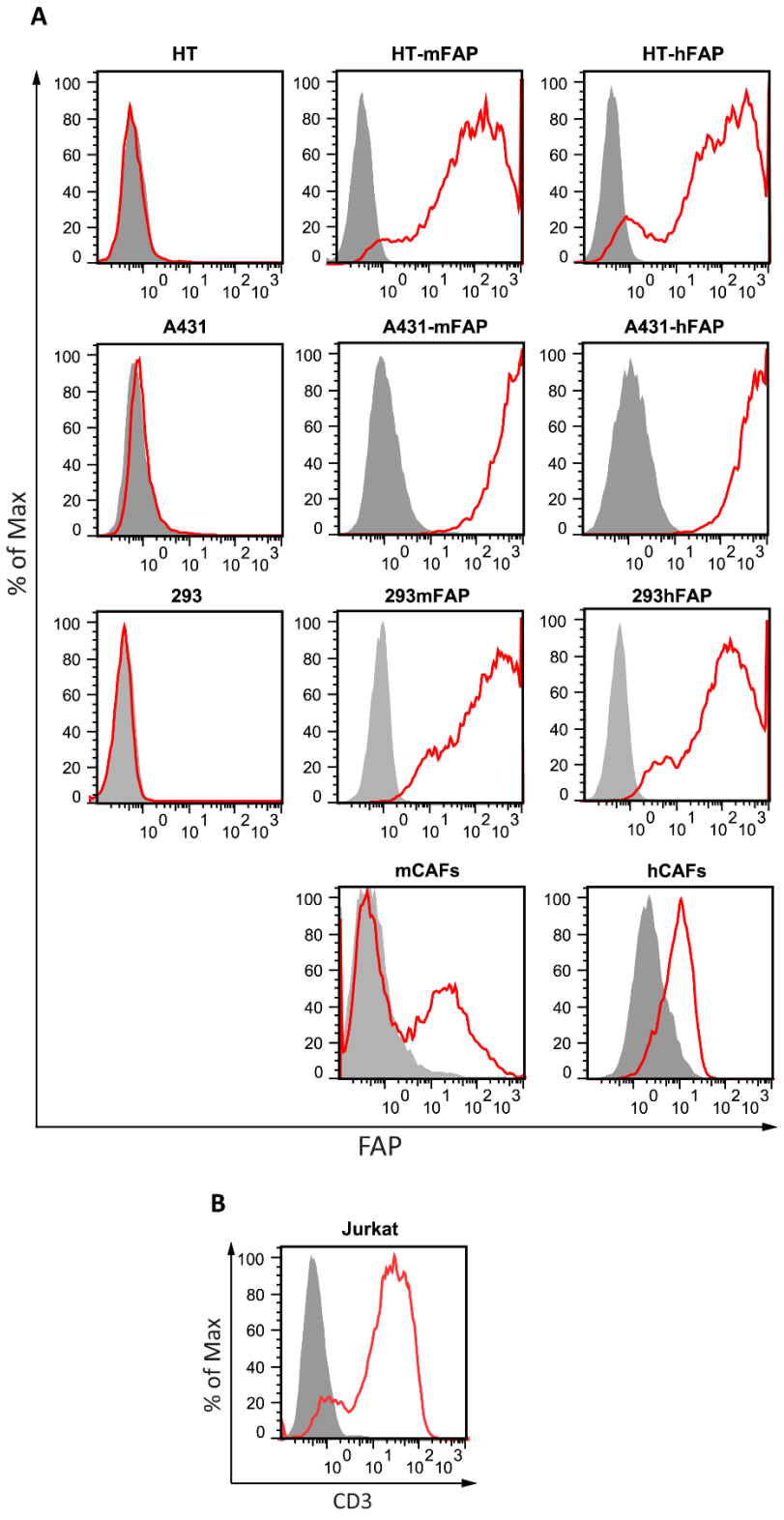

Figure 22. FAP and CD3 expression of the cell lines used in this project. A. A panel of cancer cell lines was evaluated for FAP expression by flow cytometry. Cells were incubated with an anti-FAP antibody or its corresponding isotype control, followed by the incubation with an Alexa647-coupled secondary antibody. **B.** Jurkat cells was evaluated for CD3 expression by flow cytometry. Cells were incubated with the OKT3 anti-CD3 antibody or its corresponding isotype control, followed by the incubation with an Alexa647-coupled secondary antibody.

We next determined whether FBiTEs or mFBiTEs encoded by ICO15K-modified viruses were properly secreted from cancer cells upon infection, and whether they could retain their antigen-binding specificities. To this end, we performed binding assays with HT1080 cells that had been genetically modified to express either human or murine FAP. FBiTE or mFBiTE binding was detected by flow cytometry with a fluorescently-labeled anti-FLAG antibody. FBiTE molecules were detected in both ICO15K-IIIa-FBiTE and ICO15K-40SA-FBiTE supernatants, and they bound specifically to HT-mFAP and HT-hFAP but not to the FAP-negative HT1080-parental cell line. Moreover, FBiTE molecules were also able to bind to CD3-positive Jurkat cells (**Figure 23A**). Both $CD3^+$ and FAP^+ bindings were more pronounced when ICO15K-40SA-FBiTE supernatants were used. In contrast, any conformation of concentrated mFBiTE showed to bind to FAP^+ cells (**Figure 23B**). From this point on, ICO15K-mFBiTEs were discarded for further experiments.

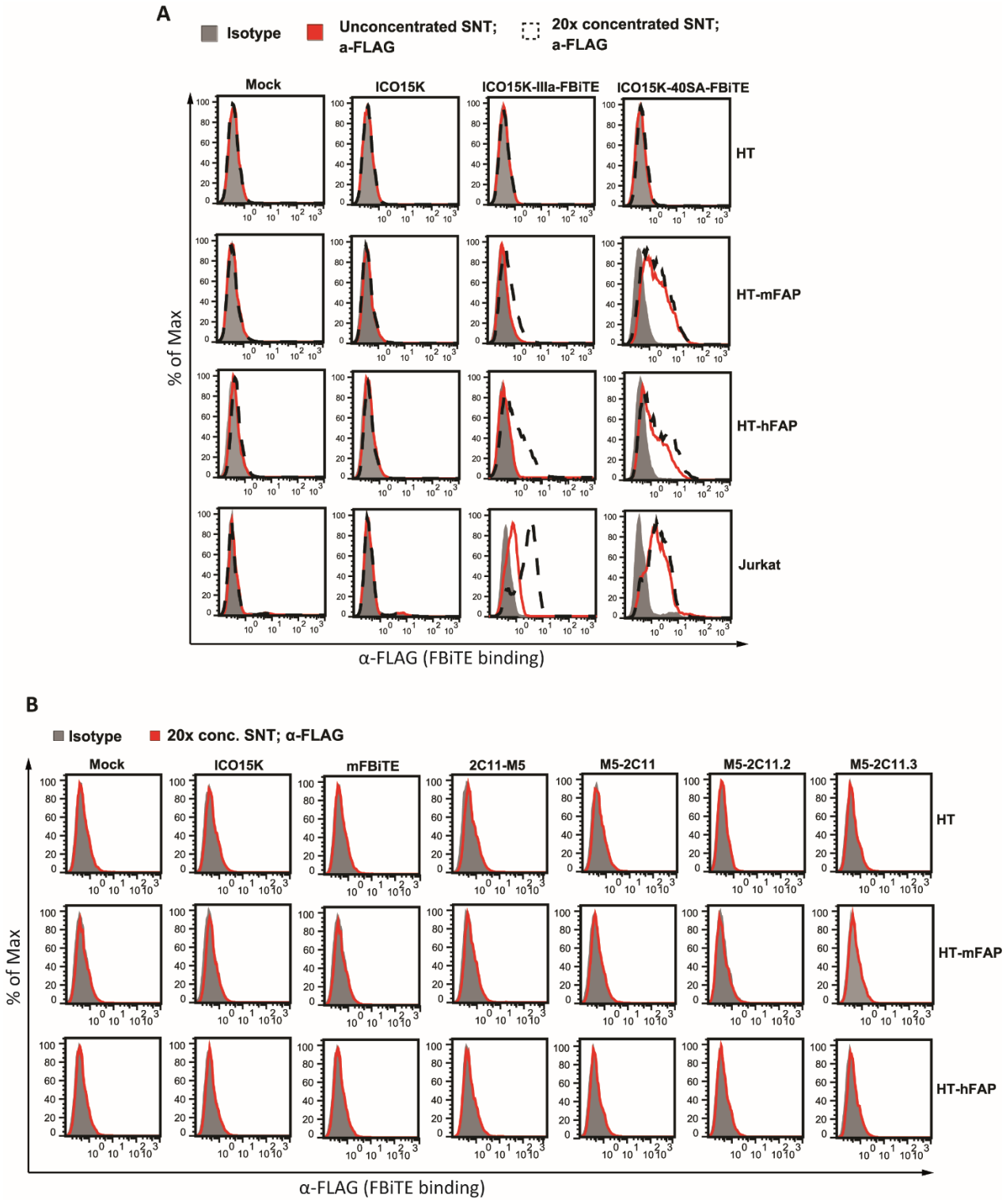

Figure 23. Binding assay of FBiTE and mFBiTE expressed by BiTE-expressing viruses. A. HT1080 (HT), HT-mFAP, HT-hFAP and Jurkat cells were incubated with mock, ICO15K, ICO15K-IIIa-FBiTE or ICO15K-40SA-FBiTE non-concentrated (solid red lines) or 20x-concentrated (dashed black lines) supernatants. FBiTE binding was detected by flow cytometry incubating cells with an FITC-conjugated anti-FLAG antibody. **B**. HT, HT-mFAP and HT-hFAP were incubated with mock, ICO15K, ICO15K-2C11-M5, ICO15K-M5-2C11, ICO15K-M5-2C11.2 or ICO15K-M5-2C11.3 20x-concentrated supernatants. In **A** and **B**, a representative result of triplicates is shown.

2.3 SUPERNATANTS FROM ICO15K-FBITE-INFECTED CELLS INDUCE ACTIVATION AND PROLIFERATION OF T CELLS

In order to detect the FBiTE-mediated T-cell effector functions, we evaluated both cytokine production and proliferation of T cells after co-culture with 293 cells, either expressing or not murine or human FAP, in the presence of supernatants from adenovirus-infected (ICO15K, ICO15K-IIIa-FBiTE or ICO15K-40SA-FBiTE) or uninfected cells (mock). After 24h of incubation, supernatants were collected and T-cell activation was assessed by quantifying IFN-ɣ, TNF-α, and IL-2 by ELISA (**Figure 24**). Significant cytokine release was observed in co-cultures of T cells and FAP-expressing cells and in the presence of ICO15K-IIIa-FBiTE and ICO15K-40SA-FBiTE supernatants. Cytokines levels were higher in the presence of murine FAP-expressing cells compared to human FAP-expressing target cells. This in line with the affinity of the FAP5 monoclonal antibody from which the scFv in our BiTE is derived, which has been reported to be 5nM for human FAP and 0.6nM for mouse FAP (Ostermann et al. 2008). Importantly, there was no cytokine production in the absence of FAP^+ targets (293 control cells) or when using supernatants from a parental virus or from non-infected cells. These data demonstrate that FBiTE molecules secreted from infected cells are able to activate T cells in FAP-expression dependent manner.

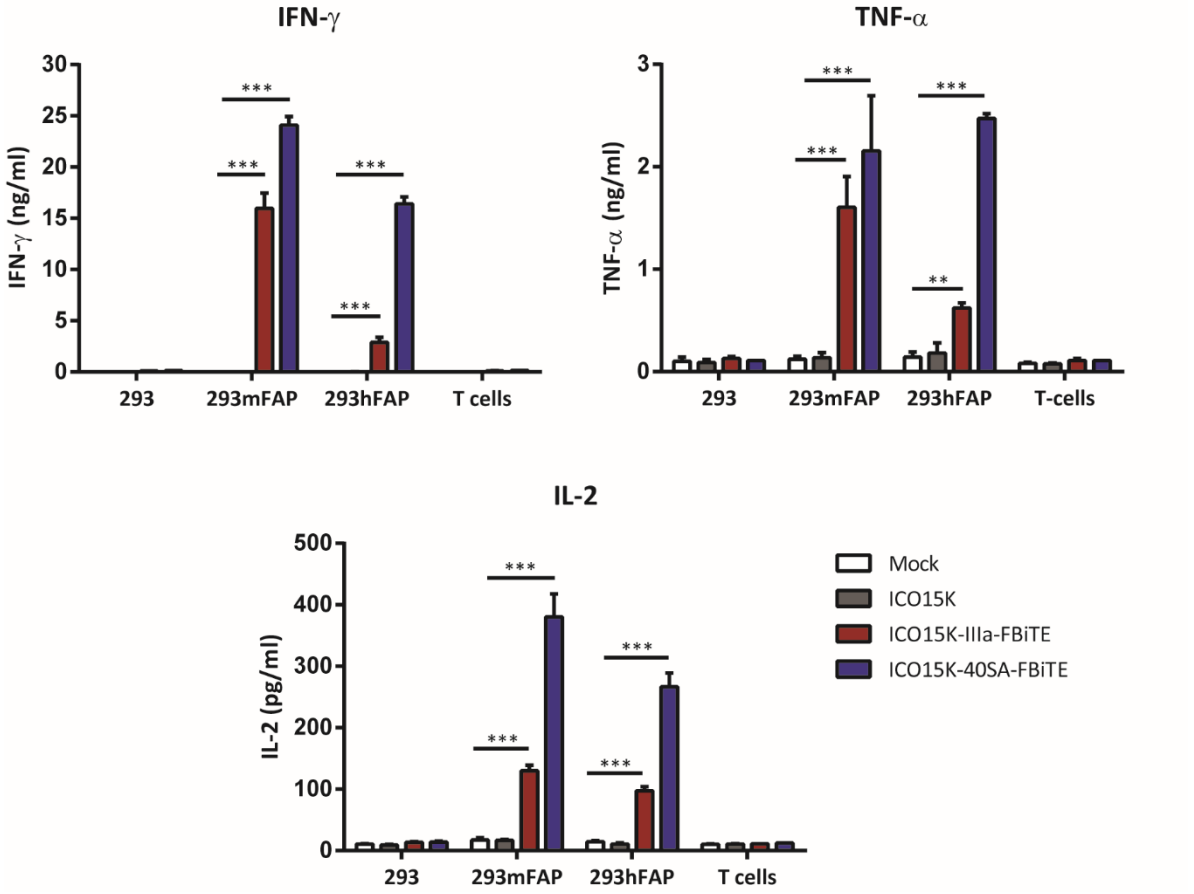

Figure 24. Evaluation of cytokine production. Average concentration values of IFN-γ, TNF-α and IL-2 cytokines were measured by ELISA assay using supernatants from 24h co-cultures of HEK293 (293), 293mFAP or 293hFAP cells with T cells (E:T=5) and indicated supernatants. Mean values ± SD are plotted (n=3). ***, ICO15K-IIIa-FBiTE and ICO15K-40SA-FBiTE significant ($P < 0.001$) versus mock or ICO15K using one-way ANOVA test with *post hoc* analysis.

To further confirm the FBiTE-mediated induction of T-cell effector functions, we evaluated T-cell proliferation after 3 days of co-culture. Both $CD4^+$ and $CD8^+$ T cells showed proliferation in the co-cultures containing FAP-expressing cells and the ICO15K-40SA-FBiTE supernatants (**Figure 25A**). ICO15K-IIIa-FBiTE supernatants only showed clear induction of $CD8^+$ T-cells proliferation when co-cultured with 293mFAP. To better assess ICO15K-IIIa-FBiTE induction of T-cell proliferation, CFSE-labeled T cells were co-cultured 3 days with target cells and the corresponding supernatants (**Figure 25B**). Both CD4+ and CD8+ T cells underwent multiple rounds of proliferation only when T cells were co-cultured with FAP-positive cells and ICO15K-IIIa-FBiTE supernatants, as evidenced by the dilution of CFSE. After performing the same analysis with PBMCs instead of isolated T cells and with 6 days of incubation, both $CD4^+$ and $CD8^+$ T cells showed strong proliferation always in the co-

cultures of PBMCs with FBiTE-containing supernatants, even in the absence of FAP-expressing cells (**Figure 25C**). These results support previous research which showed that a population of macrophages in PBMCs express FAP (Julia et al. 2013). To avoid unspecific FBiTE activation of T cells in PBMCs, we used isolated T cells for further experiments.

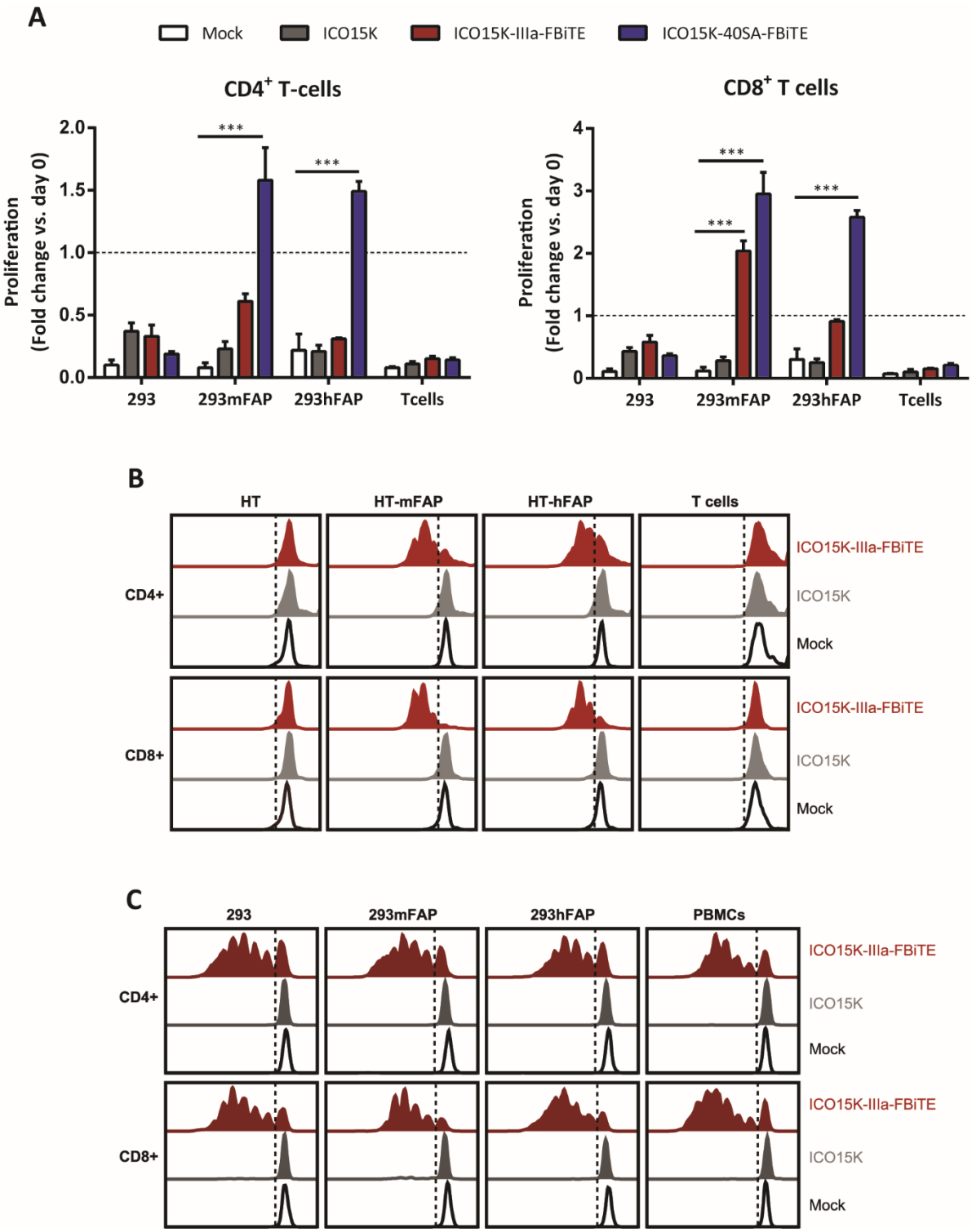

Figure 25. FBiTE molecules expressed from ICO15K-FBiTE-infected cells induce T-cell proliferation. A. T-cell proliferation following co-cultures with 293, 293mFAP and 293hFAP and indicated supernatants (E:T=5). Mean values ± SD are plotted (n=3). ***, ICO15K-IIIa-FBiTE and ICO15K-40SA-FBiTE significant ($P < 0.001$) versus mock or ICO15K using one-way ANOVA test with *post hoc* analysis. **B.** CFSE-labeled T cells were cocultured with HT and its FAP-derivative cells (E:T = 5) in the presence of the indicated supernatants. 3 days after co-culture, CFSE dilution (i.e. cell proliferation) in $CD3^+$ cells was evaluated by flow cytometry. **C**. 293, 293mFAP and 293hFAP were co-cultured with CFSE-labeled PBMCs and indicated supernatants. Six days after co-culture, the CFSE content in $CD4^+$ and $CD8^+$ T-cells was determined by flow cytometry. **B** and **C**, a representative result of triplicates is shown.

2.4 COMBINING VIRAL ONCOLYSIS WITH FBITE-MEDIATED KILLING IMPROVES THERAPEUTIC ACTIVITY *IN VITRO*

Having shown the expression of FBiTE from ICO15K-IIIa-FBiTE and ICO15K-40SA-FBiTE-infected cells, we next investigated FBiTE-mediated cytotoxicity *in vitro*. We first evaluated the effect of co-culturing HT1080 and its derivative FAP-expressing cell lines with T cells and the indicated supernatants. Marked cytotoxicity of FAP-positive engineered cell lines was observed after 24h of incubation only in the presence of both ICO15K-IIIa-FBiTE and ICO15K-40SA-FBiTE supernatants (**Figure 26A**). Surprisingly, when using the ICO15K-40SA-FBiTE supernatants, some cytotoxicity is also detected in the HT parental cell line. This result supports evidence from a recent study, which demonstrated that BiTEs can also mediate a bystander tumor cell killing of nearby cells lacking the targeted antigen (Ross et al. 2017). To evaluate this, we co-cultured CFSE stained FAP-negative cells (HT or A431) with T cells and its derivative mFAP or hFAP-positive cells, and supernatants were added. After 24h, the cytotoxicity of the CFSE-FAP-negative cells and the mFAP or hFAP-expressing cells was determined by flow cytometry. mFAP and hFAP cells were identified as a CFSE-hCD45- double negative cells. In both cell lines we observed some cytotoxicity of FAP-negative cells (from 15% to 20%) only when co-cultured together with FAP-positive cells and FBiTE-expressing viruses supernatants. This result corroborates an existing BiTE-dependent T cell-induced bystander lysis of FAP-negative cells proximal to FAP-positive cells (**Figure 26B, C**).

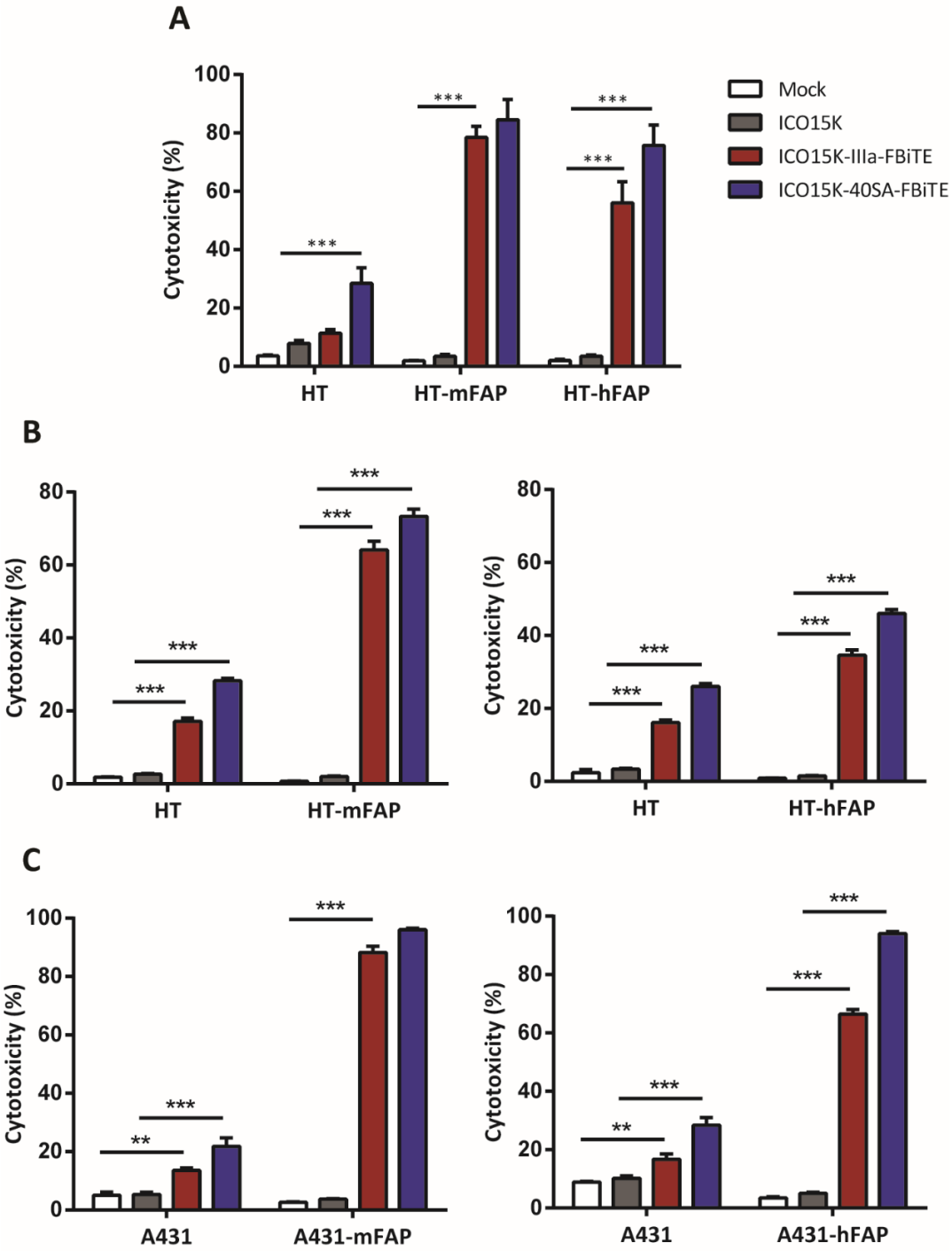

Figure 26. Enhanced FBiTE-expressing viruses-mediated cytotoxicity of FAP-positive cells. A. FBiTE-mediated cytotoxicity was evaluated by flow cytometry after 24h incubation of CFSE-stained HT1080 cell lines cultured with T cells and indicated supernatants. **B, C.** FBiTE-mediated bystander tumor cell killing. CFSE-stained HT cells (B) or A431 cells (C) were culture in the presence of T cells and its derivative mFAP- or hFAP cells and the indicated supernatants (mock, ICO15K, ICO15K-IIIa-FBiTE or ICO15K-40SA-FBiTE) were added. After 24h, cytotoxicity of HT cells (B) or A431 cells (C) and its mFAP- or hFAP-derivative cells were evaluated by flow cytometry. Mean values ± SD are plotted in A, B and C (n=3). ***, significant ($P < 0.001$) by one-way ANOVA test with *post hoc* analysis compared to mock and ICO15K. **, significant ($P < 0.01$) by one-way ANOVA test with *post hoc* analysis compared to mock and ICO15K.

We next investigated the potential of combining viral oncolysis and FBiTE-mediated killing of FAP-positive non-infected cells. To this end, A549 cells were infected with ICO15K-IIIa-FBiTE, ICO15K-40SA-FBiTE or parental ICO15K at an MOI 20. After 4h of incubation, cells were washed and co-cultured with HT or HT-FAP-CFSE-stained cells and T cells. In this setup, A549 cells act as FBiTE producers whereas HT cells represent the target cells. The presence of OAd-infected cells specifically increased the cytotoxicity of FAP-positive target tumor cells (**Figure 27**). These results demonstrate that expression of FBiTE is compatible with viral replication and sufficient to achieve the combined oncolysis and FBiTE T cell-mediated killing of the non-infected targeted cells *in vitro*.

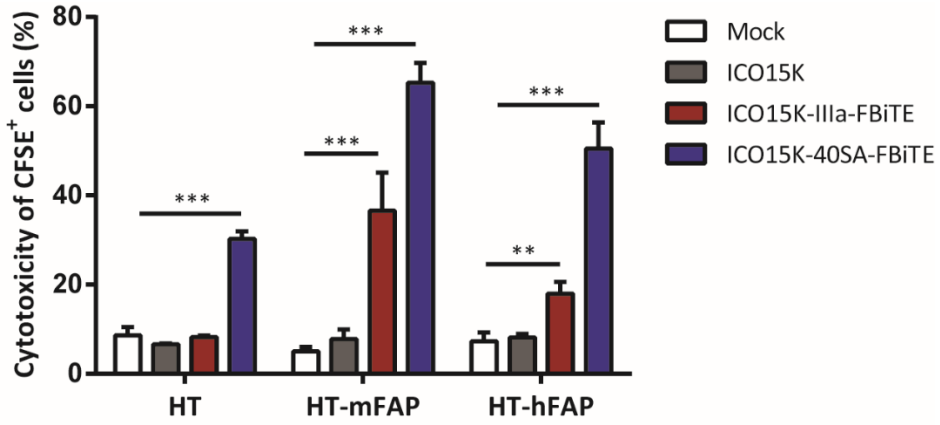

Figure 27. FBiTE-mediated killing of FAP-positive non-infected cells. CFSE-stained target cells were co-cultured with A549-infected cells and T cells (E:T=5). After four days of incubation, specific cytotoxicity of CFSE-stained cells was determined by flow cytometry. Mean values ± SD are plotted (n=3). **, ICO15K-40SA-FBiTE significant ($P < 0.01$) and ***, ICO15K-IIIa-FBiTE significant ($P < 0.001$) by one-way ANOVA test with *post hoc* analysis compared to mock and ICO15K.

Although the above-mentioned experiments prove the FBiTE-mediated killing of FAP-expressing cancer cell lines, the ultimate goal of the secreted FBiTE is to target the FAP^+ CAFs in the tumor microenvironment. To demonstrate the therapeutic potential of the FBiTE in that context, cytotoxicity experiments were performed by co-culturing murine CAFs (mCAFs) and human CAFs (hCAFs) with human T cells and the different supernatants. As shown in **Figure 28**, T-cell-mediated killing of both mCAFs and hCAFs was observed in co-cultures containing the ICO15K-IIIa-FBiTE and ICO15K-40SA-FBiTE supernatants. These results not only confirm the cytotoxic potential of the secreted FBiTE, but also demonstrate that mCAFs can be targeted and killed by human T cells, a prerequisite for the

use of *in vivo* xenograft models in which the stroma is from mouse origin and the anti-CD3 side of FBiTE binds only to human T cells.

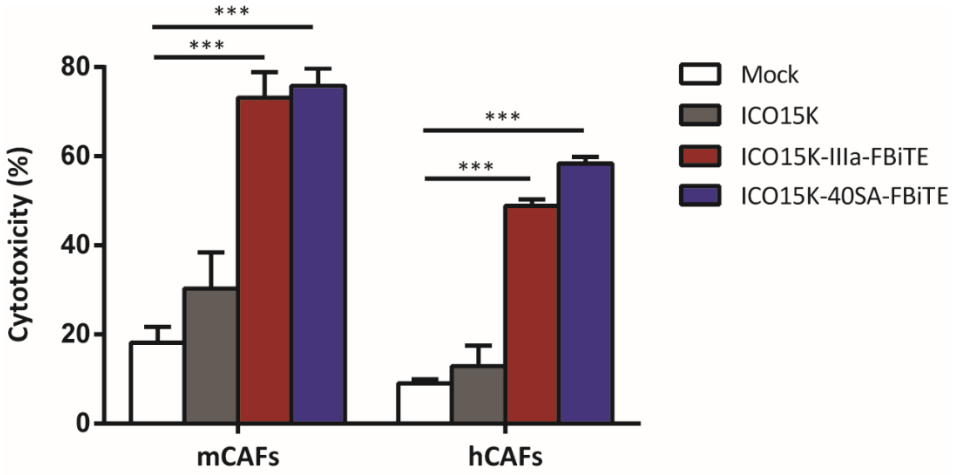

Figure 28. **Cytotoxicity of CFSE-stained-murine or human CAFs**. CFSE-stained target cells were co-cultured with T cells (E:T=5) and indicated supernatants. After 24h of incubation, killing of CFSE-stained cells was determined by flow cytometry. Mean values ± SD are plotted (n=3). ***, FBiTE-expressing viruses significant ($P < 0.001$) by one-way ANOVA test with *post hoc* analysis compared to mock and ICO15K.

2.5 ICO15K-FBITE INCREASES TUMOR T-CELL RETENTION AND ACCUMULATION *IN VIVO*

In order to evaluate T-cell trafficking to ICO15K-FBiTE-treated tumors, a biodistribution imaging study was performed. Preactivated T cells were transduced with a lentiviral vector expressing GFP and the Click Beetle Green (CBG) luciferase. We obtained 64% GFP-CBG-positive cells (**Figure 29A**), of which 64% were $CD4^+$ and 33% were $CD8^+$ (**Figure 29B**).

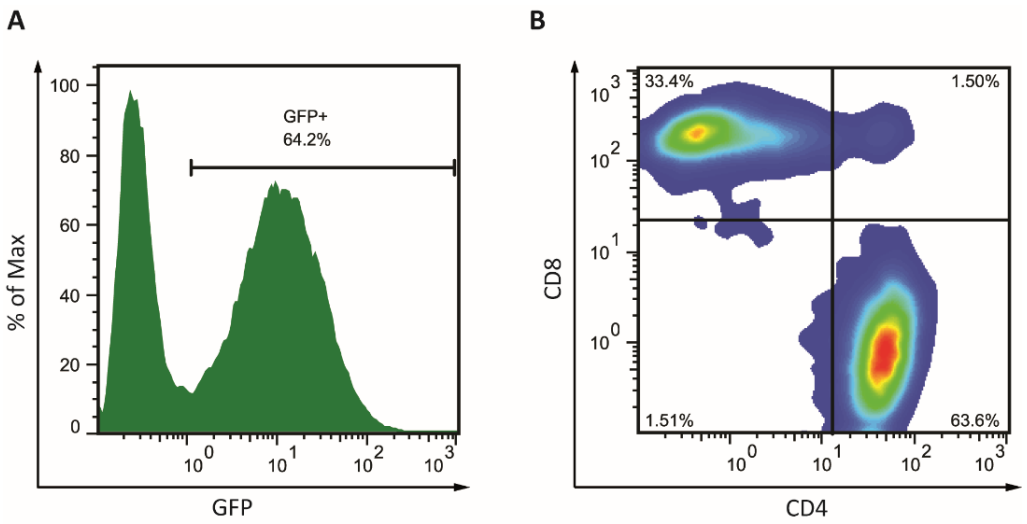

Figure 29. Characterization of GFP- and CBG Luciferase-expressing T cells. A. Flow cytometry analysis of GFP expression of preactivated T cells that had been transduced with a lentiviral vector encoding GFP and the click beetle green (CBG) luciferase. **B**. Percentages of CD4 and CD8 LUC-T cell populations determined by flow cytometry.

Once we obtained the LUC-T cells, tumors were injected with PBS, ICO15K or ICO15K-IIIa-FBiTE when reached approximately 120mm^3, and four days post-treatment 1x10^7 LUC-T cells were intravenously injected to all mice groups. Mice were imaged every day until sacrificed. ICO15K-IIIa-FBiTE-treated tumors showed significant enhanced T-cell retention and accumulation from the first day post-injection, increasing daily unto reaching a peak at day 6 (**Figure 30**). This result proved the feasibility of the bystander therapy in an *in vivo* scenario.

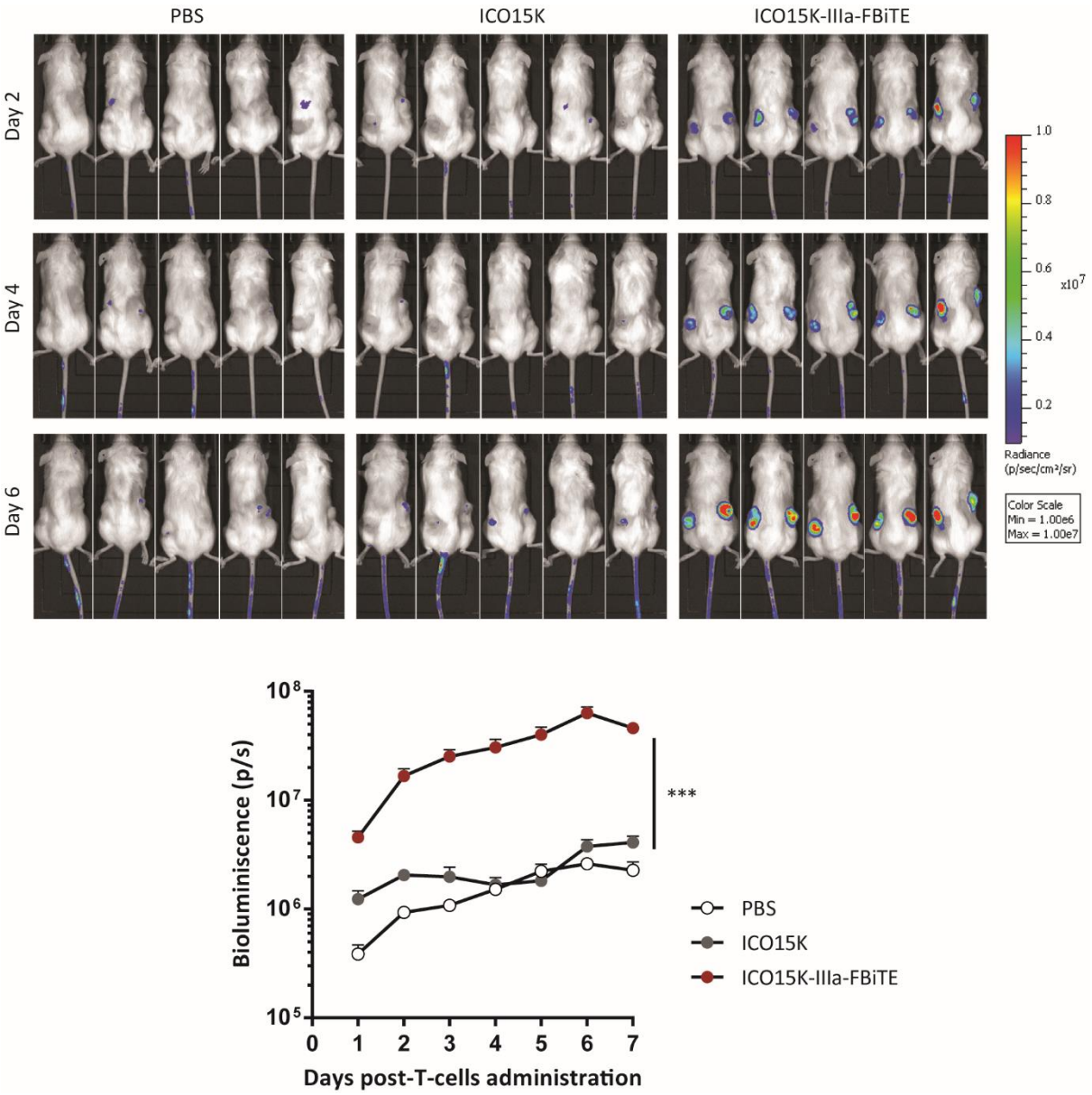

Figure 30. Increased T cell accumulation in ICO15K-FBiTE tumors. NSG mice bearing A549 (lung carcinoma) tumors were intratumorally treated with PBS, ICO15K, or ICO15K-IIIa-FBiTE ($1x10^9$ vp/tumor). Four days post-virus treatment, all mice received an intravenous injection of $1x10^7$ LUC-T cells (64% GFP^+). Luciferase activity was analyzed by bioluminescence imaging (IVIS) daily until day 7. Mean values ± SEM with ≥5 animals per group are shown. ***, ICO15K-FBiTE significant ($P < 0.001$) by one-way ANOVA test with *post hoc* analysis compared to PBS and ICO15K groups.

2.6 ICO15K-FBITE-MEDIATED ONCOLYSIS ENHANCES ANTITUMOR EFFICACY *IN VIVO*

We next assessed whether the accumulation of FAP-targeted-T cells observed in ICO15K-IIIa-FBiTE-treated mice could improve the antitumor efficacy in A549 (human lung cancer)

and HPAC (human pancreatic) tumor models. It has previously shown that these tumor models generate FAP^+ stroma once implanted subcutaneosly in NSG mice (Lo et al. 2015; Tran et al. 2013). First, A549 tumor-bearing mice were randomized into treatment groups and treated with a single intratumoral administration of PBS, ICO15K, ICO15K-IIIa-FBiTE or ICO15K-40SA-FBiTE ($1x10^9$ vp/tumor) when the tumor volume reached a mean of $120mm^3$. To assess the antitumor activity in presence of T cells (**Figure 31A-D**), four days post-virus-treatment $1x10^7$ preactivated human T cells were injected intravenously twice to all mice-treated groups. In the slow-growing A549 model, there were no differences in tumor growth among the different groups up to day 15 (**Figure 31A**). After this day, the mean tumor growth among treated groups were statistically different. Contrary to expectations based on all the previous results *in vitro*, tumors treated with the ICO15K-40SA-FBiTE did not present any antitumor efficacy advantage compared to the ICO15K-IIIa-FBiTE treated tumors. Given that the production of high amounts of BiTE by the ICO15K-40SA-FBiTE decreased the replication of the virus *in vitro* (**Figure 21**) and did not confer better antitumor efficacies *in vivo*, we decided to discard this virus for further experiments. Then, we next performed the same efficacy study with the HPAC tumor model where mice were only treated with PBS, ICO15K, or ICO15K-IIIa-FBiTE. In contrast to the A549 model, in the fast-growing HPAC model, significant differences started earlier, from day 9 (**Figure 31B**) but tumor growth was more difficult to control. In both tumor models, tumors growth of tumors treated with the FBiTE-expressing adenovirus were significantly smaller when compared with the tumors treated with PBS or with the control virus. This treament also improved significantly the survival of mice (sacrificed when tumors reached approximately $2000mm^3$) (**Figure 31C, D**), providing evidence for the therapeutic benefit of arming an oncolytic adenovirus with the FBiTE.

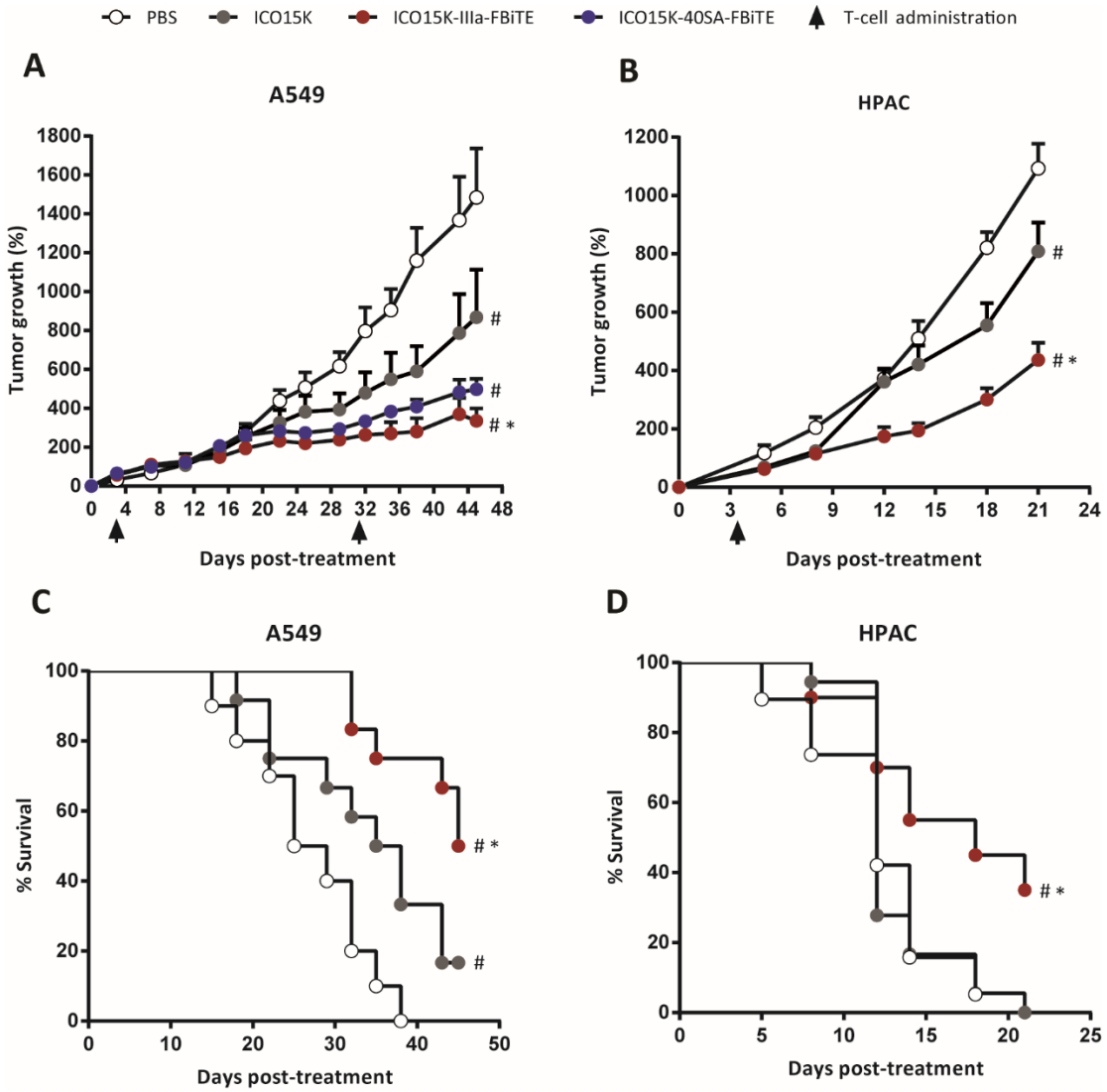

Figure 31. Enhanced antitumor efficacy of ICO15K-FBiTE in the presence of T cells. A-D. NSG mice bearing subcutaneous A549 (lung carcinoma) or HPAC (pancreatic adenocarcinoma) tumors were intratumorally treated with PBS, ICO15K, ICO15K-IIIa-FBiTE or ICO15K-40SA-FBiTE (A549) or with PBS, ICO15K or ICO15K-IIIa-FBiTE ($1x10^9$ vp/tumor). **A-D**. Antitumor efficacy in the presence of T cells. Four days after virus treatment, animals were treated once (HPAC) or twice (A549) with $1x10^7$ preactivated T cells. The mean tumor growth ± SEM of ≥ 12 tumors per group is shown. **C, D.** Kaplan-Meier survival curves of the experiments described in **A** and **B**. *, significant ($P < 0.05$) by one-way ANOVA test with *post hoc* analysis compared to ICO15K group. #, significant ($P < 0.05$) by one-way ANOVA test with *post hoc* analysis compared to PBS group.

We next wanted to demonstrate that the antitumor efficacy observed was T cell-dependent. For that, an antitumor activity experiment in the absence of T cells was performed in both tumor models (**Figure 32**). The treatment with either the FBiTE-armed or parental viruses induced a similar significant level of efficacy compared to the PBS group, indicating that the infusion of T cells is crucial to improve the antitumor efficacy in both tumor models.

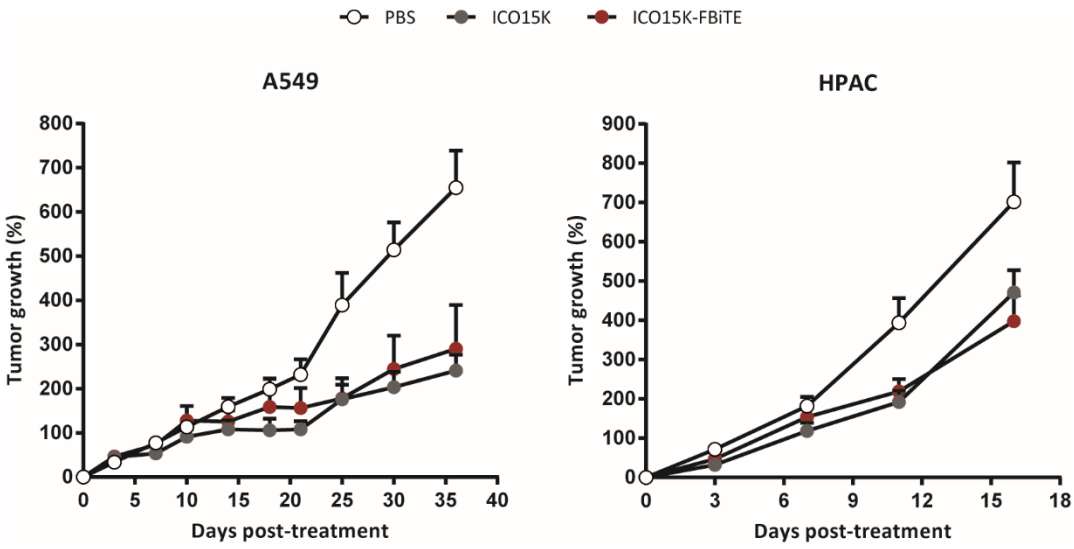

Figure 32. **Antitumor activity in absence of T cells**. NSG mice bearing subcutaneous A549 or HPAC tumors were intratumorally treated with PBS, ICO15K or ICO15K-FBiTE ($1x10^9$ vp/tumor). Mean percentage of tumor growth value ± SEM with ≥ 12 tumors per group is plotted.

2.7 ICO15K-FBITE IMPROVES THE ANTITUMOR ACTIVITY BY DEPLETION OF FAP

We analysed tumor samples from the efficacy studies described above to demonstrate that the observed improved antitumor activity was associated to the elimination of CAFs by T cells retargeted with the FBiTE expressed from the oncolytic adenovirus. We first quantified the viral genomes and the FBiTE copy numbers by real-time PCR. As expected, we observed high amounts of viral genomes only in virus-treated tumors compared to PBS-treated tumors (**Figure 33A**), indicating that both viruses are able to infect and replicate in both tumor models. This result is further supported by similar findings when the presence of virus was evaluated by an anti-E1A immunohistochemistry (**Figure 34A**). As expected, we could detect FBiTE expression only in ICO15K-FBiTE-treated tumors (**Figure 33B**). These data confirm that viruses are present in the tumor and that the FBiTE is locally expressed *in vivo* upon ICO15K-FBiTE infection.

Having shown the *in vivo* persistence of both viruses as well as the FBiTE expression by the modified virus, we next sought to demonstrate the hypothesis that the enhanced antitumor effect was associated to depletion of FAP. FAP expression was first quantified by real-time PCR. As shown in **Figure 33C**, the expression of FAP was significantly reduced in HPAC tumor model in the ICO15K-FBiTE-treated tumors compared with the PBS and the

control virus. In the A549 model, although not significant, slight reduction of FAP expression was also observed in the ICO15K-FBiTE-trated tumors. Consistent with this mRNA quantification data, the amount of FAP protein detected by staining the A549 tumors was also lower (**Figure 34B**). Altogether, these results indicate that the T cells retargeted by the FBiTE are responsible for killing the FAP-positive murine CAFs in the tumor mass.

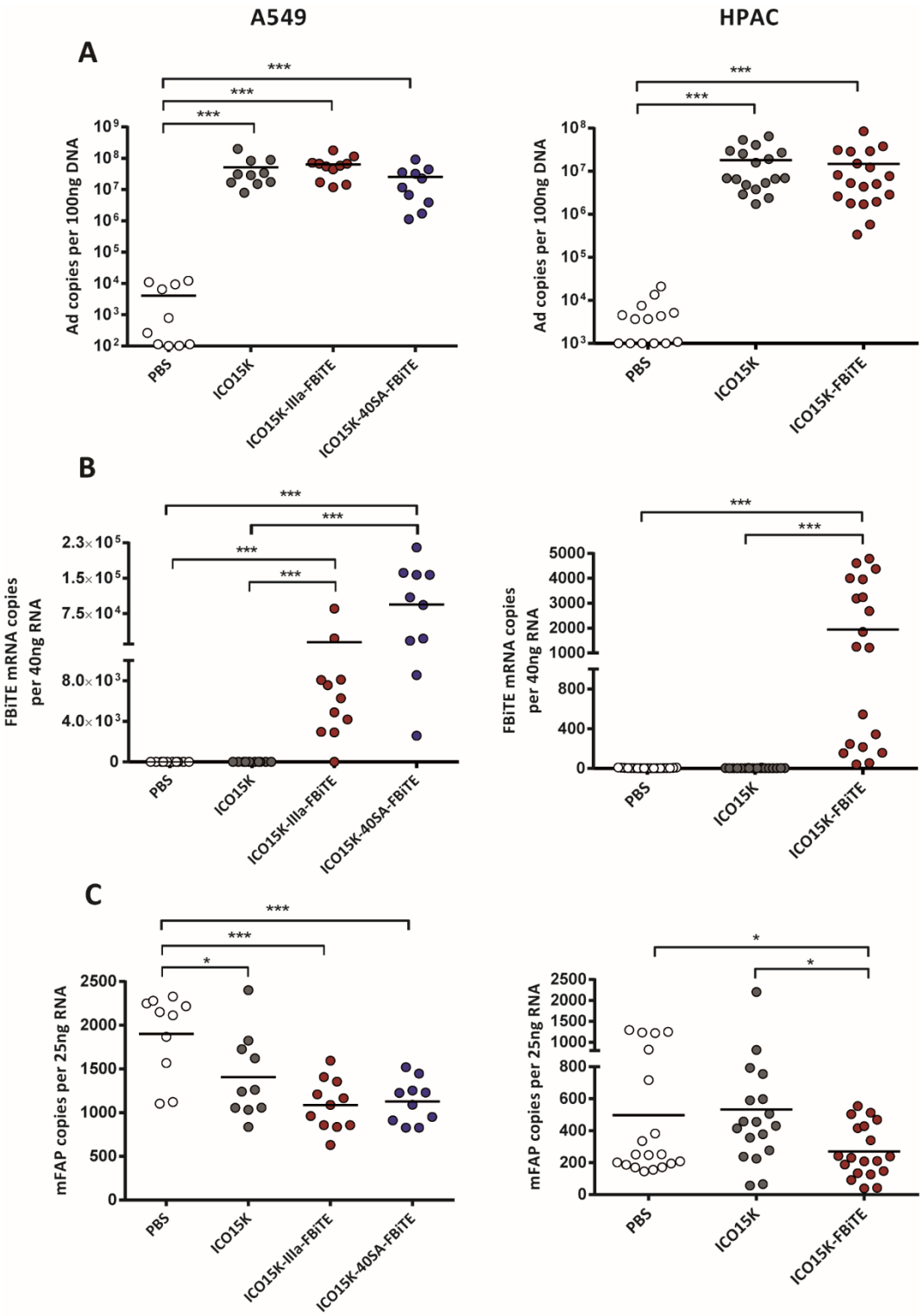

Figure 33. Depletion of tumor stroma by ICO15K-FBiTE. A549 and HPAC tumors from the antitumor efficacy studies in presence of T cells were harvested at endpoint of the experiments. **A-B.** Piece of tumor samples were mechanically homogenized, total DNA and RNA were extracted and quantification by real-time PCR-based method was performed to evaluate **A.** the virus persistence, **B.** FBiTE expression and **C.** levels of FAP expression in both tumor models. *, significant ($P < 0.05$) by two-tailed unpaired Student's *t*-test. ***, significant ($P < 0.001$) by two-tailed unpaired Student's *t*-test.

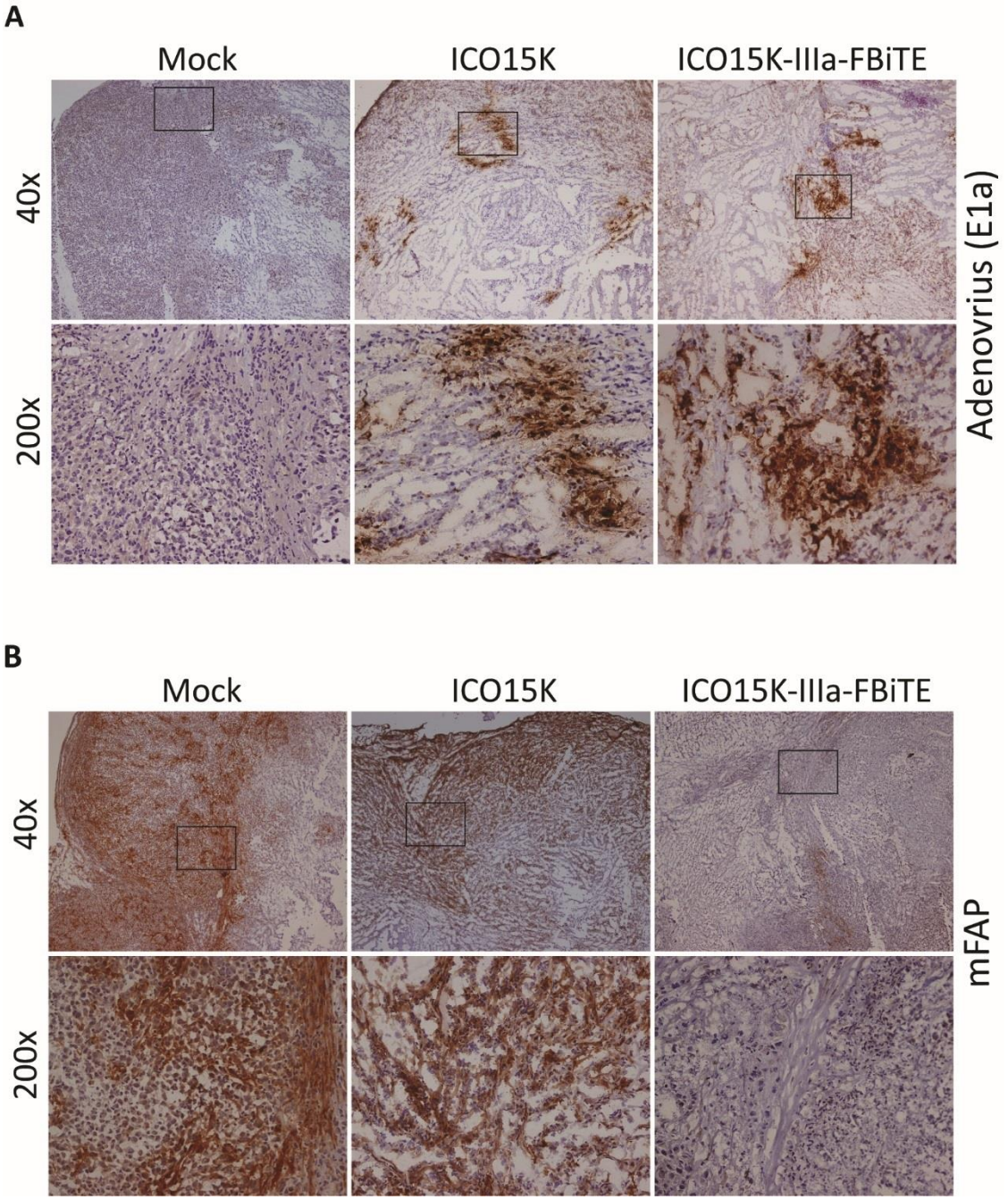

Figure 34. A549 tumor tissue characterization. Immunohistochemical stains of A549 tumors were performed to assess **A**. presence of virus by staining the early viral protein E1a and **B**. FAP expression by an anti-FAP antibody.

3. TARGETING THE TUMOR STROMA WITH AN IMMUNOTOXIN OR PRODRUG

3.1 ONCOLYTIC ADENOVIRUS EXPRESSING FAP-TARGETED IMMUNOTOXIN

3.1.1 Construction of different anti-FAP-toxin-secreting oncolytic adenoviruses

Immunotoxins are small recombinant toxins that contain either growth factor or Fv fragments as ligands. These molecules represent useful agents since they can directly bind to surface antigens that are selectively expressed on tumor cells endows cellular specificity to their cytotoxic action. In line with the chapter 2 of this thesis, where we demonstrated the advantages to specifically kill FAP-expressing CAFs in the tumor, we propose a new strategy to target the tumor stroma, which consists in the generation of an oncolytic adenovirus carrying an anti-FAP immunotoxin. Part of this study was performed in collaboration with Javier Lacadena laboratory (Universidad Complutense de Madrid), specialist in toxins and immunotoxins. With these viruses, we seek to achieve stroma disruption and significant toxicity in virus-resistant cells, improving virus spread and overall tumor efficacy.

We first chosed the toxin α-Sarcin and the antibody FAP5 (M5) for the generation of the immunotoxin. Javier Lacadena lab designed the sequence of the immunotoxin M5-Sarcin. M5-Sarcin was generated by joining the ScFv FAP5 (M5) and the engineered α-Sarcin (Gasset et al. 1995) by a GGCGGCCGC linker. α-Sarcin is a fungal ribotoxin that was chosen as a candidate for its small size, poor immunogenicity and their highly efficient ability to inactive ribosomes. As cytosolic internalization is a requirement for the toxicity of secretory ribonucleases, we decided to generate two new immunotoxin-expressing viruses, where the toxin α-Sarcin was fused to the anti-FAP antibody MO36 (Brocks et al. 2001) or to the antibody ESC11 (Fischer et al. 2012). Having three different scFv fused to the α-Sarcin the probability to an adequate internalization of the toxin was therefore higher. The designed viruses expressing these immunotoxins are shown in **Figure 35**. For proper expression of these proteins, genes were flanked by a kozak sequence and a polyadenylation signal. Immunotoxins were first inserted after the fiber of the virus genomes, but the transfection of these plasmids did not generate any virus after three

independent transfections. We secondly inserted the genes between E4 and RITR regions, which was already described to not affect the replication of the virus, and the new plasmids generated viable viruses. Immunotoxins were placed under the control of the major late promoter by including a splicing acceptor IIIa or 40SA upstream of the kozak sequence. A 6-Histidine tag (His Tag) were also included at the C-terminus of the genes for its detection. For all cases, the ICO15K platform was chosen as control backbone. The modified oncolytic adenoviruses were named ICO15K-IIIa-M5-Sarcin, ICO15K-40SA-M5-Sarcin, ICO15K-IIIa-MO36-Sarcin, ICO15K-40SA-MO36-Sarcin, ICO15K-IIIa-ESC11-Sarcin and ICO15K-40SA-ESC11-Sarcin (**Figure 35**).

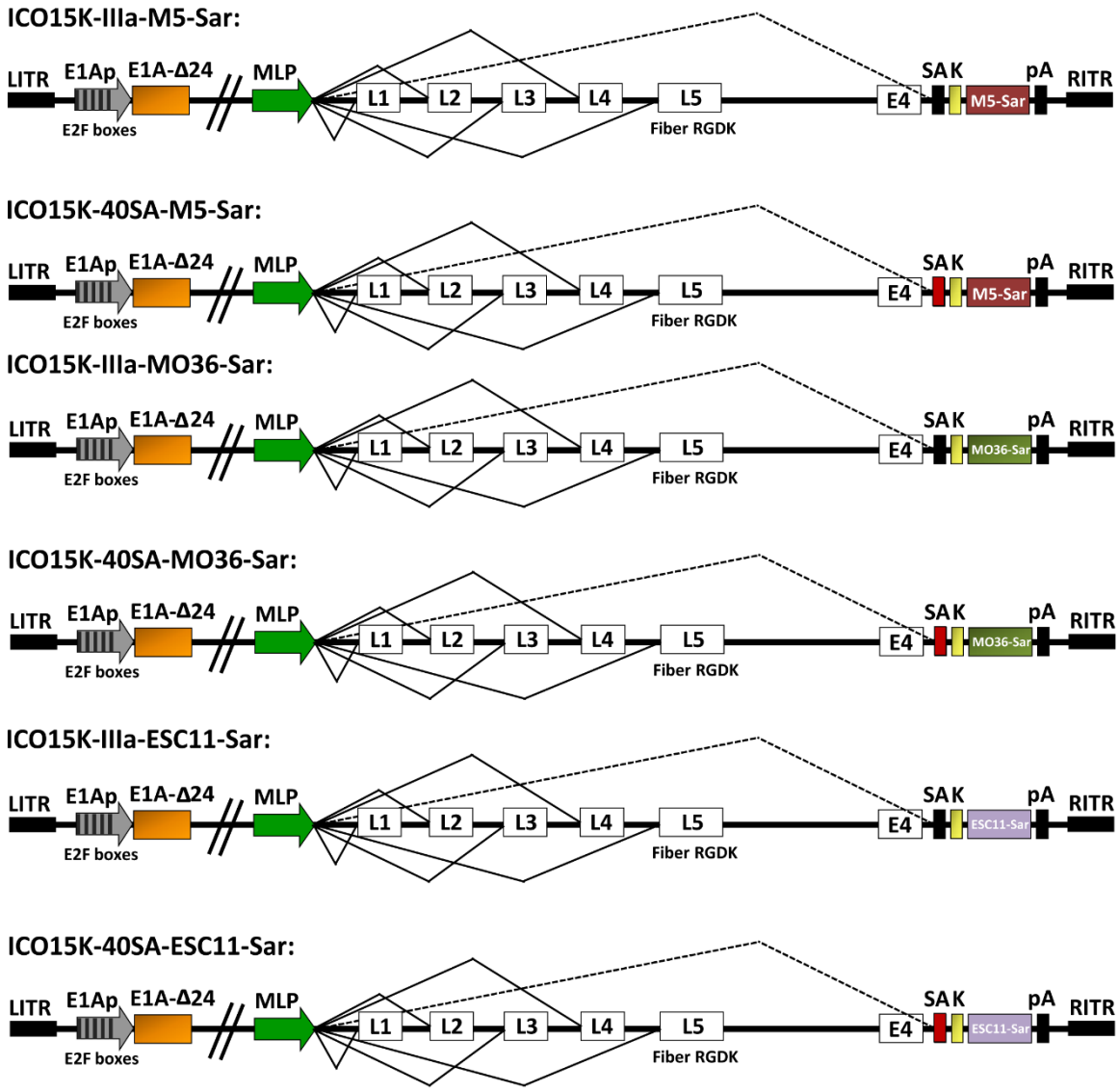

Figure 35. Schematic representation of the immunotoxin-expressing viruses used in this section. IIIa (SA, black square) or 40SA (SA, red square) splice acceptor and Kozak (K) sequences were included 5' of the

transgene. A 6-Histidine tag was inserted at the C-terminus of the immunotoxin gene to facilitate its detection. For all cases, coding DNA sequences were codon-optimized towards the human-biased codon use. MLP: major late promoter; SA: splicing acceptor K: kozak; pA: polyA.

Viable viruses were generated, and further experiments were performed with clarified cell extracts (CCE).

3.1.2 FAP-specific binding of immunotoxins secreted by infected cells

The first parameter we wanted to characterize was whether immunotoxins were properly synthesized by infected cells, secreted to the extracellular media and able to bind to FAP-positive cells. For this purpose, binding assays with HT1080 cells, its derivative FAP-expressing cells and non-concentrated supernatants were performed. Binding of immunotoxins was detected by flow cytometry with an anti-His tag antibody. As shown in **Figure 36**, although immunotoxins were detected in supernatants and they bound specifically to FAP-expressing cells but not to FAP-negative parental cell line, bindings significantly differ between them. Immunotoxins from ICO15K-M5-Sar and ICO15K-MO36-Sar supernatants were slightly detected, contrary to the ICO15K-ESC11-Sar supernatants, which high detection of the proteins was observed only when incubated with HT-hFAP cells. These differences may rely in the differences of affinities between the antibodies or in the design of the immunotoxins, which could differently affect its synthesis and properties.

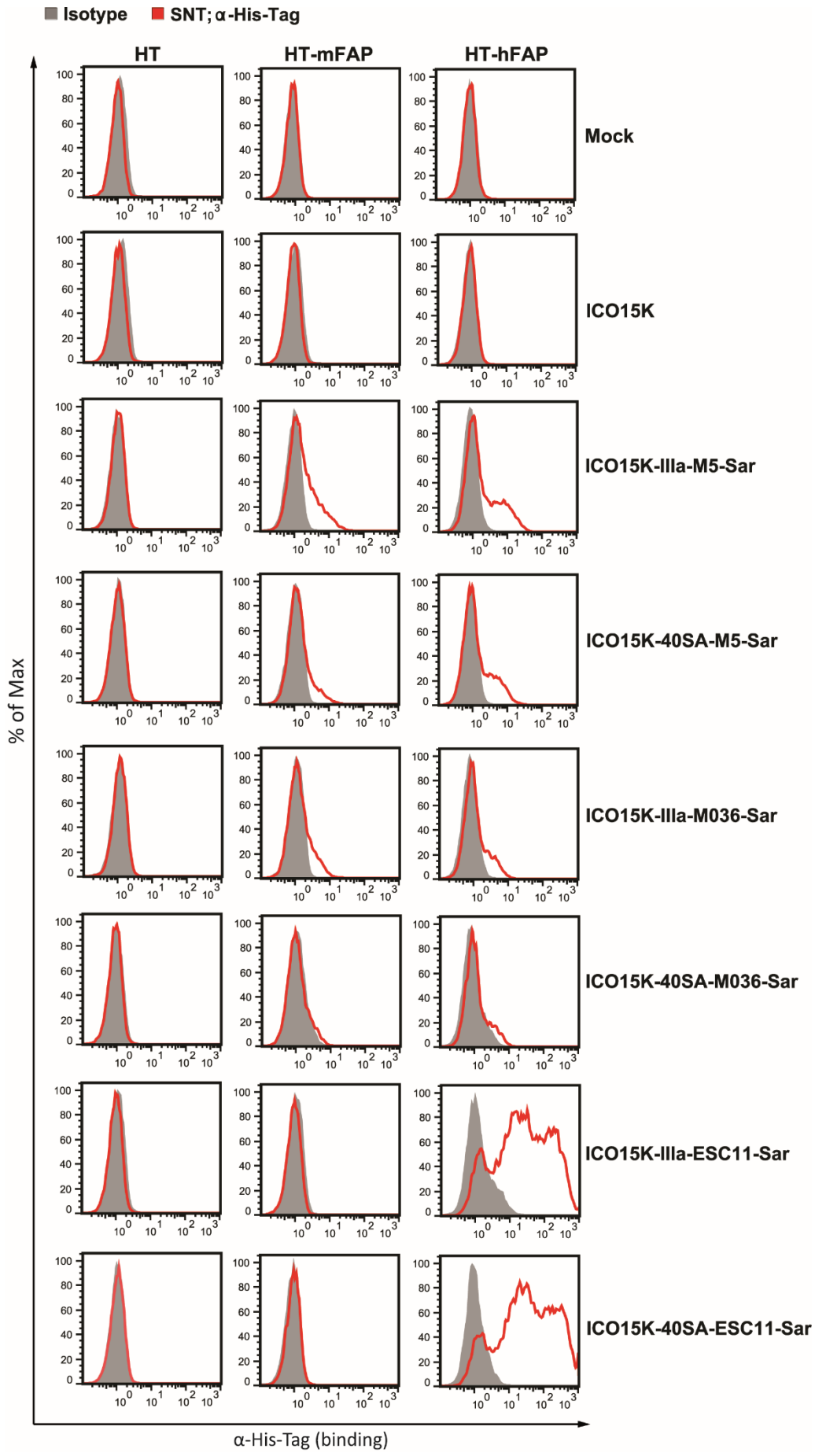
Isotype
SNT; α-His-Tag
HT
HT-mFAP
HT-hFAP
Mock
ICO15K
ICO15K-IIIa-M5-Sar
ICO15K-40SA-M5-Sar
ICO15K-IIIa-M036-Sar
ICO15K-40SA-M036-Sar
ICO15K-IIIa-ESC11-Sar
ICO15K-40SA-ESC11-Sar
% of Max
α-His-Tag (binding)

Figure 36. Binding assay of the immunotoxins secreted by infected cells. HT1080 (HT), HT-mFAP and HT-hFAP were incubated with mock, ICO15K or immunotoxin-containing non-concentrated supernatants. Immunotoxin binding was detected by flow cytometry incubating cells with an anti-His tag antibody and an Alexa647-coupled secondary antibody. A representative result of triplicates is shown.

3.1.3 *In vitro* cytotoxicity of oncolytic adenovirus expressing immunotoxin

Having demonstrated the ability of the secreted immunotoxins to bind specifically to FAP-expressing cells, we then evaluated if these immunotoxins could internalize through the cell membrane and provoke the cytotoxicity of the target cells. First, 293, 293mFAP and 293hFAP were incubated with serial dilutions of ICO15K, ICO15K-IIIa-M5-Sar or ICO15K-40SA-M5-Sar viruses. After 6 days, viability was evaluated. Although we observed significant differences in cytotoxicity between viruses, being ICO15K the more potent virus and the ICO15K-40SA-M5-Sar the less, we did not observe differences between FAP-positive or -negative cell lines (**Figure 37A**). Second, cytotoxicity of target cells was also studied using supernatants of infected cells. HT, HT-mFAP and HT-hFAP were incubated with indicated supernatants and three days post-incubation, cytotoxicity was evaluated by flow cytometry. As shown in **Figure 37B,** no significant cytotoxicities were observed between any condition. Taken together, these results evidence the inability of the M5-Sarcin immunotoxin to efficiently kill target cells. Although the lack of toxicity remain still unknown, possible reasons could be the inability of the scFv to properly internalize into the cell, the viral bioselection of those viruses expressing non-functional toxins, an insufficient concentration of the immunotoxin to kill the cells, etc.

Aiming to optimize the antitumor potential of the engineered immunotoxins, we next decided to test whether the MO36-Sarcin or the ESC11-Sarcin, which have different anti-FAP scFv, could properly internalize and reach the ribosome from the target cell. To this end, same cytotoxicity assay than described in **Figure 37B** was performed with the new supernatants (ICO15K-IIIa-MO36-Sar, ICO15K-40SA-MO36-Sar, ICO15K-IIIa-ESC11-Sar or ICO15K-40SA-ESC11-Sar). As result in **Figure 38** shows, again no advantage could be achieved by the expression of the new immunotoxins in A549 cells.

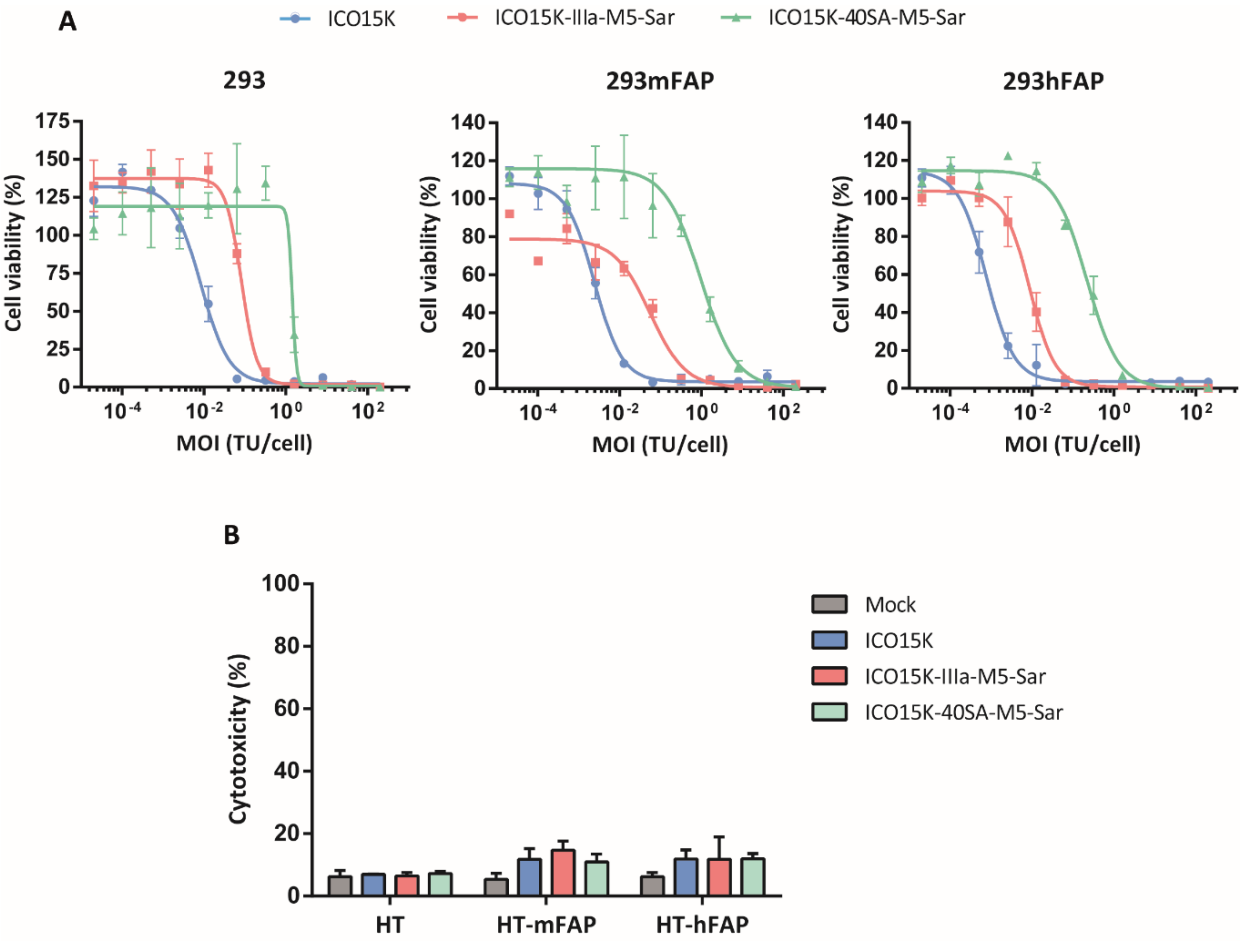

Figure 37. Cytotoxicity of M5-Sarcin-expressing viruses. A. 293, 293mFAP and 293hFAP were incubated with serial dilution of ICO15K, ICO15K-IIIa-M5-Sar or ICO15K-40SA-M5-Sar. After 6 days of incubation, cell viability was measured by BCA protein assay. Dose-response curves are shown along with the IC50 values for each virus and condition. **B.** HT, HT-mFAP and HT-hFAP cells were co-cultured with supernatants from Mock/ICO15K/ICO15K-IIIa-M5-Sar/ICO15K-40SA-M5-Sar-infected A549 cells. 72h after co-culture, cells were stained with LIVE/DEAD and the percentage of cytotoxicity was determined by flow cytometry. In **A** and **B**, the mean ± SD of triplicates is shown.

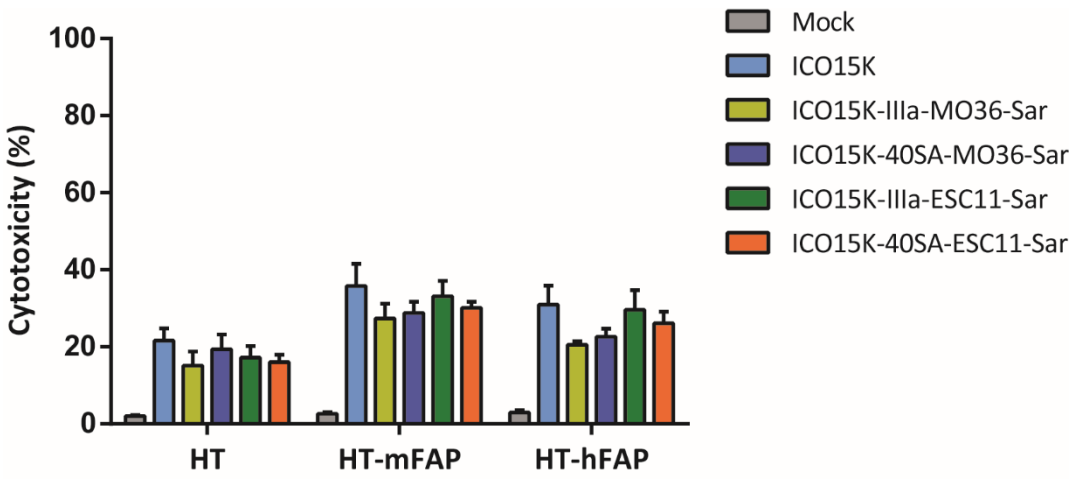

Figure 38. Immunotoxin-mediated cytotoxicity. HT, HT-mFAP and HT-hFAP cells were co-cultured with indicated supernatants. After 72h of incubation, cells were stained with LIVE/DEAD and the percentage of cytotoxicity was determined by flow cytometry. Mean ± SD of triplicates is shown.

Since there is no certainty of the functionality of the Sarcin toxin, we decided not to continue with this toxin and change the strategy to generate another immunotoxin. Sarcin was then replaced by Onconase, a ribonuclease found in the oocytes of the Northern Leopard Frog, and which had already been used and validated as an immunotoxin against EGFR-expressing cancer cells (Fernández-Ulibarri et al. 2015). We designed the new immunotoxin, termed ONCO-FAP, by joining a toxin Onconase and the scFv derived from the anti-FAP5 (M5) described above. The ONCO-FAP was arranged with the toxin located at N-terminus and the anti-FAP placed at the C-terminus to improve the functionality of the immunotoxin. This gene also included the splicing acceptor 40SA, kozak, signal peptide, Hist tag and polyA sequenced described for the other immunotoxins. The genome of ICO15K was genetically engineered by homologous recombination in bacteria to place the ONCO-FAP construct between E4 and LITR under the control of the MLP (**Figure 39A**). As performed with the above-described immunotoxins, we next tested whether ICO15K-ONCO-FAP infected cells could produce and secrete functional immunotoxin ONCO-FAP. To assess the production and effectiveness of the ONCO-FAP, *in vitro* cytotoxicity was evaluated in HT and its FAP-derivative cell lines. Cells were infected at gradually decreasing MOIs of the parental ICO15K and ICO15K-ONCO-FAP viruses, and the percentage of cell viability was determined. Both adenoviruses presented a similar cytotoxic profile in all cell lines tested (**Figure 39B**), indicating that no advantage in cell death could be attributed to ONCO-FAP from the supernatants.

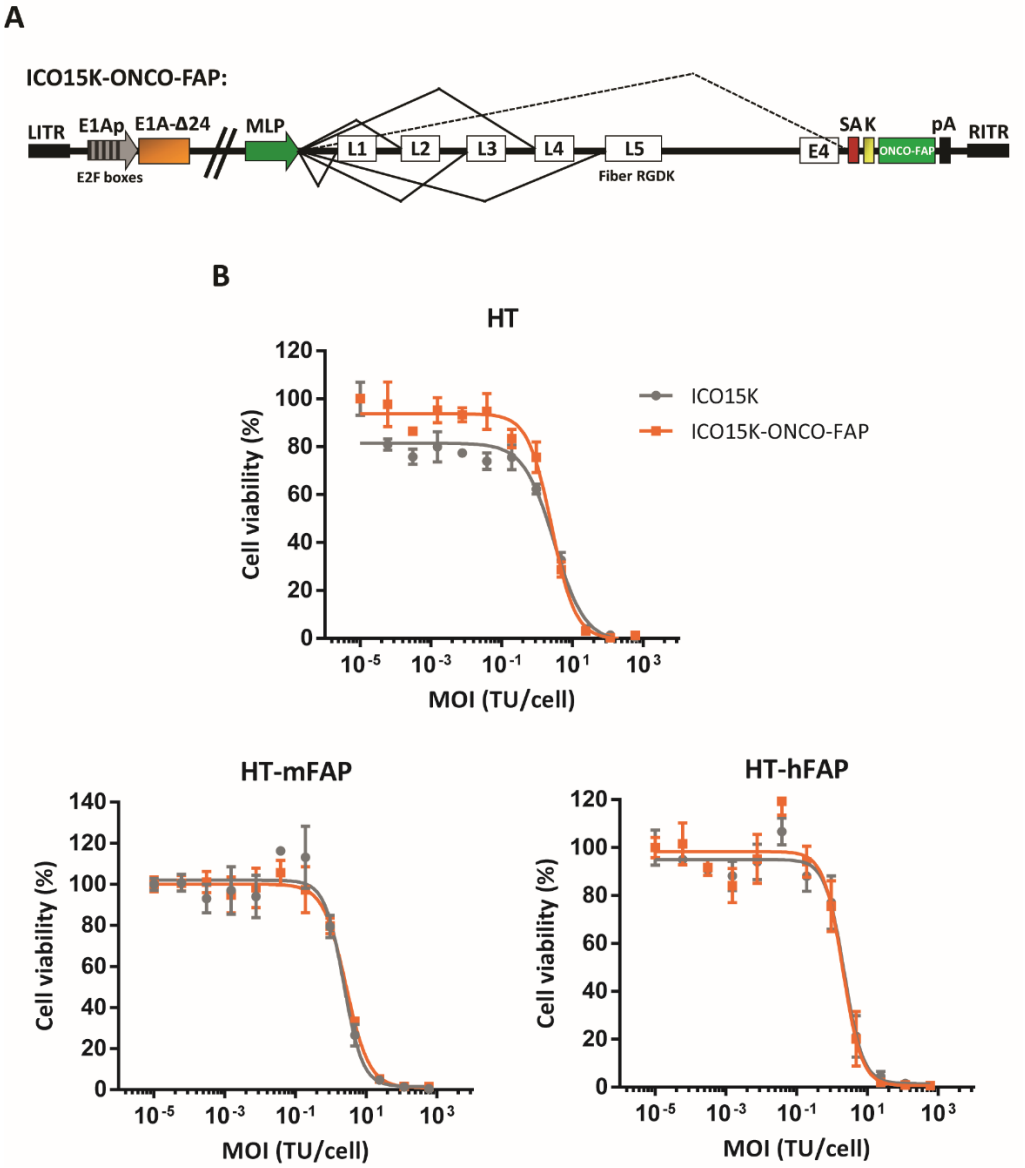

Figure 39. Construction and *in vitro* characterization of ICO15K-ONCO-FAP. A. Schematic representation of the genome of ICO15K-ONCO-FAP. ONCO-FAP transgene was cloned after E4, flanked by the 40SA splicing acceptor (SA) and Kozak (K) sequence in N-terminus and the polyadenylation (pA) in C-terminus. **B.** HT, HT-mFAP and HT-hFAP were infected with serial dilutions of ICO15K or ICO15K-ONCO-FAP, and on day 6 post-infection, cell viability was determined by BCA staining. The mean of triplicates is plotted.

3.2 EXPRESSION VECTOR-ENCODED IMMUNOTOXIN

3.2.1 Generation of expression vector-encoded immunotoxin

Facing the impossibility of acquiring any cytotoxicity from a diverse panel of immunotoxins expressed from the adenovirus ICO15K (see chapter 3.1), we decided to change the strategy and express these immunotoxins from an expression vector. This strategy would

avoid any possible clonality of a virus expressing non-functional immunotoxin. The objective of this chapter was therefore to analyze the oncolytic potential and functionality of the above-described immunotoxins M5-Sarcin, ESC11-Sarcin and ONCO-FAP without the interaction of the oncolytic adenovirus. Immunotoxins were design as already described and shown in **Figure 40**. Coding sequences of the different immunotoxins were introduced after the cytomegalovirus promoter (CMVp) in a GT4082 expression vector, which is derived from the pcDNA3.1 plasmid. GT4082 contained an expression cassette CMV-GFP, in which GFP was replaced to incorporate the immunotoxin (as described in 3.2.4 section).

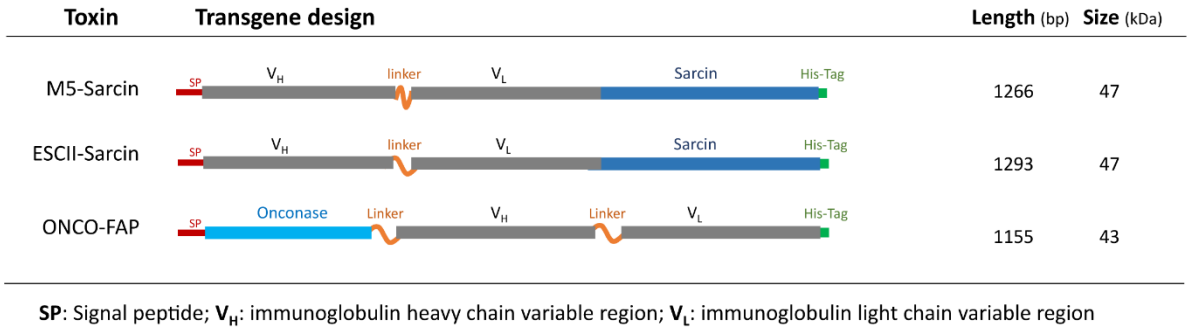

Figure 40. Diagram of the immunotoxin expressed by GT4082. Design, size and length of the immunotoxins encoded by the expression vector GT4082. Sequence are flanked by the signal peptide and the kozak sequence in N-terminus and the polyadenylation and His tag in the C-terminus.

3.2.2 Binding of secreted immunotoxin to FAP-expressing cells

As performed in immunotoxins-expressing viruses, we next wanted to evaluate whether immunotoxins-encoded expression vector could produce and secrete functional immunotoxins. To assess the production and binding of the proteins, the human 293, 293hFAP and 293mFAP and the HT, HT-hFAP and HT-mFAP were used for binding assays with concentrated and non-concentrated supernatants of HEK293-transfected cells. Immunotoxins molecules were detected in the supernatants of M5-Sarcin, ESC11-Sarcin and ONCO-FAP and they specifically bound to FAP-expressing cancer cells in both cell lines (**Figure 41A, B**). Bindings were generally more pronounced when supernatants were concentrated.

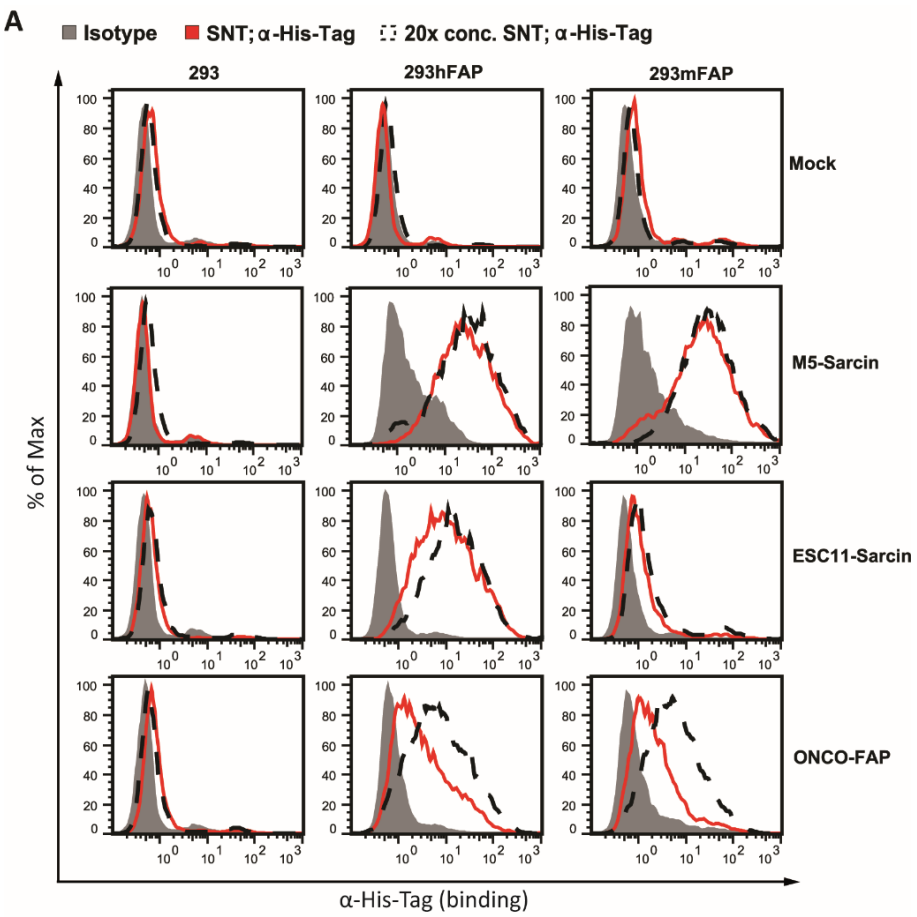
A
Isotype
SNT; α-His-Tag
20x conc. SNT; α-His-Tag
293
293hFAP
293mFAP
Mock
M5-Sarcin
ESC11-Sarcin
ONCO-FAP
% of Max
α-His-Tag (binding)

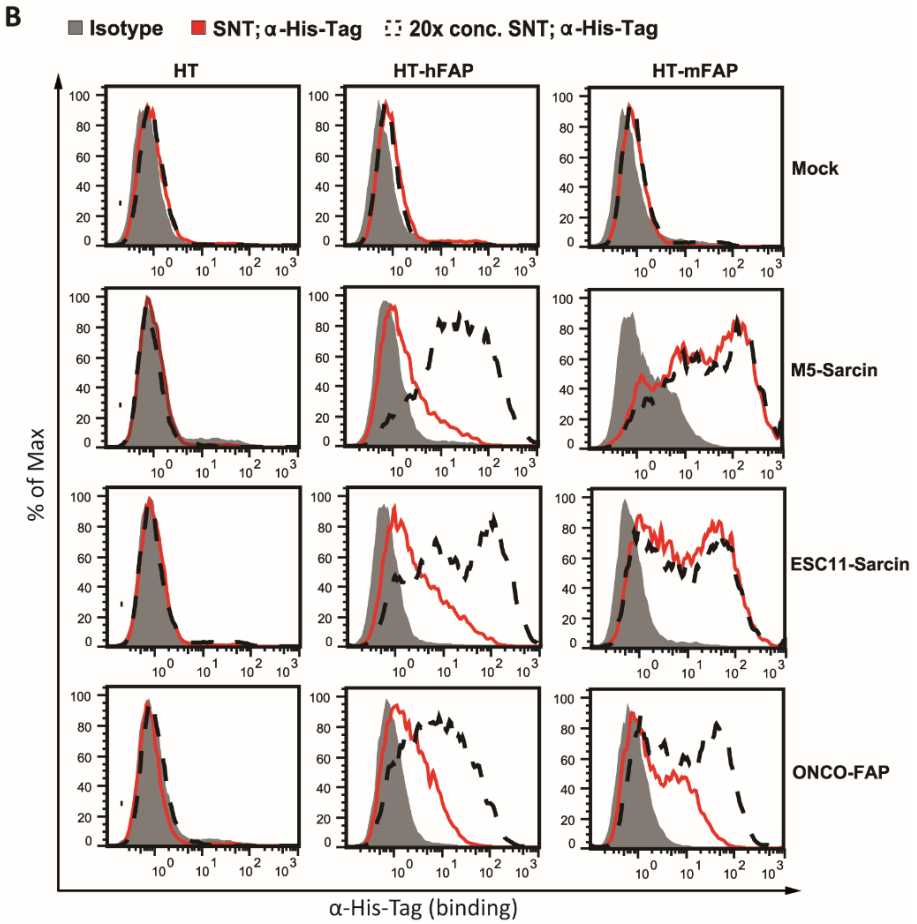
B
Isotype
SNT; α-His-Tag
20x conc. SNT; α-His-Tag
HT
HT-hFAP
HT-mFAP
Mock
M5-Sarcin
ESC11-Sarcin
ONCO-FAP
% of Max
α-His-Tag (binding)

Figure 41. Binding assays of immunotoxins expressed from HEK293-transfected cells. (**A**) 293 and its FAP-derivatives or (**B**) HT, HT-mFAP and HT-hFAP were incubated with the indicated non-concentrated (red solid lines) or 20x concentrated supernatants (black dashed lines) of HEK293-transfected cells. Supernatants from uninfected cells (mock) were used as a negative control. Immunotoxin binding was detected by flow cytometry after incubating cells with an anti-His tag antibody and an Alexa647-coupled secondary antibody.

3.2.3 Specific cytotoxicity of FAP-positive cells by supernatants-containing immunotoxin

Having observed striking binding of the different immunotoxins, we next studied its cytotoxic capacity *in vitro*. For this, we performed flow cytometry-based immunotoxin-mediated cytotoxicity assays by culturing HT and its derivative FAP-expressing cell lines with non-concentrated or 10x concentrated supernatants of HEK293 transfected cells. We could not observe any cytotoxicity benefit from any of the immunotoxins tested (**Figure 42**). Moreover, no differences between concentrated and non-concentrated supernatants were observed, indicating that the concentration of the protein would not likely be the problem of the lack of toxicity.

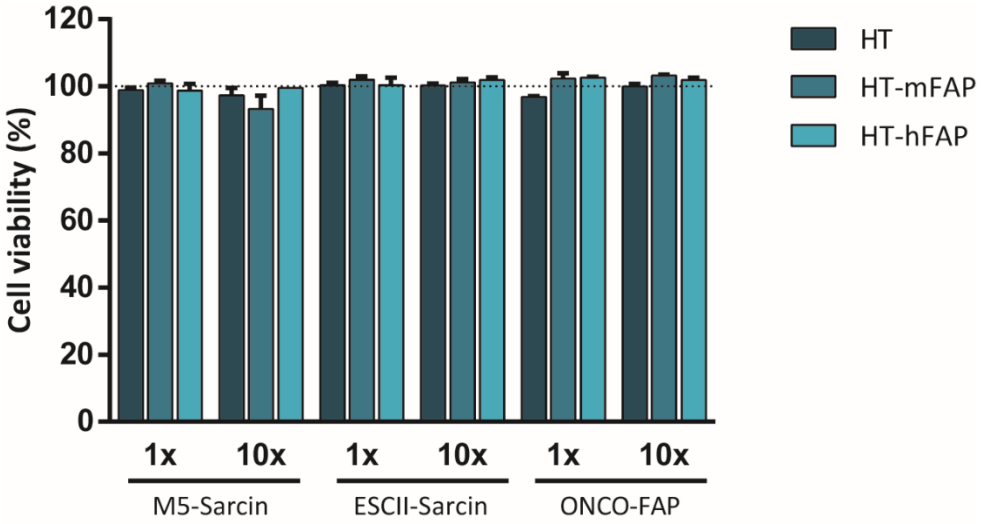

Figure 42. Cytotoxicity of immunotoxin-containing supernatants of HEK293 transfected cells. HT. HT-mFAP and HT-FAP cell lines were incubated with non-concentrated (1x) or 10x concentrated supernatants (10x) for 72 hours. Cell viability was measured by flow cytometry after LIVE/DEAD staining. Viabilities were normalized to baseline values of the same cells incubated only with media. Mean values ± SD are plotted (n=3).

Not having observed an improvement in cancer cell cytotoxicity with the ICO15K- nor the expression vector-expressing the immunotoxins, we decided to stop the immunotoxin-

related project. In both cases, we did show expression and binding of the different immunotoxins, but we could never observe a significant antitumor benefit. After different strategies tested, the reason of lack of toxicity remain unknown.

3.3 NFRA-ARMED ONCOLYTIC ADENOVIRUS

3.3.1 Generation of NfrA-secreting oncolytic adenovirus

Using the oncolytic virotherapy for delivery of prodrug activating enzymes offers the possibility for improving the distribution and level of enzyme expression within a tumor, in addition to any synergy between viral oncolysis and the targeted chemotherapy of prodrug activation. In this context, we hypothesize that arming OAds with activable-prodrugs might lead to synergistic interactions that ultimately result in increased therapeutic effects not achievable by either therapy alone. This project was performed in collaboration with the Adam Patterson lab (University of Auckland), specialist in bioreductive prodrugs.

Adam Patterson lab, which have a large library of prodrugs, provided us the best enzyme-prodrug system based on potency and availability. The chosen system consisted in the nitroreductase (NTR) NfrA from *Bacillus subtilis* and the prodrug SN34668 for *in vitro* application (5-[bis(2-bromoethyl)amino]-N-(2-hydroxyethyl)-N-methyl-4-(methylsulfonyl)-2-nitrobenzamide) and the prodrug SN25161 for the *in vivo* assays (2-[[5-[bis(2-bromoethyl)amino]-4-(methylsulfonyl)-2-nitrobenzoyl](methyl)amino]ethyl dihydrogen phosphate) (details are shown in **Table 17**). We then inserted the NfrA into the ICO15K parental backbone, generating the ICO15K-NfrA modified virus (**Figure 43**).

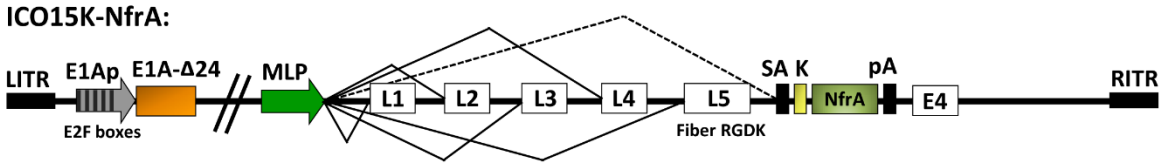

Figure 43. Construction of NfrA-expressing ICO15K. Schematic representation of the genome of ICO15K-NfrA virus. The NfrA gene was cloned after the fiber gene in the genomes of the ICO15K backbone. To drive the expression unfe the control of the major late promoter (MLP), a splicing acceptor (SA) and a polyadenylation sequence (pA) flanked the sequence of the transgene. A kozak (K) sequence was also included before the NfrA gene to increase the translational efficiency.

The objective of this study was therefore to assess the antitumor activity of the prodrug SN34668 synthesized in the Auckland Cancer Society Research Centre (ACSRC), as substrate for *Bacillus subtilis* NfrA gene (NTR) expressed by the ICO15K virus.

SN Number	Chemical Name	Molecular Weight
NTR prodrug		
SN34668 (alcohol prodrug for in vitro)	**5-[bis(2-bromoethyl)amino]-N-(2-hydroxyethyl)-N-methyl-4-(methylsulfonyl)-2-nitrobenzamide**	**531.2231**
NTR pre-prodrug		
SN35161 (phosphate pre-prodrug for in vivo)	**2-[[5-[bis(2-bromoethyl)amino]-4-(methylsulfonyl)-2-nitrobenzoyl](methyl)amino]ethyl dihydrogen phosphate**	**611.2031**

Table 17. Description of the NTR prodrug or pre-prodrug used *in vitro* and *in vivo* assays.

3.3.2 *In vitro* characterization of oncolytic adenovirus expressing NfrA

Once the virus was generated, amplified and purified, a comparative study was performed to characterize the effects of the synergistic therapy compared to the virus therapy alone. The reference physical and functional titers obtained after virus purification (performed as explained in Materials and Methods section) are presented in **Table 18**. Both viruses showed similar proper bioactivity, which enabled easy and comparable manipulation for both *in vitro* and *in vivo* assays.

Virus	Physical titer (vp/mL)	Functional titer (TU/mL)	Physical:Functional ratio
ICO15K	2.1×10^{12}	2.06×10^{11}	10.19
ICO15K-NfrA	2.74×10^{12}	2.80×10^{11}	9.8

Table 18. Characterization of purified virus.

Cytotoxic features of the viruses were tested in the permissive A549 and in the semi-permissive CMT-64.6 cell lines. IC_{50} values from curves are shown in **Figure 44**. No significant differences were detected in both cell lines, suggesting that the transgene-expressing virus could retain the cytotoxic traits of their parental ICO15K virus.

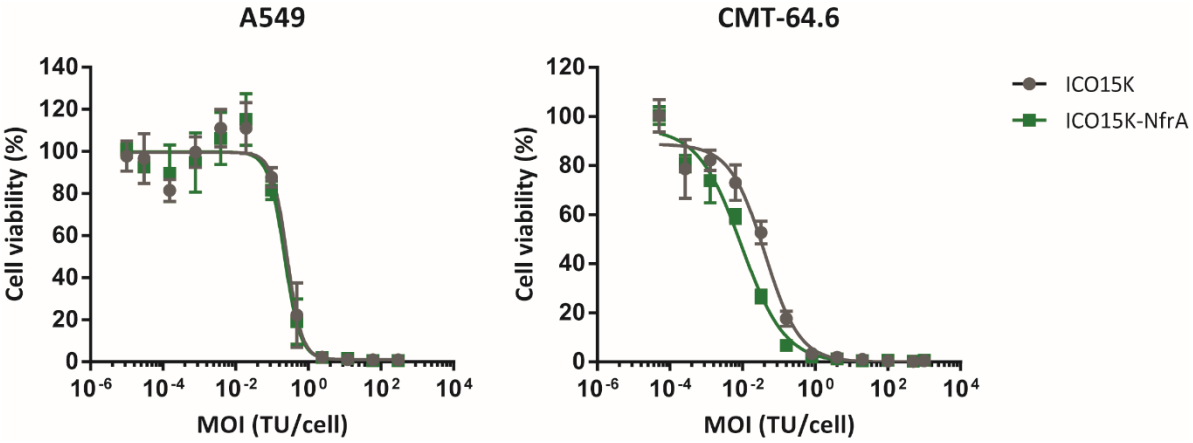

Cell line	IC_{50} ICO15K	IC_{50} ICO15K-NfrA	Fold change vs. ICO15K
A549	0.2576±0.143	0.2179±0.122	1x
CMT-64.6	0.04059±0.025	0.00928±0.0055	-4x

Figure 44. Cytotoxic curves of viruses in permissive and semi-permissive cell lines. A549 or CMT-64.6 cell lines were infected with serial dilutions of ICO15K parental virus or the NfrA-encoded virus and on day 5 (A549) or day 7 (CMT-64.6) post-infection cell viability was determined and IC_{50} were calculated. Mean values ± SD are plotted (n=3).

Once demonstrated that the NfrA-expressing virus conserved the cytotoxic capacities compared to its counterpart, we next wanted to analyze the expression and functionality of the NfrA inserted in the virus genome. In an attempt to answer this point, Adam Patterson provided us a fluorogenic NTR prodrug, the SN29884 (1-methyl-6-nitro-4(1H)-quinolinone) (**Figure 45A**). To establish the cell line dependence of NTR expression kinetics and amplitude following ICO15K-NfrA infection, a panel of four human or murine cell lines were exposed at MOI 3 or MOI 50 (**Figure 45B**). Similar expression patterns were observed across the cell lines, which a peak of intensity between 48 or 72h post-infection. As expected, human cell lines showed better expressions of the protein, in contrast to murine cell lines, which slight expression was only seen in the CMT-64.6 cell line. These results are in line with the permissively of the cell lines, which demonstrate that the expression of the NfrA is effectively restricted to the replication of the virus, avoiding therefore possible undesirable toxicities leaking out of the tumor.

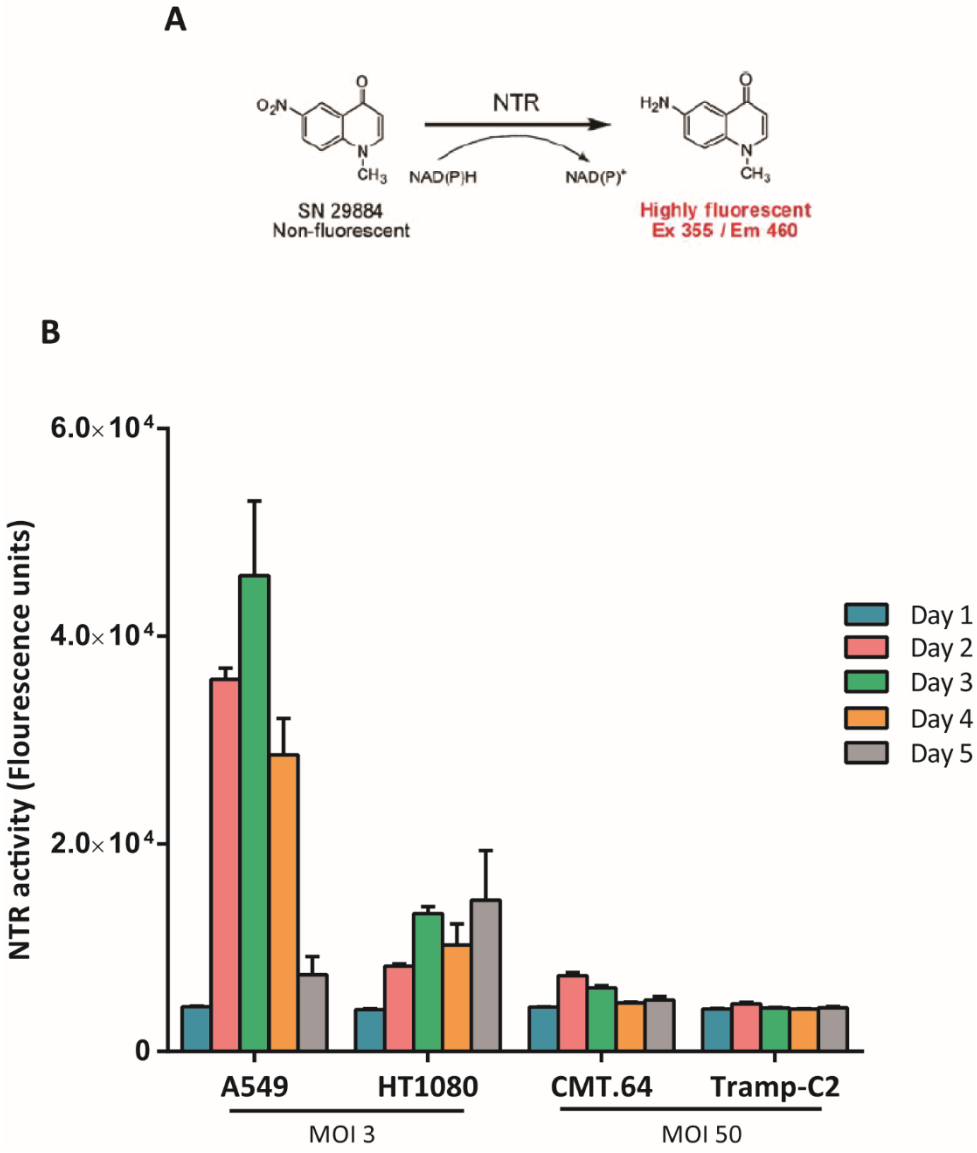

Figure 45. Activity of NfrA expressed by ICO15K-NfrA. A. Fluorescent characterization of a cell-permeable nitroreductase probe for monitoring of cellular nitroreductase (NTR) activity. SN29884 (1-methyl-6-nitro-4(1H)-quinolinone) was diluted from 50mM DMSO stock to 300 µM and used to characterize the enzymatic activity of the NfrA expressed by the modified virus. **B.** SN29884 was added to the cells and after 2h of incubation, fluorescence excitation 350 nm and emission 450 nm were scanned daily. Dependence of NTR expression on time (5 days) using A549, HT1080, CMT-64.6 and Tramp-C2 cells. Mean values ± SD are plotted (n=3).

Having demonstrated desired expression and activity of the NTR-encoded ICO15K, we then evaluated if the reduction of the SN34668 prodrug by the NTR could provoke the cytotoxicity of the target cells *in vitro*. To test this without the interfering cytotoxicity of the virus, we sought a cell line which could partly resist ICO15K infection for 72h. Previous results in our lab reported low percentages of adenovirus infectivity and insignificant

replication in the murine cell line Tramp-C2, and we therefore decided to use this cell line as a candidate for a cytotoxicity assay. In order to have a stable fluorescent signal for flow cytometry discrimination of these cells or for assessing the viability of target cells by measuring the luminescence signal with a plate reader (Victor), a GFP- and luciferase-expressing version of the Tramp-C2 cell line (Tramp-C2-GL) was generated. Then, Tramp-C2-GL cells were co-cultured with ICO15K- or ICO15K-NfrA infected A549 cells in the presence of 50µM SN34668 prodrug for 3 days. Thus, in this setting, A549 act as NfrA producers, while Tramp-C2-GL cells represent the target of the drug. ICO15K-NfrA infected A549 cells induced a decreased in the relative luminescence units (RLU) compared to ICO15K-infected cells when co-cultured with the SN34668 prodrug (**Figure 46**). In this condition, although not significant, total survival of target cells decreased a 30% compared to the ICO15K parental virus.

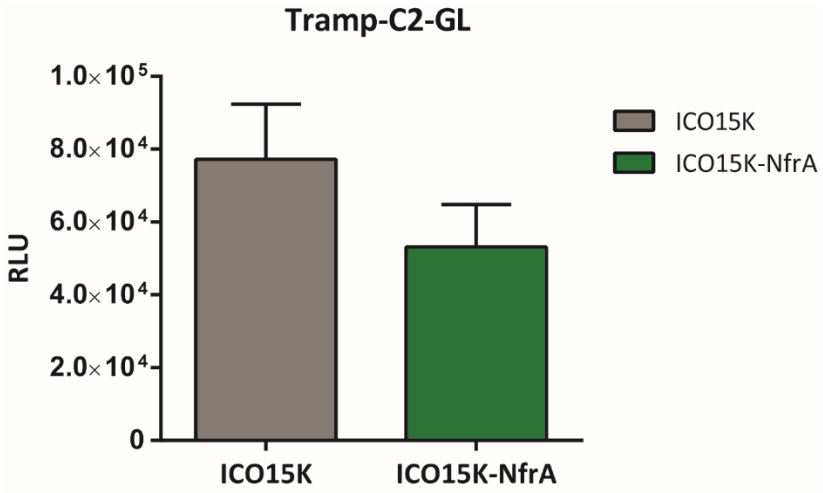

Figure 46. NTR-dependent bystander effect of SN34668. A549 cells were infected with ICO15K or ICO15K-NfrA at MOI of 20 for 4 hours. After washing the excess of virus, A549-infected cells were co-cultured with Tramp-C2-GL cells (1:1 ratio). Three days after infection, viability of Tramp-C2-GL cells was determined measuring its luminescence. Te mean ± SD of triplicates is shown. RLU: relative luminescence units.

DISCUSSION

OAds represent promising therapeutic agents that promote antitumor effects through a dual mechanism: selective tumor cell killing and the induction of antitumor immunity. However, several clinical trials with OAds generated promising albeit modest results (Ahn and Bekaii-Saab 2017). Novel strategies are therefore needed to overcome the obstacles that prevent successful application of OAds, such as eliminating the tumor stroma that prevents efficient virus spread and preventing the immunodominance of the adenoviral epitopes that promotes fast virus clearance (Schirmbeck et al. 2008; Zou 2005). In this thesis, we have focused on overcoming these two main limitations through different strategies.

1. OPTIMIZATION OF REPLICATION-DEPENDENT TRANSGENE EXPRESSION FROM AN ONCOLYTIC ADENOVIRUS

In addition to directly inducing lysis and stimulating antitumor immunity, OVs can be engineered to encode therapeutic proteins that are expressed locally as the virus replicates. Insertion of transgenes into the genome of oncolytic adenoviruses aims at the destruction of neighboring and distant uninfected cancer cells by transgene-encoded therapeutic proteins or RNAs. This strategy aims to increase the efficacys of these agents as cancer therapeutics. Importantly, next to the selection of the candidate transgene, the appropriate amount of transgene expression and a location of transgene insertion into the virus genome compatible with virus replication are pivotal for this approach. Although our group have already demonstrated the feasibility of expressing therapeutic transgenes from the OAd, its success in tumors has still been limited (Arias 2017; Fajardo et al. 2017; Sonia Guedan et al. 2010). Thus, transgene expression may be required to increase the antitumor activity. A major effort in this regard is to express high levels of transgenes in a tumor-specific manner without affecting virus replication. In the first chapter of this thesis, we hypothesized that increasing the transgene expression from OAd without affecting virus replication could improve the potency of our armed OAds. We therefore explored and compared the IIIa- and 40SA-splice acceptor sites in two different locations, after-fiber (as an L6 transcription unit) or between E4 and RITR into the genomes of the parental ICO15K virus, in both cases using a rightward orientation to connect the splicing acceptor to the major late promoter Cytotoxicity capacities and expression levels of an inserted luciferase gene were compared.

Different strategies have been pursued to achieve transgene expression by OAds (Hermiston and Kuhn 2002; Nettelbeck 2008). In some cases, autonomous transgene cassettes including promoters and polyadenylation signals were inserted into various positions of the Ad genome. In other cases, transgenes were connected to viral transcription units using splicing acceptors (SA), internal ribosome entry sites (IRES), or self-cleaved fusions with viral proteins. These latter strategies possess two advantages. They exploit viral mechanisms that ensure efficient gene expression, and second, they facilitate the timing of transgene expression within the viral replication cycle. For example, genes inserted into the late Ad transcription unit are expressed with late kinetics. Such late kinetics of therapeutic gene expression and activity may decrease interference with virus replication. Transgenes have been inserted into the late viral transcription unit either by replacing viral genes or as additional reading frames using IRES or SA sites.

Among these strategies, we decided to evaluate the transgene expression driven by the adenoviral MLP comparing two different splice-acceptors sites. Therefore, OAds with the transgene under the control of the MLP will show reduced expression in non-tumor cells and this may reduce toxicity caused by the transgene. Transgene toxicity is a particular concern upon systemic virus delivery. Notably, high liver toxicity has already been reported following systemic infusion of replication-deficient adenoviral vectors carrying prodrug-converting enzymes under control of a constitutive promoter (Brand et al. 1997; Van der Eb et al. 1998; Qiao et al. 2002). These reports highlight the importance of tumor-restricted transgene expression, which is the strategy used in all chapters of this thesis. Splice acceptor sequences can be used to control transgene expression from endogenous Ad promoters and this represents an approach to arm oncolytic Ads that spares genomic space, which is important as adenovirus 5 genome cannot exceed 38 Kb (Bett, Prevec, and Graham 1983). While packaging of therapeutic genes is generally not an issue for large viruses like HSV, which nearly 50% of HSV genes are nonessential for viral replication (Roizman 1996), and vaccinia, where it is estimated that the virus may be able to package approximately 50 kb of foreign DNA (Moss 1996), for smaller viruses like Ad, this is a considerable hurdle. One strategy has been to generate multiple genes from a single transcript through the use of IRES (Rivera et al. 2004; Rohmer et al. 2009). However, a combination of several genes would be ideal, but the maximum genome size that can fit within the capsid is only 2 kb over the wild-type size. Although the transgene can be inserted as an expression cassette with its own promoter and polyA signal, as usual in

adenoviral vectors used for gene therapy or vaccination, the design of OAd using endogenous viral promoters to express the transgene also saves space and allows a better tuning of the expression with the replication cycle of the virus. In addition, it avoids creating directed or inverted repeats by repetition of promoter or regulatory sequences that result in rearrangements and genome instability. To obtain more than 2 kb of cloning space, deletion of dispensable E3 genes has also been considered. These proteins are non-essential for viral replication *in vitro* and they have been totally replaced with antigen-expression cassettes with exogenous promoters or partially replaced, preserving the E3 promoter and different E3 genes (Bauzon et al. 2003; Rohmer et al. 2009; Zhu et al. 2005). Nonetheless, it has been reported that viruses with an intact E3 region showed higher replication and antitumor responses in immunocompetent models (Y. Wang et al. 2003). Therefore, a different strategy rather than deleting adenoviral genes was required to overcome low transgene expression.

To date, different splicing acceptors signals that have already been tested derive from the Ad genes, such as the IIIa gene (Fajardo et al. 2017; S. Guedan et al. 2008; Sonia Guedan et al. 2010; Muhlemann et al. 2002), Ad41 long fiber (C. Fuerer and Iggo 2004), Ad40 long fiber gene (Carette et al. 2005), or from a consensus splicing signal including branch point, a polypyrimidine track, and a splice acceptor sequence (BPSA) (Fernández-Ulibarri et al. 2015; Jin, Kretschmer, and Hermiston 2005). In our study, we chose the IIIa (also named 3VDE) endogenous splicing acceptor from the IIIa protein of the Ad5 , which is the splicing acceptor currently used in our group, and the 40SA, the splicing acceptor of the long fiber gene of the Ad40, which has been reported to be one of the strongest splicing acceptors (Carette et al. 2005). Both splicing acceptors were evaluated in a position after the fiber or between E4 and the right ITR, in the same orientation of the major late promoter, which means that proteins where expressed at late stages of virus life cycle. For expression of some transgenes by OAds, for example, for pro-apoptotic or cytotoxic genes, restriction of gene expression to late stages of virus replication would facilitate a better compatibility of OAd replication (Fernández-Ulibarri et al. 2015; S. Guedan et al. 2008). Since in this thesis we worked with immunotoxins, late expression of the proteins was a requisite. This decision discarded the evaluation of other strategies based on early expression of transgenes, such as to link the transgene to E1A using IRES (Rivera et al. 2004) or a 2A ribosome skipping or self-cleaving sequence. Our group is currently evaluating the

expression of presumably less toxic protein, such as hyaluronidase PH20, at early expression by the insertion of a 2A linker.

Generation of cLUC-expressing viruses and further amplification in eukaryotic cells allowed effective purification of all viruses and yielded good physical/functional ratios. However, we observed striking loss of cytotoxicity in A549 cells when cLUC cDNA was located after-fiber of the viruses, and significantly more when using the 40SA splicing acceptor. These results seem to be consistent with our experience with several OAds carrying MLP-IIIa-driven transgenes, which consistently show reduced *in vitro* cytotoxic potential compared to the parental virus when tested in this cell line. Regarding the splice-acceptor site 40SA, surprisingly Carette *et al.* reported that the introduction of this splicing acceptor into the genome of an OAd did not decrease its oncolytic activity (Carette et al. 2005). There are, however, some possible explanations for this discrepancy. Although the sequence of the splicing acceptor is exactly the same, there are differences in the virus design between the two studies. We placed the transgene downstream of the fiber gene in a non-E3 deleted OAd-24Δ-based virus (ICO15K), while Carette *et al.* inserted it upstream of the fiber gene in the deleted E3 region of the OAd24Δ, suggesting that the exact position of the splicing acceptor and/or the deletion of E3 gene may be important determinants for the cytotoxic properties of the virus and for the efficiency of the splicing. Another possible explanation might be more related to the codon usage of the proteins. It has been described that optimizing the engineered protein could have a negative effect in its own synthesis and on viral fitness, thus impacting viral activity (Villanueva, Martí-Solano, and Fillat 2016). In line with this, Quirin *et al.* reported that transgenes can interfere in a sequence-specific manner with splicing. For example, they showed that efficient transgene expression was lost by replacing the luciferase cDNA with the FCU1 cDNA, and that this ineffective splicing could be restored by insertion of a luciferase gene-derived spacer downstream of the splicing acceptor in combination with switching codons (Quirin et al. 2010). These studies suggest that not only the location of the insertion, or the strategy of the expression, but also the sequence of the transgene can also impact in viral cytotoxicity and transgene expression. However, this loss of cytotoxicity observed was partially rescued when using the semi-permissive murine CMT-64 cell line, but still the after-fiber location had some deleterious effect. The reason for this may be related to the permissively of the cell line. The amount of ICO15K virus produced in one round of replication in A549 is near to 9000 TU/cell and in CMT-64 is only 6 TU/cell. Thus, after serial rounds of replication, the virus

particles released from the CMT-64 cells are probably too poor to observe the same cytotoxic differences than when using a permissive cell line. In contrast to the after-fiber location, the insertion between E4 and RITR did not have a deleterious effect on virus life cycle.

Using the luciferase gene as a sensitive reporter for monitoring transgene expression, we show lower transgene expression *in vitro* when inserted between the E4 genes and right ITR of the Ad genome in both the E4-IIIa-cLUC and the E4-40SA-cLUC viruses. These findings are supported by previous results in our group and by others, which also observed decreased transgene expression in this location (Arias 2017; Fernández-Ulibarri et al. 2015). Conversely, in a transposon-based scan insertion study for SA-transgene cassettes in the Ad genome, Herminston *et al.* reported that E4 insertion site afforded the strongest transgene expression and the best late transgene expression kinetics (Jin, Kretschmer, and Hermiston 2005). Given that we did not used the same splicing acceptor sequence neither the same orientation of the insertion of the transgene, these parameters remain to be investigated in direct comparisons. Taken together, we observe a clear direct correlation between less cytotoxicity and more transgene expression, which is likely the result of the competition between the cLUC and viral genes for the transcription and translation machinery of the cell. The location after the fiber leads to higher transgene expression but the location upstream to the RITR leads to a tighter replication-dependent expression, which may be more adequate for toxic proteins (corroborated with the results obtained in chapter 3). Nevertheless, since our main goal was to obtain more transgene expression, we decided to discard the viruses with the transgene between E4 and RITR for further *in vivo* experiments. With regard to splicing acceptors, luciferase expression levels were markedly higher in40SA-cLUC viruses-infected cells than levels obtained with IIIa, especially at late stages of infection. These findings broadly supports the work of other studies in this area (Carette et al. 2005; Fernández-Ulibarri et al. 2015), who described the 40SA splicing acceptor as the strongest splicing acceptor.

In vivo studies in both A549 and CMT-64 cell lines in the immunocompromised SCID/Beige mice also showed clear differences in luciferase expression. The lack of an appropriate animal model to evaluate OAds is one of the main drawbacks for the progress in the field. This problem derives from the fact that Ads are species-specific and consequently, human Ads replicate very poorly in murine cell lines (Jogler et al. 2006). Precisely for this reason, in

this chapter we also wanted to evaluate the feasibility of expressing transgenes from virus infected-murine cell lines. Consistent with our *in vitro* assays, we observed significant higher luciferase expression with the 40SA splicing acceptor compared to the IIIa splicing acceptor (both located after-fiber). Importantly, luciferase expression was detected in both mice models. Nevertheless, lack of antitumor efficacy, less transgene levels, and shorter persistence of luciferase expression were observed in CMT-64 model compared to A549 model. These results may be explained by the lower virus replication in murine CMT-64 cell line, leading to a rapid virus clearance even in the absence of the immune system. This agrees with earlier observations which showed that virus antitumor efficacy in CMT-64 in an immunocompetent model was lost in the absence of the immune system (Al-Zaher et al. 2018). Remarkably, in the A549 mice model the loss of cytotoxicity by the 40SA-cLUC carrying virus *in vitro* did not translated to a loss of antitumor efficacy. This result encouraged us to evaluate whether more expression by 40SA of a therapeutic transgene would enhance the overall antitumor efficacy *in vivo*. Nevertheless, higher expression of an anti-EGFR-armed OAd did not provide any therapeutic advantage. There are two possible explanations for these results. One is that the loss of cytotoxicity of the 40SA-cBiTE virus observed *in vitro* is compensated *in vivo* by the higher number of BiTE molecules expressed in the tumor. Thus, more concentration of BiTEs may mediate better activation of T cells to kill the stroma, balancing therefore the antitumor efficacy between the two viruses, but at the end, not contributing to improve the efficacy over the IIIa-cBiTE virus. Another explanation may be related with the lack of adequate model mice. It is probable that although more molecules of BiTE are available when using the 40SA splicing acceptor, the lack of enough functional T cells in NSG model would finally limit the antitumor activity (this limitation is further discussed in section 2). Despite this discouraging result, furtehr studies could be done to determine whether the 40SA splicing acceptor is a suitable candidate or not. For example, other therapeutic transgenes that do not depend of a third component (T cells in the case of the BiTE) and that have different sequences could clarify conclusions.

In summary, we have constructed a panel of replication-dependent strategies for transgene expression by OAd. However, the inverse correlation of transgene expression and oncolytic potency of the virus poses a dilemma to select the best candidate virus. Overall, our results clearly reveal that the efficiency of transgene expression depend on the strategy of transgene insertion into the transcription unit but most importantly, it might

require optimization for individual transgenes. New avenues should be pursued to further improve transgene expression without impairing virus potency. For example, a more detailed analysis of both early and late insertion sites, mutations of endogenous splicing acceptors, design of new promoters and splice-acceptor sites, or viral promoter reconstitution could help to reduce the adverse effects on viral gene expression and replication or to improve transgene expression. Ideally, more strategies should be compared with different transgenes. In line with this, ongoing projects in our group are evaluating both novel transgene insertion sites and the maximum transgene size compatible with viral replication following the transposon-based approach developed by Kretschmer *et al.* (Kretschmer et al. 2005).

2. FBITE-ARMED ONCOLYTIC ADENOVIRUS

The induction of antiviral T cell responses is a well-documented consequence of the viral infection of normal tissues. As discussed above, many OVs induce an inflammatory form of cell death (ICD) with potential to reverse tumor immune suppression. OV-triggered inflammation in the tumor bed has been shown to alter the chemokine and cytokine milieu in such a way as to increase tumor infiltration with T cells, from a “cold” to a “hot” or lymphocyte-infiltrated tumor (Garcia-Carbonero et al. 2017; Ribas et al. 2017; Dmitriy Zamarin and Wolchok 2014). However, the main side effect of the host immune system is the efficient clearance of the virus counteracting the oncolytic effect of the treatment. Thus, a critical determinant of OV efficacy may be the balance between antiviral and antitumor immune responses.

One of the major obstacles to successful oncolytic therapy is the presence of stroma in tumors. CAFs, which comprise the main component of the tumor stroma, not only form a thick layer surrounding the tumor vasculature that limits virus spread within the tumor (Salmon et al. 2012), but also induce the formation of an altered ECM responsible for the acceleration of tumor progression, modulate inflammatory response, activate angiogenesis, and stimulate the progression and invasive capacity of tumor cells (Feig et al. 2013; Kalluri 2016; Pardoll 2012). We therefore hypothesized that arming OAds with BiTEs that redirect immune response towards tumor stroma cells would solve these key challenges in oncolytic virotherapy (**Figure 47**).

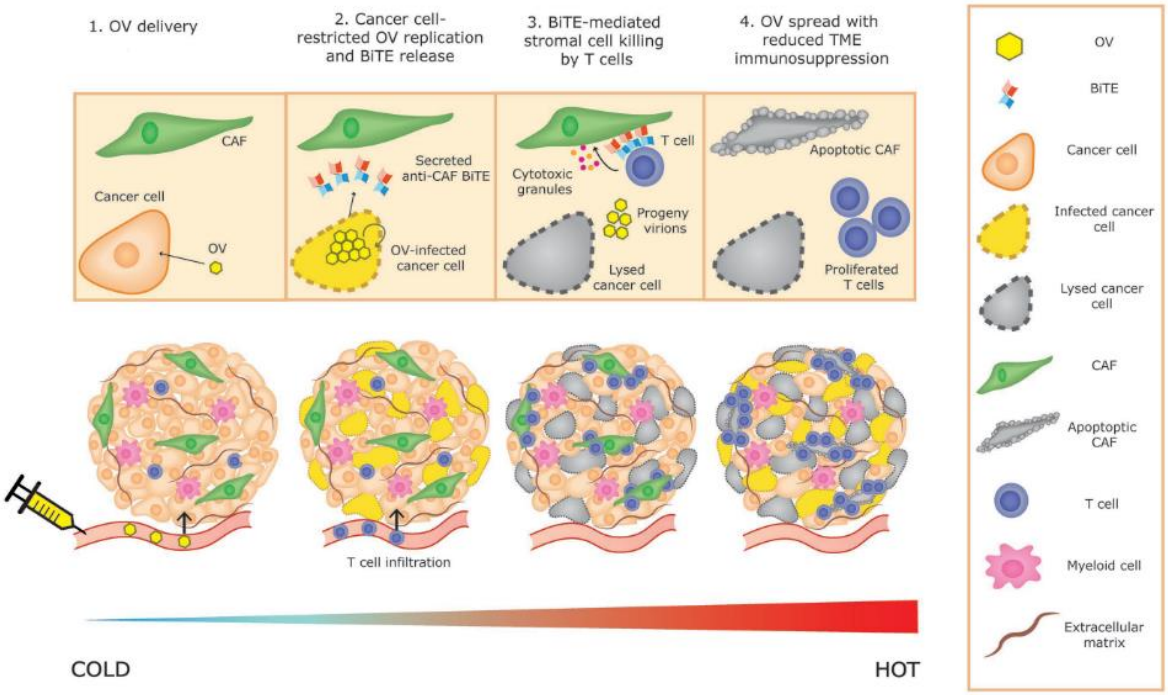

Figure 47. Dual targeting of cancer and tumor stroma using OVs encoding stromal cell-targeted BiTEs. Systemic delivery of BiTE-armed OVs leads to infection of cancer cells (1). Cancer cell-restricted virus replication (infected cells shown yellow) leads to localized BiTE secretion (2) and stroma cells-targeted BiTEs. will redirect the cytotoxicity of endogenous and infiltrating polyclonal T cells to CAFs. Meanwhile, progeny virions released from dying cancer cells (gray) can spread to neighboring cancer cells (3). Continued cycles of virus replication and cancer cell lysis will lead to OV spread throughout the tumor, while BiTE-mediated depletion of CAFs may decrease TME-mediated immunosuppression (4). In this manner, BiTE-armed OVs could convert an immunologically "cold" tumor into one that is immunologically "hot". Imaged taken from (Scott et al. 2018).

In the present work, we aimed at addressing these limitations by arming an OAd with an anti-FAP Bispecific T-cell Engager (FBiTE). We have genetically engineered the parental OAd ICO15K to encode the FBiTE, which is produced and secreted from infected cells. Among the different CAF-specific and nonspecific markers, we chose the fibroblast activation protein (FAP) as the tumor-associated antigen (TAA) being targeted by BiTEs for several reasons. FAP is a membrane-bound serine protease selectively expressed in fibroblasts and its up-regulation in CAFs makes it a prime target. The role of FAP in tumorigenesis is, however, somewhat controversial. Its silencing has shown inhibition of stromagenesis, tumor growth, and angiogenesis in lung and colon cancer murine models (Santos et al. 2009) and suppression of cell proliferation, migration, and invasion of ovarian squamous cell carcinoma cells *in vitro* and *in vivo* (H. Wang et al. 2014). These data confirms previous results suggesting that targeting FAP enhances antitumor efficacy and

might be therefore a promising approach for clinical benefits (Kakarla et al. 2013; J. Lee et al. 2005; Lo et al. 2015; Ostermann et al. 2008; Speck et al. 2018; Tran et al. 2013; Yu, Hong, and Song 2017). In contrast, other studies showed that expression of FAP decreased tumorigenicity in mouse models of melanoma (Ramirez-Montagut et al. 2004), and it was associated with longer survival in patients with invasive ductal carcinoma of the breast (Ariga et al. 2002). These conflicting observations suggest that the physiologic response to FAP may depend not only on the *in vivo* tumor microenvironment but also on the exact context of the expression within different microenvironments.

For the construction of a BiTE with potential for translation into patients (FBiTE), we chosed the scFvs derived from the monoclonal antibody L2K (anti-CD3) and FAP5 (anti-FAP). The scFv from the L2K antibody is the same that is used in the Blinatumomab BiTE, which is optimized for binding to the CD3 in this format (Brischwein et al. 2006) and has already been validated in BiTEs targeting different TAAs (Hammond et al. 2007; Oberst et al. 2014; Schlereth et al. 2005). In contrast, the scFv FAP (named M5) is comprised of the scFv from the FAP-specific antibody FAP5 (Ostermann et al. 2008). This antibody was specifically chosen for its ability to react to both mouse and human FAP, which is a prerequisite for the use of *in vivo* xenograft models in which the targeted stroma is from mouse origin. In addition, this scFv had been previously used by Tran *et al.* for the generation of an anti-FAP-CAR (Tran et al. 2013). Thus, previous validation of these two scFv would facilitate the functionality of our FBiTE.

The rationale behind the molecular design of the BiTEs described in this work was based on the previous functional BiTE designs made in our laboratory together with the literature of antibody engineering studies. To achieve bispecificity of BiTEs, factors that need to be taken into account include the special arrangement of the scFvs or size of the different target antigens. Minor changes in linker length or composition or 'switch' of domains, can be crucial determinants for functionality (Brinkmann and Kontermann 2017). An anti-EGFR-BiTE (cBiTE) was previously generated and validated in our laboratory (Fajardo et al. 2017). The cBiTE format was chosen based on the fact that all BiTEs in clinical development so far had this conformation (Baeuerle, Reinhardt, and Kufer 2008). We therefore used the cBiTE format to design a functional human anti-FAP BiTE (FBiTE). To this end, CDRs from the EGFR scFv of the anti-EGFR BiTE (cBiTE) were replaced by the specific FAP5 CDRs. This strategy allowed us to conserve the full structure of the cBiTE, minimizing therefore the

possibilities to obtain a non-functional protein. The anti-FAP (M5) and the anti-CD3 (L2K) scFv were located at the N- and C-terminus, respectively. Furthermore, it has been reported that placing the L2K anti-CD3 scFVs at the N-terminus negatively affects the binding capabilities of some BiTEs (Compte et al. 2014; Milan and Peal 2013). Following exactly the same conformation and linkers of the cBiTE, we could detect functional FBiTE in the supernatants of the ICO15K-FBiTE infected cells. Regarding the murine BiTEs (mBiTEs), we first designed the mFBiTE and the 2C11-M5 BiTEs following the literature of BiTEs engineering studies. Most of these reports observed that BiTEs containing the 145.2C11 scFv (anti-murine CD3) placed at the N-terminus improved its functionality (Schlereth et al. 2006; Stone et al. 2012b). Thus, both mFBiTE and 2C11-M5 BiTEs were designed with the 145.2C11 scFv and the M5 scFv at N- and C-terminus, respectively. The difference between both constructions was the V_L-V_H orientation and a GS linker. Nevertheless, no functional BiTEs were detected in supernatants. Given this lack of functionality, we decided to evaluate three more conformations, where the M5 scFv was located in N-terminus and the 2C11 scFv in C-terminus. Moreover, we also assessed different V_H-V_L orientations and glycine-serine linkers. However, none of these five formats showed any sign of functionality, based in binding and cytotoxicity assays. Contrary to our results, most of the BiTEs so far described with some specific orientations show superior binding and cytotoxic activities than other, but still retain binding capacities in any of the arrangements tested (Milan and Peal 2013). Altogether, these results point out the importance of the arrangements, linkers, V_H-V_L orientations and the different scFvs used when designing a BiTE. The inexistence of a “perfect format” makes this approach much more complicated. Testing further possible structure combinations would likely solve this problem, but the generation of all combinations of BiTE-armed OAds represents a huge task. A possible new strategy would be to synthesize first a panel of BiTEs from an expression vector as protein products, following by the selection of a functional candidate and finally the insertion of the candidate into the genome of the virus. This approach, in addition to allow the evaluation of more conformations, it also allows to assess the fully functionality of the protein without the interference of the virus. Although this strategy is now optimized in our laboratory, in this thesis only the human version of BiTE was further developed.

FBiTE secretion by infected cells was confirmed by flow cytometry-based binding assays. ICO15K-40SA-FBiTE infected cells showed higher signal binding compared to the IIIa-FBiTE, which confirm the hypothesis that the 40SA is a stronger splicing acceptor. Surprisingly, no

differences of binding were observed between concentrated and non-concentrated supernatants. It seems that most of the FAP or CD3 antigens expressed by the cells were already bound to a BiTE molecule even when unconcentrated supernatants were used, achieving therefore a binding saturation. In contrast, whereas the binding signal to $CD3^+$ cells was clear when using IIIa-FBiTE non-concentrated supernatant, no binding was detected to FAP^+ cells using the same supernatant. This result indicates that the binding of the FBiTE to the CD3 was of higher affinity than to the FAP, which is the contrary than has been described for Blinatumomab (Dreier et al. 2002). However, this BiTE showed potent activity as well.

Using OVs for cancer-targeted transgene expression has now been validated both preclinically and clinically. Here, we inserted the BiTE after-fiber of the genome, and its expression was regulated using the adenoviral MLP, through the IIIa- or the 40SA splicing acceptor, limiting BiTE production to cells permissive to the virus life cycle. We demonstrated by flow cytometry the secretion of FBiTE to the supernatants 72h post-infection under both the IIIa- or 40SA splicing acceptor. The IIIa splicing acceptor has been widely used by us and others to restrict transgene expression to virus replication (Sonia Guedan et al. 2010; Nettelbeck 2008; Juan J. Rojas et al. 2010). However, although BiTE antibodies have potent activities at very low concentrations (femto- to picomolar) or toward tumor antigens with low expression levels (Bargou et al. 2008; Dreier et al. 2002), modest antitumor activity with the cBiTE under the IIIa splicing acceptor evidenced the need of increasing the expression of transgenes expressed by our virus-infected cells. Since BiTE activity is dose-dependent, we wanted to evaluate if higher concentrations of BiTE molecules would therefore improve T cell-mediated cytotoxicity of target cells *in vitro* and *in vivo*. Thus, the idea of assessing the 40SA splicing acceptor from the HAd-40 long fiber aimed to produce higher amounts of BiTE from the virus-infected cells. In line with this, the after-fiber location has also shown favorable production of transgene molecules compared, for example, with the after-E4 location (tested in this thesis).

Both, IIIa- and 40SA-BiTE-armed OAds had similar cytopathic effect as the parental virus. Despite we were able to amplify both viruses to good titers and ratios, viral yield and cytotoxic properties were decreased compared to ICO15K parental virus. The size of the engineered ICO15K genomes encoding the BiTEs is approximately 37.7 kb, which represents a 105% of the original Ad5 genome size. This percentage is the packaging limit

that has been described for Ads, as inserts giving a genome size above 105% may result in unstable viruses with multiple genomic rearrangements after three to four culture passages (Berkner and Sharp 1983; Ghosh-Choudhury, Haj-Ahmad, and Graham 1987). Earlier observations in our group also showed that OAds carrying MLP-driven after-fiber transgenes slightly impaired our modified-viruses, decreasing their *in vitro* cytotoxic potential compared to the parental virus (Arias 2017; Fajardo et al. 2017; L. A. Rojas et al. 2016). Since the 105% limit is not reached, we believe this loss of cytotoxicity is more related to a consequence of the synthesis competition between the BiTE and the viral genes, rather than to the packaging limit. The fact that this loss is higher for 40SA-FBiTE virus, which expresses more BiTE molecules that the IIIa-FBiTE virus, also supports the hypothesis of an inversely proportional correlation between the synthesis of virus components and the synthesis of the transgene molecules (discussed above). In addition, a recent study has shown that incorporation of a codon-optimized transgene as an L6 unit under the control of the MLP can attenuate adenoviral fitness (Villanueva, Martí-Solano, and Fillat 2016). Despite this loss of production and cytotoxicity, carrying the FBiTE gene confers a significant cytotoxic advantage in the presence of T cells *in vitro*. Most importantly, the *in vitro* loss of cytotoxic of the IIIa-FBiTE-expressing virus did not translate into a loss in antitumor efficacy *in vivo* in the absence of T cells compared to ICO15K. This result may be explained by the excess of virus that is produced in every round of replication.

It is worth highlighting that arming OVs with BiTEs represents a combined anti-cancer therapy. Encoding BiTEs within OVs exploits the strengths of both virotherapy and immunotherapy while overcoming limitations of each agent alone. Our results show that simultaneously targeting the cancer cells with the OAds and the tumor stroma with the FBiTE enhances the overall antitumor efficacy. The potential of BiTEs encoded by OVs have already been explored. The first one was the Ephrin A2-BiTE-armed oncolytic vaccinia virus, which induced PBMCs activation and tumor cell cytotoxicity *in vitro* and *in vivo* (Yu et al. 2014). In line with that study, similar results have been described with different OVs armed with BiTEs (Fajardo et al. 2017; Freedman et al. 2017; Speck et al. 2018). However, all those studies exploited BiTEs targeting tumor-specific antigens (Fajardo et al. 2017; Freedman et al. 2017; Speck et al. 2018; Yu et al. 2014). Thus, those secreted BiTEs can target both infected and uninfected cells, thereby reducing the virus-driven BiTE production and availability in the tumor microenvironment. To overcome this limitation,

the FBiTE was designed to be expressed by the infected cancer cells and to target stromal cells, thereby avoiding the depletion of BiTE-expressing cancer cells and promoting continuous BiTE production dependent on viral oncolysis. In this regard, a recent report described the benefits of targeting the tumor stroma with a FAP-targeting BiTE-armed vaccinia virus in an immunocompetent mouse model of cancer (Yu, Hong, and Song 2017) and most relevant, Freedman *et al.* has recently published a report which demonstrate that the treatment of fresh clinical biopsies with FAP-BiTE encoding virus induced activation of tumor-infiltrating $PD1^+$ T cells to kill CAFs, depleting consequently CAF-associated factors and upregulating proinflammatory cytokines (Freedman et al. 2018). This report supports the feasibility of the clinical application of our ICO15K-FBiTE virus.

In contrast to other therapies, one of the most important advantages of using BiTEs is its MHC-I-independent mode of action (Offner et al. 2006; Schlereth et al. 2005). Loss of MHC expression is a well-documented immune evasion strategy of tumors (Garrido et al. 2016). It is noteworthy that both cytotoxic strategies that are immediately engaged by BiTE-armed OVs operate independently of MHC class I by the tumor cells, and therefore can be employed to kill cancer cells even when tumor cells have lost MHC expression. In fact, BiTEs force T cells and tumor cells to come in close contact, forming an immunological synapse that shows all the hallmarks of a synapse formed by T cell receptor-MHC class I-peptide induced synapses. Therefore, encoding a BiTE specific against FAP by the OAd would ideally redirect antiviral lymphocytes to attack the tumor stroma, independent of MHC I presentation. In line with this, it has been recently reported that BiTEs can engage cytomegalovirus-specific enriched CTLs to kill cancer cells *in vitro*, supporting the idea that redirecting Ad-specific CTLs may also be feasible (Schmittnaegel et al. 2015). In this study, we have demonstrated that once the FBiTE is expressed and secreted from infected cells, it can successfully activate both CD4 and CD8 T cells. This activation leads to T-cell-mediated cytotoxicity of the FAP-expressing cells *in vitro*. Unexpectedly, there was some non-specific cytotoxicity of FAP-negative cells when co-cultured together with its mFAP- or hFAP-derived cells. However, this result is in accord with a recent study, which demonstrated that T cells activated by BiTEs in the presence of target-positive cells release cytokines that diffuse locally and bind to proximal target-negative cells (Ross et al. 2017). These cytokines do not lead to direct cytotoxicity effects but upregulate cell surface molecules, such as ICAM-1 and FAS, on bystander cells, leading to T cell-mediated killing of target-negative cells even in the absence of a regular cytolytic synapse (pseudo-synapse). The authors also

show that diffusion of T cell-derived cytokines is restricted to nearby bystander cells in solid tumors, limiting therefore extratumoral toxicities. In all *in vitro* functional assays, FBiTE construct shows higher affinity for the mouse FAP than for the human FAP. This is in line with the affinity of the FAP5 monoclonal antibody from which the scFV in our BiTE is derived, which has been reported to be 5 nM for human FAP and 0.6 nM for mouse FAP (Ostermann et al. 2008). We further demonstrated that ICO15K-FBiTE promotes T-cell infiltration into tumors and has superior antitumor activity compared to the parental virus in presence of T cells.

The evaluation of our FBiTE-armed OAds *in vivo* was one of the major challenges in this thesis. The anti-CD3 used derives from the BiTE Blinatumomab, which only binds human or chimpanzee CD3 (Benjamin and Stein 2016), and the Ad5-derived OVs replicates and expresses the BiTE only in human tumor cells. The evaluation of the ICO15K-FBiTE was therefore restricted to immunodeficient mouse models bearing human-derived tumor xenografts in which human PBMCs or T cell were transferred to mice. Conversely, the fact that the anti-FAP scFv used can bind to both murine and human FAP allowed the evaluation of targeting the murine CAFs infiltrated into the human tumors. As a model target cell we had the possibility to use lentiviral transduced FAP-expressing tumor cell lines (*e.g.* HT1080-mFAP). Targeting FAP-expressing tumor cell lines *in vivo* would validate our FBiTE-expressing virus but would represent the same approach than the already published with anti-tumor antigen BiTEs-expressing viruses. For this reason, our *in vivo* setting, although more challenging, represent a more realistic scenario. In summary, the BiTE mechanism of action in this setting was to target the infused human PBMCs or T cells towards the FAP antigen in mouse CAFs.

Contrary to the anti-EGFR-BiTE-expressing virus previous developed in our laboratory, NOD/*scid*/*IL2rγ*$^{-/-}$ (NSG) mice instead of SCID/Beige mice were used for the *in vivo* experiments. Although other immunodeficient mice, such as Nude, NOD/SCID or SCID/Beige have been used for the preclinical of BiTE antibodies and CART cells (Avanzi et al. 2018; Hammond et al. 2007; Schlereth et al. 2005; Yu et al. 2014), NSG have rapidly becoming the superior choice of host for the creation of “human immune system” mice since this strain supports high levels of human PBMC engraftment without the requirement of pre-conditioning regimens such as total body irradiation or depletion of host macrophages, that were pre-requisites for successful engraftment in previous

generations of immunodeficient mice. Consistently, short T cell persistence demonstrated in our previous results evidenced the need to use another strain for the current *in vivo* experiments. As there is a population of macrophages in PBMCs that express FAP, we had to perform all the *in vitro* and *in vivo* experiments with isolated T cells. Using preactivated T cells instead of unstimulated T cells is not essential to induce a BiTE-mediated T-cell activation, proliferation and cytotoxicity. Proliferation of both $CD4^+$ and $CD8^+$ population of T cells was observed when unstimulated PBMCs were incubated with FAP-expressing cells *in vitro*. This result is supported by our previous work (Fajardo et al. 2017) where EGFR-BiTE-armed OAd induced PBMCs activation and tumor cell cytotoxicity *in vitro* and *in* vivo, and by Dreier *et al.,* who reported that an anti-CD19/anti-CD3 BiTE could redirect unstimulated cytotoxic T cells against CD19-positive cells in a potent, rapid and specific manner (Dreier et al. 2002). However, the use of preactivated rather than unstimulated T cells has technical advantages. To work with preactivated T cells allows to easily amplify around 35-40 times the initial number of isolated T cells, which is crucial to perform the *in vivo* experiments. Working with unstimulated T cells for *in vivo* experiments, although not impossible, would be more challenging and costly.

The dose and route of administration of the human T cells transferred to NSG mice were also important factors to take into account for our *in vivo* model. Several strategies have been used for preclinical evaluation of BiTEs. Some studies performed a co-implantation of cancer cells and PBMCs before the BiTE treatment (Hammond et al. 2007; Schlereth et al. 2005; Yu et al. 2014). However, these studies are focused in the prevention in tumor formation, which it is not our objective. To assess the efficacy of BiTEs in established tumors, T cells or PBMCs have been injected through several routes: intratumorally, intraperitoneally or intravenously (Speck et al. 2018; Stadler et al. 2016). With this broad range of possibilities, we decided to use intravenously administration for several reasons. Intratumoral administration of T cells was discarded because this strategy does not mimic what happens in an immunocompetent model or in a patient. One of the major hurdles for treating solid tumors using BiTEs is precisely the density and types of T cells already in the tumor bed. Thus, administrating cytotoxic T cells directly into the tumor would probably induce better antitumor efficacy, but it would only represent the best case: the efficacy in a highly infiltrated tumor. On the other hand, the intraperitoneal administration would require the migration of T cells from the peritoneal cavity to the circulation, likely delaying their biodistribution in the mice. We therefore decided that intravenously administration

of preactivated T cells in a 100-130 mm^3 tumors-bearing NSG mice would be the best option for the evaluation of our FBiTE. The rationale of treating the animals around this size is based in our preliminary studies. A tumor volume around 120 mm^3 represents a bigger tumor compared to what may be treated in humans but is usually difficult to measure xenografts tumors whose size is below an average of 80 mm^3. Another important reason is that it is normally hard to control tumor growth when we start the treatment of larger tumors.

A major concern of these *in vivo* experiments was the potential development of T cell-mediated graft versus host disease (GvHD), which is well-described in experiments involving adoptive transfer of human PBMCs or T cells to highly immunodeficient mice. It has been described that NSG mice at 6–12 weeks of age injected intravenously with 10^7 human PBMC via the tail vein developed GvHD consistently with accelerated weight loss and significantly fast disease development, with a median survival time of 40 days (Ali et al. 2012). Consistently, most of the studies that have administrated human PBMCs or T cells intravenously have injected not more than 10^7 cells. We decided therefore to administrate 10^7 human T cells. With this amount, we did not observe any signs of GvHD in our fast-growing HPAC model and importantly, neither with the slow-growing A549 xenograft model, based on body weight and general animal behavior.

The most challenging issue was to choose a human tumor model which generated FAP^+ stroma from mouse origin. A549 (human lung carcinoma) and HPAC (human pancreatic cancer) were chosen as the best models so far for two main reasons: they have shown to generate FAP^+ stroma once implanted in NSG mice (Lo et al. 2015; Tran et al. 2013), and both models had already been used and validated in our group as a permissive tumor model for adenovirus replication with adequate transgene expression (Arias 2017; Fajardo et al. 2017). In contrast, models such as FaDu (pharynx squamous cell carcinoma) were discarded for *in vivo* evaluation because despite this cell line also showed generation of a dense stroma once implanted in mice, it is highly resistant to virus infection and replication, which means that few BiTEs molecules would be synthesized by these cells in the tumor microenvironment, likely limiting BiTE-mediated induction of T cell cytotoxicity (Ostermann et al. 2008). Quantification of murine FAP expression in tumor samples confirmed the presence of murine stroma within the human tumors, but the amount of the stroma in these models still represented a low percentage of the whole tumor mass,

which do not mimic human tumors such as the pancreatic ductal adenocarcinoma (PDAC), where is well-described that the stroma plays an essential role in disease progression (Von Ahrens et al. 2017; Erkan et al. 2012). Thus, the low percentage of stroma component narrowed the therapeutic window for ICO15K-FBiTE. In future studies, to closely mimic the human tumor morphology and the interactions between stroma and cancer cells, stroma-rich orthotopic xenograft models (*e.g.* pancreatic model) could be used instead of subcutaneous xenograft models. Several reports support the idea that using orthotopic models represents a better approach to evaluate the cancer therapeutics. We next wondered which would be the best route of OV administration. It is often stated that an ideal OV should be systemically injectable (also in our group), for some good reasons: essentially, the possibility to infect both primary tumor and metastases, and the fact that this route is relatively non-invasive and injections can be frequently repeated (Fisher 2006). However, although some OVs have been administered intravenously to human patients without severe side effects, the most used route is the local (intratumoral) injection (Marelli et al. 2018). This is the case also for the approved OV T-VEC. Intratumoral delivery is usually chosen because of safety concerns after intravenous injection, or, especially in the case of HSV-1, to minimize the chance that preexisting circulating antibodies might neutralize the virus before it reaches its target (Fukuhara, Ino, and Todo 2016). Nevertheless, as mentioned above, in the case of T-VEC, despite the intratumoral injection, uninjected skin lesions and occasionally even visceral metastases displayed a regression, likely due to the immune response elicited by the virus (Andtbacka et al. 2015). Despite the preferred intravenous injection of the virus in our group, tumors were treated intratumorally for some reasons. The lack of a rich-stroma model and all the hurdles that the virus has to bypass when it is systemically administered represent a drawback for our efficacy studies. For these reasons, we thought that viral intratumoral administration would promote a higher BiTE molecules concentration within the tumor, facilitating therefore the detection of the advantages of our BiTE-expressing virus (proof of concept). Despite this apparent advantage, the dose of viral administration was $1x10^9$ vps/tumor, which represent 50 times lower than the one used for efficacy studies of ICO15K in systemic administrations. Moreover, the distribution of the virus within the tumor is usually more homogenous when given systemically than when injected in one point of the tumor. Given that both routes of administration may not be directly compared, future

studies should be focused in evaluating the efficacy and toxicity of intravenous administration of the ICO15K-FBiTE in the same mice models.

We demonstrated the significant improvement on survival for both models upon one (HPAC) or two (A549) T cell administrations. One of the reasons to inject one or two times was the different growth rates of the models used. Based on our pilot studies which classified HPAC tumors as fast growing, only a single dose of T cells was performed. In contrast, with the A549, which is a model that grows much more slowly than HPAC, mice were treated twice with T cells. However, the decision to inject once in the HPAC model also comes from the fact that injecting two times in the A549 model did not apparently confer any advantage. This is in line with our earlier observations (Fajardo et al. 2017), which showed that two or even three T cell administrations did not improve antitumor efficacy. In previous experiments, we evaluated the biodistribution of luciferase-expressing T cells when readministered to tumor-bearing mice which had received either PBS, ICO15K or ICO15K-cBiTE (OAd encoding the EGFR-targeting BiTE). We observed that after the initial T cell administration, luciferase signal (i.e. T cells) accumulated in tumors treated with ICO15K-cBiTE. However, after administering a second dose of T cells, only one out of six of the tumors that had previously shown luciferase signal, showed increased signal again. This result was independent of the presence of the virus, as we could detect the presence of the virus in tumors by immunofluorescence of tumor sections at the end of the experiment. This suggests that the main antitumor efficacy observed in our *in vivo* experiments are mediated by the first T cell administration. The reason behind this event is still under investigation. We speculate that some major changes in the tumor microenvironment after the initial round of virus replication and BiTE-mediated T-cell lysis might be affecting subsequent T-cell function.

Adenovirus detection at the end of the antitumor efficacy experiments showed similar adenovirus content in tumors between different treatments. Nevertheless, quantification of FAP expression in these samples revealed that in A549 model the ICO15K, besides the ICO15K-FBiTE, had some cytotoxicity against FAP-expressing cells (FAP expression in ICO15K treated-tumor is reduced compared to PBS) whereas in the HPAC model this parental virus does not decrease the amount of FAP-expressing cells. Although we do not know the reason for this difference between the models, this could be related to the twice faster growth rate of HPAC tumors. In the slow growing A549 tumors, the parental virus

better controls the overall tumor growth and has more time to infect and replicate in CAFs, which are quite resistant to adenovirus-mediated cytotoxicity. However, even in this model, the FBiTE-expressing adenovirus still represents an advantage over ICO15K, as it is able to induce higher percentage of T cell-mediated CAFs death in tumors and, consequently, enhanced antitumor efficacy. This result also supports the hypothesis that we would probably observe a greater advantage of our FBiTE-expressing virus compared to the parental virus in permissive tumor models with higher percentage of stroma. However, only few human tumor models are well-described to generate substantial stroma once implanted subcutaneously in NSG mice, limiting therefore the possibility to explore this with further tumor models.

One of the major concerns when targeting non-specific tumor antigens, such as FAP, is the potential toxicity. Despite the controversial toxicity effect related with immune targeting, fatal adverse effects have already been reported (Teachey et al. 2013). In this regard, successful growth inhibition without signs of toxicity by FAP-targeted CARs T-cells has been reported (Kakarla et al. 2013; Lo et al. 2015; L. Wang et al. 2014). In contrast, Tran *et al. r*eported that FAP-targeting with FAP5-CAR-transduced T cells led to cachexia and lethal bone toxicities due to FAP expression by multipotent bone marrow stem cells (BMSCs) (Tran et al. 2013). Other studies have shown that FAP is expressed by some normal tissues and macrophages (Bae et al. 2008; Julia et al. 2013; Roberts et al. 2013). In agreement with this, we found activation and proliferation of T cells when PBMCs were co-cultured with FBiTE-containing supernatants. Importantly, ICO15K-FBiTE treatment did not result in any significant off-target toxicity in mice. This discrepancy can be explained by the mode of action of our OV. FBiTE expression depends on the replication of the OAd in cancer cells within the tumor microenvironment, in contrast to CART-cells, which circulate freely through the body. Thus, the strategy of arming OVs with a FAP-targeting BiTE allows the continuous expression of BiTE directly in the tumor, preventing the targeting of healthy cells by the BiTE and in turn avoiding possible adverse effects. When expressed locally, the short plasma half-lives of BiTEs may become advantageous, minimizing systemic exposure and avoiding "on-target, off-tumor" toxicities (Teachey et al. 2013). In addition, we showed that a single dose of OAd is enough to obtain a continuous expression of BiTE by infected cells, avoiding the needed of repeated systemic infusion due to short half-life of BiTEs (Topp et al. 2011).

Despite the notable improvement of antitumor efficacy obtained with ICO15K-FBiTE, no complete responses were observed. These findings may be somewhat limited by the lack of adequate tumor models used. Using immunocompetent models in order to explore the impact of infiltrating T cells in the tumor after virus injection would represent a more realistic scenario. However, both the inability to design a functional murine FBiTE and the specie-specific nature of the adenovirus infection and replication restricted the appropriate evaluation in immunocompetent mouse models. The *in vivo* experiments, as already discussed, require therefore the infusion of human lymphocytes and human tumor cells in animals without an immune system (NSG). This model limits the possibility to efficiently explore the systemic antitumor immunity induced by the virus. Thus, the limited and transient presence of adoptively transferred lymphocytes in our model could explain the decrease but incomplete elimination of FAP^+ cells in treated-tumors. Another reason that could explain the incomplete tumor rejection could be related to the insufficient activation of T cells. Although is well known that the costimulation is not essential for the BiTE functionality (Dreier et al. 2002), a recent report has demonstrated that the costimulation during BiTE-engagement strongly improves the antitumor efficacy (Correnti et al. 2018). This study highlights the need of developing improved BiTE constructs in order to avoid T cell anergy or T cell exhaustion due to chronic antigen stimulation. One possibility would be to engineer our ICO15K-FBiTE to simultaneously express stimulatory molecules, such as IL-2. Thus, both FBiTEs and some stimulatory molecule will be secreted at the same time, likely improving BiTE-mediated induction of T cell functions. In this line, combining this therapy with other immuno- or chemotherapies may also represent significant advantages. For example, we have recently demonstrated that combining BiTE-armed OV with CART-cells improve CART-cell activation and proliferation *in vitro* and *in vivo*, thereby enhancing T-cell-mediated cytotoxicity (Wing et al. 2018). We and others have also shown an increase in the expression of T-cell inhibitory receptors after immune-based therapies, likely limiting the antitumor activity (Wing et al. 2018; Dmitry Zamarin et al. 2014). Preclinical evidence suggests that bispecific antibody activity under these settings can be restored or even enabled when combined with antibodies to checkpoint molecules. The blockade of the PD1-PD-L1 axis restores blinatumomab activity *in vitro* (Duell et al. 2017). Comparable data has been described with the anti-CD3 x anti-CD33 BiTE AMG330 (Kischel et al. 2015). AMG330 upregulated PD1 on T cells and PD-L1 on AML blasts *in vitro*. Lytic potential, T cell activation and proliferation are strongly enhanced

upon blockade of the PD1-PD-L1 axis (Kischel et al. 2015; Laszlo et al. 2015a). Addition of costimulatory agonistic anti-CD28 antibodies to AMG330/T cell/blast coculture boosted blast lysis (Laszlo et al. 2015b). Remarkably, Ribas *et al.* recently reported the strong enhanced immune recognition of cancer when combined talimogene laherparepvec oncolytic virus with an anti-PD1 antibody (Ribas et al. 2017). Taken together, these studies support the rationale to combine our BiTE-expressing virus with different immune checkpoint inhibitors. On the other hand, Fang *et al.* reported the benefits of combining FAP-targeted therapies with chemotherapies (Fang et al. 2016). Such results suggest that destroying the stroma not only improves virus spread but also may allow chemotherapy drugs to better penetrate into tumor. It is therefore likely that the successful application of FAP-targeted by BiTE-armed OAd in cancer patients will require the development of an optimized therapeutic approach.

In conclusion, this study establishes ICO15K-FBiTE as an effective strategy for targeting both cancer cells and FAP-positive stromal cells, killing through combined viral oncolysis and intratumoral expression of an anti-FAP BiTE. This approach offers opportunities for cancer therapy with no evidence of toxicity and further encourages the transition into clinical applications. However, future studies should be directed towards optimization of both OAd and BiTE designs and to explore the effectiveness of FAP-targeting BiTE-armed OAd in combination with other therapeutic modalities, such as chemotherapy or other immunotherapies.

3. TARGETING THE TUMOR STROMA WITH AN IMMUNOTOXIN OR A PRODRUG

As already described, intratumoral diffusion of OVs is blockedby stromal barriers of solid tumors. Briefly, the ECM constitutes a wall through which the Ad will not pass and stromal fibroblasts are very resistant to virus replication. As mentioned in previous sections, multiple strategies have been adopted to tackle this issue. In our own group, ECM-degrading viruses have been successfully developed (Sonia Guedan et al. 2010; Alba Rodríguez-García et al. 2015), enhancing virus spread and overall antitumor efficacy. Despite all these strategies offer a number of advantages, further work is still needed to overcome the barrier formed by stromal fibroblasts.

We therefore aim at overcoming limited virus spread by engineering our parental OAd ICO15K to express recombinant stroma-targeted immunotoxins. Thus, the main goal of this third chapter was to evaluate another possible strategy to deplete the tumor stroma but different from the presented FBiTE, in this case, without involving the immune system. Antibody derivatives show several advantages for arming of OVs:(i) as they are secreted by infected cells they will show bystander or paracrine activity, (ii) there are tumor-selective due to the antibody moiety and (iii) they can be easily modified by exchange of the antibody moiety, exploiting the available diversity of antibodies and/or of fused effector domains. Although the concept of immunotoxins was born in the early 1980s, there is only one report on the *in vitro* and *in vivo* benefits of encoding an immunotoxin in an oncolytic virus, an immunoRNase secreted from an oncolytic adenovirus (Fernández-Ulibarri et al. 2015). A replication-deficient Ad vector encoding an Pseudomonas exotoxin-based, Her2-specific immunotoxin had been reported previously (X. Liu et al. 2010). The immunotoxin expression and cytotoxicity for this vector was enhanced by co-administration of an OAd *in vitro*, resulting in vector replication in co-infected cells. However, the limitation of this study is that the co-infections are very unlikely to occur *in vivo* by the systemic route

For the construction of a potent immunotoxin, we first tried the combination of the scFv derived from the monoclonal antibody anti-FAP5 (named M5) and the engineered α-sarcin toxin, generating the M5-Sarcin immunotoxin. The scFv from the FAP5 antibody was the same that we used in the generation of our FBiTE. We chose this same scFV because we had previously validated it *in vitro*. In collaboration with Javier Lacadena, α-sarcin was selected as the most suitable toxin for several reasons. Ribotoxins have advantages for use in the design of immunotoxins, namely, their small size, high thermostability, resistance to proteases, and highly efficient ribonucleolytic activity (Kao et al. 2001). Remarkably, the specific action of α-sarcin is so effective that a single molecule is enough to kill a cell (Lamy, Davies, and Schindler 1992), which is an important requisite when expressed by an OAd. Furthermore, an immunotoxin based on α-sarcin and an anti-A33 scFv (colorectal cancer antigen) has demonstrated antitumor efficacy *in vitro* and *in vivo*(Tomé-Amat et al. 2015).

Based on our previous ICO15K-armed designs, insertion of M5-Sarcin after-fiber was more desirable compared to the location between E4 and RITR in order to obtain higher expression of transgene. However, this design resulted in non-viable viruses. This result

agrees with Fernández-Ulibarri *et al.,* who found that although similar constructions of virus could be rescued and amplified, all had a high physical/functional ratios (>5000) (Fernández-Ulibarri et al. 2015). This phenomenon may beattributed to an interference of the immunotoxin with virus replication, because other transgenes have not shown non-viable virus or increased physical/functional ratios. After multiple attempts we could finally obtain the ICO15K virus with M5-Sarcin after the fiber, but the interference of M5-Sarcin with OAd replication should be avoided not only during virus production, but also during the infection of patients' tumors to ensure a successful oncolysis. On the contrary, insertion of M5-Sarcin between E4 and the RITR allowed a normal level of production of the virus. These findings further support the idea that the location after the fiber leads to higher transgene expression but the location between E4 and the RITR leads to a tighter replication-dependent expression.

Flow cytometry-based binding assays resulted in expression of the protein by virus-infected cells. Nevertheless, no immunotoxin-mediated killing of FAP-positive cells was observed. These results were completely unexpected. Preliminary functional experiments with the α-sarcin moiety by the group of Javier Lacadena showed adequate ribonuclease activity. There are, however, some possible explanations for this lack of functionality. The *in vitro* toxicity of an immunotoxin depends on several molecular aspects, including antigen binding affinity, internalization rate, intracellular processing, toxin release and intrinsic toxicity (Hexham et al. 2001). However, we mainly speculate in three possible hypotheses: (i) inability of immunotoxin internalization upon binding to FAP antigen, (ii) insufficient concentration to achieve the death of cells and (iii) natural bioselection virus variants carrying non-functional immunotoxins.

Due to the lack of functional immunotoxin, and to unravel these possibilities we used another approach by generating an immunotoxin recognizing the human and murine FAP. We decided to replace the scFv M5 for the scFv MO36 (Brocks et al. 2001) and ESC11 (Fischer et al. 2012), which were both validated for internalization upon binding to the cell surface FAP antigen. Nonetheless, these two new constructions, although were also properly expressed and secreted by the infected cells, did not provide any cytotoxic advantage. This result likely suggests that the lack of functionality of the protein is likely related to the lack of α-sarcin toxicity than the internalization of the immunotoxin. In an attempt to answer whether this lack of toxicity was due to low concentration of

immunotoxin or to virus bioselection, these immunotoxins were cloned in an expression vector. Once again, flow cytometry-based binding assays revealed high concentration of immunotoxin in supernatants, but still no signs of cytotoxic activity were observed. These findings indicate that our lack of cytotoxicity was neither related with low expression of transgene nor viral bioselection. It seems that a folding or structural problem of the sarcin attached to the scFv was precluding its activity. We therefore changed the toxin. In the ONCO-FAP design, the Onconase was fused to M5 scFv. Prior studies have used Onconase in Phase II-IIIb clinical trials against non-small cell lung cancer and unresectable malignant mesothelioma, respectively. Remarkably, an anti-EGFR scFv fused to Onconase expressed from an OAd have shown an increased cytotoxicity to EGFR-positive tumor cells *in vitro* and a significant enhanced therapeutic activity in mice xenograft tumor models (Fernández-Ulibarri et al. 2015). We therefore replaced the published anti-EGFR scFv with our anti-FAP5 scFv (M5) without altering any other part of the sequence. Unfortunately, similar lack of cytotoxicity was obtained with the new toxin, and the reasons of the discrepancy with the Fernández-Ulibarri *et al.* study is not known. The use of different scFv could somewhat affect the protein folding, affecting the intrinsic toxicity of the toxin.

Given the inability to obtain a synergistic cytotoxic effect with the immunotoxin-expressing OAds, we thought that using the enzyme-prodrug therapy (DEPT) strategy could help us to achieve our main objective: deplete tumor stroma to increase viral spread and overall antitumor efficacy. In this strategy, an exogenous prodrug-converting enzyme is selectively delivered to tumor cells, to specifically sensitize them to that prodrug. A key advantage of employing an exogenous enzyme is the potential to use a prodrug substrate that is not recognized by human enzymes and thereby minimize off-target activity while maximizing toxicity within the tumor environment. Moreover, the toxic substances produced by the combination enzyme/prodrug can spread to the neighboring cancer cells and induce consecutive cell death (the bystander effect). However, a primary disadvantage is the difficulty of delivering an exogenous enzyme effectively and selectively to tumors. Thus, we hypothesized that nitroreductase (NTR)-armed ICO15K virus could might lead to synergistic interactions not achievable by either therapy alone. The selection of NTR was based on the strong bystander effect induced by this enzyme in combination with different prodrugs. In fact, the first transgene inserted in ICOVIR15 was NTR (Juan J. Rojas et al. 2010).

To date, multiple enzyme-prodrug combinations have already been explored, also in the field of virotherapy (Chen et al. 2004; C. Fuerer and Iggo 2004; Christophe Fuerer et al. 2005; Hallenbeck et al. 2005; Singleton et al. 2007). These studies have demonstrated that this strategy can substantially increase the CPE of an OAds *in vitro*, but it is often translated to poor increased efficacy in xenograft models *in vivo*, suggesting that more potent enzyme-prodrug systems, improved efficient expression strategy, or enhanced potency of OAds are needed to improve the synergistic effect of the combination of both promising therapies.

We therefore engineered ICO15K to express *B. subtilis* NfrA by introducing the nfrA gene after-fiber region under the control of the MLP via IIIa splicing acceptor. Combination of NfrA enzyme/SN34668 prodrug was chosen based on preliminary studies performed by Adam Patterson laboratory (personal communication), which showed this system as the most cytotoxic. The expression of prodrug-activating enzymes from a late viral promoter, to delay their expression after the onset of DNA synthesis, could limit the extent to which prodrug activation inhibits virus replication. Accordingly, the oncolytic potency of the resulting ICO15K-NfrA was found to be equivalent to the parental virus *in vitro*, confirming that the insertion of the enzyme did not compromise oncolytic activity. Importantly, this genome location conferred replication-dependent late gene expression, which was demonstrated by delayed NfrA activity (> 24h) in different cell lines. The NTR probe also revealed that the amplitude and duration of NTR expression is heterogeneous across cancer cell lines exposed to ICO15K-NfrA. The expression pattern likely depends on the susceptibility to initial infection, and the kinetics of E2F-driven viral life cycle. Finally, preliminary cytotoxic experiments revealed an increased cytotoxic effect of our NfrA-expressing virus *in vitro*.

It remains to be seen whether NfrA expression from our ICO15K-NfrA virus will increase their efficacy in tumor xenograft models (ongoing). Clearly, the timing of prodrug administration will be a key factor in the overall efficacy; administration too early in the course of oncolytic infection could be counterproductive, preventing virus replication and thus limiting both the oncolytic effect, and the amount and distribution of the prodrug-activating enzyme. However, with optimum timing, prodrug activation is expected to kill more cellsthan could be achieved by viral oncolysis alone.

Despite these encouraging results, more work is needed to determine the therapeutic effect both *in vitro* and *in vivo* of our ICO15K-NfrA in combination with the prodrug administration.

CONCLUSIONS

1. The insertion of a splicing acceptor and a transgene after the fiber gene of an oncolytic adenovirus leads to higher transgene expression compared to the insertion between the E4 region and the right ITR, but the location next to the RITR leads to a tighter replication-dependent expression.
2. When expressing transgenes from oncolytic adenovirus ICO15K, the strong splicing acceptor derived from the fiber gene of Ad40 provides higher transgene levels compared to the IIIa gene acceptor of Ad5, but at the expense of reduced virus replication *in vitro*.
3. FBiTE-armed oncolytic adenoviruses, either using IIIa or 40SA splicing acceptors, were successfully rescued and showed similar replication efficiency as the parental *in vitro*.
4. FBiTE molecules expressed and secreted from ICO15K-FBiTE-infected cells bound specifically to human CD3 and FAP, leading to T cell activation and proliferation, and promoting cytotoxicity against FAP^+ cells.
5. Oncolytic adenoviruses armed with different designs of FBiTEtargeting against murine CD3 and murine and human FAP were successfully rescued, but they failed to induce T cell-activation.
6. Intratumoral administration of ICO15K-IIIa-FBiTE increases the accumulation of tumor-infiltrating T cells compared to the ICO15K.
7. In a highly permissive model for adenovirus replication oncolytic adenoviruses with the FBiTE under IIIa or 40SA, improve antitumor efficacy compared to the parental control without FBiTE, but the one with IIIa shows more efficacy.
8. Treatment with intratumoral ICO15K-FBiTE and systemic human T cells decreased the amount of FAP in tumors, suggesting a FBiTE-T cell-mediated cytotoxic activity of.
9. Insertion of the designed immunotoxins after the fiber of an oncolytic adenovirus resulted in non-viable virus, whereas the insertion between E4 and RITR did generate viable viruses.
10. Immunotoxin molecules expressed and secreted by virus-infected cells bound specifically to the murine and human FAP on target cells, but without cytotoxicity.
11. Oncolytic adenoviruses expressing NfrA-activatable prodrug retain the in vitro virus replication efficiency of a non-modified virus.
12. ICO15K-NfrA shows replication-dependent NfrA enzymatic activity on target cells, leading to a bystander cytotoxic effect *in vitro*.

REFERENCES

Afkhami, Sam, Yushi Yao, and Zhou Xing. 2016. "Methods and Clinical Development of Adenovirus-Vectored Vaccines against Mucosal Pathogens." *Molecular Therapy - Methods and Clinical Development* 3(March): 16030.

Ahi, Yadvinder S., and Suresh K. Mittal. 2016. "Components of Adenovirus Genome Packaging." *Frontiers in Microbiology* 7(SEP): 1–15.

Ahn, Daniel, and Tanios Bekaii-Saab. 2017. "The Continued Promise and Many Disappointments of Oncolytic Virotherapy in Gastrointestinal Malignancies." *Biomedicines* 5(1): 10. http://www.mdpi.com/2227-9059/5/1/10.

Von Ahrens, Dagny et al. 2017. "The Role of Stromal Cancer-Associated Fibroblasts in Pancreatic Cancer." *Journal of Hematology and Oncology* 10(1): 1–8.

Al-Zaher, Ahmed Abdullah et al. 2018. "Evidence of Anti-Tumoral Efficacy in an Immune Competent Setting with an IRGD-Modified Hyaluronidase-Armed Oncolytic Adenovirus." *Molecular Therapy - Oncolytics* 8: 62–70.

Alemany, R., K. Suzuki, and D. T. Curiel. 2000. "Blood Clearance Rates of Adenovirus Type 5 in Mice." *Journal of General Virology* 81(11): 2605–9.

Ali, Niwa et al. 2012. "Xenogeneic Graft-versus-Host-Disease in NOD-Scid IL-2Rγnull Mice Display a T-Effector Memory Phenotype." *PLoS ONE* 7(8): 44219.

Andtbacka, Robert H.I. et al. 2015. "Talimogene Laherparepvec Improves Durable Response Rate in Patients with Advanced Melanoma." *Journal of Clinical Oncology* 33(25): 2780–88.

Ardelt, Wojciech, Stanislaw M Mikuslki, and Kuslima Shogen. 1991. "Amino Acid Sequence of an Anti-Tumor Protein from Rana Pipiens Oocytes and Early Embryos. Homology to Pancreatic Ribonucleases." *The Journal of biological chemistry* 266(5): 245–51.

Arias, Marcel. 2017. "Arming Oncolytic Adenoviruses with Transgenes to Engage Stroma Toxicity and Immune Stimulation as a Double Strategy Against Cancer." *Doctoral thesis*.

Ariga, Naohiro et al. 2002. "Stromal Expression of Fibroblast Activation Protein/Seprase, a Cell Membrane Serine Proteinase and Gelatinase, Is Associated with Longer Survival in Patients with Invasive Ductal Carcinoma of Breast." *International Journal of Cancer* 95(1): 67–72.

Avanzi, Mauro P. et al. 2018. "Engineered Tumor-Targeted T Cells Mediate Enhanced Anti-Tumor Efficacy Both Directly and through Activation of the Endogenous Immune System." *Cell Reports* 23(7): 2130–41. https://doi.org/10.1016/j.celrep.2018.04.051.

Bae, Sohyun et al. 2008. "Fibroblast Activation Protein α Identifies Mesenchymal Stromal Cells from Human Bone Marrow." *British Journal of Haematology* 142(5): 827–30.

Baeuerle, P A, Carsten Reinhardt, and P. Kufer. 2008. "BiTE: A New Class of Antibodies That Recruit T-Cells." *Drugs of the future* 33(2): 137.

Balkwill, Frances. 2009. "Tumour Necrosis Factor and Cancer." *Nature Reviews Cancer* 9(3): 361–71.

Bargou, Ralf et al. 2008. "Tumor Regression in Cancer of a T Cell – Engaging Antibody." *Science* 3(August): 974–78.

Bartlett, David L. et al. 2013. "Oncolytic Viruses as Therapeutic Cancer Vaccines." *Molecular Cancer* 12(1): 1–16.

Barton, Kenneth N. et al. 2008. "Phase I Study of Noninvasive Imaging of Adenovirus-Mediated Gene Expression in the Human Prostate." *Molecular Therapy* 16(10): 1761–69. http://dx.doi.org/10.1038/mt.2008.172.

Bauerschmitz, Gerd J. et al. 2006. "Triple-Targeted Oncolytic Adenoviruses Featuring the Cox2 Promoter, E1A Transcomplementation, and Serotype Chimerism for Enhanced Selectivity for Ovarian Cancer Cells." *Molecular Therapy* 14(2): 164–74. http://dx.doi.org/10.1016/j.ymthe.2006.01.010.

Bauzon, Maxine et al. 2003. "Multigene Expression from a Replicating Adenovirus Using Native Viral Promoters." *Molecular Therapy* 7(4): 526–34. http://dx.doi.org/10.1016/S1525-0016(03)00023-6.

Bayo-Puxan, N et al. 2009. "Replacement of Adenovirus Type 5 Fiber Shaft Heparan Sulfate Proteoglycan-Binding Domain with RGD for Improved Tumor Infectivity and Targeting." *Human Gene Therapy* 20(10): 1214–21.

Benjamin, Jonathan E., and Anthony S. Stein. 2016. "The Role of Blinatumomab in Patients with Relapsed/Refractory Acute Lymphoblastic Leukemia." *Therapeutic Advances in Hematology* 7(3): 142–156.

Berdiel-Acer, Mireia et al. 2014. "Differences between CAFs and Their Paired NCF from Adjacent Colonic Mucosa Reveal Functional Heterogeneity of CAFs, Providing Prognostic Information." *Molecular Oncology* 8(7): 1290–1305.

Berk, Arnold J. 2005. "Recent Lessons in Gene Expression, Cell Cycle Control, and Cell Biology from Adenovirus." *Oncogene* 24(52): 7673–85.

Berkner, Kathleen L., and Phillip A. Sharp. 1983. "Generation of Adenovirus by Transfection of Plasmids." *Nucleic Acids Research* 11(17): 6003–20.

Bett, Andrew J., Ludvik Prevec, and Frank L. Graham. 1983. "Packaging Capacity and Stability of Human Adenovirus Type." *Journal of Virology* 67(10): 5911–21.

Bewley, M. C. 1999. "Structural Analysis of the Mechanism of Adenovirus Binding to Its Human Cellular Receptor, CAR." *Science* 286(5444): 1579–83. http://www.sciencemag.org/cgi/doi/10.1126/science.286.5444.1579.

Birnboim, H.C., and J. Doly. 2009. "A Rapid Alkaline Extraction Procedure for Screening Recombinant Plasmid DNA." *Nucleic Acids Research* 7(6): 1–11. papers3://publication/uuid/928F2D41-40F1-4E91-85C5-EC153BE4E035.

Bischoff, James R et al. 1996. "Adenovirus Mutant Replicates Selectively Deficient Human Tumor That in P53- Cells." *Science* 274(5286): 373–76.

Blackford, A. N., and R. J. A. Grand. 2009. "Adenovirus E1B 55-Kilodalton Protein: Multiple Roles in Viral Infection and Cell Transformation." *Journal of Virology* 83(9): 4000–4012. http://jvi.asm.org/cgi/doi/10.1128/JVI.02417-08.

Boon, Thierry et al. 1994. "Tumor Antigens Recognized by T Lymphocytes." *Annu. Rev. Immunol* 12: 337–65.

Bosch, Fèlix, and Laia Rosich. 2008. "The Contributions of Paul Ehrlich to Pharmacology: A Tribute on the Occasion of the Centenary of His Nobel Prize." *Pharmacology* 82(3): 171–79.

Bradley, R. R. et al. 2012. "Adenovirus Serotype 5-Specific Neutralizing Antibodies Target Multiple Hexon Hypervariable Regions." *Journal of Virology* 86(2): 1267–72. http://jvi.asm.org/cgi/doi/10.1128/JVI.06165-11.

Brand, K. et al. 1997. "Liver-Associated Toxicity of the HSV-Tk/GCV Approach and Adenoviral Vectors." *Cancer Gene Therapy* 4(1): 9–16.

Brinkmann, Ulrich, and Roland E. Kontermann. 2017. "The Making of Bispecific Antibodies." *mAbs* 9(2): 182–212.

Brischwein, Klaus et al. 2006. "MT110: A Novel Bispecific Single-Chain Antibody Construct with High Efficacy in Eradicating Established Tumors." *Molecular Immunology* 43(8): 1129–43.

Bristol, J. Andrew et al. 2003. "In Vitro and in Vivo Activities of an Oncolytic Adenoviral Vector Designed to Express GM-CSF." *Molecular Therapy* 7(6): 755–64. http://dx.doi.org/10.1016/S1525-0016(03)00103-5.

Brocks, Bodo et al. 2001. "Species-Crossreactive ScFv Against the Tumor Stroma Marker " Fibroblast Activation Protein " Selected by Phage Display From an Immunized FAP Ɑ/Ɑ Knock-Out Mouse." *Molecular Medicine* 7(7): 461–69.

Bunuales, Maria et al. 2012. "Evaluation of Monocytes as Carriers for Armed Oncolytic Adenoviruses in Murine and Syrian Hamster Models of Cancer." *Human Gene Therapy* 23(12): 1258–68. http://online.liebertpub.com/doi/abs/10.1089/hum.2012.043.

Capasso, Cristian et al. 2016. "Oncolytic Adenoviruses Coated with MHC-I Tumor Epitopes Increase the Antitumor Immunity and Efficacy against Melanoma." *OncoImmunology* 5(4): 1–11. http://dx.doi.org/10.1080/2162402X.2015.1105429.

Carette, Jan E. et al. 2005. "Replication-Dependent Transgene Expression from a Conditionally Replicating Adenovirus via Alternative Splicing to a Heterologous Splice-Acceptor Site." *Journal of Gene Medicine* 7(8): 1053–62.

Cattaneo, Roberto, Tanner Miest, Elena V. Shashkova, and Michael A. Barry. 2008. "Reprogrammed Viruses as Cancer Therapeutics: Targeted, Armed and Shielded." *Nature Reviews Microbiology* 6(7): 529–40.

Cawood, Ryan et al. 2009. "Use of Tissue-Specific MicroRNA to Control Pathology of Wild-Type Adenovirus without Attenuation of Its Ability to Kill Cancer Cells." *PLoS Pathogens* 5(5).

———. 2011. "MicroRNA Controlled Adenovirus Mediates Anti-Cancer Efficacy without Affecting Endogenous MicroRNA Activity." *PLoS ONE* 6(1).

Cerullo, Vincenzo et al. 2010. "Oncolytic Adenovirus Coding for Granulocyte Macrophage Colony-Stimulating Factor Induces Antitumoral Immunity in Cancer Patients." *Cancer Research* 70(11): 4297–4309.

Chen, M. J. et al. 2004. "Enhanced Efficacy of Escherichia Coli Nitroreductase/CB1954 Prodrug Activation Gene Therapy Using an E1B-55K-Deleted Oncolytic Adenovirus Vector." *Gene Therapy* 11(14): 1126–36.

Coffin, Robert. 2016. "Interview with Robert Coffin, Inventor of T-VEC: The First Oncolytic Immunotherapy Approved for the Treatment of Cancer." *Immunotherapy* 8(2): 103–6.

Compte, Marta et al. 2014. "Functional Comparison of Single-Chain and Two-Chain Anti-CD3-Based Bispecific Antibodies in Gene Immunotherapy Applications." *OncoImmunology* 3(5).

Correnti, Colin E. et al. 2018. "Simultaneous Multiple Interaction T-Cell Engaging (SMITE) Bispecific Antibodies Overcome Bispecific T-Cell Engager (BiTE) Resistance via CD28 Co-Stimulation." *Leukemia* 32(5): 1239–43.

Coughlan, Lynda et al. 2010. "Tropism-Modification Strategies for Targeted Gene Delivery Using Adenoviral Vectors." *Viruses* 2(10): 2290–2355.

Cripe, Timothy P. et al. 2001. "Fiber Knob Modifications Overcome Low, Heterogeneous Expression of the Coxsackievirus-Adenovirus Receptor That Limits Adenovirus Gene Transfer and Oncolysis for Human Rhabdomyosarcoma Cells." *Cancer Research* 61(7): 2953–60.

Darzynkiewicz, Z. et al. 1988. "Cytostatic and Cytotoxic Effects of Pannon (P-30 Protein), a Novel Anticancer Agent." *Cell tissue Kinetics* 21(3): 169–82.

Diaconu, Iulia et al. 2012. "Immune Response Is an Important Aspect of the Antitumor Effect Produced by a CD40L-Encoding Oncolytic Adenovirus." *Cancer Research* 72(9): 2327–38.

Dias, J. D. et al. 2012. "Targeted Cancer Immunotherapy with Oncolytic Adenovirus Coding for a Fully Human Monoclonal Antibody Specific for CTLA-4." *Gene Therapy* 19(10): 988–98.

Dine, Jennifer et al. 2017. "Immune Checkpoint Inhibitors: An Innovation in Immunotherapy for the Treatment and Management of Patients with Cancer." *Asia Pac J Oncol Nurs* 4(2): 95–97. https://www.ncbi.nlm.nih.gov/pmc/articles/PMC5412150/pdf/APJON-4-127.pdf.

Dmitriev, I et al. 1998. "An Adenovirus Vector with Genetically Modified Fibers Demonstrates Expanded Tropism via Utilization of a Coxsackievirus and Adenovirus Receptor-Independent Cell Entry Mechanism." *Journal of virology* 72(12): 9706–13. http://www.ncbi.nlm.nih.gov/pubmed/9811704%0Ahttp://www.pubmedcentral.nih.gov/articlerender.fcgi?artid=PMC110480.

Dock, G. 1904. "The Influece of Complicating Disease upon Leukemia." *The American journal of the Medical Sciences* 127: 563–92.

Doniną, Simona et al. 2015. "Adapted ECHO-7 Virus Rigvir Immunotherapy (Oncolytic Virotherapy) Prolongs Survival in Melanoma Patients after Surgical Excision of the Tumour in a Retrospective Study." *Melanoma Research* 25(5): 421–26.

Dranoff, Glenn. 2003. "GM-CSF-Secreting Melanoma Vaccines." *Oncogene* 22(20): 3188–92.

Dreier, Torsten et al. 2002. "Extremely Potent, Rapid and Costimulation-Independent Cytotoxic T-Cell Response against Lymphoma Cells Catalyzed by a Single-Chain Bispecific Antibody." *International Journal of Cancer* 100(6): 690–97.

Du, T. et al. 2014. "Tumor-Specific Oncolytic Adenoviruses Expressing Granulocyte Macrophage Colony-Stimulating Factor or Anti-CTLA4 Antibody for the Treatment of Cancers." *Cancer Gene Therapy* 21(8): 340–48.

Duell, J. et al. 2017. "Frequency of Regulatory T Cells Determines the Outcome of the T-Cell-Engaging Antibody Blinatumomab in Patients with B-Precursor ALL." *Leukemia* 31(10): 2181–90. http://dx.doi.org/10.1038/leu.2017.41.

Duffy, Margaret R., Alan L. Parker, Angela C. Bradshaw, and Andrew H. Baker. 2012. "Manipulation of Adenovirus Interactions with Host Factors for Gene Therapy Applications." *Nanomedicine* 7(2): 271–78.

Van der Eb, M. M. et al. 1998. "Severe Hepatic Dysfunction after Adenovirus-Mediated Transfer of the Herpes Simplex Virus Thymidine Kinase Gene and Ganciclovir Administration." *Gene Therapy* 5(4): 451–58.

Erkan, Mert et al. 2012. "The Role of Stroma in Pancreatic Cancer: Diagnostic and Therapeutic Implications." *Nature Reviews Gastroenterology and Hepatology* 9(8): 454–67. http://dx.doi.org/10.1038/nrgastro.2012.115.

Fajardo, Carlos Alberto et al. 2017. "Oncolytic Adenoviral Delivery of an EGFR-Targeting t-Cell Engager Improves Antitumor Efficacy." *Cancer Research* 77(8): 2052–63.

Fang, Jinxu et al. 2016. "A Potent Immunotoxin Targeting Fibroblast Activation Protein for Treatment of Breast Cancer in Mice." *International Journal of Cancer* 138(4): 1013–23.

Fausther-Bovendo, Hugues, and Gary P. Kobinger. 2014. "Pre-Existing Immunity against Ad Vectors: Humoral, Cellular, and Innate Response, What's Important?" *Human Vaccines and Immunotherapeutics* 10(10): 2875–84.

Feig, C. et al. 2013. "Targeting CXCL12 from FAP-Expressing Carcinoma-Associated Fibroblasts Synergizes with Anti-PD-L1 Immunotherapy in Pancreatic Cancer." *Proceedings of the National Academy of Sciences*.

Fernández-Ulibarri, Inés et al. 2015. "Genetic Delivery of an ImmunoRNase by an Oncolytic Adenovirus Enhances Anticancer Activity." *International Journal of Cancer* 136(9): 2228–40.

Fischer, Eliane et al. 2012. "Radioimmunotherapy of Fibroblast Activation Protein Positive Tumors by Rapidly Internalizing Antibodies." *Clinical Cancer Research*.

Fisher, K. 2006. "Striking out at Disseminated Metastases: The Systemic Delivery of Oncolytic Viruses." *Current opinion in molecular therapeutics* 8(4): 301–13.

FitzGerald, David J., Alan S. Wayne, Robert J. Kreitman, and Ira Pastan. 2011. "Treatment of Hematologic Malignancies with Immunotoxins and Antibody-Drug Conjugates." *Cancer Research* 71(20): 6300–6309.

Flint, Jane, Vincent R. Racaniello, Glenn F. Rall, and Anna Marie Skalka. 2015. *Principles of Virology Volume I: Molecular Biology*.

Frahm, Nicole et al. 2012. "Human Adenovirus-Specific T Cells Modulate HIV-Specific T Cell Responses to an Ad5-Vectored HIV-1 Vaccine." *Journal of Clinical Investigation* 122(1): 359–

67.

Freedman, Joshua D. et al. 2018. "An Oncolytic Virus Expressing a T-Cell Engager Simultaneously Targets Cancer and Immunosuppressive Stromal Cells." *Cancer Research* 78(24): 6852–65.

Freedman, Joshua D et al. 2017. "Oncolytic Adenovirus Expressing Bispecific Antibody Targets T-cell Cytotoxicity in Cancer Biopsies." *EMBO Molecular Medicine* 9(8): 1067–87. http://embomolmed.embopress.org/lookup/doi/10.15252/emmm.201707567.

Fuerer, C., and R. Iggo. 2004. "5-Fluorocytosine Increases the Toxicity of Wnt-Targeting Replicating Adenoviruses That Express Cytosine Deaminase as a Late Gene." *Gene Therapy* 11(2): 142–51.

Fuerer, Christophe et al. 2005. "Late Expression of Nitroreductase in an Oncolytic Adenovirus Sensitizes Colon Cancer Cells to the Prodrug CB1954." *Human Gene Therapy* 16: 051201064535001.

Fueyo, Juan et al. 2000. "A Mutant Oncolytic Adenovirus Targeting the Rb Pathway Produces Anti-Glioma Effect in Vivo." *Oncogene* 19(1): 2–12.

Fukuhara, Hiroshi, Yasushi Ino, and Tomoki Todo. 2016. "Oncolytic Virus Therapy: A New Era of Cancer Treatment at Dawn." *Cancer Science* 107(10): 1373–79.

Gabrilovich, Dmitry I. et al. 1999. "Antibodies to Vascular Endothelial Growth Factor Enhance the Efficacy of Cancer Immunotherapy by Improving Endogenous Dendritic Cell Function." *Clinical Cancer Research* 5(10): 2963–70.

Gabrilovich, Dmitry I., and Srinivas Nagaraj. 2009. "Myeloid-Derived Suppressor Cells as Regulators of the Immune System." *Nature Reviews Immunology* 9(3): 162–74.

Ganesh, Shanthi et al. 2007. "Relaxin-Expressing, Fiber Chimeric Oncolytic Adenovirus Prolongs Survival of Tumor-Bearing Mice." *Cancer Research* 67(9): 4399–4407.

Ganly, Ian et al. 2000. "A Phase I Study of Onyx-015, an E1B Attenuated Adenovirus, Administered Intratumorally to Patients with Recurrent Head and Neck Cancer." *Clinical Cancer Research* 6(3): 798–806.

Garcia-Carbonero, Rocio et al. 2017. "Phase 1 Study of Intravenous Administration of the Chimeric Adenovirus Enadenotucirev in Patients Undergoing Primary Tumor Resection." *Journal for ImmunoTherapy of Cancer* 5(1): 1–13.

García-Ortega, Lucía et al. 2010. "Cleavage of the Sarcin-Ricin Loop of 23S RRNA Differentially Affects EF-G and EF-Tu Binding." *Nucleic Acids Research* 38(12): 4108–19.

Garrido, Federico et al. 2016. "The Urgent Need to Recover MHC Class I in Cancers for Effective Immunotherapy." *Current Opinion in Immunology* 39: 44–51. http://dx.doi.org/10.1016/j.coi.2015.12.007.

Gasset, Marfa et al. 1995. "Thermal Unfolding of the Cytotoxin A-Sarcin: Phospholipid Binding Induces Destabilization of the Protein Structure." *Biochimica et biophysica acta* 1252: 126–34.

Gavilanes, José G. et al. 2012. "Production and Characterization of a Colon Cancer-Specific Immunotoxin Based on the Fungal Ribotoxin -Sarcin." *Protein Engineering Design and*

Selection 25(8): 425–35.

Ghosh-Choudhury, G, Y Haj-Ahmad, and F L Graham. 1987. "Protein IX, a Minor Component of the Human Adenovirus Capsid, Is Essential for the Packaging of Full Length Genomes." *The EMBO journal* 6(6): 1733–39. http://www.ncbi.nlm.nih.gov/pubmed/3038533%0Ahttp://www.pubmedcentral.nih.gov/articlerender.fcgi?artid=PMC553549.

Gibson, Heather et al. 2015. "Immunotherapeutic Intervention with Oncolytic Adenovirus in Mouse Mammary Tumors." *OncoImmunology* 4(1): 984523.

Glasgow, J. N., M. Everts, and D. T. Curiel. 2006. "Transductional Targeting of Adenovirus Vectors for Gene Therapy." *Cancer Gene Therapy* 13(9): 830–44.

Goebeler, Maria Elisabeth et al. 2016. "Bispecific T-Cell Engager (BiTE) Antibody Construct Blinatumomab for the Treatment of Patients with Relapsed/Refractory Non-Hodgkin Lymphoma: Final Results from a Phase I Study." *Journal of Clinical Oncology* 34(10): 1104–11.

Goradel, Nasser Hashemi et al. 2018. "Oncolytic Adenovirus: A Tool for Cancer Therapy in Combination with Other Therapeutic Approaches." *Journal of Cellular Physiology* (December). http://doi.wiley.com/10.1002/jcp.27850.

Guedan, S. et al. 2008. "Syncytia Formation Affects the Yield and Cytotoxicity of an Adenovirus Expressing a Fusogenic Glycoprotein at a Late Stage of Replication." *Gene Therapy* 15(17): 1240–45.

Guedan, Sonia et al. 2010. "Hyaluronidase Expression by an Oncolytic Adenovirus Enhances Its Intratumoral Spread and Suppresses Tumor Growth." *Molecular Therapy* 18(7): 1275–83.

Hall, Kathryn, Maria E. Blair Zajdel, and G. Eric Blair. 2010. "Unity and Diversity in the Human Adenoviruses: Exploiting Alternative Entry Pathways for Gene Therapy." *Biochemical Journal* 431(3): 321–36. http://biochemj.org/lookup/doi/10.1042/BJ20100766.

Hallenbeck, Paul et al. 2005. "Systemic Gene-Directed Enzyme Prodrug Therapy of Hepatocellular Carcinoma Using a Targeted Adenovirus Armed with Carboxypeptidase G2." *Cancer Research* 65(12): 5003–8.

Hammond, Scott A. et al. 2007. "Selective Targeting and Potent Control of Tumor Growth Using an EphA2/CD3-Bispecific Single-Chain Antibody Construct." *Cancer Research* 67(8): 3927–35.

Harrington, Laurie E, R. v. d. Most, J Lindsay Whitton, and Rafi Ahmed. 2002. "Recombinant Vaccinia Virus-Induced T-Cell Immunity: Quantitation of the Response to the Virus Vector and the Foreign Epitope." *Journal of Virology* 76(7): 3329–37. http://jvi.asm.org/cgi/doi/10.1128/JVI.76.7.3329-3337.2002%5Cnhttp://www.pubmedcentral.nih.gov/articlerender.fcgi?artid=136038&tool=pmcentrez&rendertype=abstract.

Havunen, Riikka et al. 2017. "Oncolytic Adenoviruses Armed with Tumor Necrosis Factor Alpha and Interleukin-2 Enable Successful Adoptive Cell Therapy." *Molecular Therapy - Oncolytics* 4(March): 77–86. http://dx.doi.org/10.1016/j.omto.2016.12.004.

Hermiston, Terry W., and Irene Kuhn. 2002. "Armed Therapeutic Viruses: Strategies and Challenges

to Arming Oncolytic Viruses with Therapeutic Genes." *Cancer Gene Therapy* 9(12): 1022–35.

Hernandez-Alcoceba, R, M Pihalja, M S Wicha, and M F Clarke. 2000. "A Novel, Conditionally Replicative Adenovirus for the Treatment of Breast Cancer That Allows Controlled Replication of E1a-Deleted Adenoviral Vectors [In Process Citation]." *Hum. Gene Ther.* 11(14): 2009–24.

Hesse, A., D. Kosmides, R. E. Kontermann, and D. M. Nettelbeck. 2007. "Tropism Modification of Adenovirus Vectors by Peptide Ligand Insertion into Various Positions of the Adenovirus Serotype 41 Short-Fiber Knob Domain." *Journal of Virology* 81(6): 2688–99. http://jvi.asm.org/cgi/doi/10.1128/JVI.02722-06.

Hexham, J. Mark et al. 2001. "Influence of Relative Binding Affinity on Efficacy in a Panel of Anti-CD3 ScFv Immunotoxins." *Molecular Immunology* 38(5): 397–408.

Hirvinen, Mari et al. 2015. "Immunological Effects of a TNF-Alpha Armed Oncolytic Adenovirus." *Human gene therapy* 144(March): 1–38. http://www.ncbi.nlm.nih.gov/pubmed/25557131.

Howley, Peter M., and David M. Livingston. 2009. "Small DNA Tumor Viruses: Large Contributors to Biomedical Sciences." *Virology* 384(2): 256–59. http://dx.doi.org/10.1016/j.virol.2008.12.006.

Hynes, Richard O., and Alexandra Naba. 2012. "Overview of the Matrisome-An Inventory of Extracellular Matrixfile:///C:/Users/Neil/Downloads/1052.Full.Pdf Constituents and Functions." *Cold Spring Harbor Perspectives in Biology* 4(1).

Inoue, H., and K. Tani. 2014. "Multimodal Immunogenic Cancer Cell Death as a Consequence of Anticancer Cytotoxic Treatments." *Cell Death and Differentiation* 21(1): 39–49. http://dx.doi.org/10.1038/cdd.2013.84.

Ison, Michael G. 2006. "Emerging Infections: Adenovirus Infections in Transplant Recipients." *Clinical Infectious Diseases* 43(3): 331–39. https://academic.oup.com/cid/article-lookup/doi/10.1086/505498%0Ahttp://cid.oxfordjournals.org/lookup/doi/10.1086/505498.

Jiang, Hong et al. 2017. "Oncolytic Adenovirus and Tumor-Targeting Immune Modulatory Therapy Improve Autologous Cancer Vaccination." *Cancer Research* 77(14): 3894–3907.

Jin, Fang, Peter J. Kretschmer, and Terry W. Hermiston. 2005. "Identification of Novel Insertion Sites in the Ad5 Genome That Utilize the Ad Splicing Machinery for Therapeutic Gene Expression." *Molecular Therapy* 12(6): 1052–63.

Jogler, Christian et al. 2006. "Replication Properties of Human Adenovirus in Vivo and in Cultures of Primary Cells from Different Animal Species." *Journal of virology* 80(7): 3549–58. http://www.ncbi.nlm.nih.gov/pubmed/16537623%0Ahttp://www.pubmedcentral.nih.gov/articlerender.fcgi?artid=PMC1440393.

Julia, Tchou et al. 2013. "Fibroblast Activation Protein Expression by Stromal Cells and Tumor-Associated Macrophages in Human Breast Cancer." *Human Pathology* 44(11): 2549–57.

Kakarla, Sunitha et al. 2013. "Antitumor Effects of Chimeric Receptor Engineered Human T Cells Directed to Tumor Stroma." *Molecular Therapy* 21(8): 1611–20.

Kalluri, Raghu. 2016. "The Biology and Function of Fibroblasts in Cancer." *Nature Reviews Cancer* 16(9): 582–98. http://dx.doi.org/10.1038/nrc.2016.73.

Kanerva, Anna et al. 2013. "Antiviral and Antitumor T-Cell Immunity in Patients Treated with GM-CSF-Coding Oncolytic Adenovirus." *Clinical Cancer Research* 19(10): 2734–44.

Kao, R. et al. 2001. "Mitogillin and Related Fungal Ribotoxins." In *Methods in Enzymology*, , 324–35.

Kelkar, Samir A., Kevin K. Pfister, Ronald G. Crystal, and Philip L. Leopold. 2004. "Cytoplasmic Dynein Mediates Adenovirus Binding to Microtubules." *Journal of Virology* 78(18): 10122–32.

Khuri, Fadlo R. et al. 2000. "A Controlled Trial of Intratumoral ONYX-015, a Selectively-Replicating Adenovirus, in Combination with Cisplatin and 5-Fluorouracil in Patients with Recurrent Head and Neck Cancer." *Nature Medicine* 6(8): 879–85.

Kim, Joo Hang et al. 2006. "Relaxin Expression from Tumor-Targeting Adenoviruses and Its Intratumoral Spread, Apoptosis Induction, and Efficacy." *Journal of the National Cancer Institute* 98(20): 1482–93.

Kimball, Kristopher J. et al. 2010. "A Phase I Study of a Tropism-Modified Conditionally Replicative Adenovirus for Recurrent Malignant Gynecologic Diseases." *Clinical Cancer Research* 16(21): 5277–87.

Kischel, R et al. 2015. "Blockade of the PD-1/PD-L1 Axis Augments Lysis of AML Cells by the CD33/CD3 BiTE Antibody Construct AMG 330: Reversing a T-Cell-Induced Immune Escape Mechanism." *Leukemia* 30(2): 484–91.

Kreitman, Robert J. 2009. "Recombinant Immunotoxins Containing Truncated Bacterial Toxins for the Treatment of Hematologic Malignancies." *BioDrugs* 23(1): 1–13.

Kretschmer, Peter J., Fang Jin, Cecile Chartier, and Terry W. Hermiston. 2005. "Development of a Transposon-Based Approach for Identifying Novel Transgene Insertion Sites within the Replicating Adenovirus." *Molecular Therapy* 12(1): 118–27.

Lacadena, Javier et al. 2007. "Fungal Ribotoxins: Molecular Dissection of a Family of Natural Killers." *FEMS Microbiology Reviews* 31(2): 212–37.

———. 2016. "A Deimmunised Form of the Ribotoxin, α-Sarcin, Lacking CD4+ T Cell Epitopes and Its Use as an Immunotoxin Warhead." *Protein Engineering Design and Selection* 29(11): 531–40.

Ladd, Brendon, Jessica J. O'konek, Leo J. Ostruszka, and Donna S. Shewach. 2011. "Unrepairable DNA Double Strand Breaks Initiate Cytotoxicity with HSV-TK/Ganciclovir." *Cancer Gene Therapy* 18(10): 751–59.

Lamy, B, J Davies, and Daniel G Schindler. 1992. "The Aspergillus Ribonucleolytic Toxins (Ribotoxins)." *Targeted Diagnosis and Therapy* 7: 237–58.

Laszlo, G. S., C. J. Gudgeon, K. H. Harrington, and R. B. Walter. 2015a. "T-Cell Ligands Modulate the Cytolytic Activity of the CD33/CD3 BiTE Antibody Construct, AMG 330." *Blood Cancer Journal* 5(8): e340-6. http://dx.doi.org/10.1038/bcj.2015.68.

———. 2015b. "T-Cell Ligands Modulate the Cytolytic Activity of the CD33/CD3 BiTE Antibody Construct, AMG 330." *Blood Cancer Journal* 5(8): e340-6.

Lee, Jaewoo et al. 2005. "Tumor Immunotherapy Targeting Fibroblast Activation Protein, a Product Expressed in Tumor-Associated Fibroblasts." *Cancer Research* 65(23): 11156–63.

Lee, Young Sook et al. 2006. "Enhanced Antitumor Effect of Oncolytic Adenovirus Expressing Interleukin-12 and B7-1 in an Immunocompetent Murine Model." *Clinical Cancer Research* 12(19): 5859–68.

Li, Yang et al. 2016. "CCL21/IL21-Armed Oncolytic Adenovirus Enhances Antitumor Activity against TERT-Positive Tumor Cells." *Virus Research* 220: 172–78. http://dx.doi.org/10.1016/j.virusres.2016.05.002.

Liu, Guang Yao et al. 2015. "Enhanced Growth Suppression of TERT-Positive Tumor Cells by Oncolytic Adenovirus Armed with CCL20 and CD40L." *International Immunopharmacology* 28(1): 487–93. http://dx.doi.org/10.1016/j.intimp.2015.07.005.

Liu, Xinjian et al. 2010. "Enhanced Pancreatic Cancer Gene Therapy by Combination of Adenoviral Vector Expressing C-Erb-B2 (Her-2=neu)-Targeted Immunotoxin with a Replication-Competent Adenovirus or Etoposide." *Human Gene Therapy* 21(2): 157–70. http://ovidsp.ovid.com/ovidweb.cgi?T=JS&PAGE=reference&D=emed11&NEWS=N&AN=358345827.

Lo, A. et al. 2015. "Tumor-Promoting Desmoplasia Is Disrupted by Depleting FAP-Expressing Stromal Cells." *Cancer Research* 75(14): 2800–2810.

Lopez, M. Veronica et al. 2012. "A Tumor-Stroma Targeted Oncolytic Adenovirus Replicated in Human Ovary Cancer Samples and Inhibited Growth of Disseminated Solid Tumors in Mice." *Molecular Therapy* 20(12): 2222–33. http://dx.doi.org/10.1038/mt.2012.147.

Lopez, M. Verónica et al. 2009. "Tumor Associated Stromal Cells Play a Critical Role on the Outcome of the Oncolytic Efficacy of Conditionally Replicative Adenoviruses." *PLoS ONE* 4(4).

Lyons, Mark et al. 2006. "Adenovirus Type 5 Interactions with Human Blood Cells May Compromise Systemic Delivery." *Molecular Therapy* 14(1): 118–28. http://dx.doi.org/10.1016/j.ymthe.2006.01.003.

Marchini, Antonio, Eleanor M Scott, and Jean Rommelaere. 2016. "Overcoming Barriers in Oncolytic Virotherapy with HDAC Inhibitors and Immune Checkpoint Blockade." *Viruses* 8(1).

Marelli, Giulia, Anwen Howells, Nicholas R. Lemoine, and Yaohe Wang. 2018. "Oncolytic Viral Therapy and the Immune System: A Double-Edged Sword against Cancer." *Frontiers in Immunology* 9(APR): 1–8.

Martínez-Ruiz, Antonio, Richard Kao, Julian Davies, and A Martínez del Pozo. 1999. "Ribotoxins Are a More Widespread Group of Proteins within the ® Lamentous Fungi than Previously Believed." 37: 1549–63.

Mathew, Mrudula, and Rama S Verma. 2009. "Humanized Immunotoxins: A New Generation of Immunotoxins for Targeted Cancer Therapy." *Cancer Science* 100(8): 1359–65.

Matsui, Hayato et al. 2011. "Enhanced Transduction Efficiency of Fiber-Substituted Adenovirus Vectors by the Incorporation of RGD Peptides in Two Distinct Regions of the Adenovirus Serotype 35 Fiber Knob." *Virus Research* 155(1): 48–54.

http://dx.doi.org/10.1016/j.virusres.2010.08.021.

Mellman, Ira, George Coukos, and Glenn Dranoff. 2011. "Cancer Immunotherapy Comes of Age." *Nature Reviews* 480: 481–89. http://dx.doi.org/10.1038/nature10673.

Mikulski, S. M. et al. 1990. "Striking Increase of Survival of Mice Bearing M109 Madison Carcinoma Treated with a Novel Protein from Amphibian Embryos." *Journal of the National Cancer Institute* 82(2): 151–53.

———. 1993. "Phase I Human Clinical Trial of ONCONASE (P-30 Protein) Administered Intravenously on a Weekly Schedule in Cancer Patients with Solid Tumors." *International Journal of Oncology* 3(1): 57–64. http://ovidsp.ovid.com/ovidweb.cgi?T=JS&PAGE=reference&D=emed3&NEWS=N&AN=1993284537.

Mikuslki, Stanislaw M et al. 2002. "Phase II Trial of a Single Weekly Intravenous Dose of Ranpirnase in Patients With Unresectable Malignant Mesothelioma." *Journal of clinical o* 20(1): 274–81.

Milan, David, and David Peal. 2013. "(12) Patent Application Publication (10) Pub . No .: US 2002/0187020 A1." 1(19).

Mocellin, Simone, Carlo Riccardo Rossi, Pierluigi Pilati, and Donato Nitti. 2005. "Tumor Necrosis Factor, Cancer and Anticancer Therapy." *Cytokine and Growth Factor Reviews* 16(1): 35–53.

Moss, B. 1996. "Genetically Engineered Poxviruses for Recombinant Gene Expression, Vaccination, and Safety." *Proceedings of the National Academy of Sciences* 93(21): 11341–48.

Muhlemann, O., B.-G. Yue, S. Petersen-Mahrt, and G. Akusjarvi. 2002. "A Novel Type of Splicing Enhancer Regulating Adenovirus Pre-MRNA Splicing." *Molecular and Cellular Biology* 20(7): 2317–25.

Murakami, Miho et al. 2010. "Chimeric Adenoviral Vectors Incorporating a Fiber of Human Adenovirus 3 Efficiently Mediate Gene Transfer into Prostate Cancer Cells." *Prostate* 70(4): 362–76.

Nagorsen, Dirk, Peter Kufer, Patrick A. Baeuerle, and Ralf Bargou. 2012. "Blinatumomab: A Historical Perspective." *Pharmacology and Therapeutics* 136(3): 334–42. http://dx.doi.org/10.1016/j.pharmthera.2012.07.013.

Nakashima, Hiroshi, Balveen Kaur, and E. A. Chiocca. 2010. "Directing Systemic Oncolytic Viral Delivery to Tumors via Carrier Cells." *Cytokine and Growth Factor Reviews* 21(2–3): 119–26. http://dx.doi.org/10.1016/j.cytogfr.2010.02.004.

Nemerow, G. R. 2000. "Cell Receptors Involved in Adenovirus Entry." *Virology* 274(1): 1–4.

Nettelbeck, Dirk M. 2003. "Virotherapeutics: Conditionally Replicative Adenoviruses for Viral Oncolysis." *Anti-Cancer Drugs* 14(8): 577–84.

———. 2008. "Cellular Genetic Tools to Control Oncolytic Adenoviruses for Virotherapy of Cancer." *Journal of Molecular Medicine* 86(4): 363–77.

"New Drugs/Drug News." 2014. *Pharmacology and Therapeutics* 39(11).

Newton, Dianne L. et al. 2001. "Potent and Specific Antitumor Effects of an Anti-CD22-Targeted Cytotoxic Ribonuclease: Potential for the Treatment of Non-Hodgkin Lymphoma." *Blood* 97(2): 528–35.

Nishio, Nobuhiro et al. 2014. "Armed Oncolytic Virus Enhances Immune Functions of Chimeric Antigen Receptor-Modified T Cells in Solid Tumors." *Cancer Research* 74(18): 5195–5205.

O'Shea, Clodagh C. et al. 2004. "Late Viral RNA Export, Rather than P53 Inactivation, Determines ONYX-015 Tumor Selectivity." *Cancer Cell* 6(6): 611–23.

Oberst, Michael D et al. 2014. "CEA/CD3 Bispecific Antibody MEDI-565/AMG 211 Activation of T Cells and Subsequent Killing of Human Tumors Is Independent of Mutations Commonly Found in Colorectal Adenocarcinomas." *mAbs* 6(6): 1571–84.

Offner, Sonja et al. 2006. "Induction of Regular Cytolytic T Cell Synapses by Bispecific Single-Chain Antibody Constructs on MHC Class I-Negative Tumor Cells." *Molecular Immunology* 43(6): 763–71.

Olombrada, Miriam et al. 2014. "The Acidic Ribosomal Stalk Proteins Are Not Required for the Highly Specific Inactivation Exerted by α-Sarcin of the Eukaryotic Ribosome." *Biochemistry* 53(10): 1545–47.

Olson, B H et al. 1965. "Alpha Sarcin, a New Antitumor Agent." *Applied microbiology* 13(3): 314–21. http://www.ncbi.nlm.nih.gov/pubmed/14330325%0Ahttp://www.pubmedcentral.nih.gov/articlerender.fcgi?artid=PMC1058251%0Ahttp://www.ncbi.nlm.nih.gov/pubmed/14325268%0Ahttp://www.pubmedcentral.nih.gov/articlerender.fcgi?artid=PMC1058250.

Ostermann, Elinborg et al. 2008. "Effective Immunoconjugate Therapy in Cancer Models Targeting a Serine Protease of Tumor Fibroblasts." *Clinical Cancer Research* 14(14): 4584–92.

Pardoll, Drew M. 2012. "The Blockade of Immune Checkpoints in Cancer Immunotherapy." *Nature Reviews Cancer* 12(4): 252–64. http://dx.doi.org/10.1038/nrc3239.

Pastan, Ira, Raffit Hassan, David J Fitzgerald, and Robert J Kreitman. 2007. "Immunotoxin Treatment of Cancer." *Annual review of medicine* 58: 221–37.

Pishvaian, Michael et al. 2016. "Phase 1 Dose Escalation Study of MEDI-565, a Bispecific T-Cell Engager That Targets Human Carcinoembryonic Antigen, in Patients With Advanced Gastrointestinal Adenocarcinomas." *Clinical Colorectal Cancer* 15(4): 345–51. http://dx.doi.org/10.1016/j.clcc.2016.07.009.

Polyak, Kornelia. 2011. "China Approves World ' s First Oncolytic." *OncoImmunology* 121(10): 3786–88. http://www.tandfonline.com/doi/full/10.1080/2162402X.2015.1115641%0Ahttp://dx.doi.org/10.1080/2162402X.2015.1115942.

Puig-Saus, Cristina, Alena Gros, Ramon Alemany, and Manel Cascalló. 2012. "Adenovirus I-Leader Truncation Bioselected against Cancer-Associated Fibroblasts to Overcome Tumor Stromal Barriers." *Molecular Therapy* 20(1): 54–62.

Qiao, J. et al. 2002. "Tumor-Specific Transcriptional Targeting of Suicide Gene Therapy." *Gene Therapy* 9(3): 168–75.

Quirin, Christina et al. 2010. "Selectivity and Efficiency of Late Transgene Expression by Transcriptionally Targeted Oncolytic Adenoviruses Are Dependent on the Transgene Insertion Strategy." *Human Gene Therapy* 22(4): 389–404. http://www.liebertonline.com/doi/abs/10.1089/hum.2010.100.

Ramesh, Nagarajan et al. 2006. "CG0070, a Conditionally Replicating Granulocyte Macrophage Colony-Stimulating Factor - Armed Oncolytic Adenovirus for the Treatment of Bladder Cancer." *Clinical Cancer Research* 12(1): 305–13.

Ramirez-Montagut, Teresa et al. 2004. "FAPα, a Surface Peptidase Expressed during Wound Healing, Is a Tumor Suppressor." *Oncogene* 23(32): 5435–46.

Ranki, Tuuli et al. 2016. "Phase I Study with ONCOS-102 for the Treatment of Solid Tumors - an Evaluation of Clinical Response and Exploratory Analyses of Immune Markers." *Journal for ImmunoTherapy of Cancer* 4(1): 1–18. http://dx.doi.org/10.1186/s40425-016-0121-5.

Restifo, Nicholas P. 2001. "Hierarchy, Tolerance, and Dominance in the Antitumor T-Cell Response." 24(3): 193–94.

Ribas, Antoni et al. 2017. "Oncolytic Virotherapy Promotes Intratumoral T Cell Infiltration and Improves Anti-PD-1 Immunotherapy." *Cell* 170(6): 1109–1119.e10. http://dx.doi.org/10.1016/j.cell.2017.08.027.

Rivera, Angel A. et al. 2004. "Mode of Transgene Expression after Fusion to Early or Late Viral Genes of a Conditionally Replicating Adenovirus via an Optimized Internal Ribosome Entry Site in Vitro and in Vivo." *Virology* 320(1): 121–34.

Roberts, Edward W. et al. 2013. "Depletion of Stromal Cells Expressing Fibroblast Activation Protein-α from Skeletal Muscle and Bone Marrow Results in Cachexia and Anemia." *The Journal of Experimental Medicine* 210(6): 1137–51. http://www.jem.org/lookup/doi/10.1084/jem.20122344.

Rodríguez-García, A. et al. 2015. "Insertion of Exogenous Epitopes in the E3-19K of Oncolytic Adenoviruses to Enhance TAP-Independent Presentation and Immunogenicity." *Gene Therapy* 22(7): 596–601.

Rodríguez-García, Alba et al. 2015. "Safety and Efficacy of VCN-01, an Oncolytic Adenovirus Combining Fiber HSG-Binding Domain Replacement with RGD and Hyaluronidase Expression." *Clinical Cancer Research* 21(6): 1406–18.

Rodríguez García, Alba. 2015. "Enhancing the Antitumor Activity of Oncolytic Adenoviruses by Combining Tumor Targeting with Hyaluronidase Expression or by Increasing the Immunogenicity of Exogenous Epitopes." *Doctoral thesis*.

Rohmer, Stanimira et al. 2009. "Transgene Expression by Oncolytic Adenoviruses Is Modulated by E1B19K Deletion in a Cell Type-Dependent Manner." *Virology* 395(2): 243–54. http://dx.doi.org/10.1016/j.virol.2009.09.030.

Roizman, B. 1996. "The Function of Herpes Simplex Virus Genes: A Primer for Genetic Engineering of Novel Vectors." *Proceedings of the National Academy of Sciences* 93(21): 11307–12.

Rojas Expósito, Luis Alfonso. 2017. "Blood Barriers for Oncolytic Adenovirus Efficacy: Study of

Binding to Erythrocytes via CAR and Albumin-Mediated Evasion of Neutralizing Antibodies." *Doctoral thesis*. http://hdl.handle.net/2445/112693.

Rojas, J. J. et al. 2012. "Improved Systemic Antitumor Therapy with Oncolytic Adenoviruses by Replacing the Fiber Shaft HSG-Binding Domain with RGD." *Gene Therapy* 19(4): 453–57.

Rojas, Juan J. et al. 2010. "Minimal RB-Responsive E1A Promoter Modification to Attain Potency, Selectivity, and Transgene-Arming Capacity in Oncolytic Adenoviruses." *Molecular Therapy* 18(11): 1960–71.

Rojas, Luis Alfonso et al. 2016. "Albumin-Binding Adenoviruses Circumvent Pre-Existing Neutralizing Antibodies upon Systemic Delivery." *Journal of Controlled Release* 237: 78–88.

Ros, Xavier Bofill-De, Eneko Villanueva, and Cristina Fillat. 2015. "Late-Phase MiRNA-Controlled Oncolytic Adenovirus for Selective Killing of Cancer Cells." *Oncotarget* 6(8).

Ross, Sandra L. et al. 2017. "Bispecific T Cell Engager (BiTE®) Antibody Constructs Can Mediate Bystander Tumor Cell Killing." *PLoS ONE* 12(8): 1–24.

Russell, Stephen J., Kah-Whye Peng, and John C. Bell. 2012. "Oncolytic Virotherapy." *Nature Biotechnology* 19(1): 47–56.

Russell, W. C. 2009. "Adenoviruses: Update on Structure and Function." *Journal of General Virology* 90(1): 1–20.

Salmon, Hélène et al. 2012. "Matrix Architecture Defines the Preferential Localization and Migration of T Cells into the Stroma of Human Lung Tumors." *Journal of Clinical Investigation* 122(3): 899–910.

Santos, AM, Jason Jung, Nazneen Aziz, and JL Kissil. 2009. "Targeting Fibroblast Activation Protein Inhibits Tumor Stromagenesis and Growth in Mice." *Journal of Clinical Investigation* 119(12): 3613–25. http://www.ncbi.nlm.nih.gov/pmc/articles/PMC2786791/.

Saxena, S. K. et al. 1991. "Comparison of RNases and Toxins upon Injection into Xenopus Oocytes." *Journal of Biological Chemistry* 266(31): 21208–14.

Schierer, Stephan et al. 2012. "Human Dendritic Cells Efficiently Phagocytose Adenoviral Oncolysate but Require Additional Stimulation to Mature." *International Journal of Cancer* 130(7): 1682–94.

Schindler, Daniel G, and Julian E Davies. 1977. "Specific Cleavage of Ribosomal RNA Caused by Alpha Sarcin." *Nucleic Acids Research* 4(4): 1097–1110.

Schirmbeck, Reinhold, Jörg Reimann, Stefan Kochanek, and Florian Kreppel. 2008. "The Immunogenicity of Adenovirus Vectors Limits the Multispecificity of CD8 T-Cell Responses to Vector-Encoded Transgenic Antigens." *Molecular Therapy* 16(9): 1609–16. http://dx.doi.org/10.1038/mt.2008.141.

Schlereth, Bernd et al. 2005. "Eradication of Tumors from a Human Colon Cancer Cell Line and from Ovarian Cancer Metastases in Immunodeficient Mice by a Single-Chain Ep-CAM-/CD3-Bispecific Antibody Construct." *Cancer Research* 65(7): 2882–89.

———. 2006. "Potent Inhibition of Local and Disseminated Tumor Growth in Immunocompetent Mouse Models by a Bispecific Antibody Construct Specific for Murine CD3." *Cancer Immunology, Immunotherapy* 55(7): 785–96.

Schmittnaegel, M. et al. 2015. "Committing Cytomegalovirus-Specific CD8 T Cells to Eliminate Tumor Cells by Bifunctional Major Histocompatibility Class I Antibody Fusion Molecules." *Cancer Immunology Research* 3(7): 764–76.

Scott, Eleanor M. et al. 2018. "Solid Tumor Immunotherapy with T Cell Engager-Armed Oncolytic Viruses." *Macromolecular Bioscience* 18(1).

Sedykh, Sergey E., Victor V. Prinz, Valentina N. Buneva, and Georgy A. Nevinsky. 2018. "Bispecific Antibodies : Design , Therapy , Perspectives." *Drug Design, Development and Therapy* 12: 195–208.

Sharpe, S. et al. 2001. "Induction of Simian Immunodeficiency Virus (SIV)-Specific CTL in Rhesus Macaques by Vaccination with Modified Vaccinia Virus Ankara Expressing SIV Transgenes: Influence of Pre-Existing Anti-Vector Immunity." *Journal of General Virology* 82(9): 2215–23.

Singleton, D. C. et al. 2007. "The Nitroreductase Prodrug SN 28343 Enhances the Potency of Systemically Administered Armed Oncolytic Adenovirus ONYX-411NTR." *Cancer Gene Therapy*.

Siurala, Mikko et al. 2016. "Syngeneic Syrian Hamster Tumors Feature Tumor-Infiltrating Lymphocytes Allowing Adoptive Cell Therapy Enhanced by Oncolytic Adenovirus in a Replication Permissive Setting." *OncoImmunology* 5(5): 1–10. http://dx.doi.org/10.1080/2162402X.2015.1136046.

Smith, Elspeth, Jessica Breznik, and Brian D. Lichty. 2011. "Strategies to Enhance Viral Penetration of Solid Tumors." *Human Gene Therapy* 22(9): 1053–60. http://www.liebertonline.com/doi/abs/10.1089/hum.2010.227.

Sobol, Paul T. et al. 2011. "Adaptive Antiviral Immunity Is a Determinant of the Therapeutic Success of Oncolytic Virotherapy." *Molecular Therapy* 19(2): 335–44. http://dx.doi.org/10.1038/mt.2010.264.

Speck, Tobias et al. 2018. "Targeted Bite Expression by an Oncolytic Vector Augments Therapeutic Efficacy against Solid Tumors." *Clinical Cancer Research* 24(9): 2128–37.

Stadler, Christiane R. et al. 2016. "Characterization of the First-in-Class T-Cell-Engaging Bispecific Single-Chain Antibody for Targeted Immunotherapy of Solid Tumors Expressing the Oncofetal Protein Claudin 6." *OncoImmunology* 5(3).

Stanton, Richard J. et al. 2008. "Re-Engineering Adenovirus Vector Systems to Enable High-Throughput Analyses of Gene Function." *BioTechniques* 45(6): 659–68.

Stavropoulos, Tom A., and Craig A. Strathdee. 2001. "Synergy between TetA and RpsL Provides High-Stringency Positive and Negative Selection in Bacterial Artificial Chromosome Vectors." *Genomics* 72(1): 99–104.

Stone, Jennifer D. et al. 2012a. "A Sensitivity Scale for Targeting t Cells with Chimeric Antigen Receptors (CARs) and Bispecific t-Cell Engagers (BiTEs)." *OncoImmunology* 1(6): 863–73.

———. 2012b. "A Sensitivity Scale for Targeting t Cells with Chimeric Antigen Receptors (CARs) and Bispecific t-Cell Engagers (BiTEs)." *OncoImmunology*.

Tahtinen, S. et al. 2015. "Adenovirus Improves the Efficacy of Adoptive T-Cell Therapy by Recruiting Immune Cells to and Promoting Their Activity at the Tumor." *Cancer Immunology Research* 3(8): 915–25. http://cancerimmunolres.aacrjournals.org/cgi/doi/10.1158/2326-6066.CIR-14-0220-T.

Takahashi, Hideyuki et al. 2017. "Cancer-Associated Fibroblasts Promote an Immunosuppressive Microenvironment through the Induction and Accumulation of Protumoral Macrophages." *Oncotarget* 8(5): 8633–47. http://www.oncotarget.com/abstract/14374.

Teachey, David T. et al. 2013. "Cytokine Release Syndrome after Blinatumomab Treatment Related to Abnormal Macrophage Activation and Ameliorated with Cytokine-Directed Therapy." *Blood* 121(26): 5154–57.

Tian, Tianhai, Sarah Olson, James M. Whitacre, and Angus Harding. 2011. "The Origins of Cancer Robustness and Evolvability." *Integrative Biology* 3(1): 17–30.

Tomé-Amat, Jaime et al. 2015. "Efficient in Vivo Antitumor Effect of an Immunotoxin Based on Ribotoxin α-Sarcin in Nude Mice Bearing Human Colorectal Cancer Xenografts." *SpringerPlus* 4(1).

Topp, Max S. et al. 2011. "Targeted Therapy with the T-Cell-Engaging Antibody Blinatumomab of Chemotherapy-Refractory Minimal Residual Disease in B-Lineage Acute Lymphoblastic Leukemia Patients Results in High Response Rate and Prolonged Leukemia-Free Survival." *Journal of Clinical Oncology* 29(18): 2493–98.

Toyoda, Eiji et al. 2008. "Adenovirus Vectors with Chimeric Type 5 and 35 Fiber Proteins Exhibit Enhanced Transfection of Human Pancreatic Cancer Cells." *International Journal of Oncology* 33(6): 1141–47.

Tran, Eric et al. 2013. "Immune Targeting of Fibroblast Activation Protein Triggers Recognition of Multipotent Bone Marrow Stromal Cells and Cachexia." *The Journal of Experimental Medicine* 210(6): 1125–35. http://www.jem.org/lookup/doi/10.1084/jem.20130110.

Trinchieri, Giorgio, Stefan Pflanz, and Robert A Kastelein. 2003. "The IL-12 Family of Heterodimeric Cytokines." *Immunity* 19(5): 641–44. http://www.sciencedirect.com/science/article/pii/S1074761303002966.

Tsukuda, Kazunori et al. 2002. "An E2F-Responsive Replication-Selective Adenovirus Targeted to the Defective Cell Cycle in Cancer Cells: Potent Antitumoral Efficacy but No Toxicity to Normal Cell." *Cancer Research* 62(12): 3438–47.

Verma, Inder M., and Matthew D. Weitzman. 2005. "GENE THERAPY: Twenty-First Century Medicine." *Annual Review of Biochemistry* 74(1): 711–38. http://www.annualreviews.org/doi/10.1146/annurev.biochem.74.050304.091637.

Villanueva, Eneko, Maria Martí-Solano, and Cristina Fillat. 2016. "Codon Optimization of the Adenoviral Fiber Negatively Impacts Structural Protein Expression and Viral Fitness." *Scientific Reports* 6.

Wang, H. et al. 2014. "Downregulation of FAP Suppresses Cell Proliferation and Metastasis through PTEN/PI3K/AKT and Ras-ERK Signaling in Oral Squamous Cell Carcinoma." *Cell Death and Disease* 5(4): 1–11.

Wang, LC. et al. 2014. "Targeting Fibroblast Activation Protein in Tumor Stroma with Chimeric Antigen Receptor T Cells Can Inhibit Tumor Growth and Augment Host Immunity without Severe Toxicity." *Cancer Immunology Research* 2(2): 154–66. http://cancerimmunolres.aacrjournals.org/cgi/doi/10.1158/2326-6066.CIR-13-0027.

Wang, Shuwen, Yuanjun Zhao, Melanie Leiby, and Jiyue Zhu. 2009. "A New Positive/Negative Selection Scheme for Precise BAC Recombineering." *Molecular Biotechnology* 42(1): 110–16.

Wang, Yaohe et al. 2003. "E3 Gene Manipulations Affect Oncolytic Adenovirus Activity in Immunocompetent Tumor Models." *Nature Biotechnology* 21(11): 1328–35.

Wiethoff, C. M., H. Wodrich, L. Gerace, and G. R. Nemerow. 2005. "Adenovirus Protein VI Mediates Membrane Disruption Following Capsid Disassembly." *Journal of Virology* 79(4): 1992–2000. http://jvi.asm.org/cgi/doi/10.1128/JVI.79.4.1992-2000.2005.

Wing, Anna et al. 2018. "Improving CART-Cell Therapy of Solid Tumors with Oncolytic Virus–Driven Production of a Bispecific T-Cell Engager." *Cancer Immunology Research*. http://cancerimmunolres.aacrjournals.org/lookup/doi/10.1158/2326-6066.CIR-17-0314.

Wolf, Evelyn et al. 2005. "BiTEs: Bispecific Antibody Constructs with Unique Anti-Tumor Activity." *Drug Discovery Today* 10(18): 1237–44.

Woller, Norman et al. 2011. "Virus-Induced Tumor Inflammation Facilitates Effective DC Cancer Immunotherapy in a Treg-Dependent Manner in Mice." *Journal of Clinical Investigation* 121(7): 2570–82.

———. 2015. "Viral Infection of Tumors Overcomes Resistance to PD-1-Immunotherapy by Broadening Neoantigenome-Directed T-Cell Responses." *Molecular Therapy* 23(10): 1630–40. http://dx.doi.org/10.1038/mt.2015.115.

Wrzesinski, Stephen H., Yisong Y. Wan, and Richard A. Flavell. 2007. "Transforming Growth Factor-β and the Immune Response: Implications for Anticancer Therapy." *Clinical Cancer Research* 13(18): 5262–70.

Yoon, A. Rum, Jin Woo Hong, and Chae Ok Yun. 2017. "Adenovirus-Mediated Decorin Expression Induces Cancer Cell Death through Activation of P53 and Mitochondrial Apoptosis." *Oncotarget* 8(44): 76666–85.

Yu, Feng et al. 2014. "T-Cell Engager-Armed Oncolytic Vaccinia Virus Significantly Enhances Antitumor Therapy." *Molecular Therapy* 22(1): 102–11.

Yu, Feng, Bangxing Hong, and Xiao-Tong Song. 2017. "A T-Cell Engager - Armed Oncolytic Vaccinia Virus to Target the Tumor Stroma." *Cancer Transl Med* 3(4): 122–32.

Yuraszeck, T., S. Kasichayanula, and J. E. Benjamin. 2017. "Translation and Clinical Development of Bispecific T-Cell Engaging Antibodies for Cancer Treatment." *Clinical Pharmacology and Therapeutics* 101(5): 634–45.

Zamarin, Dmitriy, and Jedd D. Wolchok. 2014. "Potentiation of Immunomodulatory Antibody Therapy with Oncolytic Viruses for Treatment of Cancer." *Molecular Therapy - Oncolytics* 1(June): 14004. http://dx.doi.org/10.1038/mto.2014.4.

Zamarin, Dmitry et al. 2014. "Localized Oncolytic Virotherapy Overcomes Systemic Tumor Resistance to Immune Checkpoint Blockade Immunotherapy . TGF- β Upregulates CD70 Expression and Induces Exhaustion of Effector Memory T Targeted Depletion of an MDSC Subset Unmasks Pancreatic Ductal." 6(226).

Zhang, Jin, Vijay Kale, and Mingnan Chen. 2015. "Gene-Directed Enzyme Prodrug Therapy." *The AAPS journal* 17(1): 102–10.

Zhu, Mingzhu et al. 2005. "Linked Tumor-Selective Virus Replication and Transgene Expression from E3-Containing Oncolytic Adenoviruses †." *Journal of virology* 79(9): 5455–65.

Ziani, Linda, Salem Chouaib, and Jerome Thiery. 2018. "Alteration of the Antitumor Immune Response by Cancer-Associated Fibroblasts." *Frontiers in Immunology* 9(MAR).

Zou, Weiping. 2005. "Immunosuppressive Networks in the Tumour Environment and Their Therapeutic Relevance." *Nature Reviews Cancer* 5(4): 263–74.

ANNEX

Sostoa et al. Journal for ImmunoTherapy of Cancer (2019) 7:19
https://doi.org/10.1186/s40425-019-0505-4

Journal for ImmunoTherapy of Cancer

RESEARCH ARTICLE Open Access

Targeting the tumor stroma with an oncolytic adenovirus secreting a fibroblast activation protein-targeted bispecific T-cell engager

Jana de Sostoa[1], Carlos Alberto Fajardo[1], Rafael Moreno[1], Maria D. Ramos[1], Martí Farrera-Sal[1,2] and Ramon Alemany[1*]

Abstract

Background: Oncolytic virus (OV)-based therapies have an emerging role in the treatment of solid tumors, involving both direct cell lysis and immunogenic cell death. Nonetheless, tumor-associated stroma limits the efficacy of oncolytic viruses by forming a barrier that blocks efficient viral penetration and spread. The stroma also plays a critical role in progression, immunosuppression and invasiveness of cancer. Fibroblast activation protein-α (FAP) is highly overexpressed in cancer-associated fibroblasts (CAFs), the main cellular component of tumor stroma, and in this study we assessed whether arming oncolytic adenovirus (OAd) with a FAP-targeting Bispecific T-cell Engager (FBiTE) could retarget infiltrated lymphocytes towards CAFs, enhancing viral spread and T cell-mediated cytotoxicity against the tumor stroma to improve therapeutic activity.

Methods: The bispecific T-cell Engager against FAP was constructed using an anti-human CD3 single-chain variable fragment (scFv) linked to an anti-murine and human FAP scFv. This FBiTE was inserted in the oncolytic adenovirus ICOVIR15K under the control of the major late promoter, generating the ICO15K-FBiTE. ICO15K-FBiTE replication and potency were assessed in HT1080 and A549 tumor cell lines. The expression of the FBiTE and the activation and proliferation of T cells that induced along with the T cell-mediated cytotoxicity of CAFs were evaluated by flow cytometry *in vitro*. *In vivo*, T-cell biodistribution and antitumor efficacy studies were conducted in NOD/*scid*/*IL2rg*$^{-/-}$ (NSG) mice.

Results: FBiTE expression did not decrease the infectivity and replication potency of the armed virus. FBiTE-mediated binding of CD3^{+} effector T cells and FAP^{+} target cells led to T-cell activation, proliferation, and cytotoxicity of FAP-positive cells *in vitro*. *In vivo,* FBiTE expression increased intratumoral accumulation of T cells and decreased the level of FAP, a marker of CAFs, in tumors. The antitumor activity of the FBiTE-armed adenovirus was superior to the parental virus.

Conclusions: Combination of viral oncolysis of cancer cells and FBiTE-mediated cytotoxicity of FAP-expressing CAFs might be an effective strategy to overcome a key limitation of oncolytic virotherapy, encouraging its further clinical development.

Keywords: Oncolytic adenovirus, Bispecific T-cell engager, Fibroblast activation protein, Tumor-associated stroma

* Correspondence: ralemany@iconcologia.net
[1]ProCure Program, IDIBELL-Institut Català d'Oncologia, l'Hospitalet de Llobregat, El Prat de Llobregat, Spain
Full list of author information is available at the end of the article

Background

Oncolytic viruses (OVs) are emerging as promising anti-tumor agents in cancer treatment, offering an attractive combination of tumor-specific cell lysis and intratumoral immune stimulation. Engineered OVs have been tested in several Phase I-III clinical trials, and Talimogene laherparepvec (Imlygic®), an Herpes Simplex Virus (HSV) expressing the granulocyte macrophage colony stimulating factor (GM-CSF), has been recently approved by FDA and EMA for the treatment of melanoma. Despite their potential, OVs have several limitations that should be tackle to improve their efficacy.

One of the major obstacles to successful oncolytic therapy is the presence of stroma in tumors, formed by different types of cells and extracellular matrix (ECM) compounds. Stroma not only creates physical barriers that limit oncolytic adenovirus (OAd) spread across the tumor, but also induces tumor progression by enhancing the survival, proliferation, stemness, metastasis, and an immunosuppressive microenvironment that limits tumor immunity, ultimately promoting cancer progression, but also enhancing resistance to therapy [1]. One attractive stromal target is the fibroblast activation protein-α (FAP), a transmembrane serine protease that is highly expressed on the cell surface of cancer-associated fibroblasts (CAFs), which represent the key component in the tumor microenvironment of many cancers [2]. Accordingly, several immunotherapeutic strategies to deplete FAP-expressing stromal cells have already been explored [3–11].

Another important hurdle for the efficacy of OVs is the host immune response to the OV. Antiviral immune responses can intrinsically limit OV infection, spread, and overall therapeutic efficacy. However, there is increasing evidence that virus-mediated destruction or damage of tumors can lead to an antitumor immune response [12]. Thus, novel strategies to minimize the antiviral immune response for successful virus growth and retreatment, but to stimulate antitumor responses, would provide an opportunity to tilt this balance in favor of the therapeutic benefit.

Based on the pro-tumorigenic functions of tumor stroma and the strong antiviral immune responses that limit OV therapy, the destruction of CAFs by arming OVs with FAP-targeting Bispecific T-cell Engagers (BiTEs) may mitigate the key limitations of OVs [3]. BiTE antibody constructs comprise tandemly-arranged single-chain variable fragments (scFvs). One scFv binds the TCR CD3ε subunit and the other binds a tumor-associated surface antigen (TAA). The simultaneous binding of the BiTE to the CD3 on T cells and to the TAA on target cells leads to the formation of the immunological synapse due to the close proximity of both membranes, leading to polyclonal T-cell activation, expansion and lysis of the protein-expressing target cells. Blinatumomab (Blincyto®), a first-in-class BiTE, has shown promise results for treating relapsed/refractory precursor B cell acute lymphoid leukemia (ALL) [13]. We have previously generated an anti-EGFR BiTE-armed OAd, which showed to improve T cell-mediated killing of cancer cells both *in vitro* and *in vivo* [14].

Here we report the development of the OAd ICO15K-FBiTE encoding FAP-targeting BiTE to retarget infiltrated lymphocytes against FAP-expressing CAFs. We show the ability of ICO15K-FBiTE to induce strong and specific T-cell activation and proliferation upon infection, leading to T cell-mediated cytotoxicity of CAFs *in vitro* and enhanced antitumor activity due to FAP depletion *in vivo*.

Methods

Cell lines

Human cell lines A549 (lung adenocarcinoma), HEK293 (embryonic kidney), HT1080 (fibrosarcoma), A431 (vulval epidermoid carcinoma), Jurkat (T-cell leukemia) and HPAC (pancreatic adenocarcinoma) were obtained from the American Type Culture Collection (ATCC). Human CAFs pf179 (named as hCAFs) were kindly provided by Varda Rotter (Weizmann Insitute of Science, Israel). 293, 293mFAP and 293hFAP cell lines were obtained from Dr. Eric Tran (National Institutes of Health, Bethesda, MD). Murine CAFs were isolated from HPAC tumors as described [15]. To generate FAP-expressing cell lines, HT1080 and A431 cells were transduced with a lentivirus encoding either the mouse or the human FAP cDNA (Dharmacon). FAP-expressing cells were sorted and expanded. HT1080 cells stably expressing mouse FAP or human FAP are designated as HT-mFAP and HT-hFAP, respectively. A431 cells are designated as A431-mFAP and A431-hFAP. All tumor cell lines were maintained in Dulbecco's modified Eagle's medium (DMEM) supplemented with inactivated 10% fetal bovine serum (FBS, Invitrogen Carlsbad) and 1X Penicillin/Streptomycin (PS, Gibco) at 37 °C, 5% CO_2 incubator, except for Jurkat cells which were maintained in RPMI-1640 medium. All cell lines were routinely tested for mycoplasma.

Preparation of peripheral blood mononuclear cells and T cell isolation

All experiments were approved by the ethics committees of the University Hospital of Bellvitge and the Blood and Tissue Bank (BST) from Catalonia. Blood samples were obtained from the BST from Catalonia. Peripheral blood mononuclear cells (PBMCs) were isolated by ficoll density gradient centrifugation. PBMCs were treated with ACK lysis buffer (Lonza) and resuspended in RPMI-1640 medium supplemented with 10% FBS. T

cells were isolated using the Rosette-Sep Human T Cell Enrichment Cocktail (STEMCELL Technologies). For stimulation, T cells were cultured with CD3/CD28-activating Dynabeads (Thermo Fisher Scientific) at 1:3 bead-to-cell ratio. For bioimaging studies, T cells were transduced with a lentivirus expressing GFP and the click beetle green luciferase (CBG) (multiplicity of infection (MOI) of 7) 24 h hours after activation. Cells were counted and fed every day until day 10, time point at which they were either used for functional assays or cryopreserved.

FBiTE and construction of recombinant adenoviruses

FBiTE was generated by joining the scFvs anti-FAP and anti-CD3ε with a GGGGS flexible linker. The anti-CD3 scFv sequence of the Blinatumomab BiTE was obtained from patent application WO2004106381. The anti-FAP sequence (FAP5) was derived from patent application US 2009/0304718 A1 and showed affinities of 5 nM for human FAP and 0.6 nM for mouse FAP [10]. The FAP5 and anti-CD3 variable regions were connected by a $(G_4S_1)_3$ and a $(G_2S_1)_4GG$ linker, respectively. The FBiTE was arranged V_L(FAP5)-V_H(FAP5)-V_H(CD3)-V_L(CD3) and contained an N-terminal signal peptide derived from the mouse immunoglobulin light chain for mammalian secretion, and a FLAG tag at the C-terminal for detection. The FBiTE construct was optimized for human codon usage and synthesized by Baseclear (pUC57-FBiTE plasmid, Baseclear). The genome of ICO15K-FBiTE was obtained by recombineering in bacteria as described [16]. HEK293 cells were transfected with the resulting plasmid pAdZ-ICO15K-FBiTE with calcium phosphate standard protocol. ICO15K-FBiTE was plaque-purified and further amplified in A549 cells. Viruses were double purified by cesium chloride gradient centrifugation and tittered using anti-hexon staining.

Production of FBiTE-containing supernatants

A549 cells (1×10^7) were infected at MOI of 20 with ICO15K or ICO15K-FBiTE. 72 h post-infection, supernatants were collected and centrifuged 5 min at 1200 g to eliminate detached cells. Supernatants from uninfected cells were used as a mock control. For binding assays, supernatants were concentrated (approximately 20x) with Amicon Ultra-15 filter units with a molecular weight cutoff of 30 kDa (Merck Millipore). Aliquots of the supernatant were stored at − 20 °C for future analysis.

Antibodies and flow cytometry

Flow cytometry analysis was performed on a Gallios cytometer (Beckman Coulter) and data was processed with FlowJo v7.6.5 (Tree Star). Murine FAP expression was detected with the mouse 73.3 antibody kindly provided by Dr. Ellen Puré (Abramson Family Cancer Research Institute, Philadelphia, Pennsylvania) and human FAP expression was detected with F19 hybridoma (ATCC). For analysis of T cell populations, antibodies CD3 (clone OKT3), CD4 (OKT4) and CD8 (SK1) (Biolegend) were used. The FITC-conjugated anti-FLAG M2 monoclonal antibody (Sigma Aldrich) was used to detect the BiTE in binding assays. In each case, appropriated isotype controls were used (Santa Cruz Biotechnology).

Binding assays

Binding assays were performed with HT1080 cells transfected with either human or murine FAP antigen or $CD3^+$ Jurkat cells. HT1080 (2×10^5) or Jurkat (1×10^5) cells were incubated on ice for one hour with the concentrated or unconcentrated supernatants. BiTE binding was determined by flow cytometry using anti-FLAG M2-FITC antibody (Sigma Aldrich).

In vitro co-culture experiments

Tumor cells (3×10^5) and PBMCs or T cells (effector--to-target ratio of 5) were seeded in 96-well plates in 100 μl of medium. For cytokine production assays, 100 μl of the supernatants were added to the wells. Supernatants were collected after 24 h of incubation and assessed for human IFN-ɣ, TNF-α, and IL-2 using the ELISA MAX Deluxe set (Biolegend), following the manufacturer's protocol. For PBMCs or T-cell proliferation assays, PBMCs or T cells were labeled with 1 μmol/L Carboxyfluorescein succinimidyl ester (CFSE) (Sigma Aldrich) and co-cultured as described above for 6 days (PBMCs) or 3 days (T cells). Cells were then stained for cell viability with LIVE/DEAD (Thermo Fisher Scientific) and for CD4 and CD8 (Biolegend). Flow cytometry analysis was performed by acquiring a total of 20,000 events.

Cytotoxicity assays

Viral cytotoxicity assays were performed as previously described [17]. IC50 was calculated with GraphPad Prsim v6.02 (GraphPad Software Inc.) by a dose-response non-linear regression with a variable slope.

To assess FBiTE-mediated cytotoxicity, CFSE-labeled target cells (HT1080, mCAFs (3×10^4) or hCAFs (1×10^4)) were cultured with $1{,}5 \times 10^5$ T cells (E:T = 5) in 96-well plates or 48-well plates, respectively. 100 μl of mock, ICO15K or ICO15K-FBiTE supernatants were added. After 24 h of incubation, cocultures were trypsinized and stained with LIVE/DEAD® (Thermo Fisher Scientific). Cells were analyzed by flow cytometry and the percentage of $CFSE^+$/LIVE and $DEAD^+$ was determined.

For bystander killing assays, FAP-negative cells (HT1080 and A431) were cultured in the presence of T

cells and its derivative mFAP or hFAP cells (E:T = 5) and 100 μl of supernatants were added. After 24 h, the cytotoxicity of the FAP-negative cells and mFAP or hFAP cells were determined by flow cytometry. mFAP- and hFAP-expressing cells were identified as a CFSE-hCD45- double negative cells. The percentage of $CFSE^+$/LIVE and $DEAD^+$ cells and $CFSE^{-/}hCD45^-$/LIVE and $DEAD^+$ cells was determined.

FBiTE-mediated cytotoxicity of FAP-positive non-infected cells was assessed infecting A549 cells in suspension with ICO15K or ICO15K-FBiTE (MOI = 20). After 4 h, infected cells were washed thrice with PBS. 3×10^4 A549-infected cells were mixed with 3×10^4 CFSE-labeled target cells (1:1), T cells (E:T = 5) and supernatants (100 μl). After three days of incubation, co-cultures were stained and analyzed as described above.

Xenograft mouse models

All animal experiments were approved by the Ethics Committee for Animal Experimentation from Biomedical Research Institute of Bellvitge (IDIBELL). A549 (4×10^6) or HPAC (2×10^6) cells were subcutaneously injected into each flank of female, 8-week-old, NOD/*scid*/*IL2rg*$^{-}$/$^{-}$ (NSG) mice (bred in house). Once tumors reached a median volume of 120 mm^3, mice were randomized prior to treatment.

To evaluate T-cell trafficking to the tumor, mice bearing A549 tumors were treated intratumorally with PBS, ICO15K, or ICO15K-FBiTE (1×10^9 vp/tumor). Four days later, 1×10^7 preactivated GFP- and CBG-luciferase-expressing T cells (LUC-T-cells) were intravenously injected to treated mice. Mice were given an intraperitoneal injection of 15 mg/mL D-luciferin potassium salt solution (Byosinth AG) and imaged daily for 7 days using IVIS Lumina XRMS Imaging System (PerkinElmer).

For antitumor efficacy studies, mice were treated intratumorally with PBS or the indicated viruses (1×10^9 vp/tumor). Tumors were measured twice or thrice a week with a digital caliper and tumor volume was determined with the eq. V (mm^3) = $\pi/6 \times W^2 \times L$, where W and L are the width and the length of the tumor, respectively.

Immunohistochemistry

To detect FAP and E1A-Adenovirus expression in tumors, immunohistochemistry (IHC) was performed using OCT-embedded sections (5 μm thick) of freshly frozen tumor tissues. Sections were fixed with 2% of PFA at room temperature and endogenous peroxidases were blocked by incubation in 3% H_2O_2. Next, sections were blocked for 1 h with 10% of normal goat serum diluted in 1% BSA, PBS-Tween. For FAP detection, primary antibody incubation was performed overnight at 4 °C using a biotinylated polyclonal sheep anti-human/mouse FAP antibody (5 μg/ml) or its isotype sheep IgG (R&D systems) in 5% of goat serum. For adenovirus detection, the primary antibody used was an anti-Ad2/5 E1A antibody (Santa Cruz Biotechnology) diluted 1/200 in PBS. The next day, sections were incubated with ABC-HRP kit (Vectastain) for 30 min, followed by 5 min incubation with DAKO-DAB substrate (EnVision). Slides were dehydrated using standard protocols and counterstained with haematoxylin.

DNA/RNA quantification by qPCR

Frozen tumor samples were disrupted using a mortar and pestle under liquid nitrogen. RNA and DNA were isolated from approximately 25 mg of homogenized tissue with the DNA/RNA/protein kit (IBI Scientific). RNA samples were treated with the TURBO DNA-*free* kit (Thermo Fisher Scientific) to remove traces of genomic DNA. RNA (1 μg) was retrotranscribed with the High-Capacity cDNA Reverse Transcription kit (Thermo Fisher Scientific). Real-time analysis was performed in a LightCycler 480 Instrument II (Roche). To quantify the viral genomes and FBiTE transcripts in the tumor, 100 ng of DNA and 40 ng of cDNA in the presence of SYBR Green I Master (Roche) were used, respectively. PCR conditions were: 95 °C 10 min, 40 cycles of 95 °C 15 s, 60 °C 1 min and 72 °C 7 min. Viral genome primers were Ad18852: 5'-CTTCGATGATGCCGCAGTG-3′ and Ad19047R: 5'-ATGAACCGCAGCGTCAAACG-3′ and FBiTE primers were qBiTEF: 5'-CGGCGAGAA AGTGACAATGAC-3′ and qBiTER: 5'-TTGGTGAGG TGCCACTTTTC-3′. Standard curves for viral genomes and FBiTE were prepared by serial dilutions of known copy numbers of adenovirus plasmid and pUC57-FBiTE, respectively. To assess murine FAP expression, 25 ng of cDNA were analyzed with the TaqMan Gene Expression Assay ref. Mm01329177_m1 (Thermo Fisher Scientific). PCR conditions were: 50 °C 2 min, 95 °C 10 min, 40 cycles of 95 °C 15 s and 60 °C 1 min. A standard curve was prepared by serial dilutions of known copy numbers of a murine FAP-expressing plasmid. Human FAP-expressing plasmid was also included as negative control. In all cases, non-retrotranscribed RNA samples, in a quantity equivalent to the amount cDNA loaded in the PCR, were used for PCR to discard genomic DNA contamination.

Statistical analysis

Statistical analyses were performed using GraphPad Prism software v6.02. All results were expressed as means ±SD or SEM, as indicated. Two-tailed unpaired Student's *t*-test was used to evaluate the statistical significance between two groups. One-way ANOVA with Tukey *post hoc* tests was used for differences between three or more groups in a single condition or time point. $P < 0.05$ was taken as the level of significance.

Results

Generation and characterization of an oncolytic adenovirus secreting a FAP-targeting BiTE

We have recently reported the generation of an oncolytic adenovirus armed with a BiTE targeting the EGFR on tumor cells (ICO15K-cBiTE) [14]. This approach, however, does not address the presence of a tumor stroma which can impair virus spread in the tumor. In order to simultaneously target cancer cells through virus-mediated oncolysis and to re-direct immune responses towards tumor stroma fibroblasts, we engineered the genome of the oncolytic adenovirus ICO15K to express a FAP-targeting BiTE (FBiTE) (named as ICO15K-FBiTE). The FBiTE molecule was engineered by joining with flexible linkers (GS linkers) two scFv, one specific for human CD3ε and the other for murine and human FAP (Fig. 1a). FAP scFv sequence was specifically chosen to bind both murine and human to be able to target the murine CAFs infiltrated in xenograft tumors in the *in vivo* experiments. We have previously demonstrated that the insertion of a transgene after the fiber gene using an adenoviral splicing acceptor favors its expression in a replication-dependent manner without interfering with viral oncolysis [14, 18]. Using this strategy, the FBiTE was inserted under the control of the adenovirus major late promoter (Fig. 1a).

To evaluate whether the FBiTE insertion affected the viability and the oncolytic properties of the virus, we first compared the replication kinetics of ICO15K and ICO15K-FBiTE in A549 cells. We observed a minor, although not significant, loss in the production yields from cell extracts and supernatants of ICO15K-FBiTE compared to the parental virus (Fig. 1b). We next assessed the killing kinetics of the virus in dose-response cytotoxicity assays in three cancer cell lines (A549, HT1080 and hCAF). As shown, the FBiTE-expressing adenovirus conserved oncolytic properties despite slight increases in IC_{50} values compared to the parental virus.

We next determined whether FBiTEs encoded by ICO15K-FBiTE were properly secreted from cancer cells upon infection, and whether they could retain their antigen-binding specificities. To this end, we performed binding assays with HT1080 cells that had been genetically modified to express either human or murine FAP. FBiTE binding was detected by flow cytometry with a fluorescently-labeled anti-FLAG

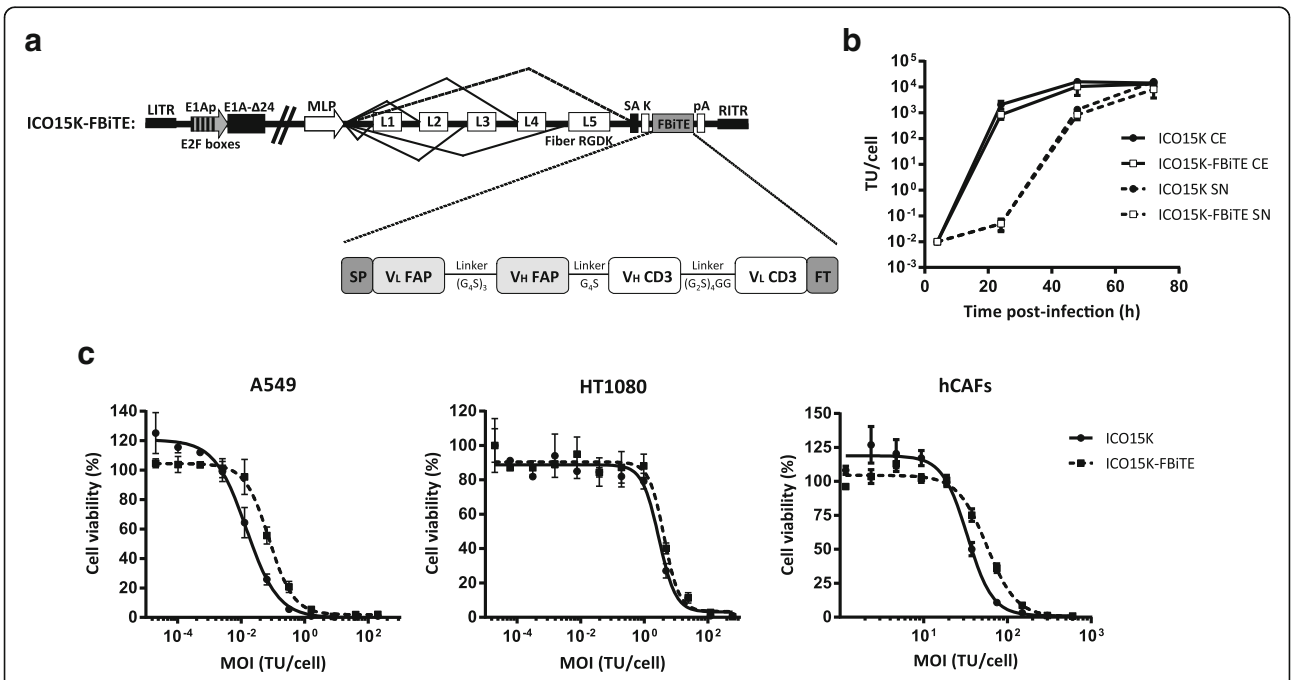

Fig. 1 *In vitro* characterization of ICO15K-FBiTE. **a** Schematic structure representation of ICO15K-FBiTE. V_L and V_H domains of anti-mhFAP and CD3Ɛ are connected by glycine and serine flexible linkers, flanked by the light chain immunoglobulin signal peptide (SP) and the FLAG tag (FT). FBiTE is inserted after the adenovirus fiber gene under the control of the major late promoter (MLP). **b** Viral production from cell extracts (CE) and supernatants (SN) of ICO15K-FBiTE. A549 cell line was infected with ICO15K or ICO15K-FBiTE. At indicated time points, cell extracts and supernatants were harvested and titrated by an anti-hexon staining-based method. **C**. Comparative cytotoxicity profile of ICO15K-FBiTE. A549, HT1080 and hCAFs cells were infected with serial dilutions of ICO15K or ICO15K-FBiTE. Cell viability was measured at day 6 post-infection for A549 and HT1080 and at day 7 for hCAFs. Mean values ± SD are plotted in B and C ($n = 3$). TU, transducing units: number of functional viral particles capable of transducing a cell

antibody. FBiTE molecuels were detected in the ICO15K-FBiTE supernatants, and they bound specifically to HT-mFAP and HT-hFAP but not to the FAP-negative HT1080-parental cell line (Fig. 2a upper and middle panels). Moreover, FBiTE molecules were also able to bind to CD3-positive Jurkat cells (Fig. 2a lower panels). $CD3^+$ bindings were more pronounced when supernatants were concentrated (dashed lines) but FAP^+ bindings were only detected when concentrated.

Supernatants from ICO15K-FBiTE-infected cells induce activation and proliferation of T cells

In order to detect the FBiTE-mediated T-cell effector functions, we evaluated both cytokine production and proliferation of T cells after co-culture with 293 cells, either expressing or not murine or human FAP, in the presence of supernatants from adenovirus-infected (ICO15K or ICO15K-FBiTE) or uninfected cells (mock). After 24 h of incubation, supernatants were collected

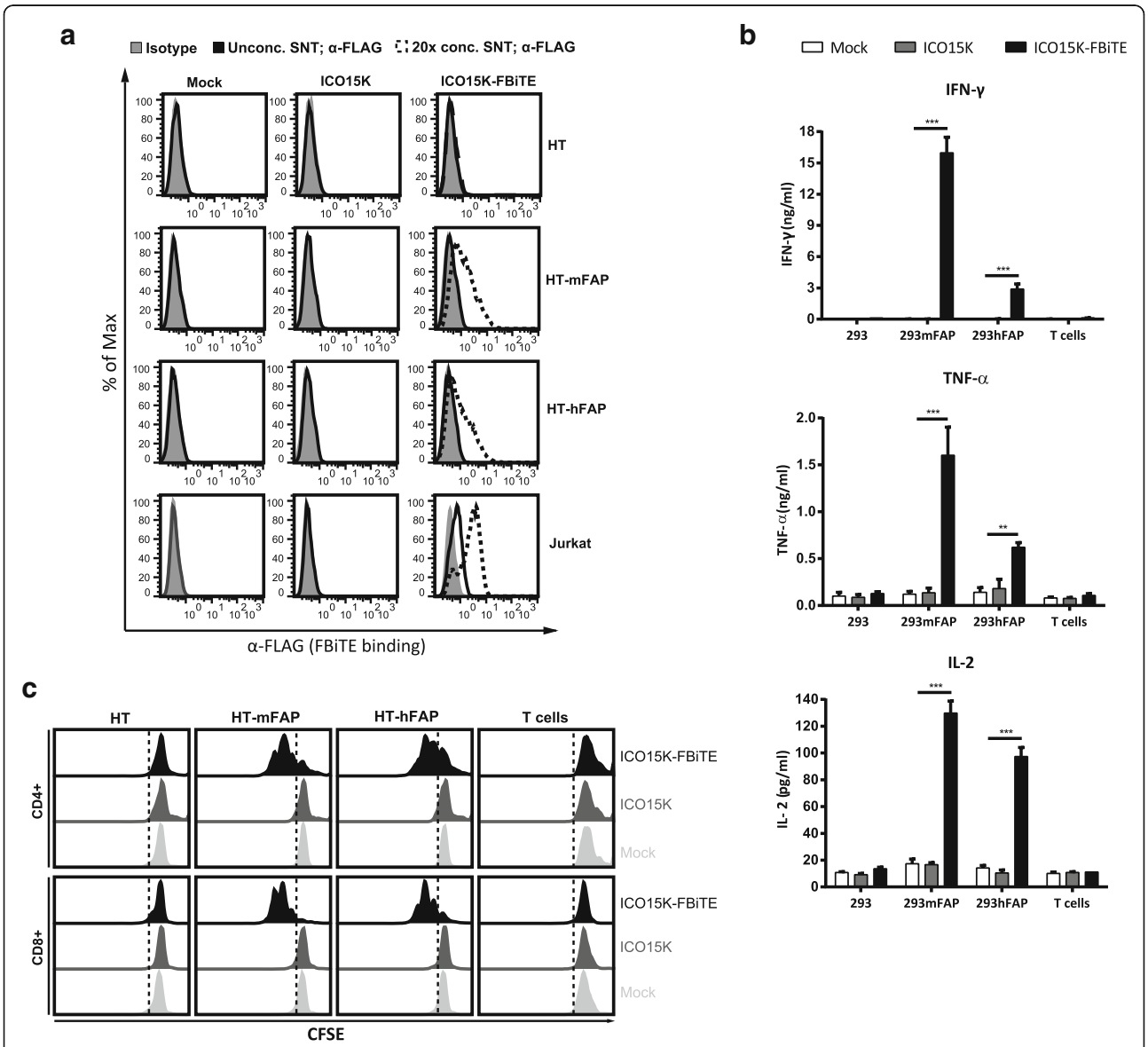

Fig. 2 FBiTE expressed by ICO15K-FBiTE specifically binds to both target and effector cells and is able to activate T cells. **a** HT1080 (HT), HT-mFAP, HT-hFAP and Jurkat cells were incubated with mock, ICO15K, or ICO15K-FBiTE supernatants and FBiTE binding was detected by flow cytometry. **b** Average concentration values of IFN-ɣ, TNF-α and IL-2 cytokines were measured by ELISA assay using supernatants from 24 h co-cultures of HEK293 (293), 293mFAP or 293hFAP cells with T cells (E:T = 5) and indicated supernatants. **c** T-cell proliferation following co-cultures with target cells and indicated supernatants (E:T = 5). A representative result of triplicates is shown. ***, ICO15K-FBiTE significant ($P < 0.001$) versus mock or ICO15K using one-way ANOVA test with post hoc analysis

and T-cell activation was assessed by quantifying IFN-ɣ, TNF-α, and IL-2 by ELISA (Fig. 2b). Significant cytokine release was observed in co-cultures of T cells and FAP-expressing cells and in the presence of ICO15K-FBiTE supernatants. Cytokines levels were higher in the presence of murine FAP-expressing cells compared to human FAP-expressing target cells. This in line with the affinity of the FAP5 monoclonal antibody from which the scFv in our BiTE is derived, which has been reported to be 5 nM for human FAP and 0.6 nM for mouse FAP [10]. Importantly, there was no cytokine production in the absence of FAP^+ targets (293 control cells) or when using supernatants from a parental virus or from non-infected cells. These data demonstrate that FBiTE molecules secreted from infected cells are able to activate T cells in FAP-expression dependent manner.

To further confirm the FBiTE-mediated induction of T-cell effector functions, we evaluated T-cell proliferation after 3 days of co-culture. Both $CD4^+$ and $CD8^+$ T cells showed proliferation only in the co-cultures containing FAP-expressing cells and the ICO15K-FBiTE supernatants (Fig. 2c). After performing the same analysis with PBMCs instead of isolated T cells, both $CD4^+$ and $CD8^+$ T cells showed strong proliferation always in the co-cultures of PBMCs with FBiTE-containing supernatants, even in the absence of FAP-expressing cells (Additional file 1). These results support previous research which showed that a population of macrophages in PBMCs express FAP [19]. To avoid unspecific FBiTE activation of T cells in PBMCs, we used isolated T cells for further experiments.

Combining viral oncolysis with FBiTE-mediated killing improves therapeutic activity *in vitro*

Having shown the expression of FBiTE from ICO15K-FBiTE-infected cells, we next investigated FBiTE-mediated cytotoxicity *in vitro*. We first evaluated the effect of co-culturing HT1080 and its derivative FAP-expressing cell lines with T cells and the indicated supernatants. Marked cytotoxicity of FAP-positive engineered cell lines was observed after 24 h of incubation only in the presence of ICO15K-FBiTE supernatants (Fig. 3a). A recent study demonstrated that BiTEs can also mediate a bystander tumor cell killing of nearby cells lacking the targeted antigen [20]. To evaluate this, we co-cultured CFSE stained FAP-negative cells (HT or A431) with T cells and its derivative mFAP or hFAP-positive cells, and supernatants were added. After 24 h, the cytotoxicity of the CFSE-FAP-negative cells and the mFAP or hFAP-expressing cells was determined by flow cytometry. mFAP and hFAP cells were identified as a CFSE- hCD45- double negative cells. In both cell lines we observed some cytotoxicity of FAP-negative cells (from 15 to 20%) only when co-cultured together with FAP-positive cells and ICO15K-FBiTE supernatants. This result supports an existing BiTE-dependent T cell-induced bystander lysis of FAP-negative cells proximal to FAP-positive cells (Additional file 2).

We next investigated the potential of combining viral oncolysis and FBiTE-mediated killing of FAP-positive non-infected cells. To this end, A549 cells were infected with ICO15K-FBiTE or parental ICO15K at an MOI 20. After 4 h of incubation, cells were washed and co-cultured with HT or HT-FAP-CFSE-stained cells and T cells. In this setup, A549 cells act as FBiTE producers whereas HT cells represent the target cells. The expression of OAd-infected cells specifically increased the cytotoxicity of FAP-positive target tumor cells (Fig. 3b). These results demonstrate that expression of FBiTE is compatible with viral replication and sufficient to achieve the combined oncolysis and FBiTE T-cell mediated killing of the non-infected targeted cells *in vitro*.

Although the above-mentioned experiments prove the FBiTE-mediated killing of FAP-expressing cancer cell lines, the ultimate goal of the secreted FBiTE is to target the FAP^+ CAFs in the tumor microenvironment. To demonstrate the therapeutic potential of the FBiTE in that context, cytotoxicity experiments were performed by co-culturing murine CAFs (mCAFs) and human CAFs (hCAFs) with human T cells and the different supernatants. As shown in Fig. 3c, T-cell-mediated killing of both mCAFs and hCAFs was observed in co-cultures containing the ICO15K-FBiTE supernatant. These results not only confirm the cytotoxic potential of the secreted FBiTE, but also demonstrate that mCAFs can be targeted and killed by human T cells, a prerequisite for the use of *in vivo* xenograft models in which the stroma is from mouse origin.

ICO15K-FBiTE increases tumor T-cell retention and accumulation in vivo

In order to evaluate T-cell trafficking to ICO15K-FBiTE-treated tumors, a biodistribution imaging study was performed. Preactivated T cells were transduced with a lentiviral vector expressing GFP and the Click Beetle Green (CBG) luciferase. We obtained 64% GFP-CBG-positive cells (Additional file 3A), of which 64% were $CD4^+$ and 33% were $CD8^+$ (Additional file 3B). Tumors were injected with PBS, ICO15K, or ICO15K-FBiTE when reached approximately $120mm^3$, and four days post-treatment 1×10^7 LUC-T cells were intravenously injected to all mice groups. Mice were imaged every day until sacrificed. ICO15K-FBiTE-treated tumors showed significant enhanced T-cell retention and accumulation from the first day post-injection, increasing daily unto reaching a peak at day 6 (Fig. 4). This result proved the feasibility of the bystander therapy in an *in vivo* scenario.

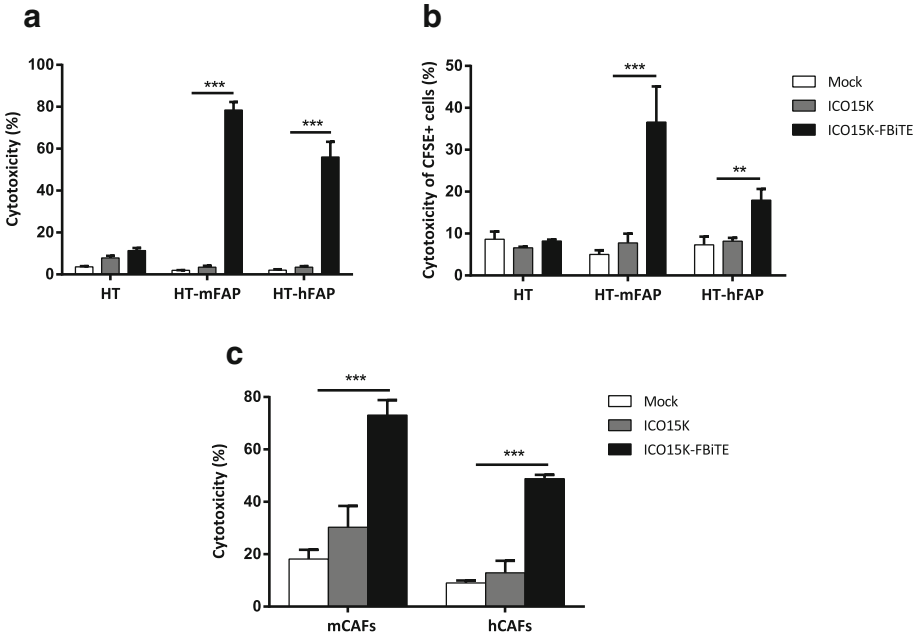

Fig. 3 Enhanced ICO15K-FBiTE-mediated cytotoxicity of FAP-positive cells. **a** FBiTE-mediated cytotoxicity was evaluated by flow cytometry after 24 h incubation of CFSE-stained HT1080 cell lines cultured with T cells and indicated supernatants. **b** CFSE-stained target cells were co-cultured with A549-infected cells and T cells (E:T = 5). After four days of incubation, specific cytotoxicity of CFSE-stained cells was determined by flow cytometry. **c** Cytotoxicity of CFSE-stained-murine or human CAFs was evaluated. Mean values ± SD are plotted in A, B and C ($n = 3$). ***, ICO15K-FBiTE significant ($P < 0.001$) by one-way ANOVA test with *post hoc* analysis compared to mock and ICO15K

ICO15K-FBiTE-mediated oncolysis enhances antitumor efficacy *in vivo*

We next assessed whether the accumulation of FAP-targeted-T cells observed in ICO15K-FBiTE-treated mice could improve the antitumor efficacy in A549 (human lung cancer) and HPAC (human pancreatic) tumor models. It has previously shown that these tumor models generate FAP^+ stroma once implanted subcutaneosly in NSG mice [5, 7]. Tumor-bearing mice were randomized into treatment groups and treated with a single intratumoral administration of PBS, ICO15K or ICO15K-FBiTE (1×10^9 vp/tumor) when the tumor volume reached a mean of $120mm^3$. We first evaluated the antitumor activity of our viruses in both tumor models in the absence of T cells (Fig. 5a). The treatment with either the FBiTE-armed or parental viruses induced a similar significant level of efficacy compared to the PBS group (Fig. 5a). Then we assessed the antitumor activity only in presence of T cells (Fig. 5b-e), therefore it should not be directly compared to Fig. 5a. Four days post-virus-treatment, 1×10^7 preactivated T cells were injected intravenously once (HPAC) or twice (A549) to all mice-treated groups. Based on our pilot studies which classified HPAC tumors as fast growing, only a single dose of T cells was performed. We observed no significant weight loss in these experiments (Additional file 4). In the A549 model, a model that grows much more slowly than HPAC, there were no differences in tumor growth among the different groups up to day 15 (Fig. 5b, Additional file 5a). After this day, the mean tumor growth among treatment groups were statistically different. In contrast, in the fast-growing HPAC model, significant differences started earlier, from day 9 (Fig. 5d, Additional file 5B) but tumor growth was more difficult to control. In both tumor models, tumors growth of tumors treated with the FBiTE-expressing adenovirus were significantly smaller when compared with the tumors treated with PBS or with the control virus. This treament also improved significantly the survival (Fig. 5c and e), providing evidence for the therapeutic benefit of arming an oncolytic adenovirus with the FBiTE.

ICO15K-FBiTE improves the antitumor activity by depletion of FAP

We analysed tumor samples from the efficacy studies described above to demonstrate that the observed improved antitumor activity was associated to the elimination of CAFs by T cells retargeted with the FBiTE expressed from the oncolytic adenovirus. We first quantified the viral genomes and the FBiTE copy numbers by real-time PCR. As expected, we observed high amounts of viral genomes only in virus-treated tumors compared

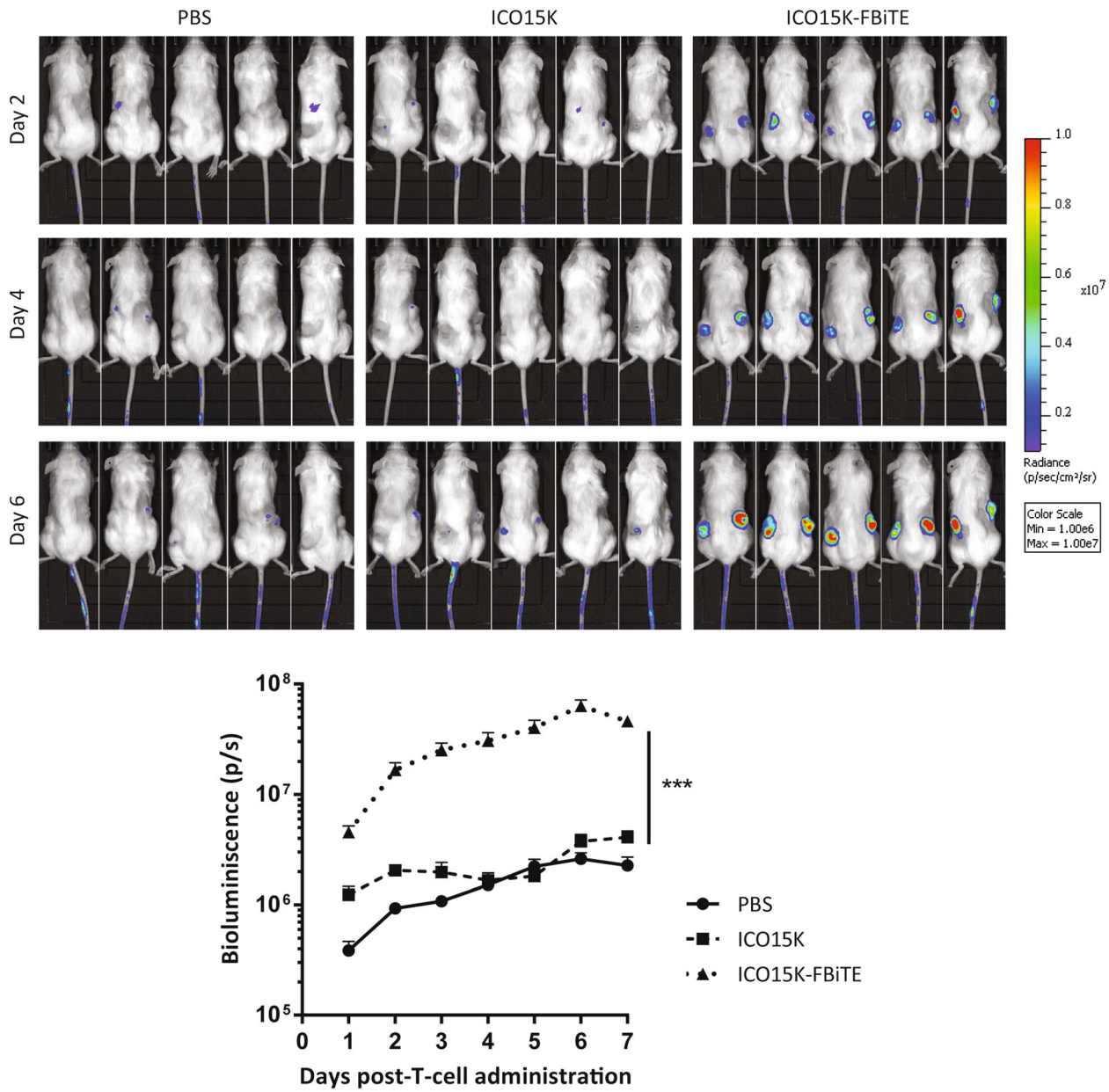

Fig. 4 Increased T cell accumulation in ICO15K-FBiTE tumors. NSG mice bearing A549 (lung carcinoma) tumors were intratumorally treated with PBS, ICO15K, or ICO15K-FBiTE (1×10^9 vp/tumor). Four days post-virus treatment, all mice received an intravenous injection of 1×10^7 LUC-T-cells (64% GFP^+). Luciferase activity was analyzed by bioluminescence imaging (IVIS) daily until day 7. Mean values ± SEM with ≥5 animals per group are shown. ***, ICO15K-FBiTE significant ($P < 0.001$) by one-way ANOVA test with *post hoc* analysis compared to PBS and ICO15K groups

to PBS-treated tumors (Fig. 6a), indicating that both viruses are able to infect and replicate in both tumor models. This result is further supported by similar findings when the presence of virus was evaluated by an anti-E1A immunohistochemistry (Fig. 6d). As expected, we could detect FBiTE expression only in ICO15K-FBiTE-treated tumors (Fig. 6b). These data confirm that viruses are present in the tumor and that the FBiTE is locally expressed in vivo upon ICO15K-FBiTE infection.

Having shown the in vivo persistence of both viruses as well as the FBiTE expression by the modified virus, we next sought to demonstrate the hypothesis that the enhanced antitumor effect was associated to depletion of FAP. FAP expression was first quantified by real-time PCR. As shown in Fig. 6c, the expression of FAP was reduced in both tumor models, in ICO15K-FBiTE-treated tumors compared with the PBS and the control virus. Consistent with this mRNA quantification data, the

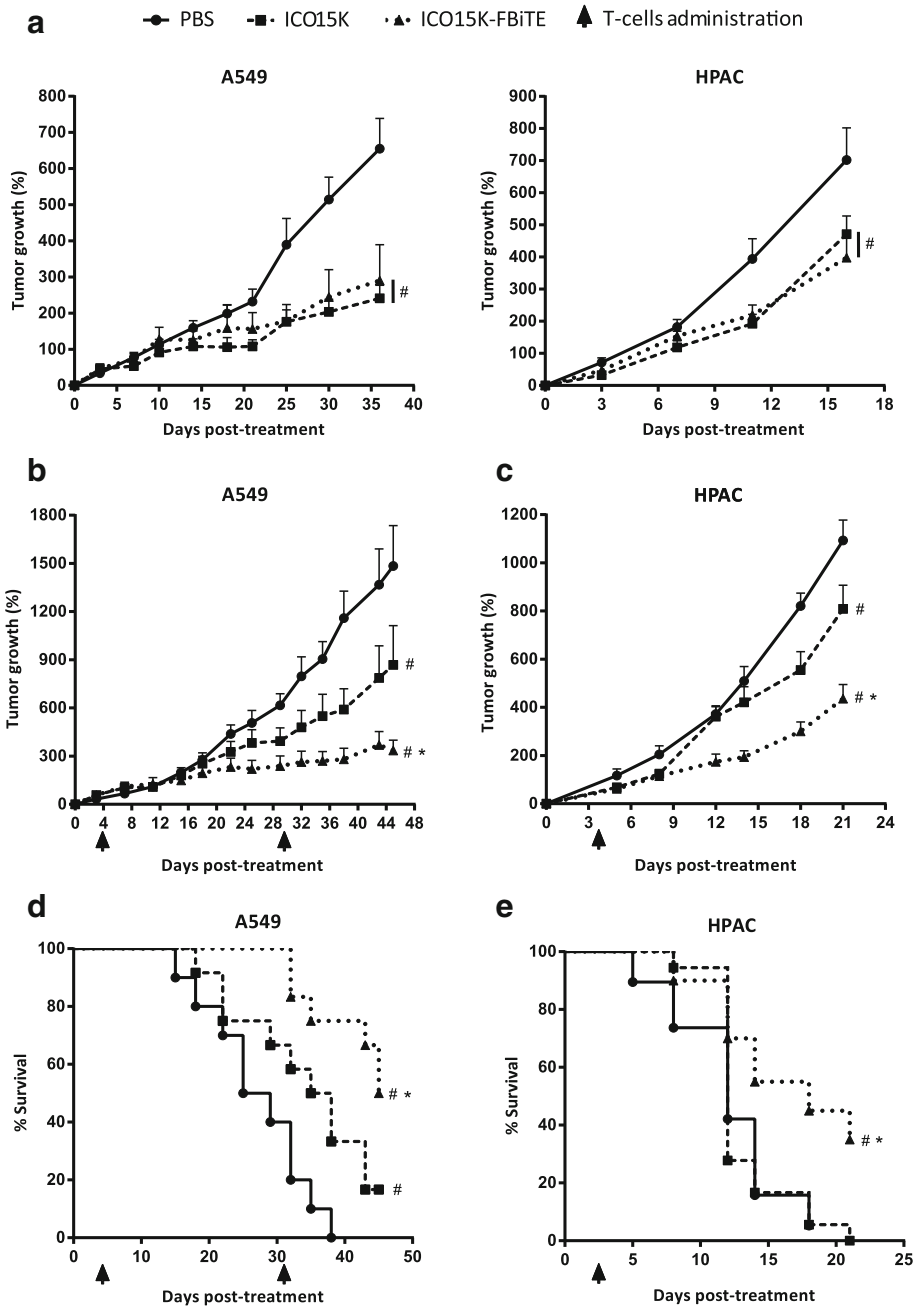

Fig. 5 Enhanced antitumor efficacy of ICO15K-FBiTE in the presence of T cells. **a**-**e** NSG mice bearing subcutaneous A549 (lung carcinoma) or HPAC (pancreatic adenocarcinoma) tumors were intratumorally treated with PBS, ICO15K, or ICO15K-FBiTE (1×10^9 vp/tumor). **a**. Antitumor activity in absence of T cells. Mean percentage of tumor growth value ± SEM with ≥12 tumors per group is plotted. **b**-**e** Antitumor efficacy in the presence of T cells. Four days after virus treatment, animals were treated once (HPAC) or twice (A549) with 1×10^7 preactivated T cells. The mean tumor growth ± SEM of ≥12 tumors per group is shown. **d**, **e** Kaplan-Meier survival curves of the experiments described in **b** and **c**. *, significant ($P < 0.05$) by one-way ANOVA test with *post hoc* analysis compared to ICO15K group. #, significant ($P < 0.05$) by one-way ANOVA test with *post hoc* analysis compared to PBS group

amount of FAP protein detected by staining the A549 tumors was also lower (Fig. 6e). Altogether, these results indicate that the T cells retargeted by the FBiTE are responsible for killing the FAP-positive murine CAFs in the tumor mass.

Discussion

Oncolytic adenoviruses (OAds) represent promising therapeutic agents that promote antitumor effects through a dual mechanism: selective tumor cell killing and the induction of antitumor immunity. However,

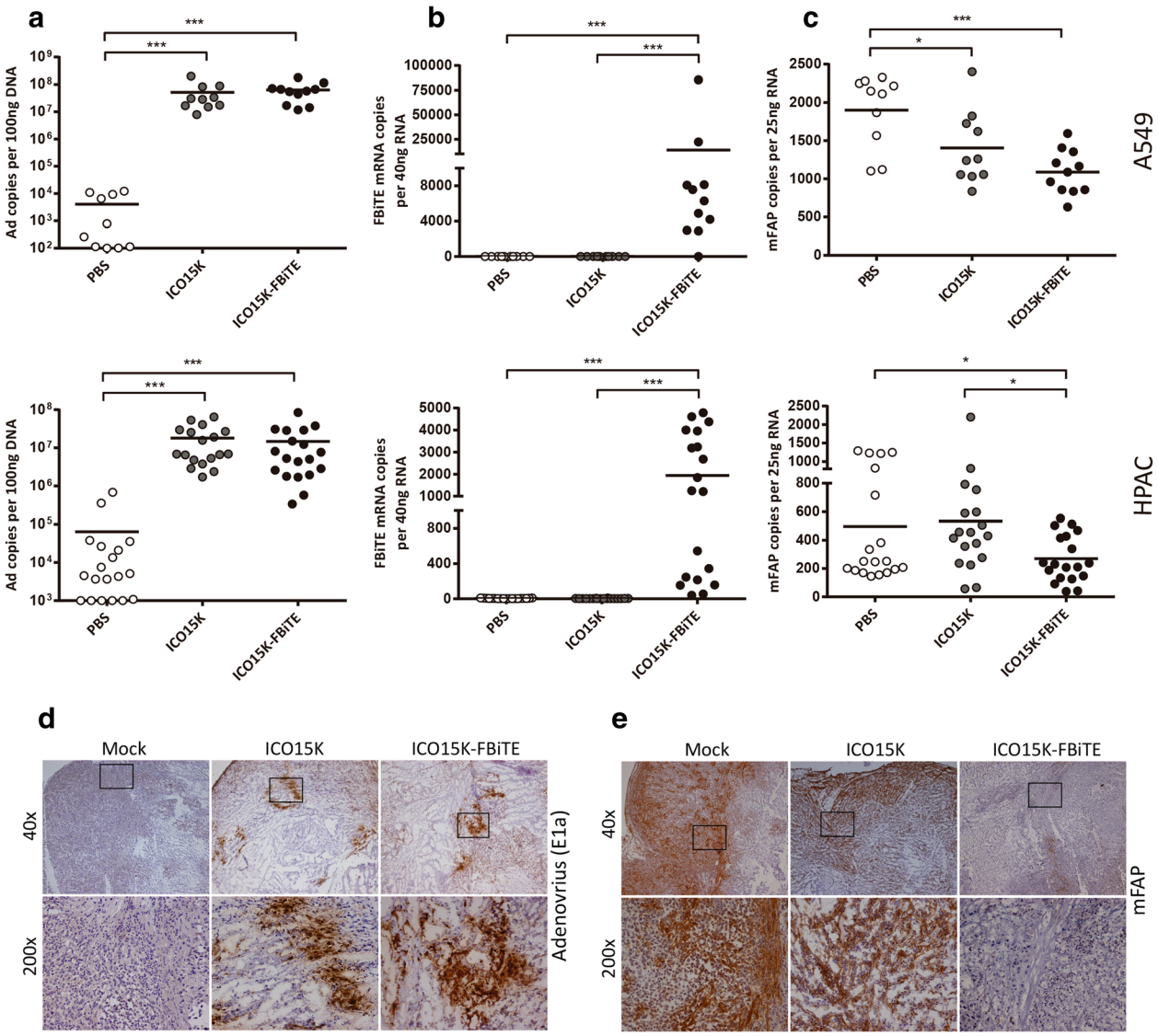

Fig. 6 Depletion of tumor stroma by ICO15K-FBiTE. A549 and HPAC tumors from the antitumor efficacy studies in presence of T cells were harvested at endpoint of the experiments. **a-c** Piece of tumor samples were mechanically homogenized, total DNA and RNA were extracted and quantification by real-time PCR-based method was performed to evaluate **a** the virus persistence, **b** FBiTE expression and **c** levels of FAP expression in both tumor models. **d, e** Immunohistochemical stainings of A549 tumors were also performed to assess **d** presence of virus by staining the early viral protein E1a and **e** FAP expression by an anti-FAP antibody. *, significant ($P < 0.05$) by two-tailed unpaired Student's *t*-test. ***, significant ($P < 0.001$) by two-tailed unpaired Student's *t*-test

several clinical trials with OAds generated promising albeit modest results [21]. Novel strategies are therefore needed to overcome the obstacles that prevent successful application of OAds, such as eliminating the tumor stroma that prevents efficient virus spread and preventing the immunodominance of the adenoviral epitopes that promotes fast virus clearance [22, 23].

In the present work, we aimed at addressing these limitations by arming an oncolytic adenovirus with an anti-FAP Bispecific T-cell Engager (FBiTE). In contrast to other therapies, one of the most important advantages of using BiTEs is its MHC-I-independent mode of action [24, 25]. BiTEs force T cells and tumor cells to come in close contact, forming an immunological synapse that shows all the hallmarks of a synapse formed by T cell receptor-MHC class I-peptide induced synapses. Therefore, encoding a BiTE specific against FAP would ideally re-direct lymphocytes to become cytotoxic against the tumor stroma, improving virus spread in the tumor microenvironment. In this study, we have demonstrated that once the FBiTE is expressed and secreted from infected cells, it can successfully activate both CD4 and

CD8 T cells. This activation leads to T-cell-mediated cytotoxicity of the FAP-expressing cells in vitro and in vivo and T-cell-induced bystander cell lysis of FAP-negative cells. Moreover, we have also demonstrated that the depletion of FAP-positive stromal cells from the tumor mass enhances the overall antitumor efficacy without increasing the toxicity. This data confirms previous results suggesting that targeting FAP enhances antitumor efficacy and might be therefore a promising approach for clinical benefits [3–10].

The use of OVs to achieve the local stimulation of the immune system against the tumor is a hot research field, leading to strong and durable responses [26]. OVs-infected cells create an inflammatory site with the consequent release of cytokines that activate the immune system, reverting the immune-suppressive tumor environment from a "cold" to a "hot" or lymphocyte-infiltrated tumor. However, the main side effect of the host immune system is the efficient clearance of the virus counteracting the oncolytic effect of the treatment. One of the advantages of arming an oncolytic virus with a BiTE is to balance the antiviral to antitumor immunity by its ability to re-direct the infiltrated antiviral lymphocytes to kill cells that express the protein targeted by the BiTE.

It is worth highlighting that arming oncolytic viruses with BiTEs represents a combined anti-cancer therapy. Our results show that simultaneously targeting the cancer cells with the oncolytic adenovirus and the tumor stroma with the FBiTE enhances the overall antitumor efficacy. Other BiTEs encoded by oncolytic viruses have already been published. The first one was the Ephrin A2-BiTE-armed oncolytic vaccinia virus, which induced PBMCs activation and tumor cell cytotoxicity *in vitro* and *in vivo* [27]. In line with that study, similar results have been described with different OVs armed with BiTEs [6, 14, 28]. However, all those studies exploited BiTEs targeting tumor-specific antigens [6, 14, 27, 28]. Thus, the secreted BiTEs can target both infected and uninfected cells, thereby reducing the virus-driven BiTE production and availability in the tumor microenvironment. To overcome this limitation, the FBiTE was designed to be expressed by the infected cancer cells and to target stromal cells, thereby avoiding the depletion of BiTE-expressing cancer cells and promoting continous BiTE production dependent on viral oncolysis. In this regard, a recent report described the benefits of targeting the tumor stroma with a FAP-targeting BiTE-armed vaccinia virus in an immunocompetent mouse model of cancer [3].

One of the major concerns when targeting non-specific tumor antigens is the potential toxicity. Despite the controversies of toxicity effects related with immune targeting, fatal adverse effects have already been reported in several studies [29]. In this regard, successful growth inhibition without signs of toxicity by FAP-targeted CARs T-cells has been reported [4, 5, 8]. In contrast, Tran et al reported that FAP-targeting with FAP5-CAR-transduced T cells led to cachexia and lethal bone toxicities due to FAP expression by multipotent bone marrow stem cells (BMSCs) [7]. Other studies have shown that FAP is expressed by some normal tissues and macrophages [19, 30, 31]. In agreement with this, we found activation and proliferation of T cells when PBMCs were co-cultured with FBiTE-containing supernatants (Additional file 1). Importantly, ICO15K-FBiTE treatment did not result in any significant off-target toxicity in mice, based on body weight and general animal behavior (Additional file 4). This discrepancy can be explained by the mode of action of our OV. FBiTE expression depends on the replication of the OAd in cancer cells within the tumor microenvironment, in contrast to CART cells, which circulate freely through the body. Thus, the strategy of arming oncolytic viruses with a FAP-targeting BiTE allows the continuous expression of BiTE directly in the tumor, preventing the targeting of healthy cells by the BiTE and in turn avoiding possible adverse effects. In addition, we showed that a single dose of oncolytic adenovirus is enough to obtain a continuous expression of BiTE by infected cells, avoiding the needed of repeated systemic infusion due to short half-life of BiTEs in serum [32].

Despite the notable improvement of antitumor efficacy obtained with ICO15K-FBiTE, no complete responses were observed. These findings may be somewhat limited by the lack of adequate tumor models used. Using immunocompetent models in order to explore the impact of infiltrating T cells in the tumor after virus injection would represent a more realistic scenario. However, the species-specific nature of the adenovirus infection and replication restricts the appropriate evaluation in immunocompetent mouse models. The limited and transient presence of adoptively transferred lymphocytes in our model could explain the decrease but incomplete elimination of FAP^+ cells in treated-tumors. Another reason that could explain the incomplete tumor rejection could be related to the insufficient activation of T cells. A recent report has demonstrated the importance of co-stimulation during BiTE-engagement in order to obtain improved antitumor efficacy [33]. This study highlights the need of developing improved BiTE constructs in order to avoid T cell exhaustion due to chronic antigen stimulation. In this line, combining this therapy with other immuno- or chemotherapies may also represent significant advantages. For example, we have recently demonstrated that combining BiTE-armed OV with CART cells improve CART-cell activation and proliferation in vitro and in vivo, thereby enhancing T-cell-mediated cytotoxicity [34]. We and others have

also shown an increase in the expression of T-cell inhibitory receptors after immune-based therapies, likely limiting the antitumor activity [34, 35]. For example, Ribas et al reported the strong enhanced immune recognition of cancer when combined talimogene laherparepvec oncolytic virus with an anti-PD1 antibody [26]. These studies support the rationale to combine our BiTE-expressing virus with different immune checkpoint inhibitors. On the other hand, Fang et al reported the benefits of combining FAP-targeted therapies with chemotherapies [11]. Such results suggest that destroying the stroma not only improves virus spread but also may allow chemotherapy drugs to better penetrate into tumor. It is therefore likely that the successful application of FAP-targeted by BiTE-armed oncolytic adenovirus in cancer patients will require the development of an optimized therapeutic approach.

Conclusion

This study establishes ICO15K-FBiTE as an effective strategy for targeting both cancer cells and FAP-positive stromal cells, killing through combined viral oncolysis and intratumoral expression of an anti-FAP BiTE. This approach offers opportunities for cancer therapy with no evidence of toxicity and further encourages the transition into clinical applications. Future studies should be directed towards optimization of both oncolytic adenovirus and BiTE designs and to explore the effectiveness of FAP-targeting BiTE-armed oncolytic adenovirus in combination with other therapeutic modalities, such as chemotherapy or other immunotherapies.

Additional files

Additional file 1: FBiTEs molecules expressed from ICO15K-FBiTE-infected cells induce T-cells proliferation when co-cultured with PBMCs. 293, 293mFAP and 293hFAP were co-cultured with CFSE-labeled PBMCs and indicated supernatants. Six days after co-culture, the CFSE content in $CD4^+$ and $CD8^+$ T-cells was determined by flow cytometry. A representative result of triplicates is shown. (DOCX 13487 kb)

Additional file 2: FBiTE-mediated bystander tumor cell killing. A, B. CFSE-stained HT cells (A) or A431 cells (B) were culture in the presence of T cells and its derivative mFAP- or hFAP cells and the indicated supernatants (mock, ICO15K or ICO15K-FBiTE) were added. After 24 h, cytotoxicity of HT cells (A) or A431 cells (B) and its mFAP- or hFAP-derivative cells were evaluated by flow cytometry. Mean values ± SD are plotted in A, B ($n = 3$). ***, significant ($P < 0.001$) by one-way ANOVA test with post hoc analysis compared to mock and ICO15K. **, significant ($P < 0.01$) by one-way ANOVA test with post hoc analysis compared to mock and ICO15K. (DOCX 168 kb)

Additional file 3: Characterization of GFP- and CBG Luciferase-expressing T cells. A. Flow cytometry analysis of GFP expression of preactivated T-cells that had been transduced with a lentiviral vector encoding GFP and the click beetle green (CBG) luciferase. B. Percentages of CD4 and CD8 LUC-T-cells populations determined by flow cytometry. (DOCX 231 kb)

Additional file 4: Body weight variation in A549 xenograft antitumoral efficacy assay. Animal body weight was monitored weekly after intratumoral injection of PBS, ICO15K or ICO15K-FBiTE (2×10^9 vp). Mean values ± SEM are plotted ($n = 6–7$). (DOCX 140 kb)

Additional file 5: Antitumor activity of ICO15K-FBiTE. NSG mice bearing subcutaneous xenografts of A549 or HPAC tumors were injected intratumorally with PBS or 2×10^9 viral particles of ICO15K or ICO15K-FBiTE. The mean tumor volume ± SEM of ≥12 tumors per group is shown. *, significant ($P < 0.05$) by one-way ANOVA test with post hoc analysis compared to ICO15K group. #, significant ($P < 0.05$) by one-way ANOVA test with post hoc analysis compared to PBS group. (DOCX 195 kb)

Abbreviations

ALL: Acute lymphoid leukemia; ATCC: American Type Culture Collection; BiTE: Bispecific T-cell engager; BST: Blood and Tissue Bank; CAF: Cancer-associated fibroblast; CBG: Click beetle green luciferase; CFSE: Carboxyfluorescein succinimidyl ester; ECM: Extracellular matrix; FAP: Fibroblast activation protein-α; FBiTE: FAP-targeting bispecific T-cell engager; GM-CSF: granulocyte macrophage colony stimulating factor; hCAFS: human CAFs; HSV: Herpes simplex virus; ICO15K-cBiTE: EGFR-BiTE-armed oncolytic adenovirus; ICO15K-FBiTE: FAP-BiTE-armed oncolytic adenovirus; IDIBELL: Biomedical Research Institute of Bellvitge; IHC: immunohistochemistry; LUC-T-cells: GFP- and CBG-luciferase-expressing T cells; mCAFs: murine CAFs; MOI: Multiplicity of infection; NSG: NOD/*scid*/*IL2rg*$^{-/-}$; OAd: Oncolytic adenovirus; OV: Oncolytic virus; PBMCs: Peripheral blood mononuclear cells; ScFv: Single-chain variable fragment; TAA: tumor-associated antigen

Acknowledgements

The authors thank Eric Tran for the gift of 293, 293mFAP and 293hFAP cells and Varda Rotter for the human CAFs pf179. We also thank Ellen Puré for providing the 73.3 anti-murine FAP antibody.

Funding

This work was supported by BIO2014–57716-C2–1-R, BIO2017–89754-C2–1-R, and Adenonet BIO2015–68990-REDT grants from the Ministerio de Economía y Competitividad of Spain, FPI-BES-2015-074427 to JdeSo, Red ADVANCE(-CAT) project COMRDI15-1-0013 from Ris3CAT, and the 2014SGR364 research grant from the 'Generalitat de Catalunya'. We thank CERCA Programme / Generalitat de Catalunya for institutional support. Co-funded by the European Regional Development Fund, a way to Build Europe.

Availability of data and materials

The data set analyzed for the current study is available from the corresponding author on reasonable request.

Authors' contributions

Conception and design: JdeSo, CAF, RA. Development of methodology: JdeSo, CAF, RA. Acquisition of data: JdeSo, CAF, RM, MDR, MF-Sal. Analysis of data: JdeSo, CAF, RA. Writing, review and/or revision of the manuscript: JdeSo, CAF, RA. All authors read and approved the final manuscript.

Ethics approval and consent to participate

All in vivo experiments were reviewed and approved by the Ethics Committee for Animal Experimentation from Biomedical Research Institute of Bellvitge (IDIBELL).

Consent for publication

Not applicable.

Competing interests

The authors declare that they have no competing interests.

Publisher's Note

Author details
[1]ProCure Program, IDIBELL-Institut Català d'Oncologia, l'Hospitalet de Llobregat, El Prat de Llobregat, Spain. [2]VCN Biosciences S.L., Grifols Corporate Offices, Sant Cugat del Vallès, Spain.

Received: 6 September 2018 Accepted: 10 January 2019
Published online: 25 January 2019

References

1. Kalluri R. The biology and function of fibroblasts in cancer. Nat Rev Cancer. 2016;16(9):582–98.
2. Park JE, Lenter MC, Zimmermann RN, Garin-chesa P, Old LJ, Rettig WJ. Fibroblast activation protein: a dual-specificity serine protease expressed in reactive human tumor stromal fibroblasts. Biol Chem. 1999;274(51):36505–12.
3. Yu F, Hong B, Song X-T. A T-cell engager - armed oncolytic vaccinia virus to target the tumor stroma. Cancer Transl Med. 2017;3(4):122–32.
4. Wang L-CS, Lo A, Scholler J, Sun J, Majumdar RS, Kapoor V, Antzis M, Cotner CE, Johnson LA, Durham AC, Solomides CC, June CH, Pure E, Albelda SM. Targeting fibroblast activation protein in tumor stroma with chimeric antigen receptor T cells can inhibit tumor growth and augment host immunity without severe toxicity. Cancer Immunol Res. 2014;2(2):154–66.
5. Lo A, Wang LCS, Scholler J, Monslow J, Avery D, Newick K, O'Brien S, Evans RA, Bajor DJ, Clendenin C, Durham AC, Buza EL, Vonderheide RH, June CH, Albelda SM, Pure E. Tumor-promoting desmoplasia is disrupted by depleting FAP-expressing stromal cells. Cancer Res. 2015;75(14):2800–10.
6. Speck T, Heidbuechel JPW, Veinalde R, Jaeger D, Von Kalle C, Ball CR, Ungerechts G, Engeland CE. Targeted bite expression by an oncolytic vector augments therapeutic efficacy against solid tumors. Clin Cancer Res. 2018;24(9):2128–37.
7. Tran E, Chinnasamy D, Yu Z, Morgan RA, Lee C-CR, Restifo NP, Rosenberg SA. Immune targeting of fibroblast activation protein triggers recognition of multipotent bone marrow stromal cells and cachexia. J Exp Med. 2013; 210(6):1125–35.
8. Kakarla S, Chow KKH, Mata M, Shaffer DR, Song XT, Wu MF, Liu H, Wang LL, Rowley DR, Pfizenmaier K, Gottschalk S. Antitumor effects of chimeric receptor engineered human T cells directed to tumor stroma. Mol Ther. 2013;21(8):1611–20.
9. Lee J, Fassnacht M, Nair S, Boczkowski D, Gilboa E. Tumor immunotherapy targeting fibroblast activation protein, a product expressed in tumor-associated fibroblasts. Cancer Res. 2005;65(23):11156–63.
10. Ostermann E, Garin-Chesa P, Heider KH, Kalat M, Lamche H, Puri C, Kerjaschki D, Rettig WJ, Adolf GR. Effective immunoconjugate therapy in cancer models targeting a serine protease of tumor fibroblasts. Clin Cancer Res. 2008;14(14):4584–92.
11. Fang J, Xiao L, Joo K-I, Liu Y, Zhang C, Liu S, Conti PS, Li Z, Wang P. A potent immunotoxin targeting fibroblast activation protein for treatment of breast cancer in mice. Int J Cancer. 2016;138(4):1013-23.
12. Sobol PT, Boudreau JE, Stephenson K, Wan Y, Lichty BD, Mossman KL. Adaptive antiviral immunity is a determinant of the therapeutic success of oncolytic virotherapy. Mol Ther. 2011;19(2):335–44.
13. Topp MS, Gökbuget N, Stein AS, Zugmaier G, O'Brien S, Bargou RC, Dombret H, Fielding AK, Heffner L, Larson RA, Neumann S, Foà R, Litzow M, Ribera JM, Rambaldi A, Schiller G, Brüggemann M, Horst HA, Holland C, Jia C, Maniar T, Huber B, Nagorsen D, Forman SJ, Kantarjian HM. Safety and activity of blinatumomab for adult patients with relapsed or refractory B-precursor acute lymphoblastic leukaemia: a multicentre, single-arm, phase 2 study. Lancet Oncol. 2015;16(1):57–66.
14. Fajardo CA, Guedan S, Rojas LA, Moreno R, Arias-Badia M, De Sostoa J, June CH, Alemany R. Oncolytic adenoviral delivery of an EGFR-targeting t-cell engager improves antitumor efficacy. Cancer Res. 2017;77(8):2052–63.
15. Berdiel-Acer M, Sanz-Pamplona R, Calon A, Cuadras D, Berenguer A, Sanjuan X, Paules MJ, Salazar R, Moreno V, Batlle E, Villanueva A, Molleví DG. Differences between CAFs and their paired NCF from adjacent colonic mucosa reveal functional heterogeneity of CAFs, providing prognostic information. Mol Oncol. 2014;8(7):1290–305.
16. Rojas LA, Condezo GN, Olié RM, Fajardo CA, Arias-Badia M, San Martín C, Alemany R. Albumin-binding adenoviruses circumvent pre-existing neutralizing antibodies upon systemic delivery. J Control Release. 2016;237:78–88.
17. Rojas JJ, Guedan S, Searle PF, Martinez-Quintanilla J, Gil-Hoyos R, Alcayaga-Miranda F, Cascallo M, Alemany R. Minimal RB-responsive E1A promoter modification to attain potency, selectivity, and transgene-arming capacity in oncolytic adenoviruses. Mol Ther. 2010;18(11):1960–71.
18. Guedan S, Rojas JJ, Gros A, Mercade E, Cascallo M, Alemany R. Hyaluronidase expression by an oncolytic adenovirus enhances its intratumoral spread and suppresses tumor growth. Mol Ther. 2010;18(7):1275–83.
19. Julia T, Paul JZ, Yingtao B, Celine S, Rajrupa M, Lo A, Haiying C, Carolyn M, June CH, Jose C, Ellen P. Fibroblast activation protein expression by stromal cells and tumor-associated macrophages in human breast Cancer. Hum Pathol. 2013;44(11):2549–57.
20. Ross SL, Sherman M, McElroy PL, Lofgren JA, Moody G, Baeuerle PA, Coxon A, Arvedson T. Bispecific T cell engager (BiTE®) antibody constructs can mediate bystander tumor cell killing. PLoS One. 2017;12(8):1–24.
21. Ahn D, Bekaii-Saab T. The continued promise and many disappointments of oncolytic Virotherapy in gastrointestinal malignancies. Biomedicines. 2017; 5(1):10.
22. Zou W. Immunosuppressive networks in the tumour environment and their therapeutic relevance. Nat Rev Cancer. 2005;5(4):263–74.
23. Schirmbeck R, Reimann J, Kochanek S, Kreppel F. The immunogenicity of adenovirus vectors limits the multispecificity of CD8 T-cell responses to vector-encoded transgenic antigens. Mol Ther. 2008;16(9):1609–16.
24. Offner S, Hofmeister R, Romaniuk A, Kufer P, Baeuerle PA. Induction of regular cytolytic T cell synapses by bispecific single-chain antibody constructs on MHC class I-negative tumor cells. Mol Immunol. 2006;43(6):763–71.
25. Schlereth B, Fichtner I, Lorenczewski G, Kleindienst P, Brischwein K, Da Silva A, Kufer P, Lutterbuese R, Junghahn I, Kasimir-Bauer S, Wimberger P, Kimmig R, Baeuerle PA. Eradication of tumors from a human colon cancer cell line and from ovarian cancer metastases in immunodeficient mice by a single-chain ep-CAM-/CD3- bispecific antibody construct. Cancer Res. 2005;65(7):2882–9.
26. Ribas A, Dummer R, Puzanov I, VanderWalde A, Andtbacka RHI, Michielin O, Olszanski AJ, Malvehy J, Cebon J, Fernandez E, Kirkwood JM, Gajewski TF, Chen L, Gorski KS, Anderson AA, Diede SJ, Lassman ME, Gansert J, Hodi FS, Long G V. Oncolytic Virotherapy promotes Intratumoral T cell infiltration and improves anti-PD-1 immunotherapy. Cell. 2017;170(6):1109–19.
27. Yu F, Wang X, Guo ZS, Bartlett DL, Gottschalk SM, Song XT. T-cell engager-armed oncolytic vaccinia virus significantly enhances antitumor therapy. Mol Ther. 2014;22(1):102–11.
28. Freedman JD, Hagel J, Scott EM, Psallidas I, Gupta A, Spiers L, Miller P, Kanellakis N, Ashfield R, Fisher KD, Duffy MR, Seymour LW. Oncolytic adenovirus expressing bispecific antibody targets T-cell cytotoxicity in cancer biopsies. EMBO Mol Med. 2017;9(8):1067–87.
29. Teachey DT, Rheingold SR, Maude SL, Zugmaier G, Barrett DM, Seif AE, Nichols KE, Suppa EK, Kalos M, Berg RA, Fitzgerald JC, Aplenc R, Gore L, Grupp SA. Cytokine release syndrome after blinatumomab treatment related to abnormal macrophage activation and ameliorated with cytokine-directed therapy. Blood. 2013;121(26):5154–7.
30. Roberts EW, Deonarine A, Jones JO, Denton AE, Feig C, Lyons SK, Espeli M, Kraman M, McKenna B, Wells RJB, Zhao Q, Caballero OL, Larder R, Coll AP, O'Rahilly S, Brindle KM, Teichmann SA, Tuveson DA, Fearon DT. Depletion of stromal cells expressing fibroblast activation protein-α from skeletal muscle and bone marrow results in cachexia and anemia. J Exp Med. 2013;210(6): 1137–51.
31. Bae S, Park CW, Son HK, Ju HK, Paik D, Jeon CJ, Koh GY, Kim J, Kim H. Fibroblast activation protein α identifies mesenchymal stromal cells from human bone marrow. Br J Haematol. 2008;142(5):827–30.
32. Topp MS, Kufer P, Gökbuget N, Goebeler M, Klinger M, Neumann S, Horst HA, Raff T, Viardot A, Schmid M, Stelljes M, Schaich M, Degenhard E, Köhne-Volland R, Brüggemann M, Ottmann O, Pfeifer H, Burmeister T, Nagorsen D, Schmidt M, Lutterbuese R, Reinhardt C, Baeuerle PA, Kneba M, Einsele H, Riethmüller G, Hoelzer D, Zugmaier G, Bargou RC. Targeted therapy with the T-cell - engaging antibody blinatumomab of chemotherapy-refractory minimal residual disease in B-lineage acute lymphoblastic leukemia patients results in high response rate and prolonged leukemia-free survival. J Clin Oncol. 2011;29(18):2493–8.
33. Correnti CE, Laszlo GS, De Van Der Schueren WJ, Godwin CD, Bandaranayake A, Busch MA, Gudgeon CJ, Bates OM, Olson JM, Mehlin C,

Walter RB. Simultaneous multiple interaction T-cell engaging (SMITE) bispecific antibodies overcome bispecific T-cell engager (BiTE) resistance via CD28 co-stimulation. Leukemia. 2018;32(5):1239–43.
34. Wing A, Fajardo CA, Posey AD, Shaw C, Da T, Young RM, Alemany R, June CH, Guedan S. Improving CART-Cell Therapy of Solid Tumors with Oncolytic Virus–Driven Production of a Bispecific T-cell Engager. Cancer Immunol Res. 2018;6(5):605-16.
35. Zamarin D, Rb H, Sk S, Js P, Mansour M, Palese P, Merghoub T, Jd W. Localized oncolytic virotherapy overcomes systemic tumor resistance to immune checkpoint blockade immunotherapy. Sci. Transl. Med. 2014;6(226): 226-32.